DETERMINATION OF SEISMIC SOURCE PARAMETERS FROM FREQUENCY DEPENDENT RAYLEIGH AND LOVE WAVE RADIATION PATTERNS

Lawrence S. Turnbull, Jr., et al

Texas Instruments, Incorporated

Prepared for:

Air Force Office of Scientific Research
Advanced Research Projects Agency

15 November 1973

UNCLASSIFIED
Security Classification

AD-778 996

DOCUMENT CONTROL DATA - R & D

(Security classification of title, body of abstract and indexing annotation must be entered when the overall report is classified)

1. ORIGINATING ACTIVITY (Corporate author)
Texas Instruments Incorporated
Equipment Group
Dallas, Texas 75222

2a. REPORT SECURITY CLASSIFICATION
UNCLASSIFIED

2b. GROUP

3. REPORT TITLE
Determination of Seismic Source Parameters From Frequency Dependent Rayleigh And Love Wave Radiation Patterns

4. DESCRIPTIVE NOTES (Type of report and inclusive dates)
Semi-Annual Technical Report No. 1-Part C, 1 May 1973 - 31 October 1973

5. AUTHOR(S) (First name, middle initial, last name)
Lawrence S. Turnbull, Jr., David F. D. Sun, and Jeffrey S. Shaub

6. REPORT DATE
15 November, 1973

7a. TOTAL NO. OF PAGES
192

7b. NO OF REFS
25

8a. CONTRACT OR GRANT NO
Contract No. F44620-73-C-0055

b. PROJECT NO.
ARPA Program Code
No. F10

c.

d.

9a. ORIGINATOR'S REPORT NUMBER(S)
ALEX(02)-TR-73-01-PART C

9b. OTHER REPORT NO(S) (Any other numbers that may be assigned this report)
AFOSR - TR - 74 - 0782

10. DISTRIBUTION STATEMENT
Approved for public release;
distribution unlimited.

11. SUPPLEMENTARY NOTES
ARPA Order No. 1827

12. SPONSORING MILITARY ACTIVITY
Advanced Research Projects Agency
Nuclear Monitoring Research Office
Arlington, Virginia 22209

13. ABSTRACT

Both exhaustive and non-linear spectral fitting procedures are applied to far-field surface wave data for determining seismic source parameters, especially depth. These procedures were applied to a series of events with decreasing control on the source parameters. High quality Rayleigh wave data from the Southeastern Missouri Earthquake of October 21, 1965 was analyzed, and the parameter corroboration with independent estimates was good, with excellent spectral fits. Two low magnitude (m_b = 4.1) Italian events were analyzed individually and by taking spectral ratios. Both techniques agreed with a nearby bodywave solution in the same tectonic region. Next, six events from Sinkiang were analyzed, again using both techniques. Results were mixed, but with better azimuthal coverage and more realistic effective Q corrections, spectral fits and depth estimates of high quality can be expected. Finally, initial efforts are directed towards determining the importance of the parameter variations; it was found that depth has the greatest effect on the shape of the spectra.

DD FORM 1 NOV 65 1473

UNCLASSIFIED
Security Classification

14. KEY WORDS	LINK A		LINK B		LINK C	
	ROLE	WT	ROLE	WT	ROLE	WT
Eurasian Earthquakes						
Surface Wave Spectra						
Determination of Source Parameters						
Narrow Band Filtering						
Non-Linear Regression						
Rayleigh Wave Attenuation Coefficient						

DETERMINATION OF SEISMIC SOURCE PARAMETERS FROM FREQUENCY DEPENDENT RAYLEIGH AND LOVE WAVE RADIATION PATTERNS

SEMI-ANNUAL TECHNICAL REPORT NO. 1 - PART C
1 MAY 1973 TO 31 OCTOBER 1973

Prepared by
Lawrence S. Turnbull, Jr., David F. D. Sun, and Jeffrey S. Shaub

TEXAS INSTRUMENTS INCORPORATED
Equipment Group
Post Office Box 6015
Dallas, Texas 75222

Contract No. F44620-73-C-0055
Amount of Contract: $148,244
Beginning 23 April 1973
Ending 31 December 1973

Prepared for

AIR FORCE OFFICE OF SCIENTIFIC RESEARCH

Sponsored by

ADVANCED RESEARCH PROJECTS AGENCY
Nuclear Monitoring Research Office
ARPA Program Code No. F10
ARPA Order No. 1827

15 November 1973

Acknowledgment: This research was supported by the Advanced Research Projects Agency, Nuclear Monitoring Research Office, under Project VELA-UNIFORM, and accomplished under the direction of the Air Force Office of Scientific Research under Contract F44620-73-C-0055.

ABSTRACT

Both exhaustive and non-linear spectral-fitting procedures are applied to far-field surface wave data for determining seismic source parameters, especially depth. The spectral fit solution is based on a minimum residual criterion between the theoretical and observed spectra. The initial efforts are directed towards determining the importance of the parameter variations; it was found that depth has the greatest effect on the shape of the spectra. We also attempted to fit a double couple source to theoretical explosion data using only Rayleigh waves. Although our analysis yielded an event at 15 km depth, indicating that an improper fit is possible, consideration of radiation patterns and spectral levels demonstrate that this is an exceptional case.

The automatic spectral fitting procedures were applied to a series of events with decreasing control on the source parameters. This procedure was supplemented by the use of a series of narrow band filters for removing multipath interference, which was successful. High quality Rayleigh wave data from the Southeastern Missouri Earthquake of October 21, 1965 was analyzed, and the parameter corroboration with independent estimates was good, with excellent spectral fits. Two low magnitude (m_b = 4.1) Italian events were analyzed individually and by taking spectral ratios. Both techniques agreed with a nearby bodywave solution in the same tectonic region. Finally, six events from Sinkiang were analyzed, again using both techniques. Results were mixed, but with better azimuthal coverage and more realistic effective Q corrections, spectral fits and depth estimates of high quality can be expected.

TABLE OF CONTENTS

TABLE OF CONTENTS
(continued)

LIST OF FIGURES

LIST OF FIGURES
(continued)

LIST OF FIGURES
(continued)

LIST OF FIGURES
(continued)

LIST OF FIGURES
(continued)

LIST OF FIGURES
(continued)

LIST OF FIGURES
(continued)

LIST OF FIGURES
(continued)

LIST OF TABLES

LIST OF TABLES
(continued)

SECTION I
INTRODUCTION

The problem of obtaining seismic source parameters from surface wave radiation patterns has been investigated by several authors over the past few years. Lambert et al. (1972) combined experience in using surface wave data with a trial-and-error approach to obtain their solutions. Mitchell (1973) used partial derivatives of the source parameters to guide a trial-and-error approach in fitting surface wave radiation patterns from the Southeastern Missouri Earthquake of 1965. Tsai and Aki (1970a, b), Tsai (1972a, b), Tsai and Shen (1972), and Weidner (1972) used essentially an exhaustive comparison scheme between the observed and theoretical spectra, with the model which yielded the minimum residual chosen as the solution. Turnbull and Alexander (1973) refined this approach, using a non-linear iterative scheme on the parameters dip(δ), slip(λ), strike(ϕ), and seismic moment(M) combined with an exhaustive variation with depth. The following report represents an attempt to refine the work of Tsai and Turnbull into a unified approach, and combine the strongest parts of their methodology.

In Section II, each part that contributes to the seismic record is discussed in detail. Our analysis of the amplitude spectra of surface waves examines the energy in the frequency band from 0.02 to 0.10 Hz (T from 10 to 50 seconds). Because the theoretical spectra of the Rayleigh and Love waves are calculated from a layered half space of nondissipating elastic medium, corrections must be made for attenuation due to anelasticity. A discussion of this correction is given, and the attenuation for a particular source-station path is given in Section VI in the analysis of the Sinkiang events. The observed spectra also are affected by interference due to

multipath arrivals. This interference takes the form of spectral modulations. Their removal was accomplished using a series of narrow band fitters as discussed by Alexander (1963). Finally, in Section II, the source excitation function is discussed in terms of the source time function, the amplitude response of the medium, the radiation pattern, and the application of Tsai's and Turnbull's combined methodology to obtain seismic source parameters.

This report is essentially a discussion of analysis techniques applied to surface wave data with various degrees of control. Section III, though, represents the beginning of a detailed study of the intrinsic capabilities of the methodology. If we do not have independent determinations of the source parameters, such as the dip(δ), slip(λ), and strike(ϕ) from body wave data, and depth from pP, we must ask ourselves the meaning of the minimum residual solution. We are investigating this problem on two fronts. First, amplitude spectra and radiation patterns were generated for many representative cases. From these, conclusions can be reached on parameter variations and spectral shapes. Secondly, in applying our theoretical double couple source model to the data, we have always assumed that the event was an earthquake. What if the data were really generated by an explosion? A discussion of the application of an earthquake source to explosion data is given for several cases.

The next three sections present applications of the methodology to multisite surface wave data with varying degrees of control on the source parameters. Each successive section analyzes data with less control than the previous one. In this way, we can get some idea of the reliability of our method. In Section IV, superior quality Rayleigh wave amplitude spectra from the Southeastern Missouri Earthquake of 1965 are analyzed. Previous solutions for the source parameters have been obtained using both the surface wave and body wave data, so comparison with our result is possible. This case demonstrates what is possible when extensive multi-azimuth, non-

multipathed data with good attenuation corrections are available. We also examine the effect of source structure on our solution.

Section V presents the analysis of data for two low magnitude Italian events (m_b about 4.0) where only three stations (VLPE) were recording. Each event is analyzed separately, and then spectral ratios of the events are used to obtain solutions. From body wave solutions for events in the same tectonic region, we can see that our solution is reasonable.

In Section VI, the analysis of six events from the Sinkiang region of southern Asia is presented. The problems inherent in de-multipathing and in the application of an attenuation correction for events from this region recorded at VLPE stations are discussed. In particular, an intensive effort was made to determine the attenuation coefficient for the Sinkiang-Chiang Mai (CHG) travel path using explosion data. No corroborative evidence of source parameter values were available at this time.

Finally, in Section VII, we give a summary of the results given in the previous sections, and the paths this investigation expects to take in the future.

SECTION II

A DISCUSSION OF THE TRANSFORMED SEISMIC RECORD AND THE APPLICATION OF SPECTRAL FITTING PROCEDURES TO THEM

Using an exhaustive approach or a non-linear regression analysis on synthetically generated data as a test for the method can be quite deceptive. It is necessary as a test for the correctness of the software, but virtually useless as a measure of its practical applicability. Considering the average quality of the VLPE data used in Section V and VI of this report, parameter estimates obtained from Rayleigh and Love wave data recorded at two sites are, in the opinion of this author, at best a first guess. The reasons for this statement lie in a detailed analysis of those factors which perturb the observed data to such a degree that our theoretical description of the seismic source is inadequate.

We can begin such an analysis by examining each of the component parts of the Fourier transform of the seismic record. The transform of the record obtained at station i resulting from event ℓ can be written:

$$R_{i\ell}(\omega) = I_i(\omega)\, U_\ell(\omega, r)$$

where: $I_i(\omega)$ - Instrument response

$U_\ell(\omega, r)$ - Frequency domain displacement

The instrument response at each of the VLPE sites is furnished on regular basis, so little error should result from this correction. The frequency domain displacement can be written as

$$U_\ell(\omega, r) = G_\ell(\omega, r)\, S_\ell(\omega)\, e^{i(\phi)}$$

where: $G_\ell(\omega, r)$ - Path transfer function

$S_\ell(\omega)$ - Source excitation function

$e^{i(\phi)}$ - Combined phase terms

The path transfer function is probably the weakest link in our analysis. It involves essentially two corrections to the observed data; a correction for effective attenuation and elimination of multipathing. Two approaches for obtaining an effective Q are given in Appendix A. One involves two or more stations nearly on the same great circle path (amplitude equalization), and the other involves multisite data from an explosion yielding an average value for a region (Tryggvasson's method). In both methods, high quality, multi-site data is required. At present, these numbers are not available for critical source-station paths from the Eurasian continent, and a concerted effort to obtain these values is highly desirable.

Elimination of multipathing has been accomplished by the use of a series of narrow band filters. This technique, first used by Alexander (1963) on surface wave data, is described in detail in Appendix B. The application of these filters produces a series of wave packets corresponding to the center frequencies of each filter. (These packets are used in the analysis of the Italian [Section V] and Sinkiang [Section VI] events). If multi-pathing exists, more than one packet will occur for the selected frequencies. By determining the group velocity of the maximum amplitude peak of each packet, and comparing these velocities to standard group velocity curves, the correct packet can be chosen. The maximum amplitude peak of this packet is then the value of the spectral amplitude corresponding to the packet frequency.

There are three main sources of inaccuracies in this type of analysis. If leakage occurs between the components, either through recording defects or improper analytical rotation, the results are essentially meaningless.

A general shift in all the packets can occur from group delays of the instruments and imprecise location of the event. Careful analysis, though, can minimize all of the above.

This technique was chosen over the complex cepstrum analysis previously applied by Tsai (1972a) because of difficulties in interpretation. The complex cepstrum technique (Linville, 1971) assumes that the multipathed signal has essentially the same dispersion as the original signal. In fact, each frequency is affected differently by lateral velocity changes, and the interpretation of the cepstrum becomes highly subjective. The cepstrum technique seems more suited for multiple event analysis.

Finally, we can write the source excitation function as:

$$S_{\ell}(\omega) = M_{\ell} L_{\ell}(\omega) k_{\ell}(\omega) N_{\ell}(\omega, h) X(\omega, \theta_{\ell}, \lambda_{\ell}, \delta_{\ell}, h_{\ell}) e^{i(\phi')}$$

where:

M_{ℓ} - Seismic moment

$k_{\ell}(\omega)$ - Rayleigh or Love wave number

$L_{\ell}(\omega)$ - Transform of source-time function

$N_{\ell}(\omega)$ - Medium amplitude response

$X_{\ell}(\omega)$ - Complex radiation pattern

The theoretical earthquake source is represented by a double couple which varies as a step function in time [source-time function $L_{\ell}(t)$] whose strength is M_{ℓ}, the seismic moment. A detailed discussion of the source time function is given in Appendix C.

The medium amplitude response $N_{\ell}(\omega)$ represents the response of the source structure to a Dirac delta function point source. This structure is in the idealized form of a plane-parallel layered half space. In Appendix D, several representative structures are displayed with their corresponding Rayleigh and Love wave group velocity curves. The effect of structure on the determination of source parameters is discussed in Section IV in the analysis of the Southeastern Missouri Earthquake of 1965.

The determination of the source parameters is achieved using a combination of Tsai's Method for a localization of a best fit, and then a non-linear regression scheme using the localized parameter values as initial values to obtain the absolute minimum residual solution. A detailed review of Tsai's Method is given in Appendix E, while the mathematics involved in the non-linear regression are given in Appendix F. The advantage of using this form of analysis is that it reduces by a significant factor the number of computer runs necessary to obtain a minimum residual solution. Tsai's Method has also been modified in terms of displaying the minimum residual solutions. Instead of examining only the 28 minimum residuals which correspond to 28 combinations of dip and slip angles, distributions of the minimum residual for each parameter over all the parameter combinations are displayed. Examples of these displays are given in the next four sections.

The need of an expanded use of the minimum residuals lies in the quality of the observed data. If the data quality is poor, knowledge of the distribution of the minimum residuals can help in making the decision of whether the absolute minimum residual is really the best parameter solution. In other words, the distribution of the minimum residual solutions should be used in making a choice between minimum residuals which have values close to each other. Also, if the use of the absolute minimum residual value of a parameter is difficult because of relatively flat distribution, then a corresponding degree of confidence should be expressed in that choice.

SECTION III

CORRELATION BETWEEN MINIMUM RESIDUAL SOLUTIONS AND SPECTRAL CHARACTERISTICS

Before we examine minimum residual solutions from data with varying degrees of control, we must first ask ourselves the meaning of the minimum residual solution. This section represents the beginning of a detailed study of the uniqueness or non-uniqueness of source parameters (particularly depth) determined from far-field surface wave data. We are approaching this analysis asking the following questions:

1) Since the minimum residual solution represents the closest match of spectral shape between the theoretical and observed spectra, what source parameter variation produces the greatest change in spectral shape?

2) Is there any readily observable spectral property which characterizes a source parameter's value, such as a spectral indicator for depth?

3) What property of the source description or of the layered half space that it is placed in affects spectral shape the most?

4) In applying a theoretical double couple source description to the observed data, we assume that the event is an earthquake. What if the data were really generated by an explosion?

In this section, we hope to supply answers to questions 1, 2, and 4, with question 3 the subject of future studies.

To address questions 1 and 2 spectra and radiation patterns were generated using a theoretical double couple point source placed in a Gutenburg plane layered half space (see Appendix F for the

theoretical formulation). Although we generated spectra and radiation patterns for many source parameter combinations, a representative set is displayed in Appendix G. From this set of figures, we can make the following observations:

- Depth variations can change spectral amplitudes of Rayleigh waves over three orders of magnitude, making this parameter, by far, the most sensitive to spectral variation (Figures G-1a, G-5a, G-6a). Love wave amplitude spectra have a smoother variation over two orders of magnitude (Figures G-1b, G-5b, G-6b). Dip variations can change spectral amplitudes of Rayleigh and Love waves about 1.5 and 1.0 orders of magnitude respectively (Figures G-2a, b, G-7a, b). Slip variations are about the same as that of the dip angle (Figures G-3a, b, G-8a, b), with strike variations, in some cases, very minimal (Figures G-4a, b, G-9a, b).

- For a vertical strike-slip fault, Rayleigh wave amplitude spectra exhibits a hole which changes frequency with depth (Figure G-7a). This hole, though, is greatly reduced for a less than perfect strike-slip fault (Figure G-5a), and completely vanishes for a dip-slip fault (Figure G-6a).

- Rayleigh spectral variations of slip for a vertical fault exhibits a common spectral point (Figure G-3a) which moves across the spectrum as depth varies (Figures not shown). This point vanishes, though, for non-vertical faults (Figure G-8a).

These observations from the amplitude spectra indicate that depth is the most sensitive parameter, but no one spectral indicator for depth is readily obvious.

Our analysis of question 4 yielded quite interesting results. Theoretical spectra for a 100 kiloton explosion in granite at shallow depth (3 km) was generated for Rayleigh waves using an approximation of the expression for a point explosive source derived by Harkrider (1964). It can be written as:

$$EXP_R(\omega) \doteq \left(\frac{2\pi}{r}\right)^{\frac{1}{2}} \cdot 4 \cdot \mu(h)\frac{\Psi(\infty)}{\omega}\ \epsilon_o(\omega)\, k_R^{\frac{1}{2}}\ A_R(\omega, h)$$

where:

- $EXP_R(\omega)$ - Spectral Amplitude of Rayleigh Wave
- $\mu(h)$ - Rigidity at depth
- ϵ_o - Ellipticity
- $\Psi(\infty)$ - Reduced displacement potential in the frequency domain; $\Psi(\infty) = \Psi_o(\infty)\ (\frac{W}{5})^{5/4}$ and W is yield in kilotons
- k_R - Wave number of Rayleigh wave
- $A_R(\omega, h)$ - Response of layered half space
- r - Distance (km)

Listed in Table III-1 are three cases where a double couple source was fitted using three different azimuthal configurations. The first two configurations are used in Sections IV and VI in actual cases, while the third could represent a possible future case. The optimal solution for each case is given in Table III-1, with residual distributions of the source parameters (see Appendix E for explanation) shown in Figures III-1, III-2, and III-3 for explosions 1, 2, and 3 respectively. If no prior knowledge of this event existed, we could assume an earthquake occurred at 15 km, with dip of 60^o, and slip of -30^o, except for the following:

- Examining the residual distributions, we see for cases 2 and 3 that optimal solutions exist at almost any strike direction, indicating a highly circular pattern. This is not

TABLE III-1

FITTING THEORETICAL EXPLOSION WITH
DOUBLE-COUPLED EARTHQUAKE MODEL

Case I. D.	Optimal Solution				
	Depth h km	Dip Angle δ^o	Slip Angle λ^o	Strike $N\phi^oE$	Moment 10^{25} dyne-cm
THEO/EXPLOSION/01	15	60	0	160	0.22 E00
THEO/EXPLOSION/02	15	60	-30	20	0.21 E00
THEO/EXPLOSION/03	15	60	-30	100	0.22 E00

THEO/EXPLOSION/01: 4-station-fit; 4 stations of LX/KIRSI/059
THEO/EXPLOSION/02: 12-station-fit; 12 stations of Mitchell's Southeastern Missouri Earthquake
THEO/EXPLOSION/03: 11-station-fit, 11 VLPE stations

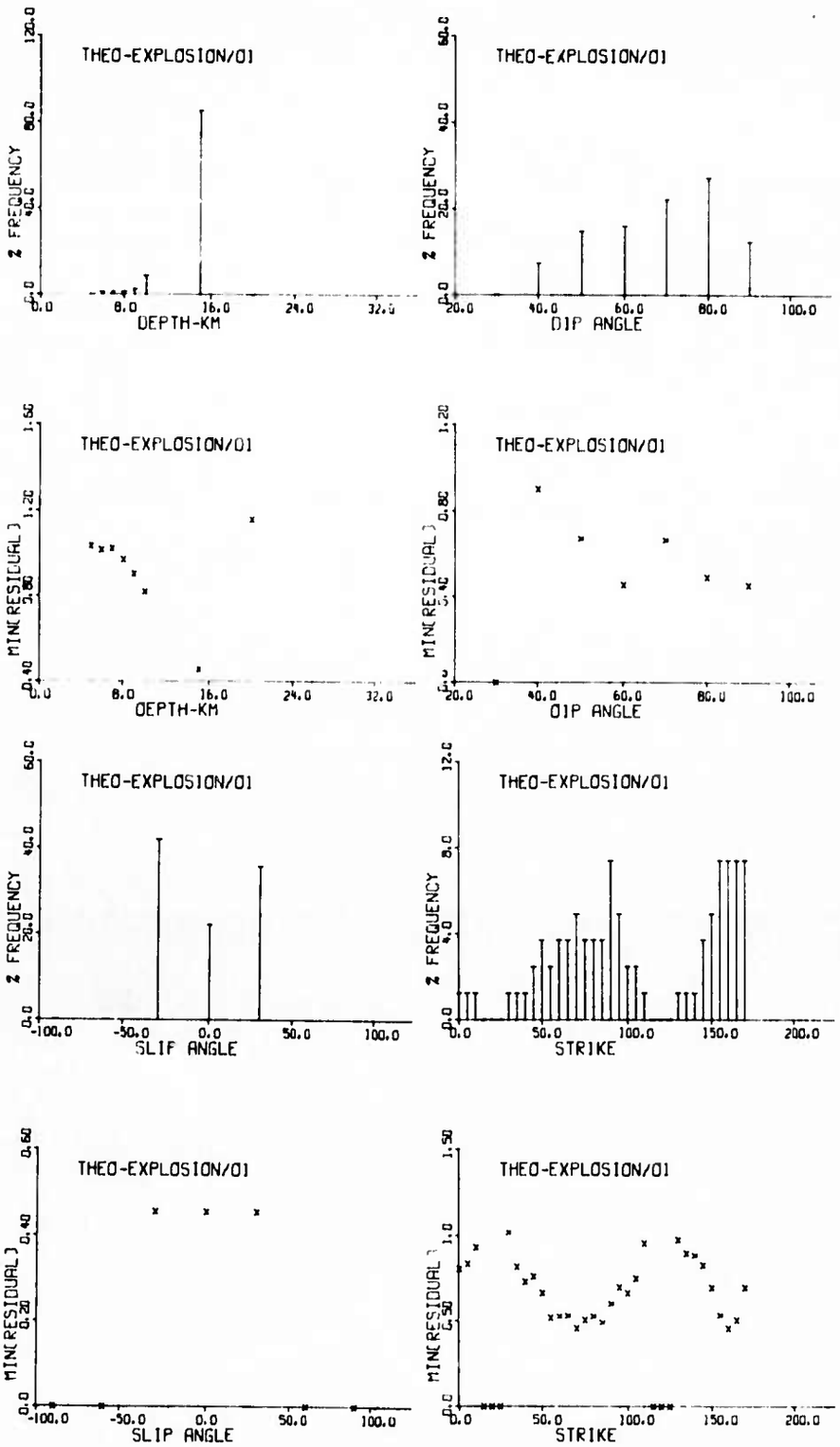

FIGURE III-1

RESIDUAL DISTRIBUTION FOR THEORETICAL EXPLOSION 1

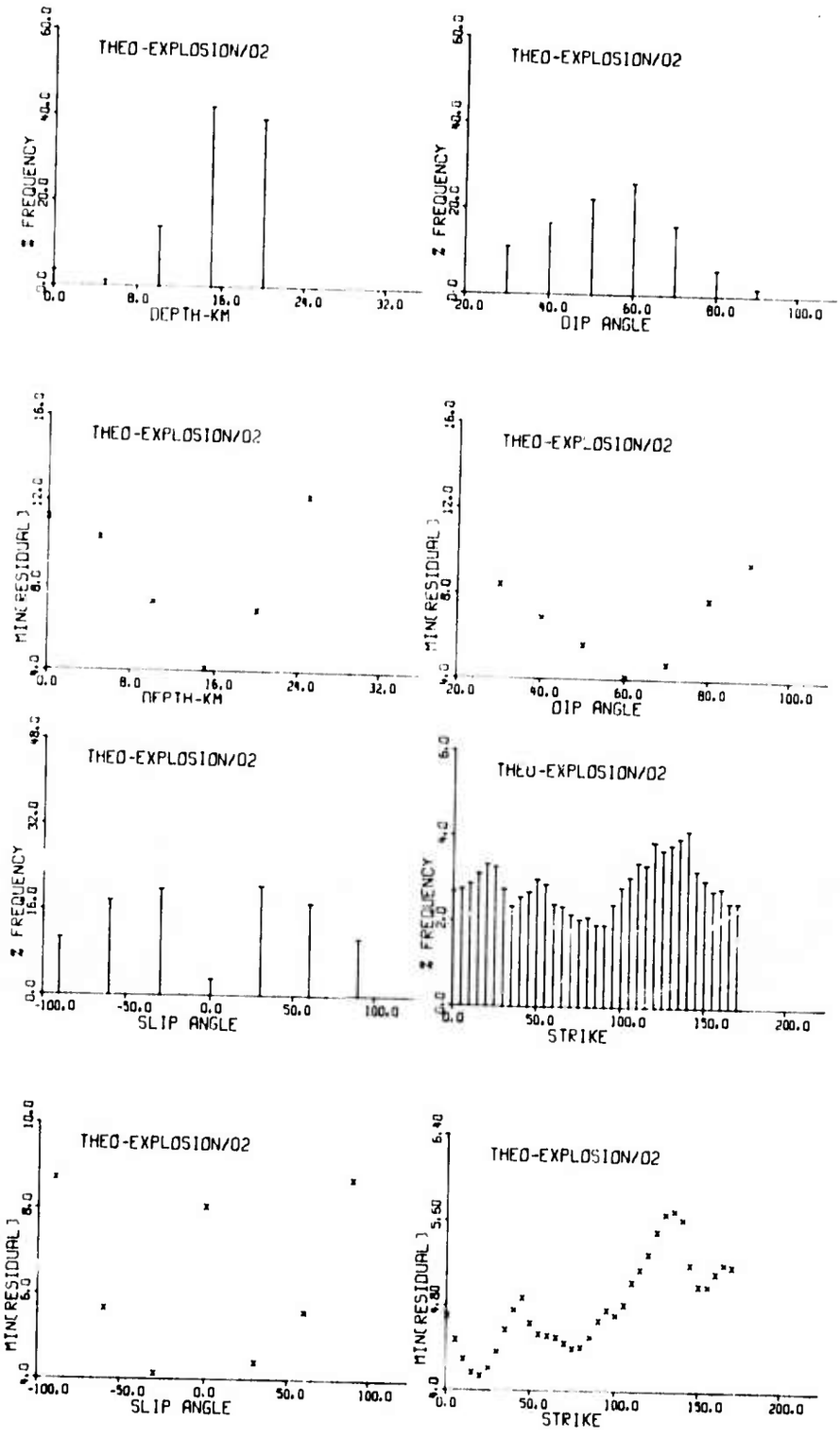

FIGURE III-2

RESIDUAL DISTRIBUTION FOR THEORETICAL EXPLOSION 2

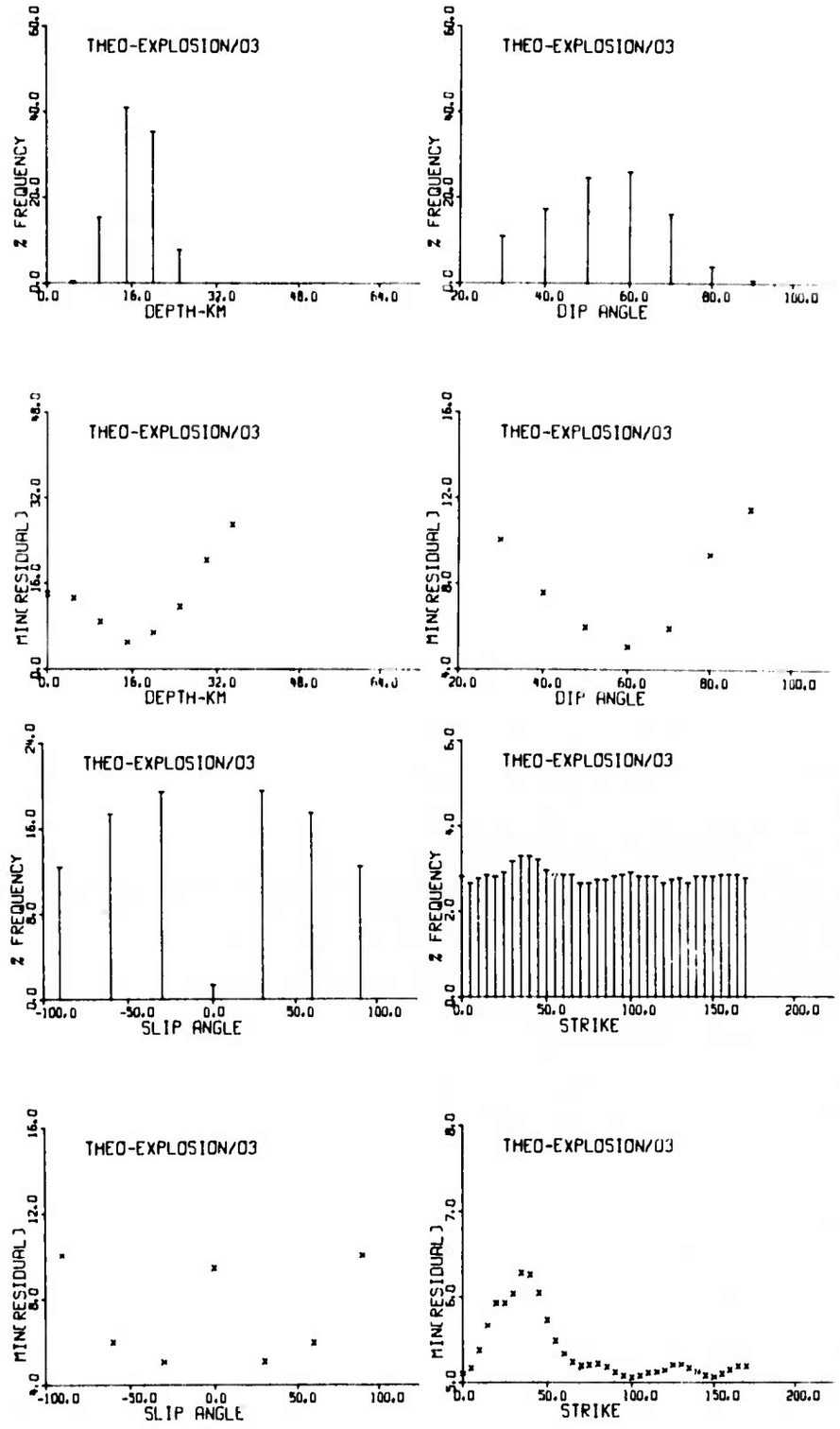

FIGURE III-3

RESIDUAL DISTRIBUTION FOR THEORETICAL EXPLOSION 3

true with case 1, where only four azimuths are used. With comprehensive azimuthal coverage, though, complete indeterminancy in the strike direction could indicate a source mismatch.

- Only Rayleigh waves have been used in the fitting procedure. Using these source parameters, we generated both Rayleigh and Love wave radiation patterns for a double couple source (Figures G-10a, b to G-14a, b) from 10 to 50 seconds. Examining the Rayleigh wave patterns, we see a progressive elimination of lobal configuration from 50 to 10 seconds, with the latter pattern being almost circular. At the same time, the Love wave patterns have sharply defined nodes.

- The circularity of the Rayleigh wave radiation pattern, though, is not enough to achieve a mis-identification; a match must also occur between the spectral shapes of the explosion and theoretical double couple. If we compare the spectra for an explosion at shallow depths (Figure III-4) with the Rayleigh wave spectra (Figure G-8a) which is approximately the same as our solution, we see that the shape is similar. In Figure III-5, a comparison of the exact spectral shapes of these two sources is shown in detail. The spectra from an explosion at or near the surface essentially averages the variation of the radiation patterns over the periods of interest. For an explosion at 4 km, this spectral averaging is not as good, and it becomes worse for deeper explosions. The uniqueness of this case becomes evident when one compares the spectral shapes of other double couple configurations where circular radiation patterns exist with shallow depth explosion spectra; the shapes are found to be quite different.

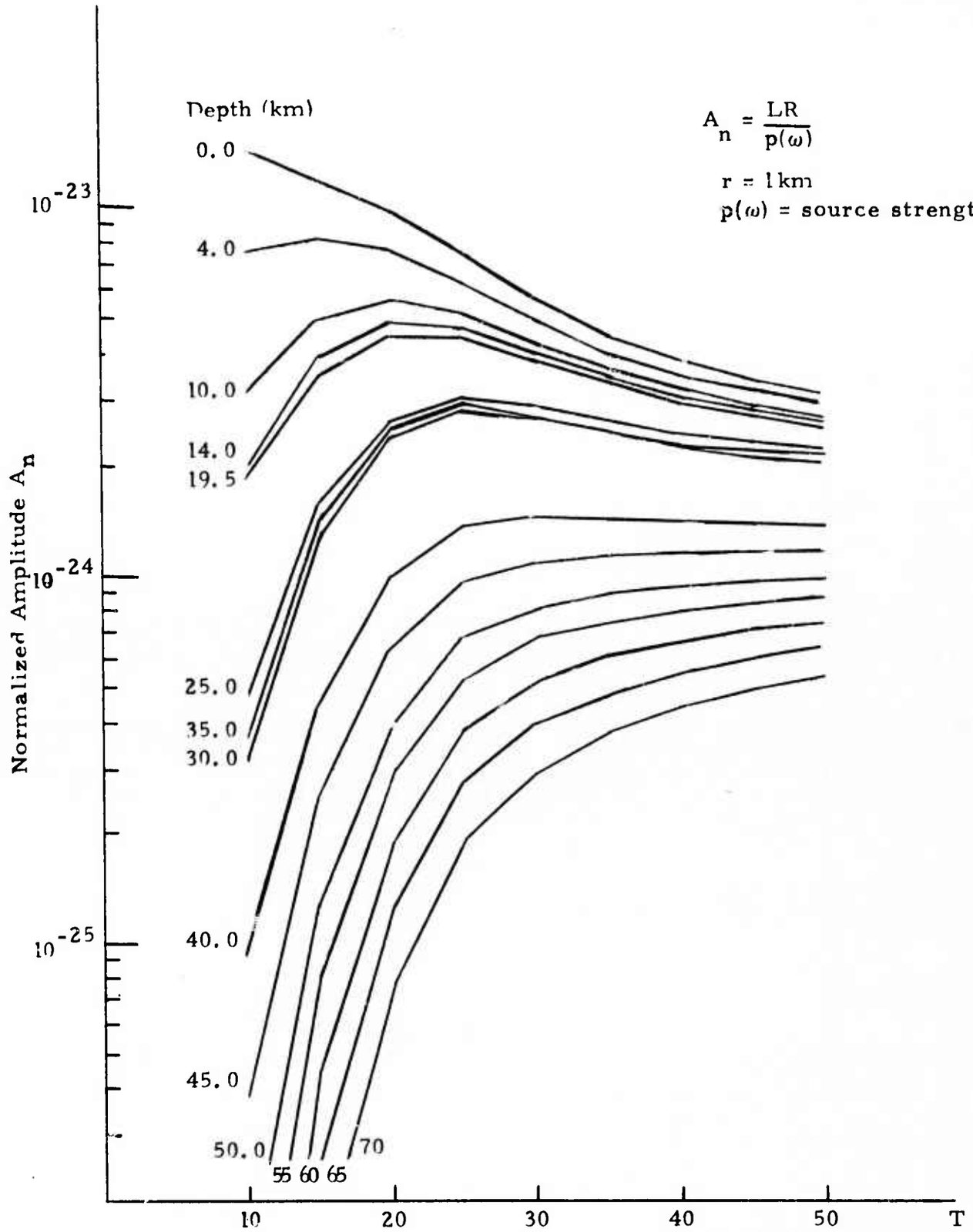

FIGURE III-4

THEORETICAL AMPLITUDE SPECTRA FOR EXPLOSIVE SOURCE

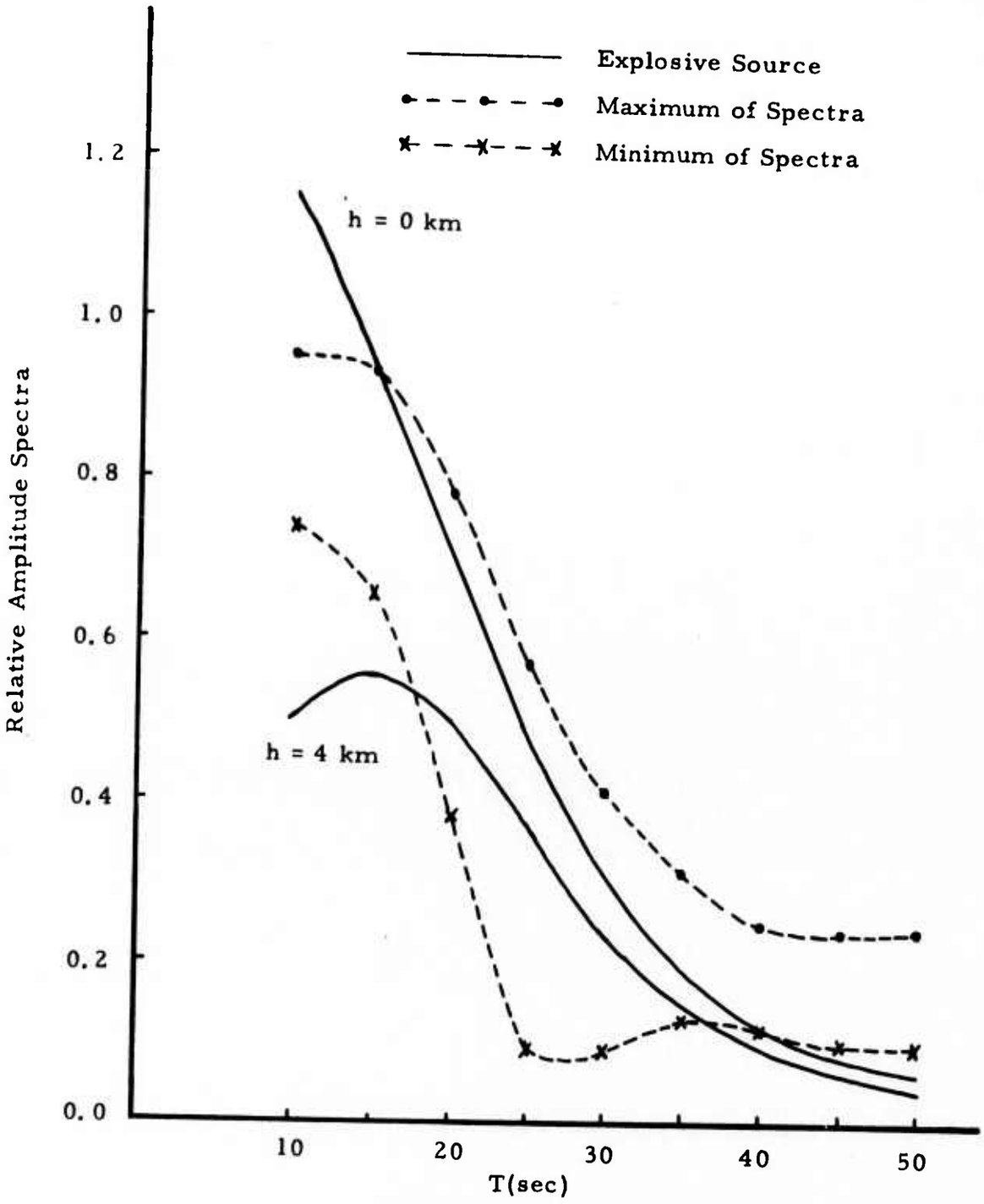

FIGURE III-5

COMPARISON OF EXPLOSIVE SOURCE SPECTRA AND A PARTICULAR DOUBLE COUPLE EARTHQUAKE SOURCE SPECTRA (h=15 km, $\delta = 60^{\circ}$, $\lambda = -30^{\circ}$)

Therefore, from the above points, we see that misidentification occurs only in a particular exceptional case, and with good azimuthal coverage, this situation can be clarified. In future studies, we will examine the problem of fitting an explosive source with an associated seismic relaxation using the same double couple source.

SECTION IV

ANALYSIS OF THE SOUTHEASTERN MISSOURI EARTHQUAKE OF OCTOBER 21, 1965

Because of the availability of high quality Rayleigh wave data for the Southeastern Missouri Earthquake of October 21, 1965 (m_b=5.2), a good opportunity existed for testing the methodology under highly controlled circumstances. In this way, we can determine what is possible when we analyze Eurasian events if we have extensive azimuthal coverage. The Rayleigh wave amplitude spectra for this event was obtained from Brian Mitchell (personal communication - 1973), having been already corrected for multipathing, higher modes, geometrical spreading, instrument response, and attenuation. Mitchell's attenuation correction is comparable with Tryggvason's (1965) for periods between 10 and 60 seconds (note discussion in Section VI). From the data, the amplitude spectra recorded at 19 observation stations were chosen for the source parameter study. The locations of these stations with respect to the epicenter are shown in Figure IV-1.

Using the modified Tsai's method (Appendix E) for residual distributions and the non-linear least squares method (Appendix F) to determine the absolute minimum residual solution, parameter estimates were obtained for several groupings of the stations. These solutions were obtained using a double couple point source placed in a layered half space which models the central United States (McEvilly, 1963). A velocity-density diagram of this structure is given in Figure D-3, with its Rayleigh and Love wave group velocities shown in Figures D-5 and D-6. The minimum residual statistics for the 12 stations east of the event are shown in Figures IV-2, with the solution deduced from the statistics given in Table IV-1. The optimal solution is (with Mitchell's solution in parenthesis):

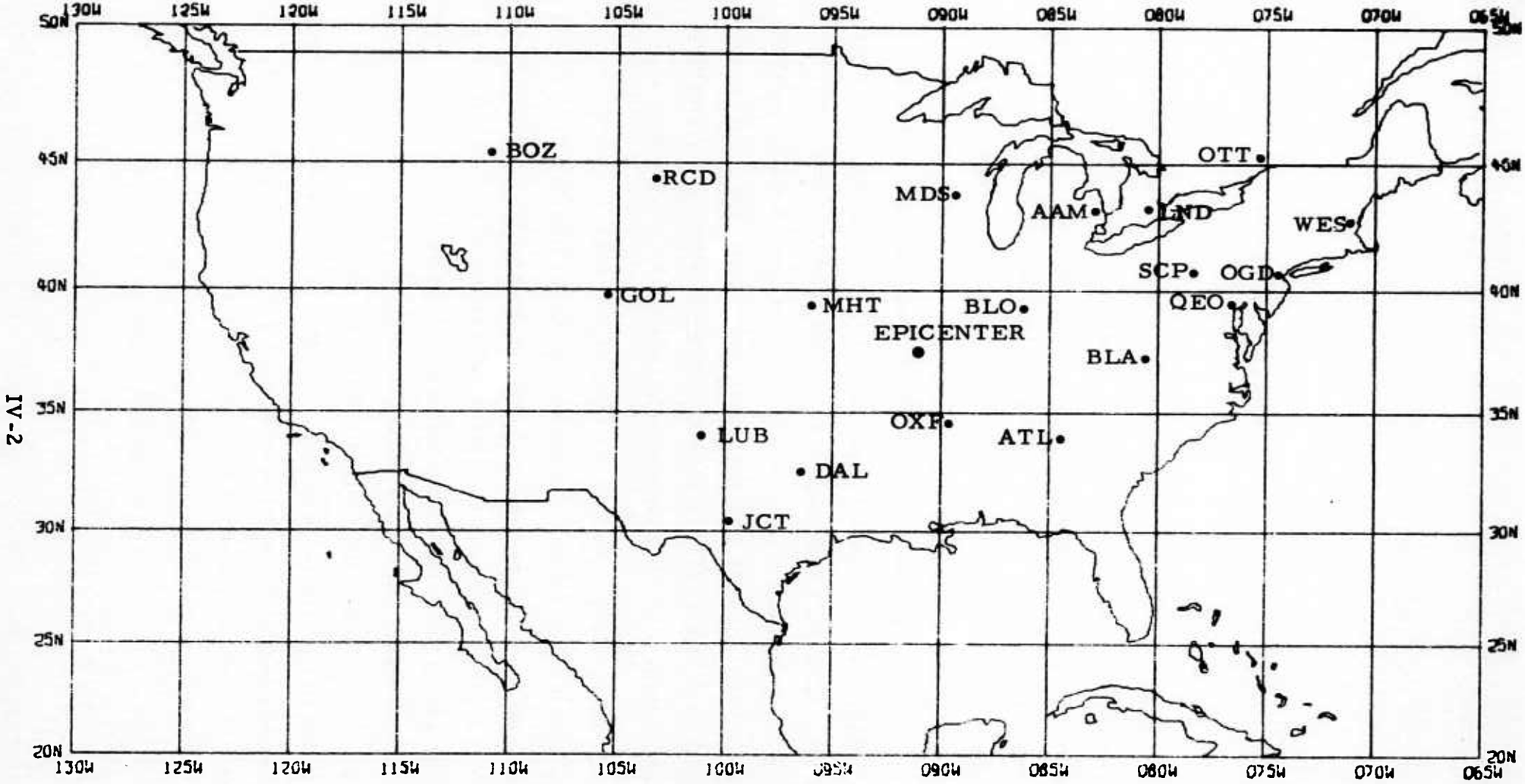

FIGURE IV-1

LOCATIONS OF THE SOUTHEASTERN MISSOURI EARTHQUAKE OF 21 OCTOBER 1965 AND WORLD WIDE NETWORK STATIONS

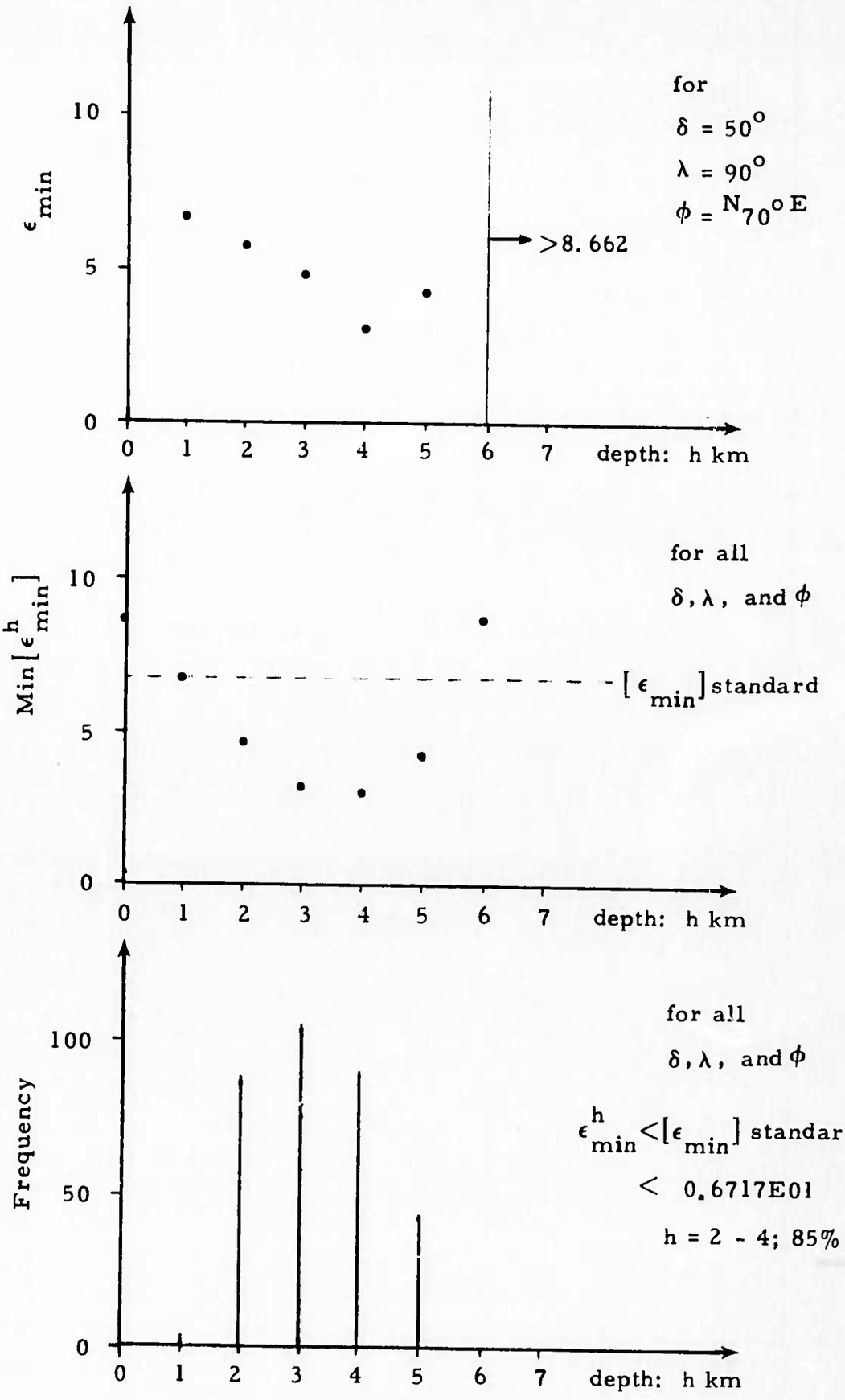

FIGURE IV-2a
VARIATION OF ϵ WITH RESPECT TO FOCAL DEPTH

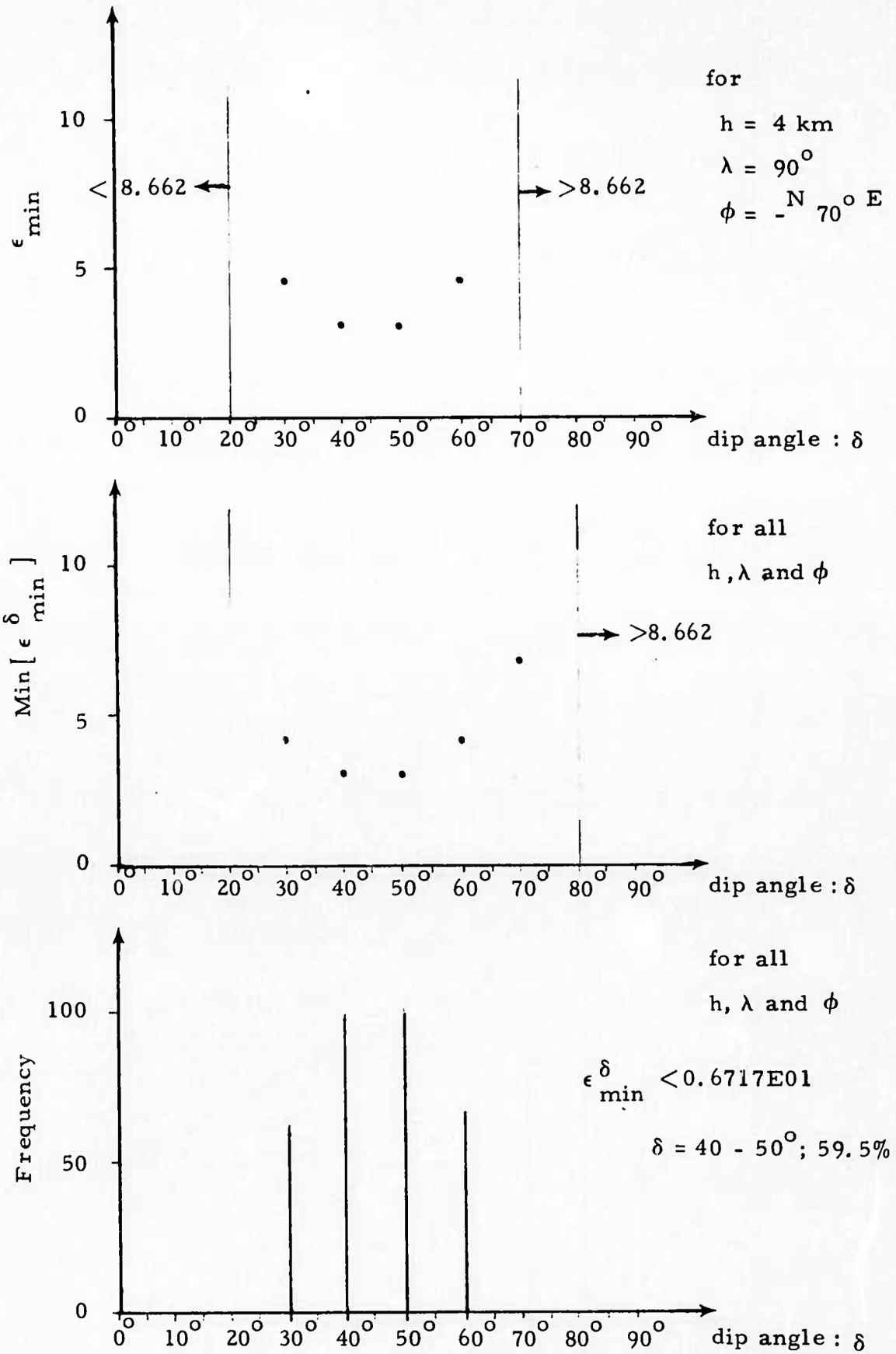

FIGURE IV-2b
VARIATION OF ϵ WITH RESPECT TO DIP ANGLE

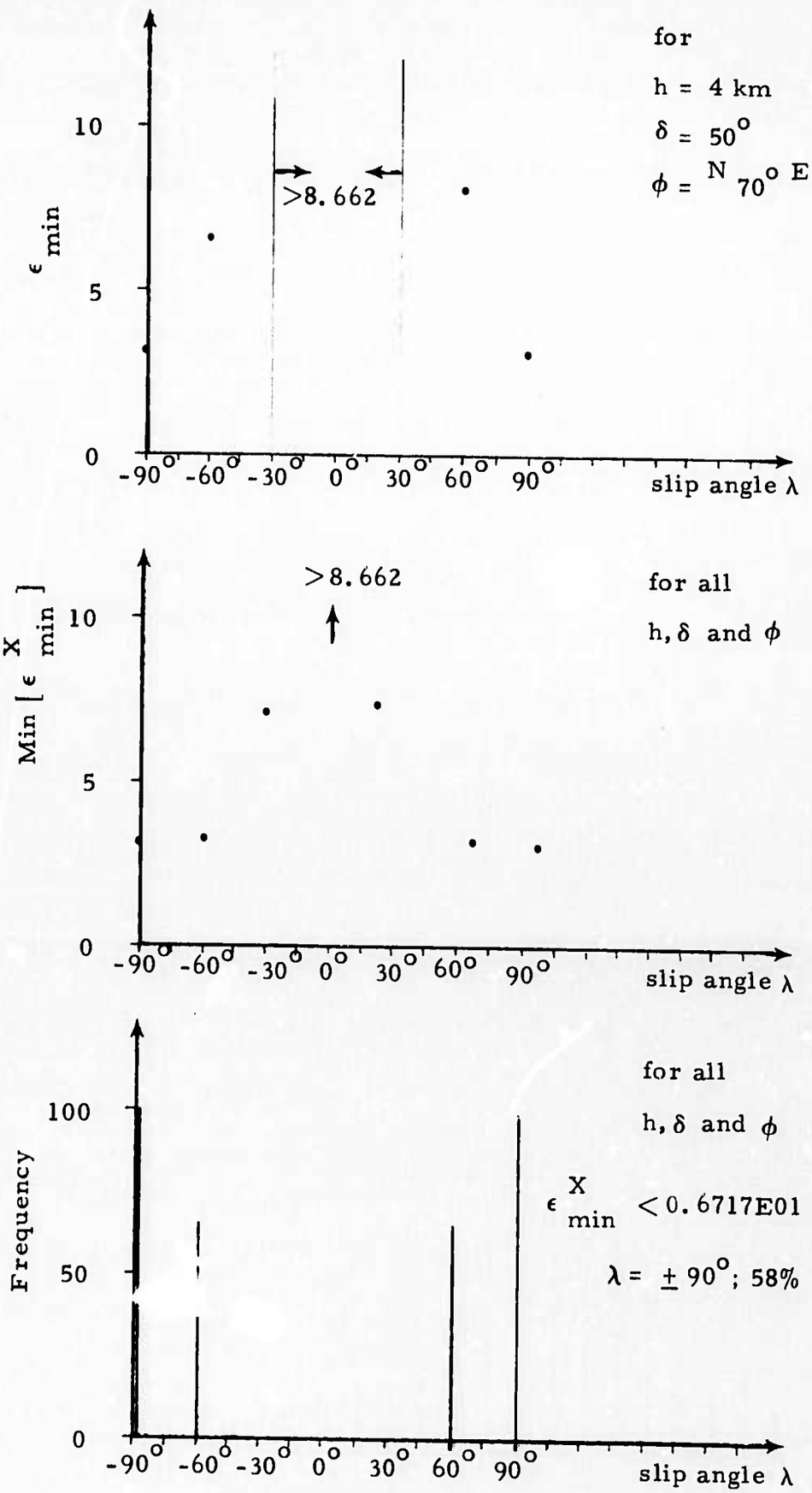

FIGURE IV-2c

VARIATION OF ε WITH RESPECT TO SLIP ANGLE

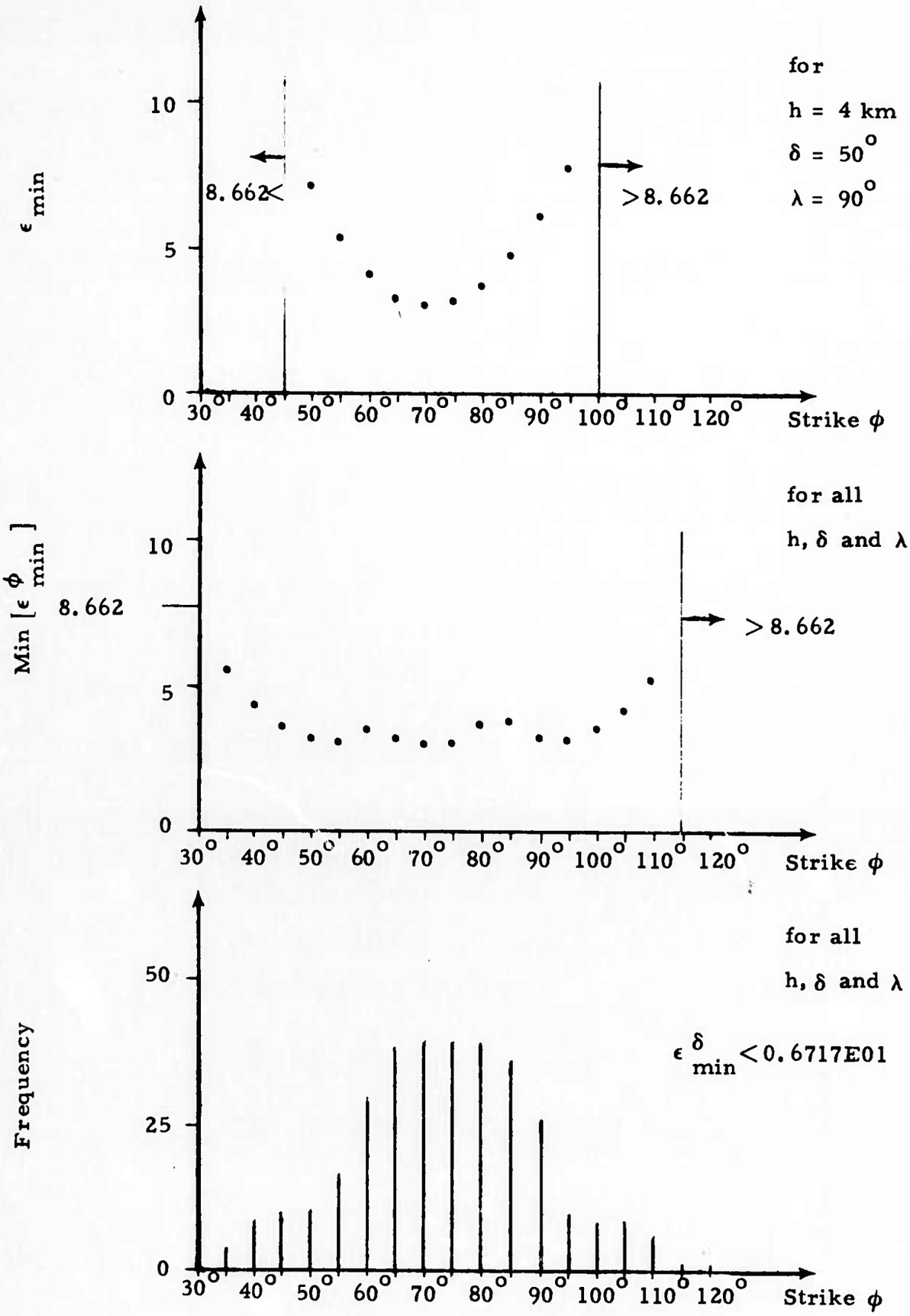

FIGURE IV-2d

VARIATION OF ϵ WITH RESPECT TO STRIKE

TABLE IV-1

SOUTHEASTERN MISSOURI EARTHQUAKE
ESTIMATION OF SEISMIC SOURCE PARAMETERS
BASED ON DISTRIBUTION-OF-MINIMUM-RESIDUAL CRITERION

Source Parameter	Probable Region	% Confidence
Focal Depth: h km	2-4	85
Dip Angle: δ^{o}	40-50	59.5
Slip Angle: λ^{o}	±90	58
Strike: $N\phi^{o}E$	60^{o}-90^{o}	75

Focal depth = 4 km	(4 km)
Dip Angle = 40° or 50°	(50°)
Slip Angle = $\pm 90^{\circ}$	($+85^{\circ}$ or $+95^{\circ}$)
Strike = $N70^{\circ}E$	($N\ 70^{\circ}E$)
Seismic Moment $\doteq 0.18 \times 10^{25}$ dyne·cm	(0.17×10^{25} dyne·cm)

We see that the solution obtained from modified Tsai's method and Mitchell's solution are in very close agreement. The distribution of minimum residuals gives us some idea of confidence regions for our parameter choices (Figures IV-2). For example, from Figure IV-2a, examination of the variation of the minimum residual with respect to depth yields the following results:

- Fixing the dip, slip, and strike at the optimal solution, variation over depth yields a minimum residual at 4 km.
- Varying all of the parameters, the minimum of the minimum residuals at each depth occurs at 4 km. A standard minimum residual is then chosen to determine the frequency solutions that occur at certain depths with minimum residuals below the standard value.
- As displayed in Figure IV-2a and listed in Table IV-1, 85 per cent of the models with minimum residuals less than the standard have depths between two and four kilometers.

As mentioned earlier, solutions were obtained for several combinations of stations. Figures IV-3 display spectra fit at six stations chosen at random. We see that the 19-station fit is almost identical to the 12-station fit. Because the amplitude of the theoretical double couple is symmetrical about 180°, the additional seven stations are not needed. Good coverage, such as this, in two successive quadrants, produce excellent results. Successive solutions were obtained by reducing the number of stations. The solution which used the fewest number of stations, and still

FIGURE IV- 3a

LR SPECTRAL AMPLITUDE:
SOUTHEASTERN MISSOURI EVENT (MITCHELL)

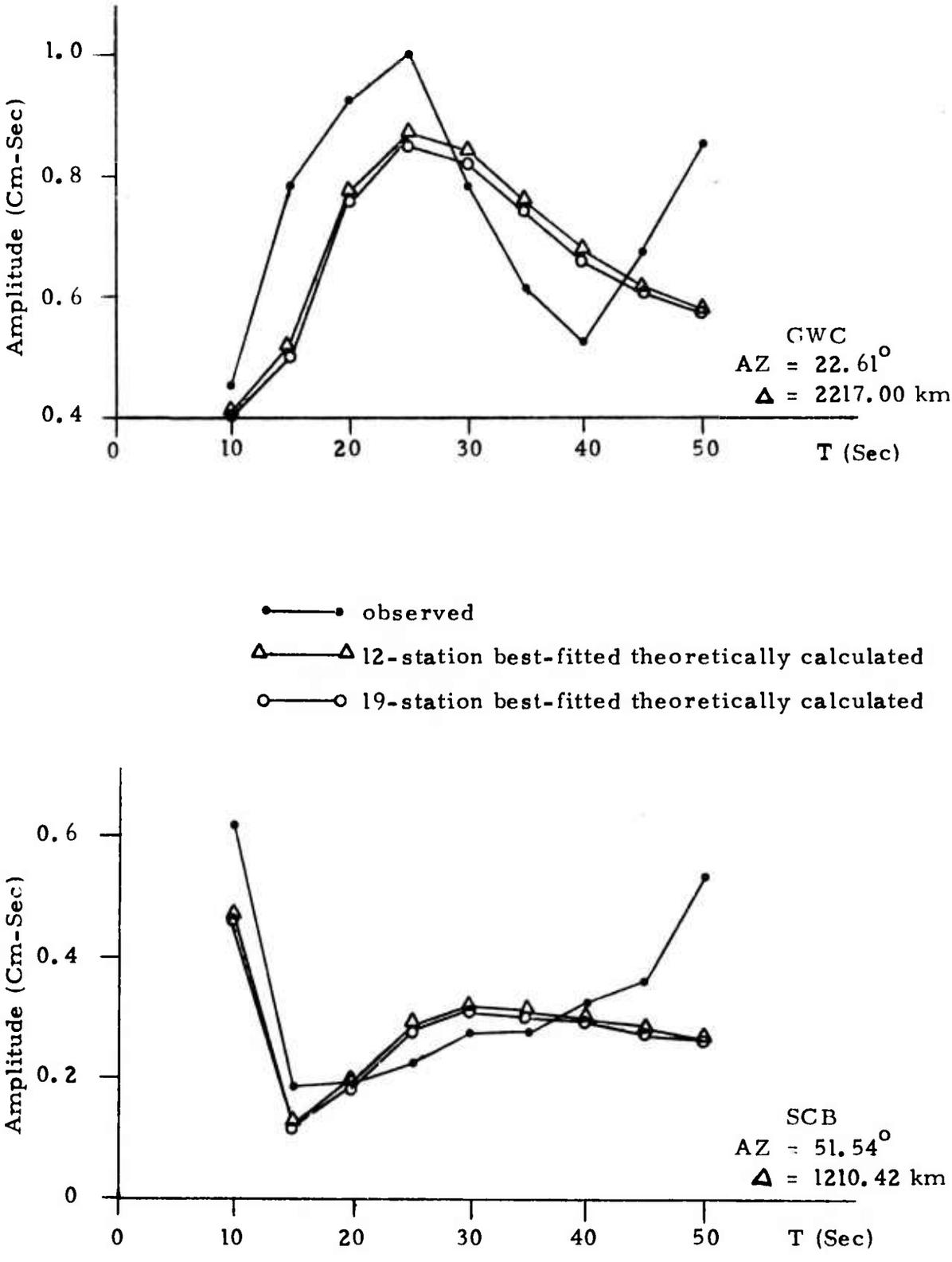

FIGURE IV-3b

LR SPECTRAL AMPLITUDE:
SOUTHEASTERN MISSOURI EVENT (MITCHELL)

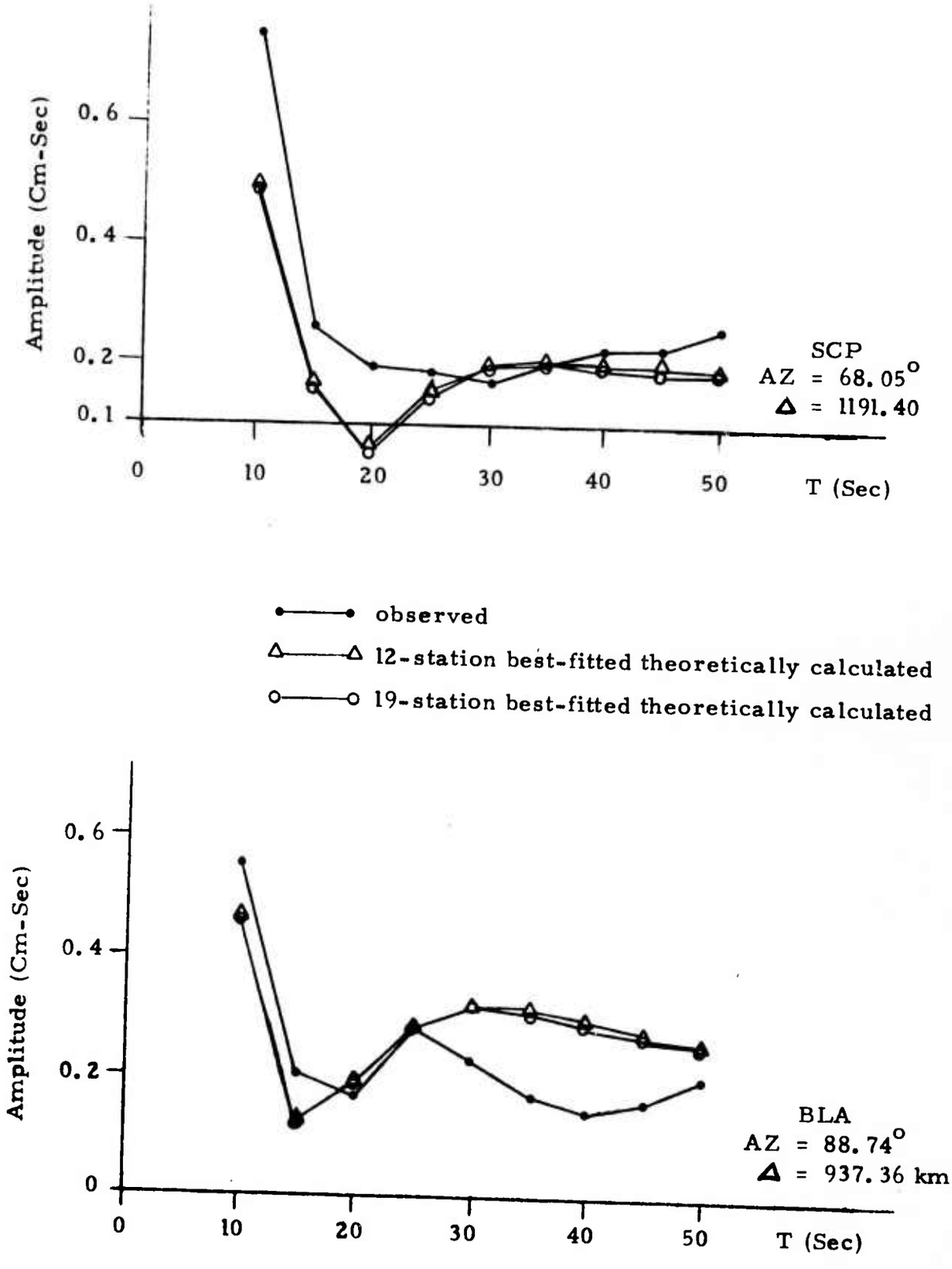

FIGURE IV- 3c

LR SPECTRAL AMPLITUDE:
SOUTHEASTERN MISSOURI EVENT (MITCHELL)

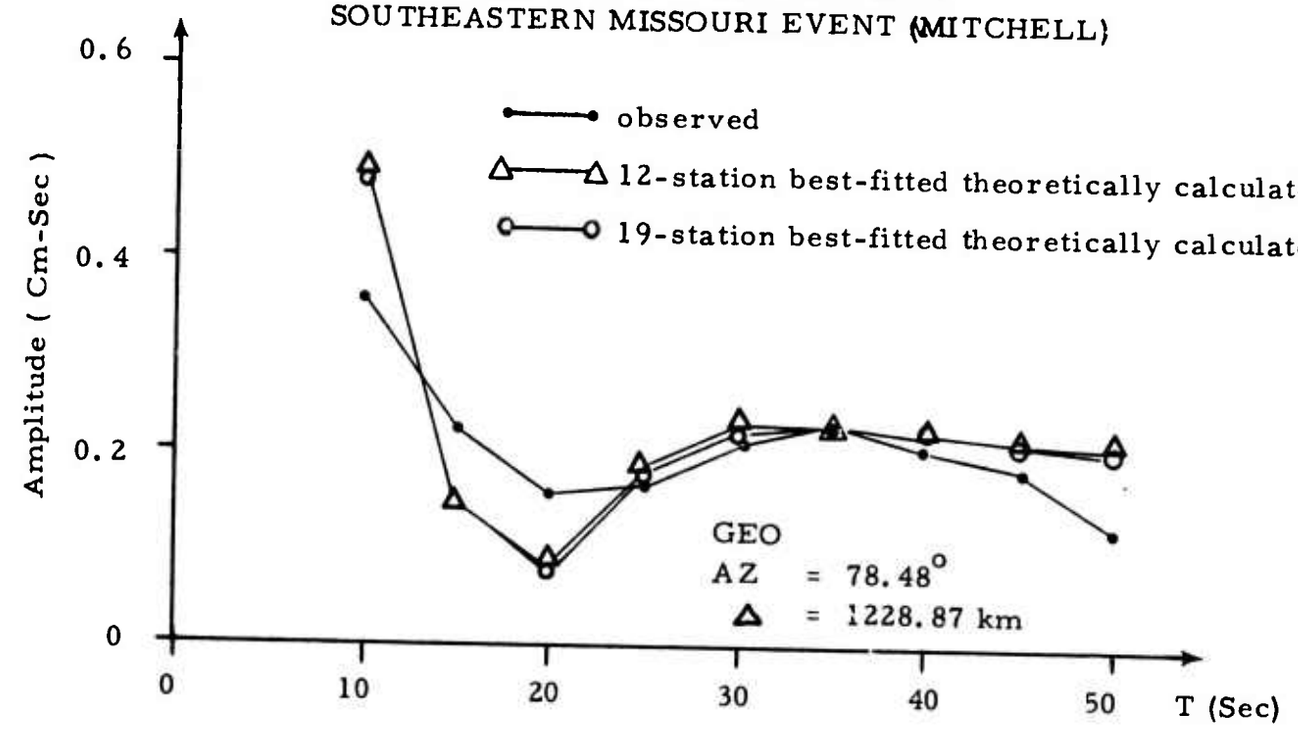

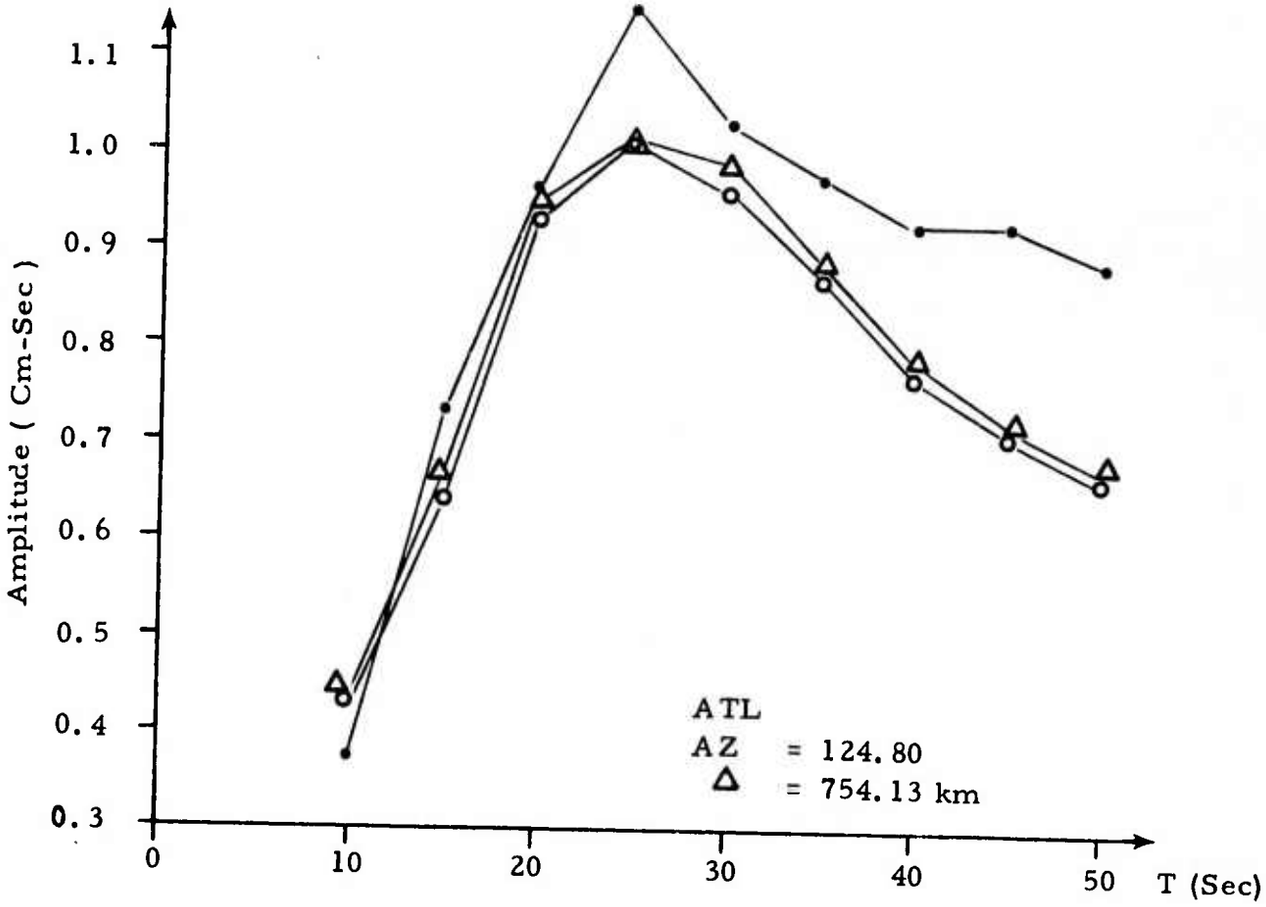

retained the same depth estimate, contained only one station in each of the eastern quadrants. These results indicate what is possible with high quality data.

Application of the non-linear regression analysis yielded the following solution:

Focal depth = 4.0 km

Dip Angle = 53.1°

Slip Angle = -79.7°

Strike = N80.4°E

Seismic Moment = 0.167×10^{25} dyne·cm
(m_b=5.4 using w^2-model [Tsai, 1972]).

This solution represents the absolute minimum residual fit. A radiation pattern plot for periods 10-50 seconds (ΔT = 5 seconds) is shown in Figures IV-4. The fits at T=25, 30, and 35 seconds are especially close.

The consistency of the depth estimate using the previous techniques is quite encouraging. Mitchell (1973), using the same data in conjunction with a trial-and-error technique guided by partial derivatives of the source parameters, obtained very much the same result. Using body wave data, Kisslinger and Nultti (1965) obtained depths of $\leq$6 km.

Before we proceed to data with less control, we should examine the effect that the layered-half space velocity structure has on the parameter estimates. As stated earlier, the solutions for this event have been obtained using the Central United States model. Three other plane layered models, namely Gutenberg-Bullen, Tibet Plateau, and Hamilton-Healy, were used in processing the same data. The velocity structure and group velocity curves for these models is given in Appendix D. All four earth models are for continental areas, with the main differences in the upper crust. Source parameter estimates using these four models are listed in Table IV-2.

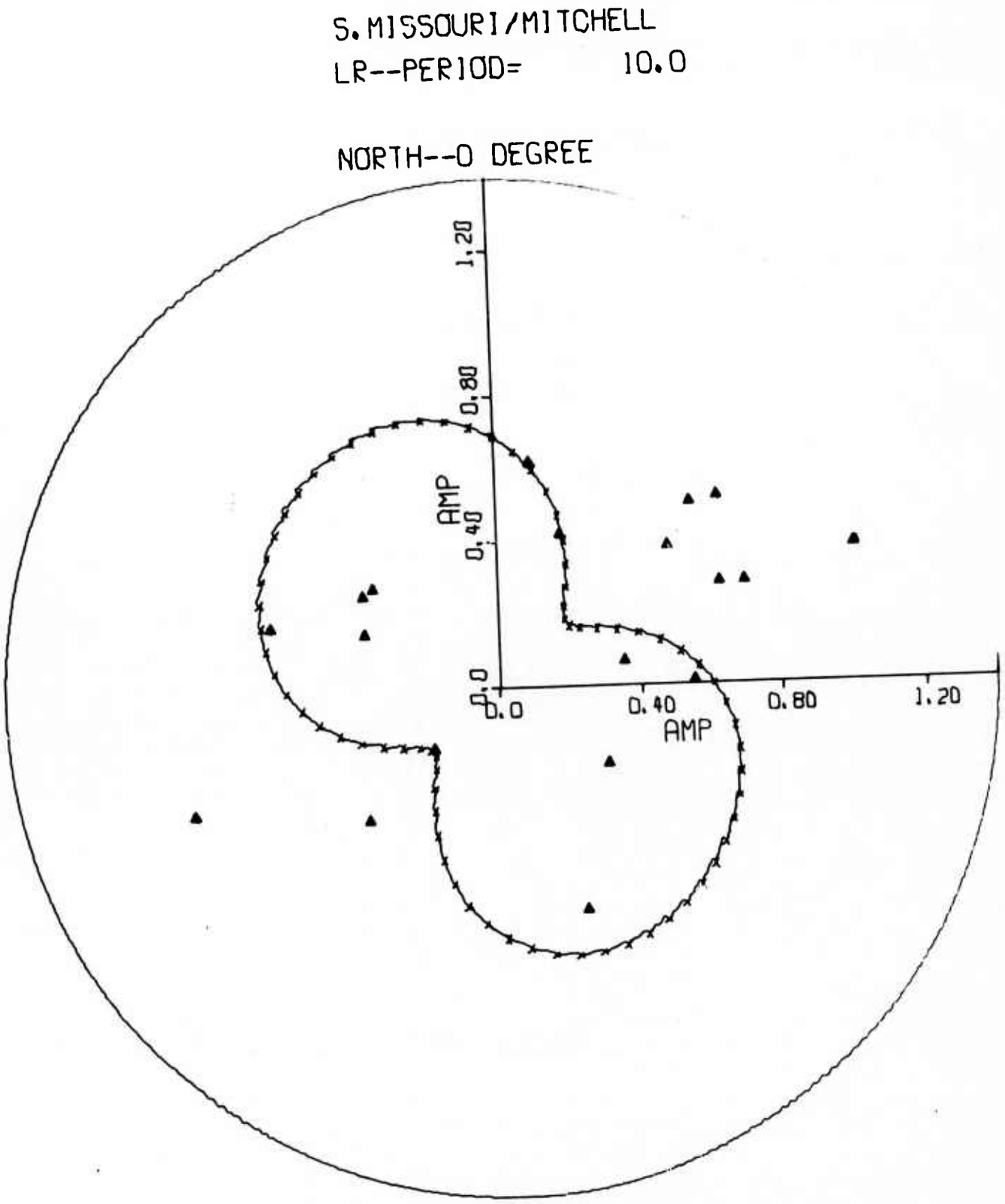

FIGURE IV-4a

RADIATION PATTERNS OBTAINED USING NON-LINEAR REGRESSION--
THE SOUTHEASTERN MISSOURI EARTHQUAKE OF OCTOBER 21, 1965

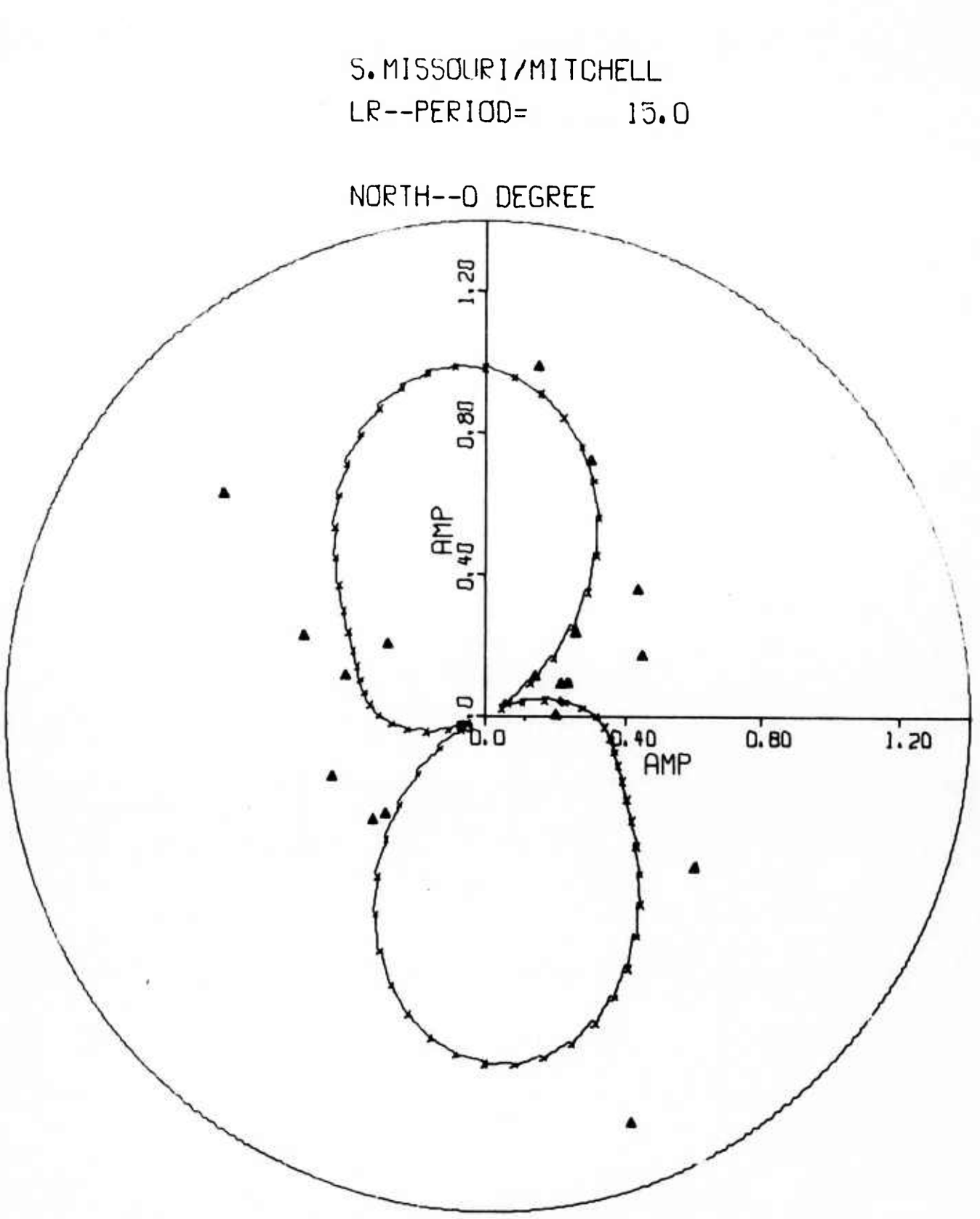

FIGURE IV-4b
RADIATION PATTERNS OBTAINED USING NON-LINEAR REGRESSION--
THE SOUTHEASTERN MISSOURI EARTHQUAKE OF OCTOBER 21, 1965

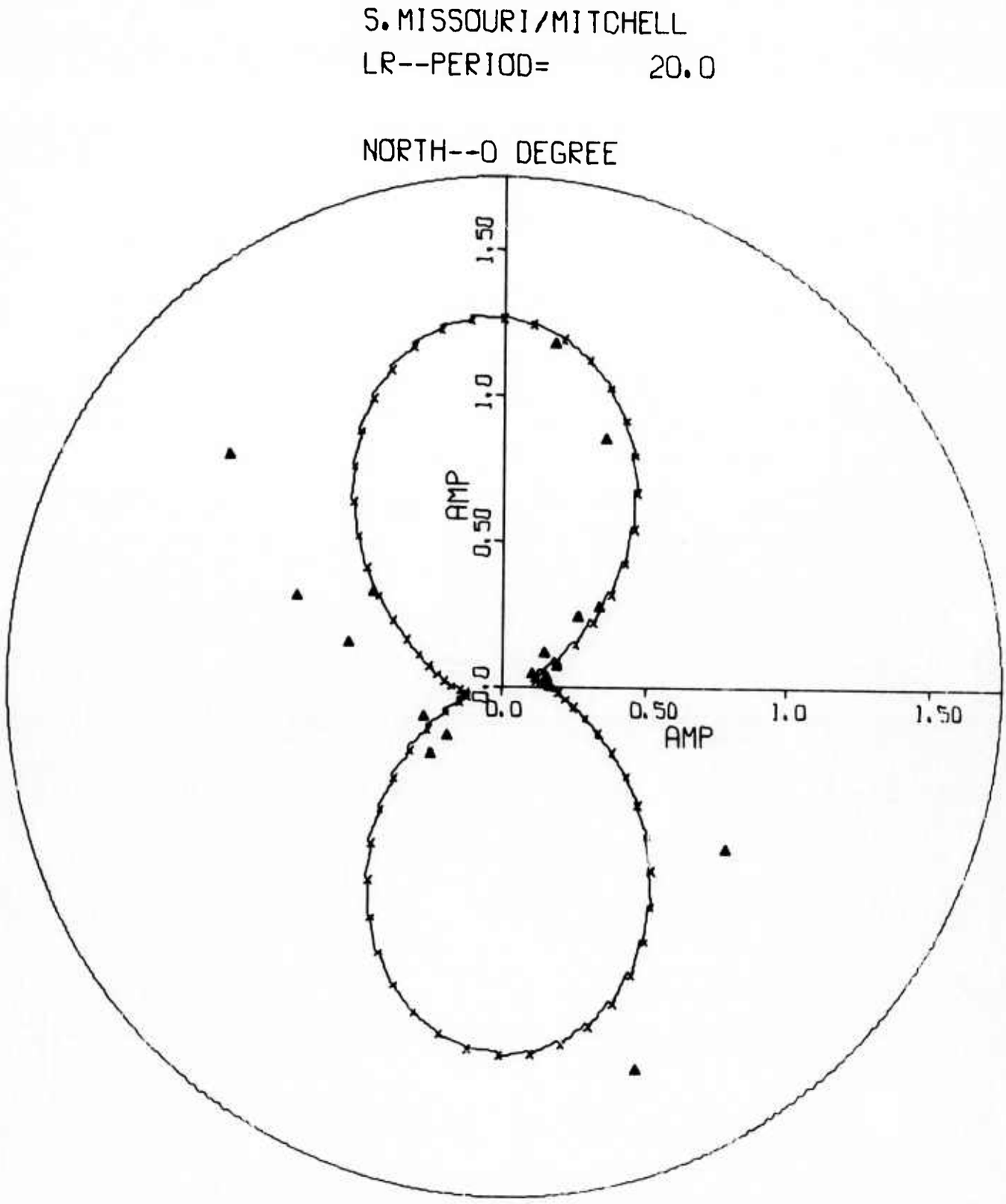

FIGURE IV-4c

RADIATION PATTERNS OBTAINED USING NON-LINEAR REGRESSION--
THE SOUTHEASTERN MISSOURI EARTHQUAKE OF OCTOBER 21, 1965

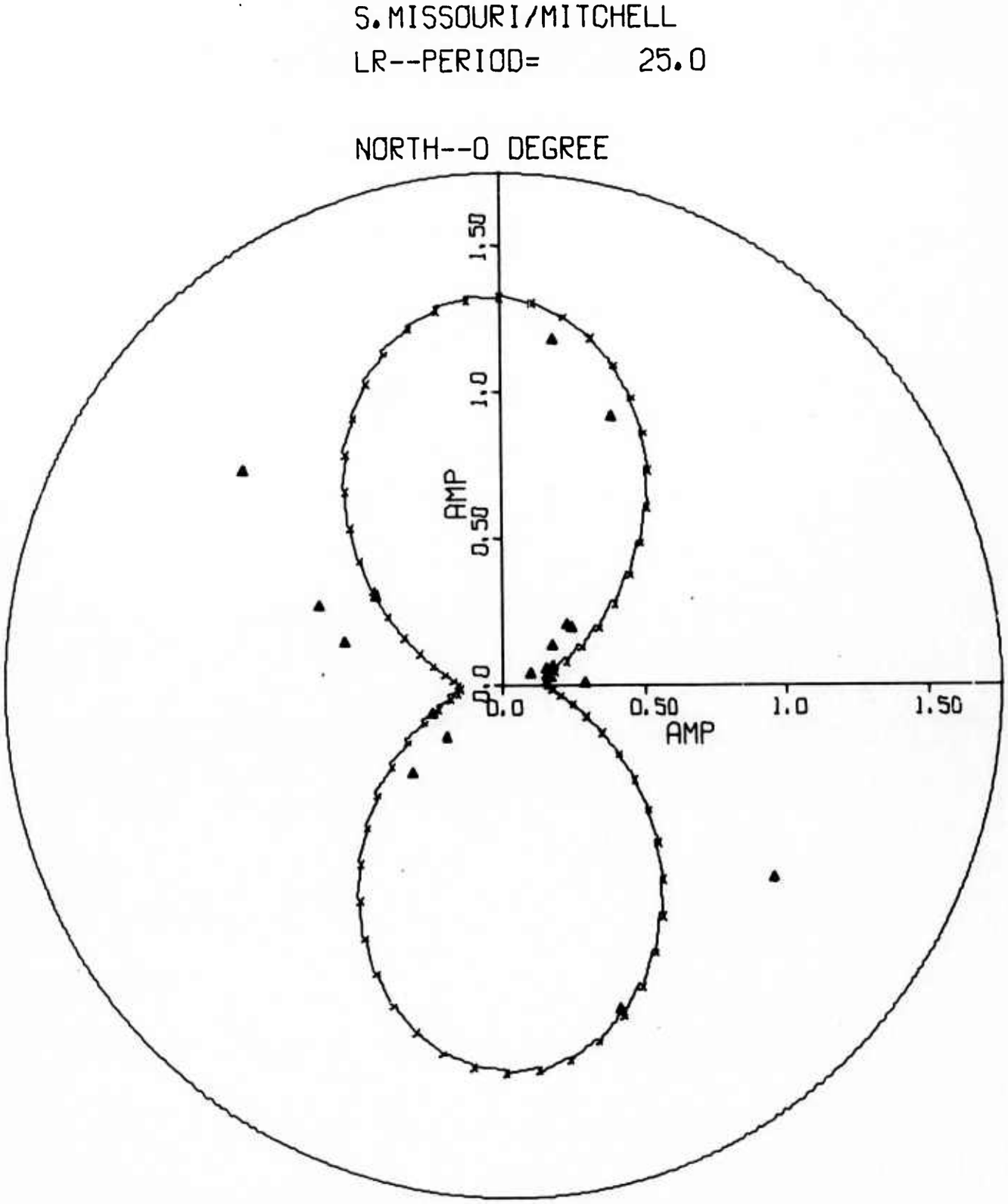

FIGURE IV-4d

RADIATION PATTERNS OBTAINED USING NON-LINEAR REGRESSION--
THE SOUTHEASTERN MISSOURI EARTHQUAKE OF OCTOBER 21, 1965

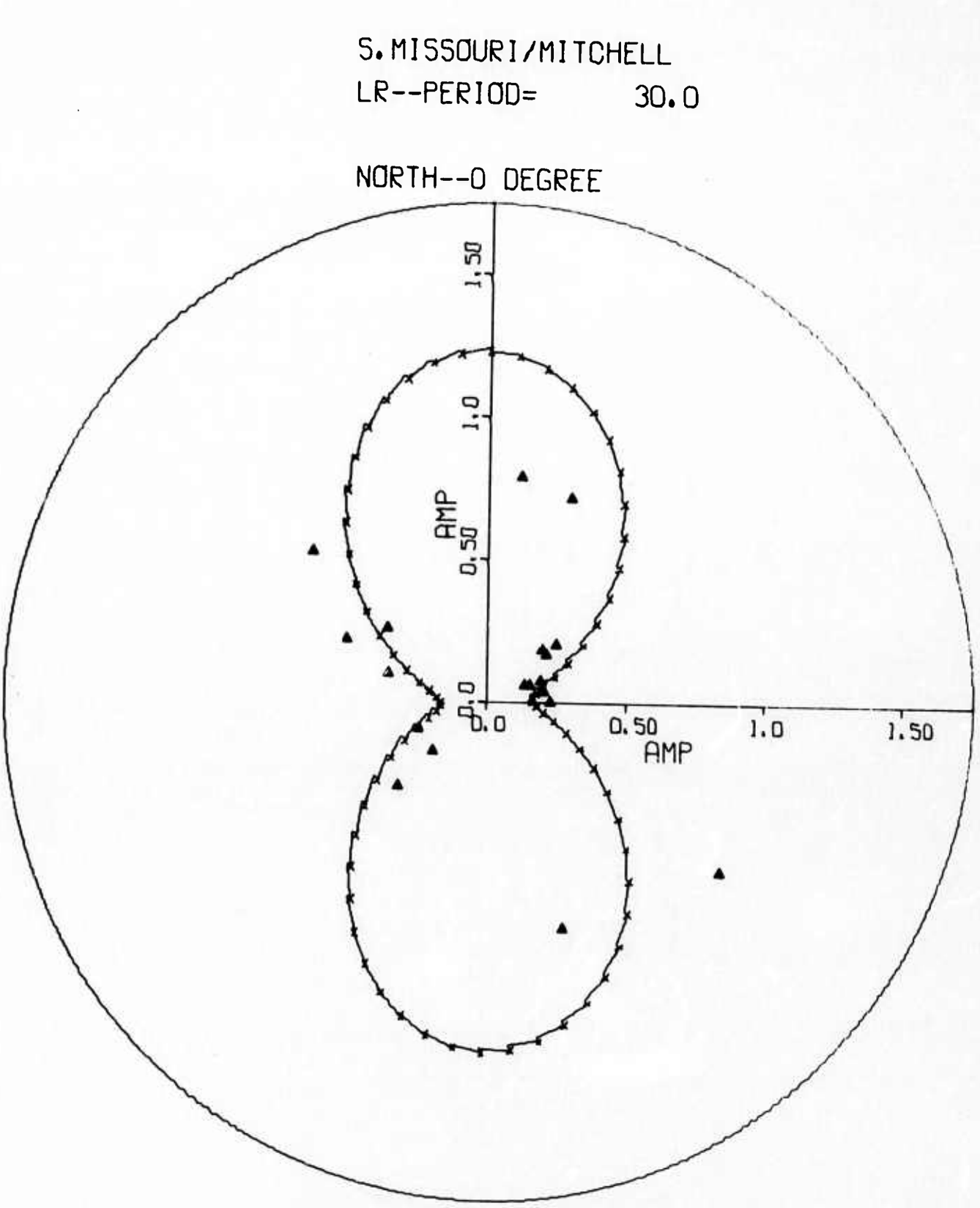

FIGURE IV-4e

RADIATION PATTERNS OBTAINED USING NON-LINEAR REGRESSION--
THE SOUTHEASTERN MISSOURI EARTHQUAKE OF OCTOBER 21, 1965

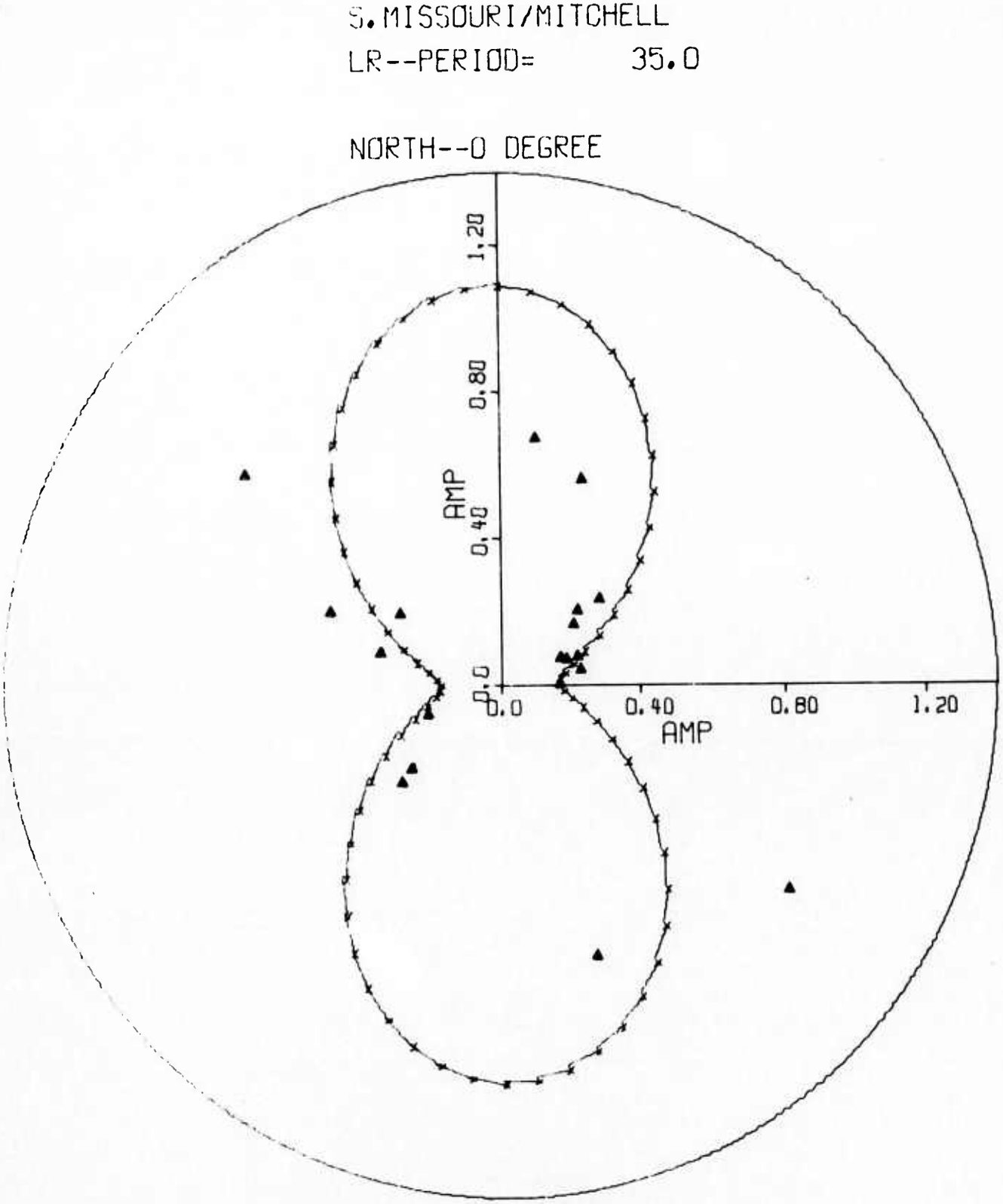

FIGURE IV-4f

RADIATION PATTERNS OBTAINED USING NON-LINEAR REGRESSION--
THE SOUTHEASTERN MISSOURI EARTHQUAKE OF OCTOBER 21, 1965

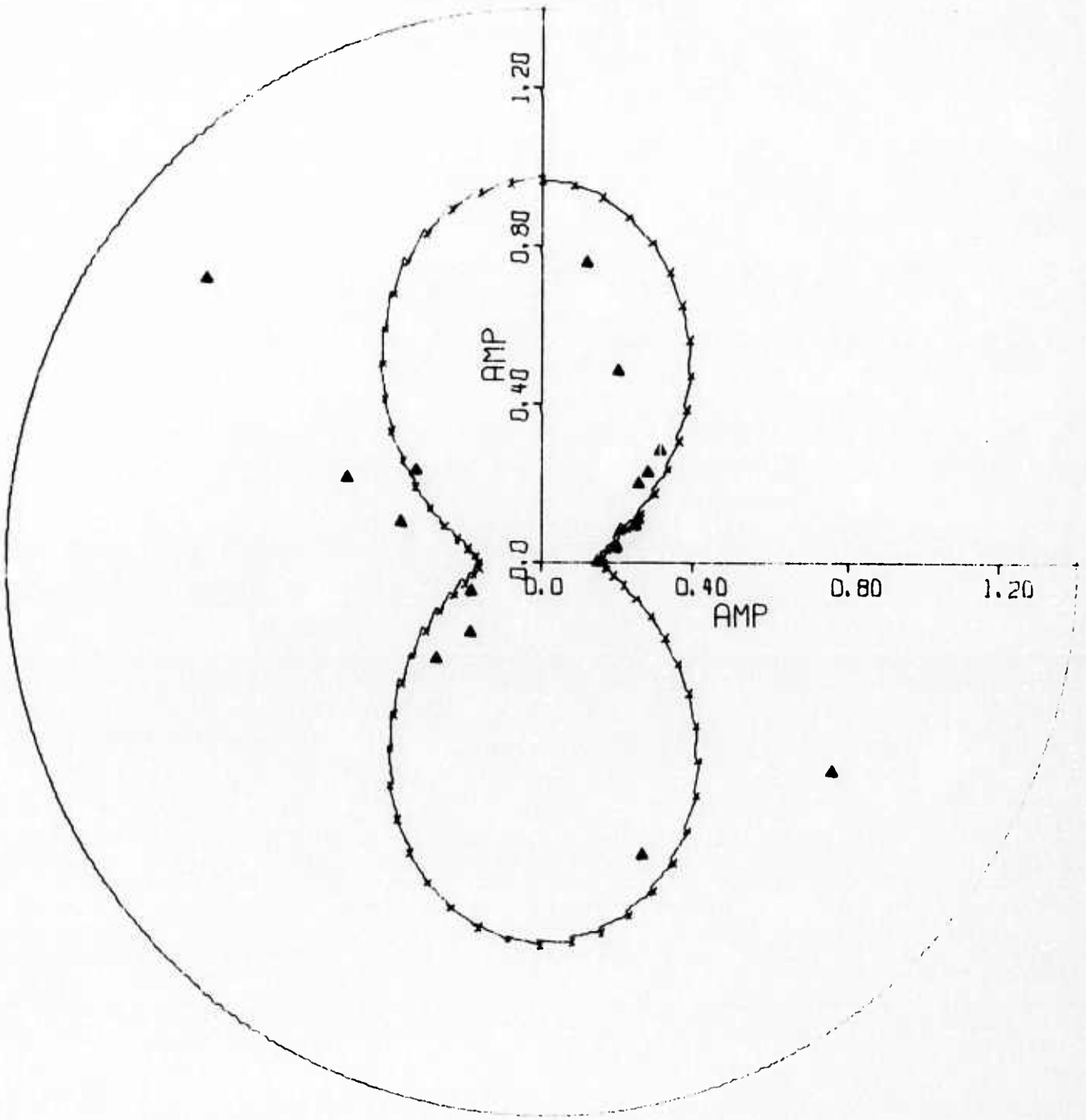

FIGURE IV-4g

RADIATION PATTERNS OBTAINED USING NON-LINEAR REGRESSION--
THE SOUTHEASTERN MISSOURI EARTHQUAKE OF OCTOBER 21, 1965

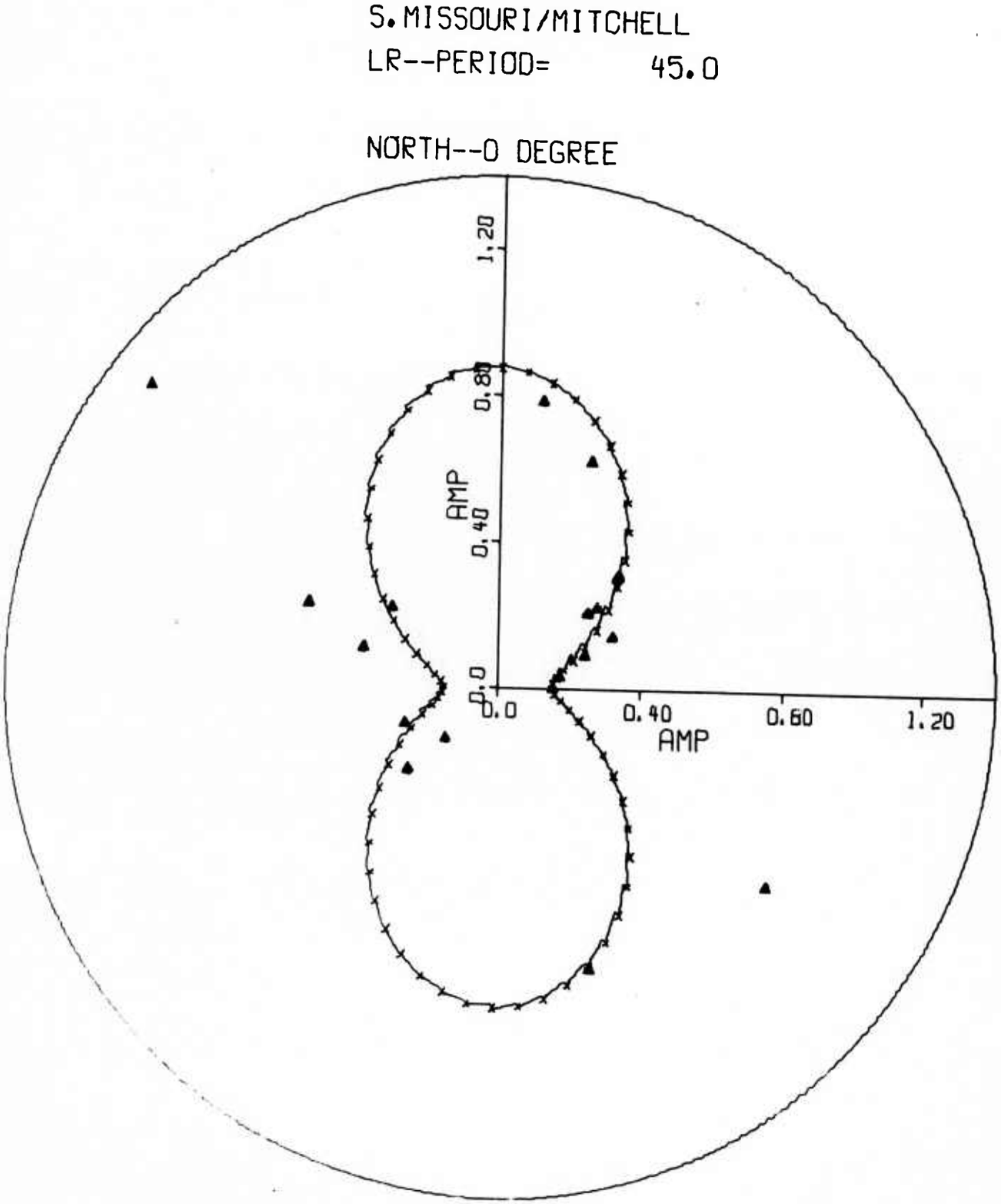

FIGURE IV-4h

RADIATION PATTERNS OBTAINED USING NON-LINEAR REGRESSION--
THE SOUTHEASTERN MISSOURI EARTHQUAKE OF OCTOBER 21, 1965

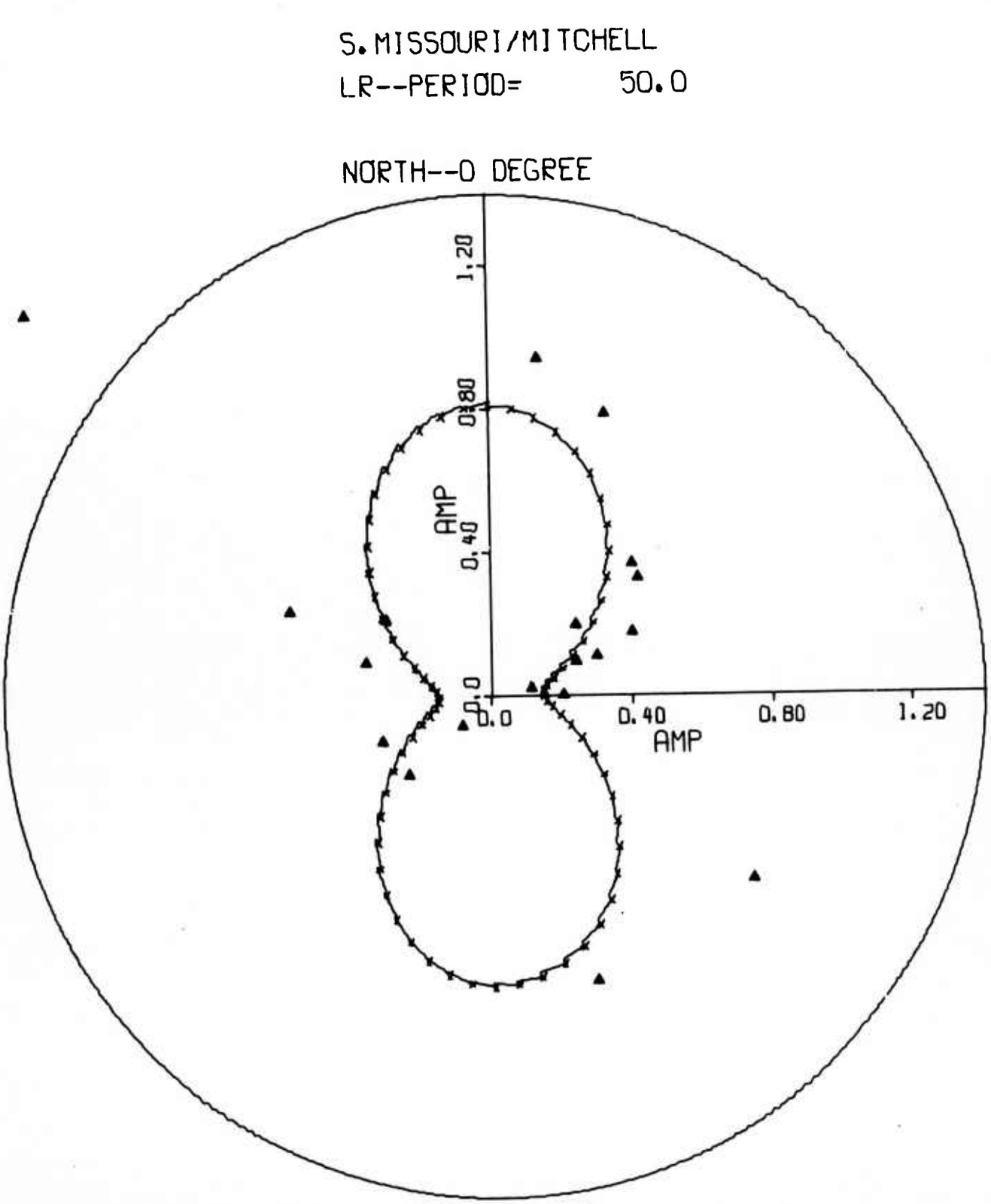

FIGURE IV-4i

RADIATION PATTERNS OBTAINED USING NON-LINEAR REGRESSION--
THE SOUTHEASTERN MISSOURI EARTHQUAKE OF OCTOBER 21, 1965

TABLE IV-2

SOUTHEASTERN MISSOURI EARTHQUAKE
VARIATION OF SEISMIC SOURCE PARAMETER
ESTIMATION WITH RESPECT TO DIFFERENT EARTH MODELS

Earth Model	Source Parameter Estimation				
	Focal Depth h km	Dip Angle δ^{o}	Slip Angle λ^{o}	Strike $N\phi^{o}E$	Moment M dyn cm
Central U. S.	4	40 50	$\pm 90^{o}$	70	0.18
56km-Tibet Plateau	3	40	-60^{o}	55	0.12
Gutenberg	4	40 50	$\pm 90^{o}$	110	0.18
Hamilton-Healy	5	40 50	$\pm 90^{o}$	70	0.13

From these results, one comes to the conclusion that structure has little effect on the depth estimate. This result is quite puzzling. The large differences between the Tibet Plateau high velocity crust and the Hamilton-Healy sedimentary crust yield only a 2 km change in the depth estimate. Future studies will examine the effect layer parameters have on depth estimation.

SECTION V

ANALYSIS OF TWO, LOW MAGNITUDE ITALIAN EVENTS

In the analysis of the Southeastern Missouri Earthquake, we were able to obtain a depth estimate, using only two stations in consecutive quadrants, which was consistent with the depth estimate obtained using 12 stations. Since this situation (a paucity of stations) usually is present in the analysis of Eurasian data, examination of just such a problem was undertaken where some control of the source parameters was available.

Two low magnitude ($m_b \doteq 4.1$) events occurred off the east coast of Italy (Figure V-1), approximately one day apart (Table V-2), and were recorded by three VLPE stations (Table V-3). Our control of the source parameters lie in the body wave solution of an event in the same tectonic region (McKenzie, 1972) along the Italian east coast (Figure V-2). The crust structure for the source region, obtained from Closs (1969), is shown in Table V-1.

Corrections from the source to the three common VLPE sites were applied using Tsai's attenuation correction (1972) for the all paths; to TLO, OGD, and KON. A series of narrow band filters were applied to the waveforms to determine if multipathing was present (see Appendix B for method), and very little was found.

Because of the uneven quality of the data, we only applied the modified Tsai's method, with the accuracy furnished by the residual distributions thought to be sufficient. The minimum residual statistics are shown in Figures V-2 for CITLY/134, and in Figures V-4 for CITLY/143 using all three VLPE stations. A summary of these statistics is given in Table V-4.

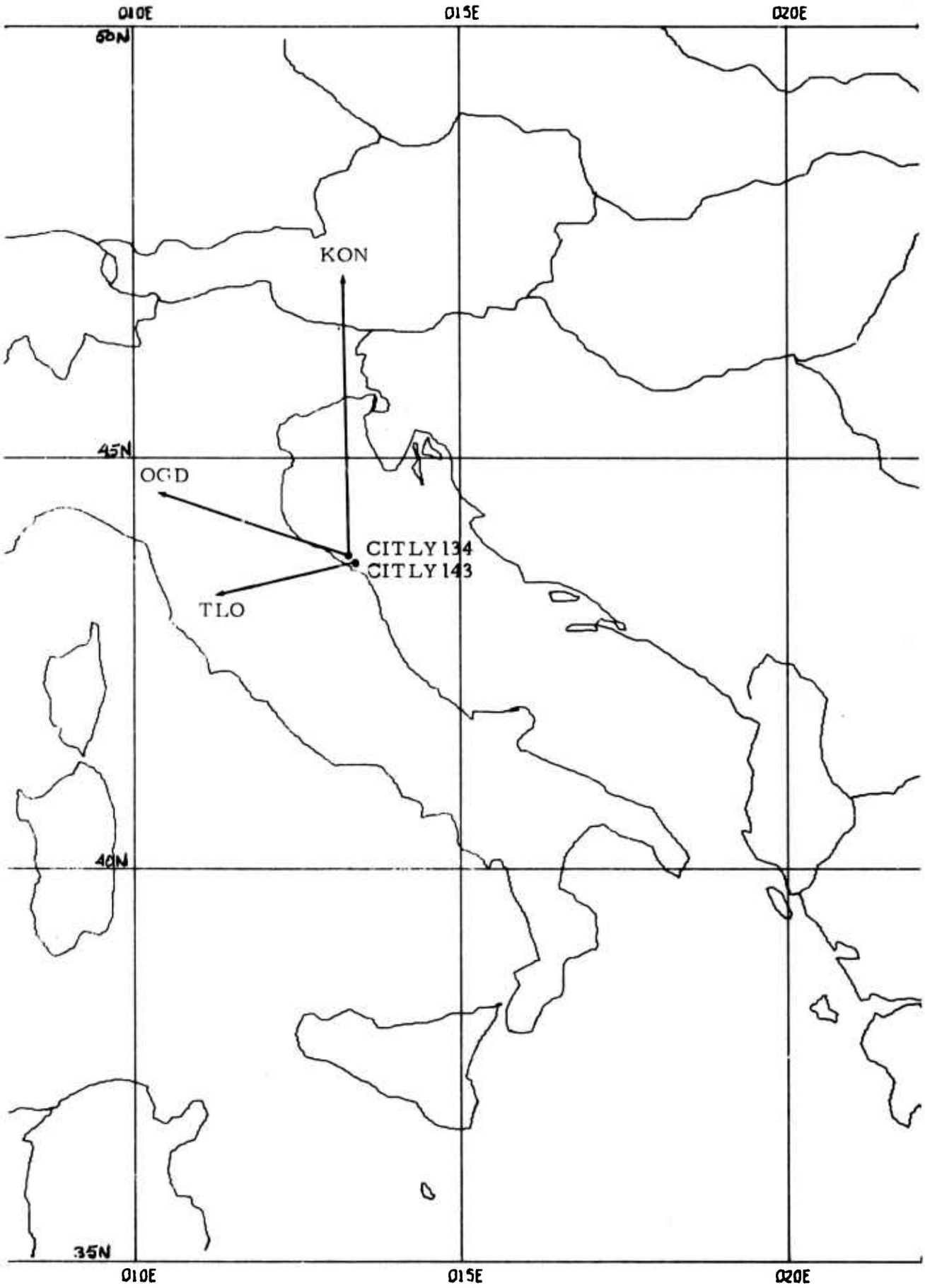

FIGURE V-1

LOCATIONS OF TWO, LOW MAGNITUDE ITALIAN EVENTS
RECORDED AT THREE VLPE STATIONS

TABLE V-1

ITALIAN EARTH MODEL

Thickness of Layer		ρ	Vp	V_s
No.	Km			
1	5	2.40	3.50	2.02
2	20	2.75	6.00	3.46
3.	20	3.00	6.50	3.75
4	13	3.30	8.20	4.73
The rest of the structure is the same as Hamilton-Healy Earth Model.				

TABLE V-2

CENTRAL ITALIAN EARTHQUAKES

Event I. D.	Location		Date & Time	M_b
	Latitude	Longitude		
LX/CITLY/143	43.7N	13.4E	02/05/72 15.14.48.0	4.2
LX/CITLY/134	43.8N	13.3E	02/04/72 17.59.52.0	4.1

TABLE V-3

OBSERVATION STATIONS FOR LX/CITLY/

1. Event: LX/CITLY/143

Site I. D.	Azimuth from Source (+ for N-E)	Δ in Degree	Δ in Km
4 TLO	-100.3	13.5	1500.3
6 KON	-7.0	16.1	1788.7
7 OGD	-58.7	61.8	6858.5

2. Event: LX/CITLY/134

Site I. D.	Azimuth from Source (+ for N-E)	Δ in Degree	Δ in Km
4 TLO	-100.9	13.5	1494.5
6 KON	-6.8	16.0	1776.7
7 OGD	-58.8	61.7	6845.9

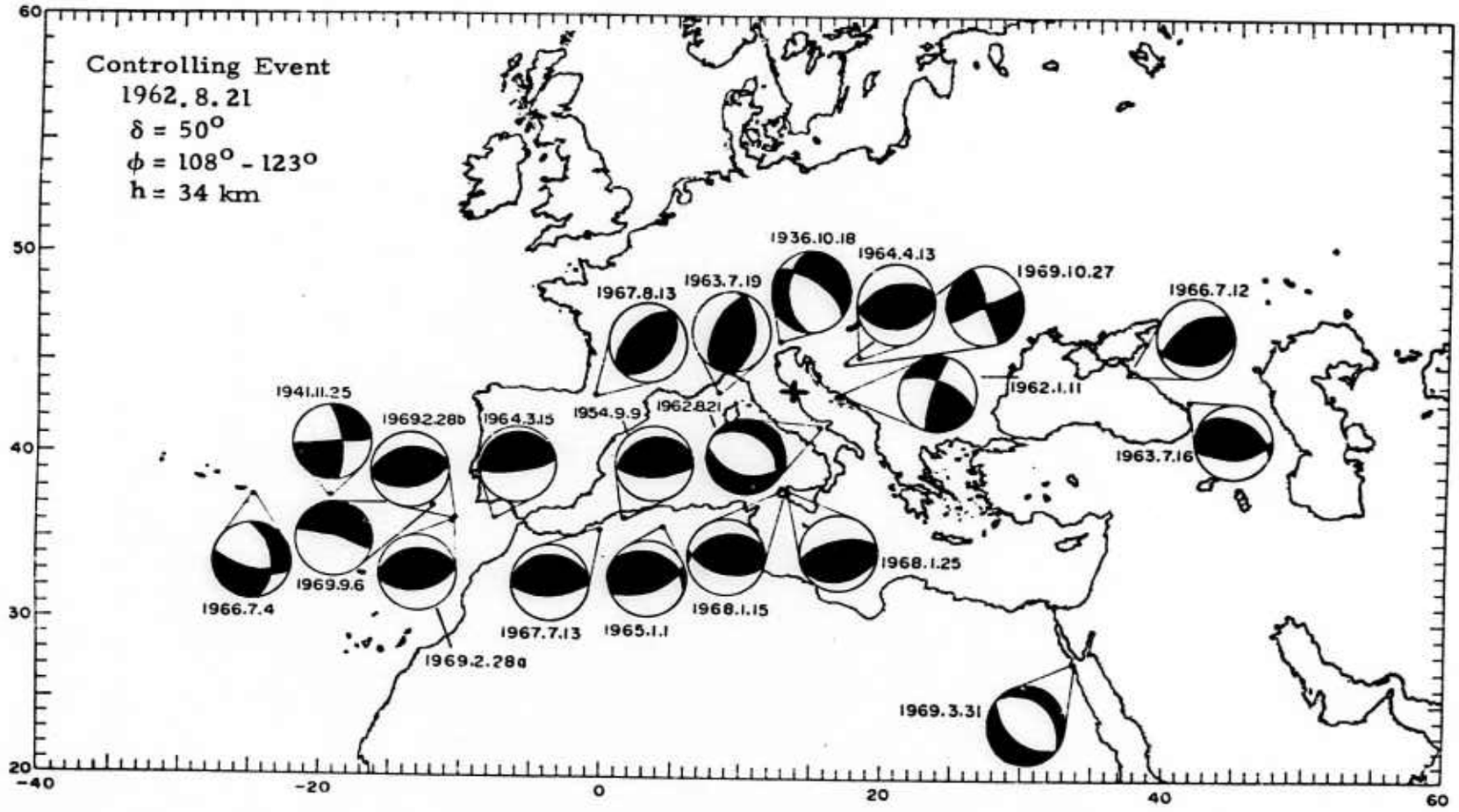

FIGURE V-2

LOCATION OF EVENTS WITH KNOWN BODY WAVE SOLUTIONS
IN RELATION TO THE TWO EVENTS ANALYZED

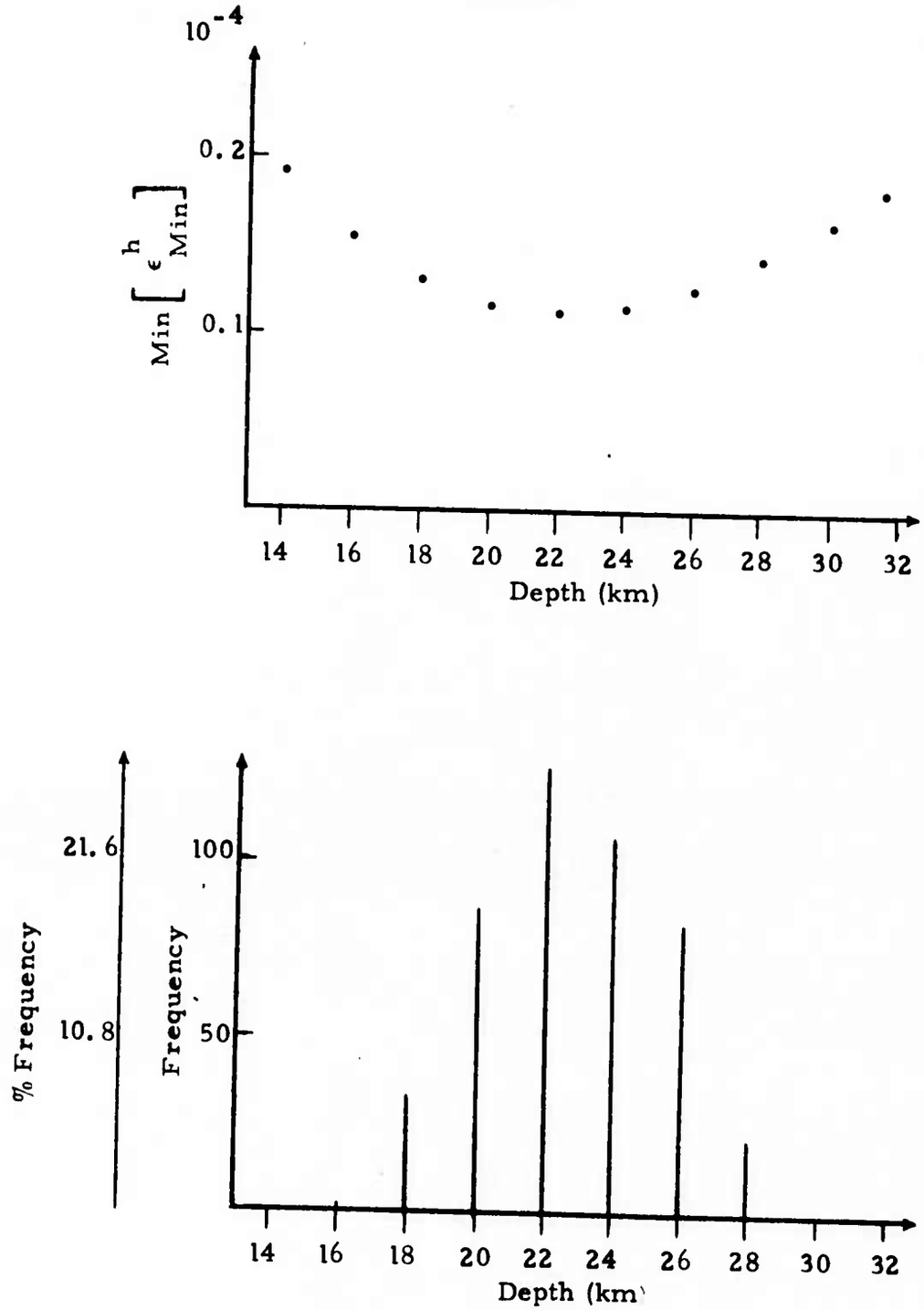

FIGURE V-3a

VARIATION OF ϵ WITH RESPECT TO DEPTH

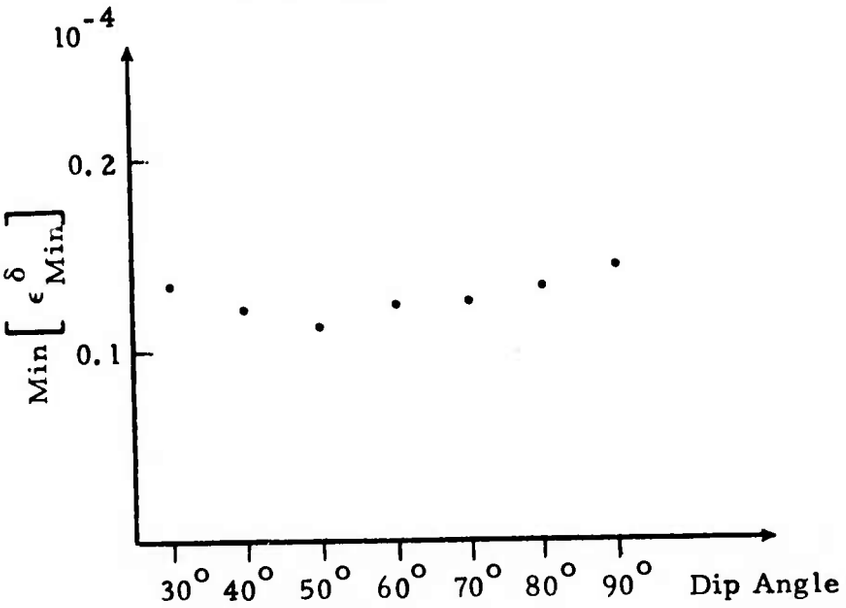

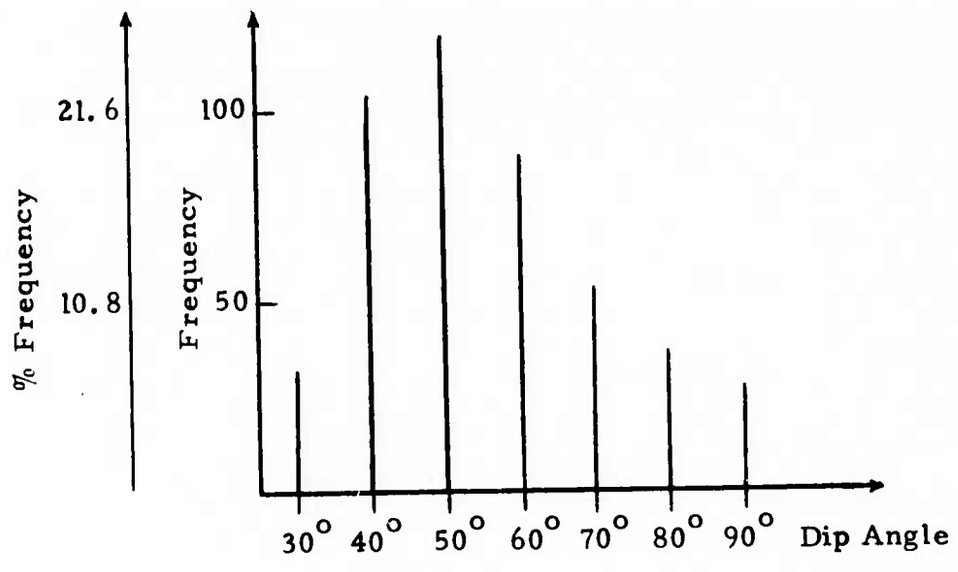

FIGURE V-3b

VARIATION OF ϵ WITH RESPECT TO DIP

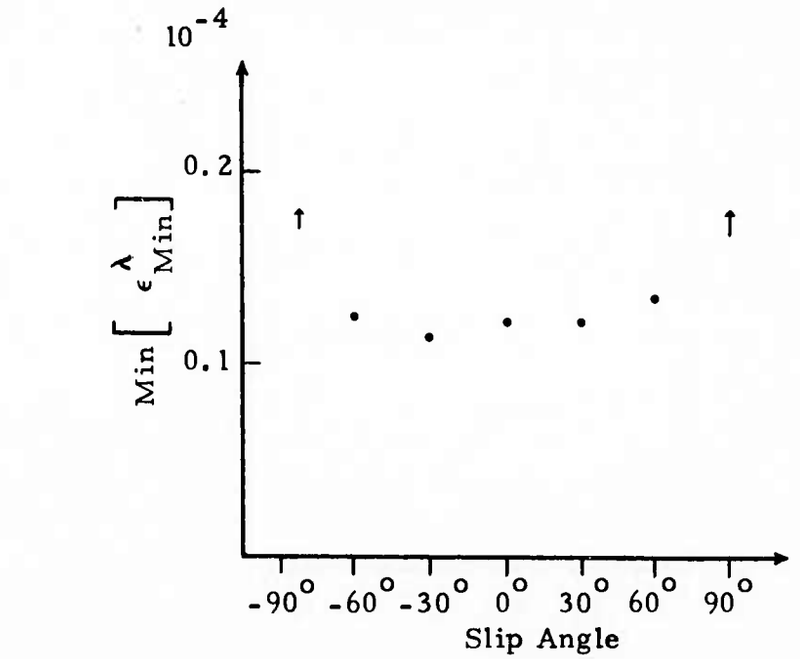

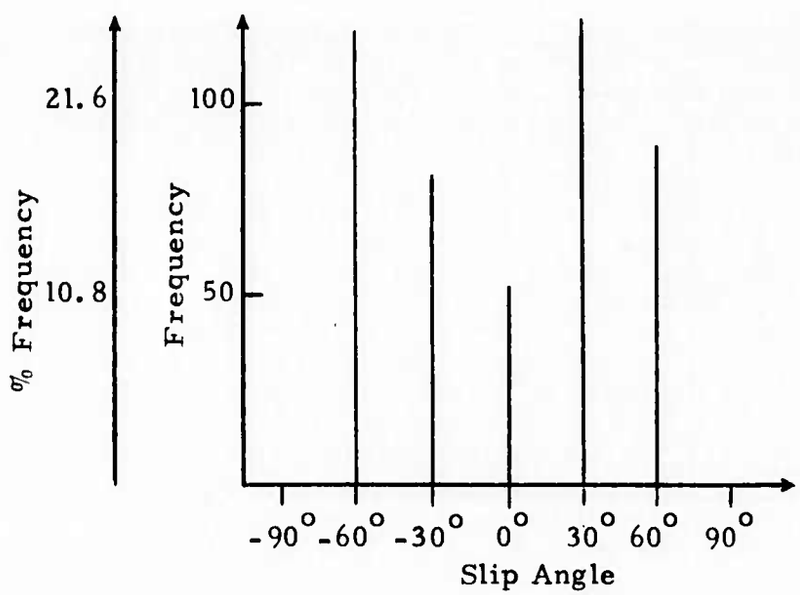

FIGURE V-3c

VARIATION OF ϵ WITH RESPECT TO SLIP

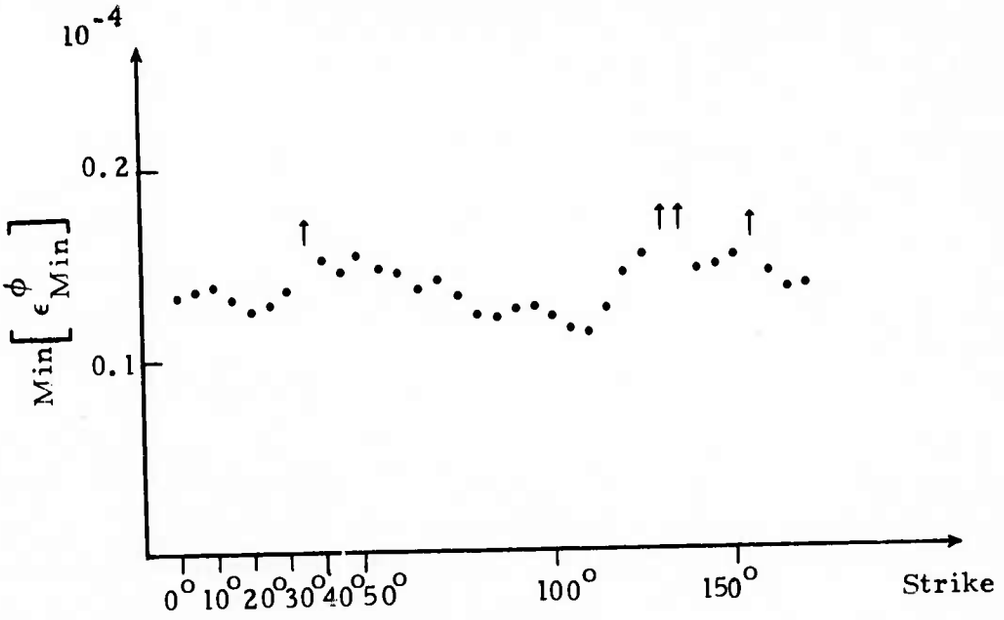

FIGURE V-3d

VARIATION OF ϵ WITH RESPECT TO STRIKE

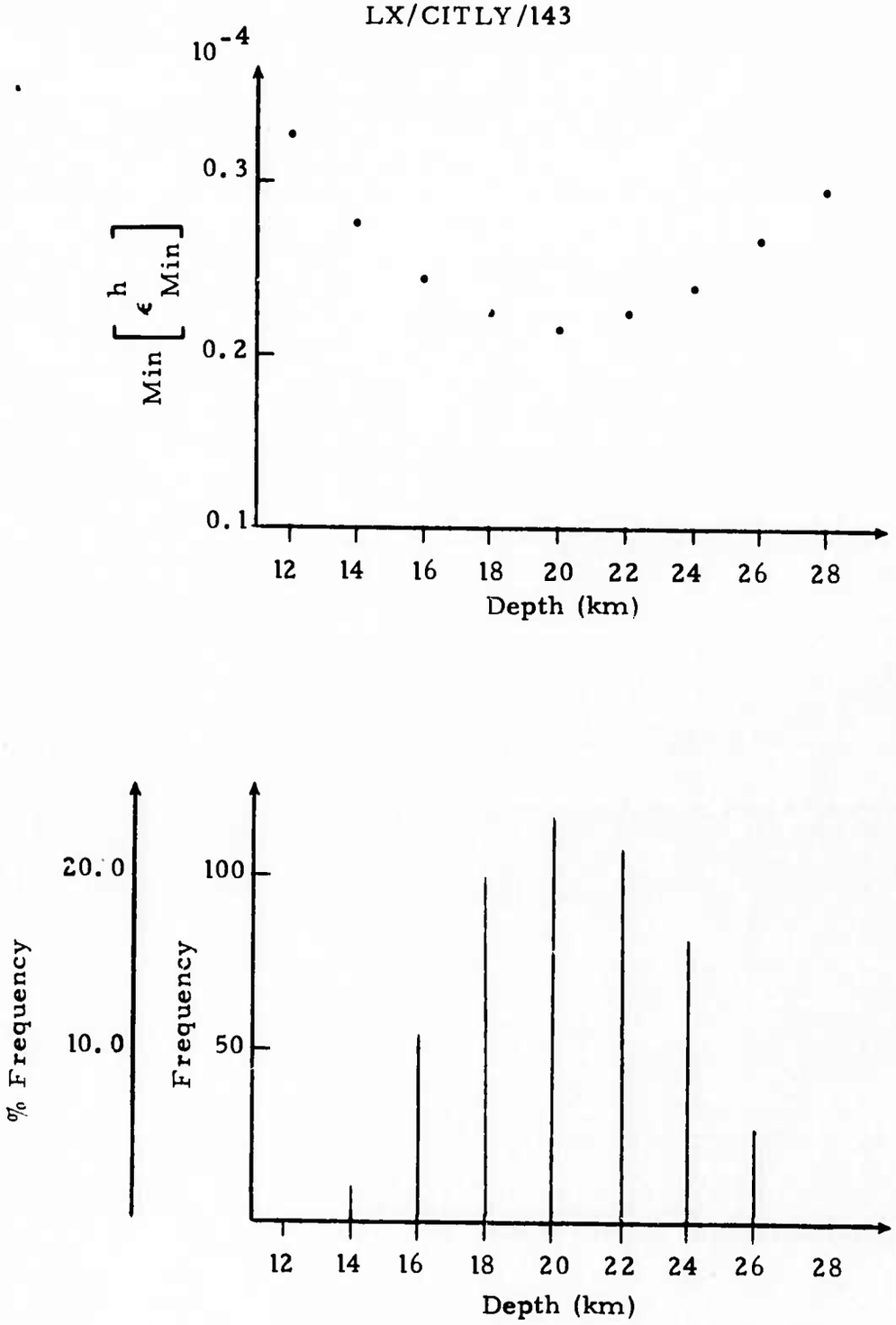

FIGURE V-4a

VARIATION OF ϵ WITH RESPECT TO DEPTH

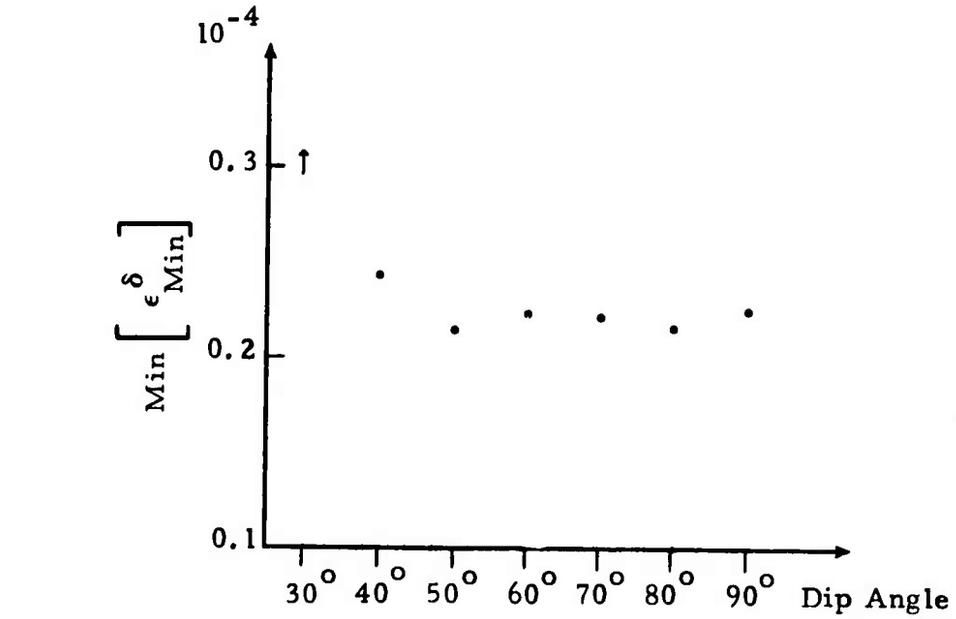

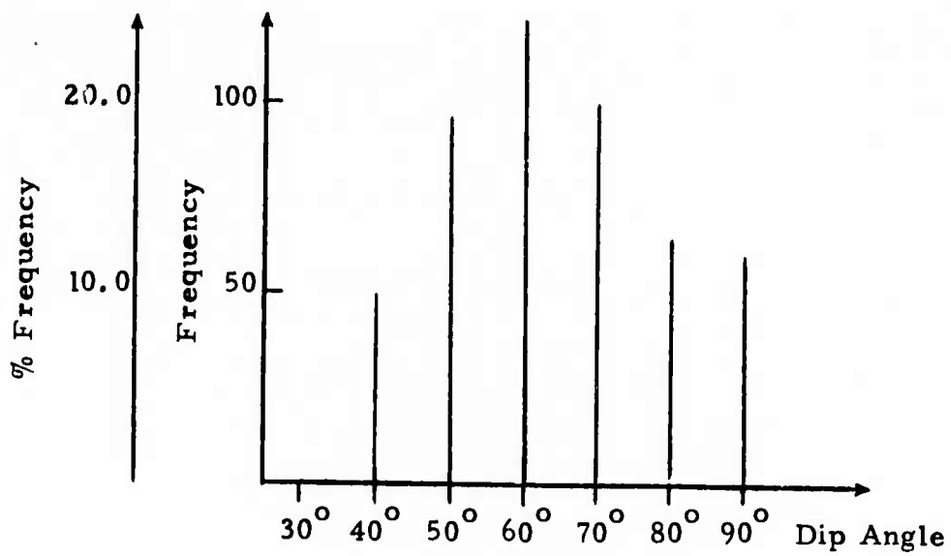

FIGURE V-4b

VARIATION OF ϵ WITH RESPECT TO DIP

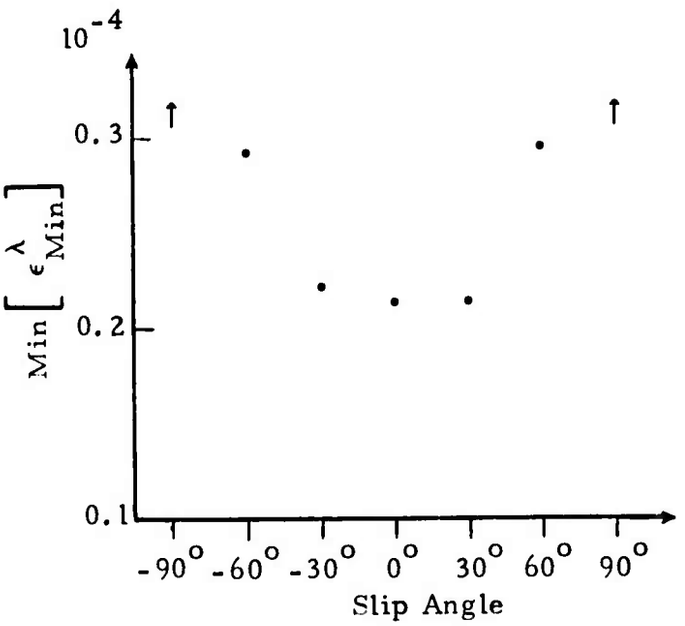

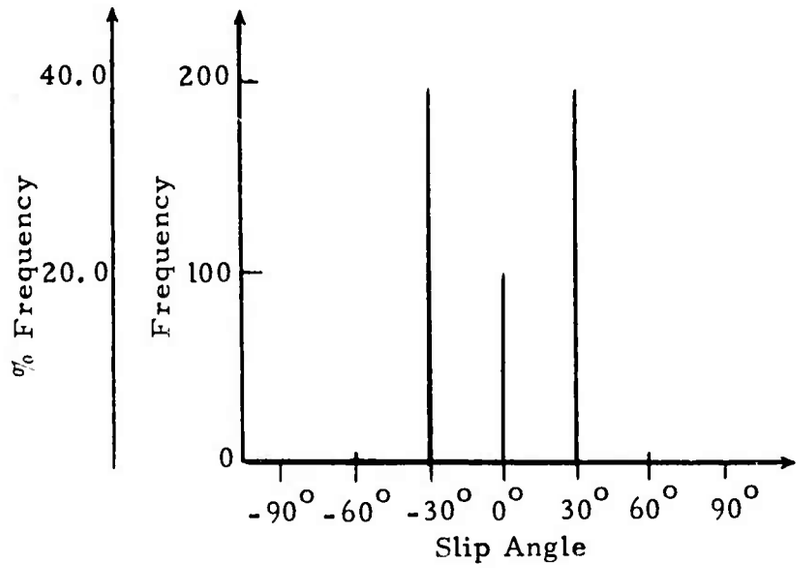

FIGURE V-4c

VARIATION OF ϵ WITH RESPECT TO SLIP

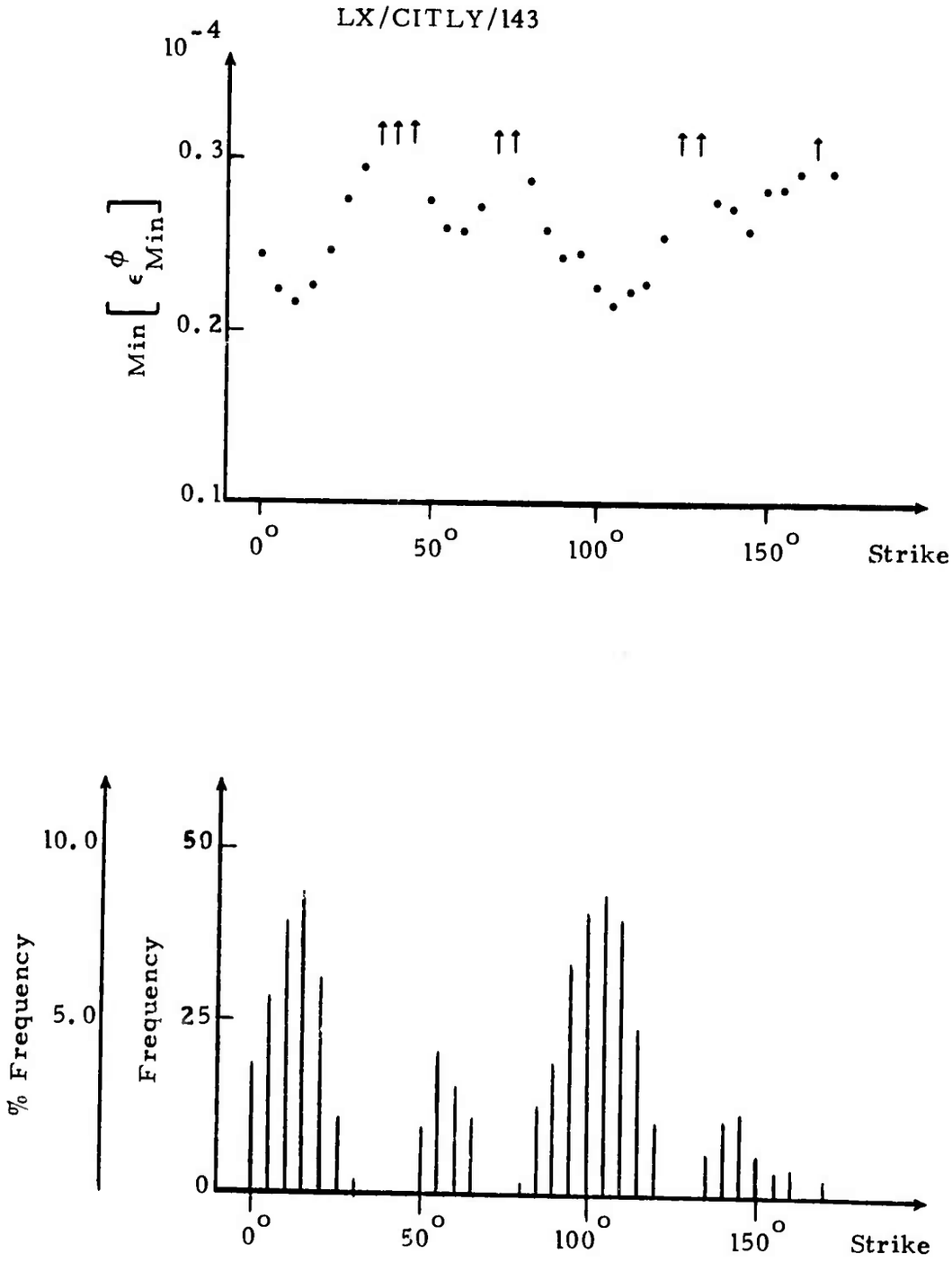

FIGURE V-4d

VARIATION OF ϵ WITH RESPECT TO STRIKE

TABLE V-4

SOLUTIONS FOR ITALIAN EVENTS

Analyzed Individually

Parameters	LX/CITLY/134 (2/4/72)		LX/CITLY/143 (2/5/72)	
	Value	Statistics	Value	Statistics
h (km)	22	20-26 ; 88%	20	18-24 ; 81%
δ	50°	$40\text{-}60^{\circ}$; 68%	50°	$50^{\circ}\text{-}70^{\circ}$; 65%
λ	-30°	$\pm 60, \pm 30^{\circ}$; 89%	0°	$-30^{\circ}\text{-}30^{\circ}$; 99%
ϕ	$N110^{\circ}E$	$80^{\circ}\text{-}110^{\circ}$; 34%	$N105^{\circ}E$	$95^{\circ}\text{-}115^{\circ}$; 37%
M (dyne-cm)	1.2×10^{21}		1.4×10^{21}	

Analyzed Using Spectral Ratio's of Events

$$\frac{S^{T}(\omega)_{\text{Trial Event}}}{S^{T}(\omega)_{\text{Ref. Event}}} = \frac{R^{OB}(\omega)_{TE}}{R^{OB}(\omega)_{RE}} = \frac{I(\omega)_{TE}\, G(\omega)_{TE}\, S^{OB}_{TE}(\omega)}{I(\omega)_{RE}\, G(\omega)_{RE}\, S^{OB}_{RE}(\omega)}$$

LX/CITLY/134 With LX/CITLY/143 As Reference

Parameters	Value	Statistics
h (km)	18	16-20 ; 87%
δ	40°	$40^{\circ}\text{-}70^{\circ}$; 74%
λ	30°	$\pm 30^{\circ}$; 61%
ϕ	$N90^{\circ}E$	$80^{\circ}\text{-}110^{\circ}$; 34%
M (dyne-cm)	1.3×10^{21}	

The source parameters for each event were similar, which should be expected because of their proximity ($< 1^{o}$). The residual distribution for depth was especially encouraging, with 80 per cent of the solutions lying within a 6 km range for both events. The dip and strike for both events are in close agreement with McKenzie's (1972) solution for the event in the same tectonic region. The seismic moments also correlate with the body wave magnitudes for each event, yielding $m_b \doteq 3.8$ to 4.0 using Tsai's ω^2-model (1972).

The almost identical location of these events offered a good opportunity to determine source parameters using spectral ratios. It is hoped that this method will enable us to examine low magnitude events using large magnitude events from the same region as a reference source. The spectral ratio is based on the assumption that one or more events from a region of interest have been rigorously analyzed, with the source parameter estimates obtained and corroborated from independent sources. Then small events in the same region, recorded at the same stations so source-station travel paths are similar, can be determined by essentially comparing source excitation functions. Examining the equation in Table V-4, we see that the path transfer functions ($G(\omega)$) and instrument response ($I(\omega)$) will cancel if we have the same source-station paths. When CITLY/134 was analyzed using CITLY/143 as a reference, we obtained parameter estimates reasonably close to those determined using only the event itself (Table V-4). The depth estimate changed 4 km.

The spectral ratio method can also give us some indication of the effectiveness of our path correction if, as in this case, individual estimates of the source parameters are known. Since multipathing was not observed, our correction for effective Q must be inaccurate for one or more paths. This is indicated if we examine the spectral fits obtained using the individual event parameter estimates. Figures V-5 show fits for CITLY/134,

FIGURE V-5a

SPECTRAL AMPLITUDE: LX/CITLY/134: KON

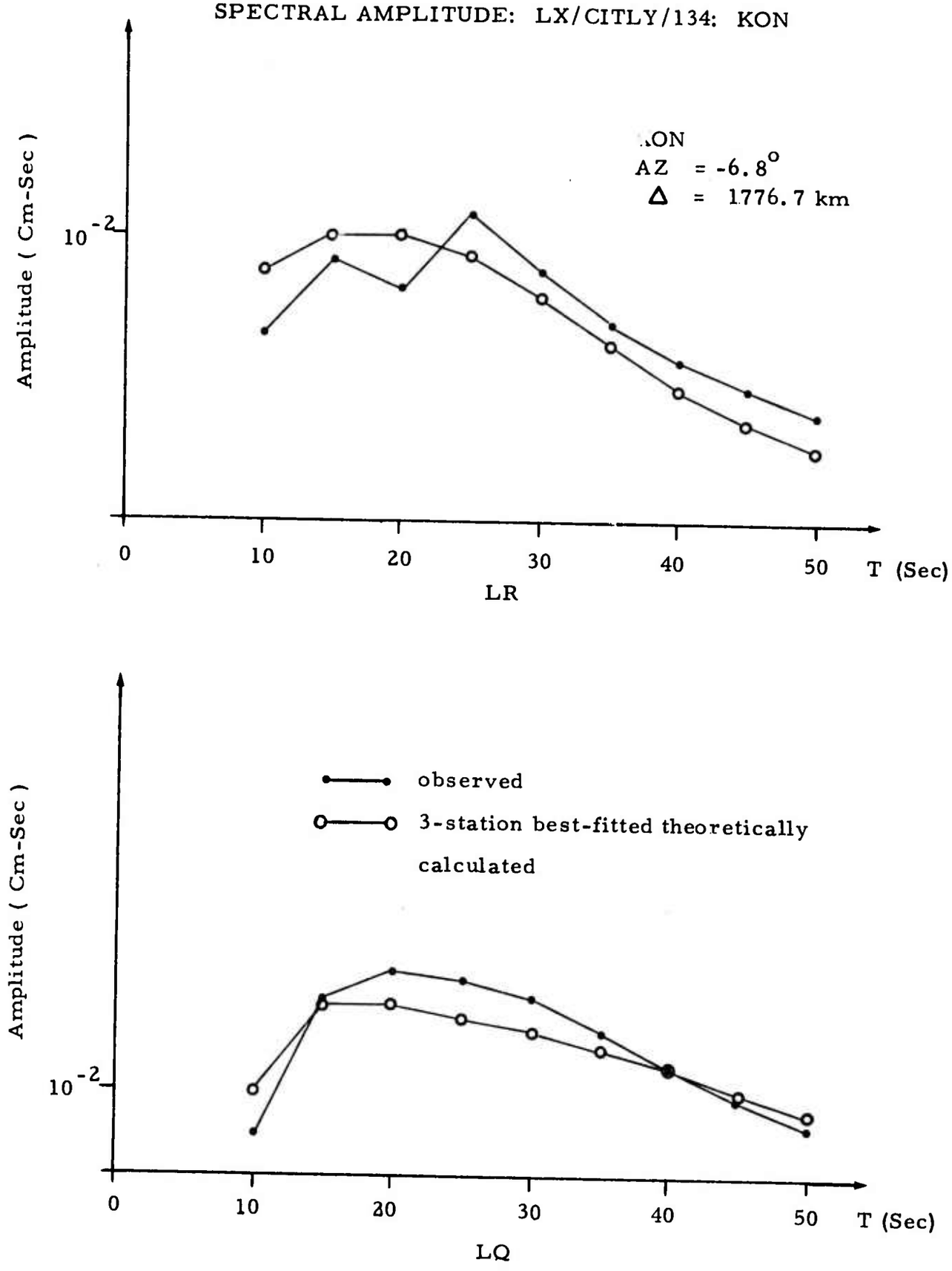

FIGURE V-5b

SPECTRAL AMPLITUDE: LX/CITLY/134: OGD

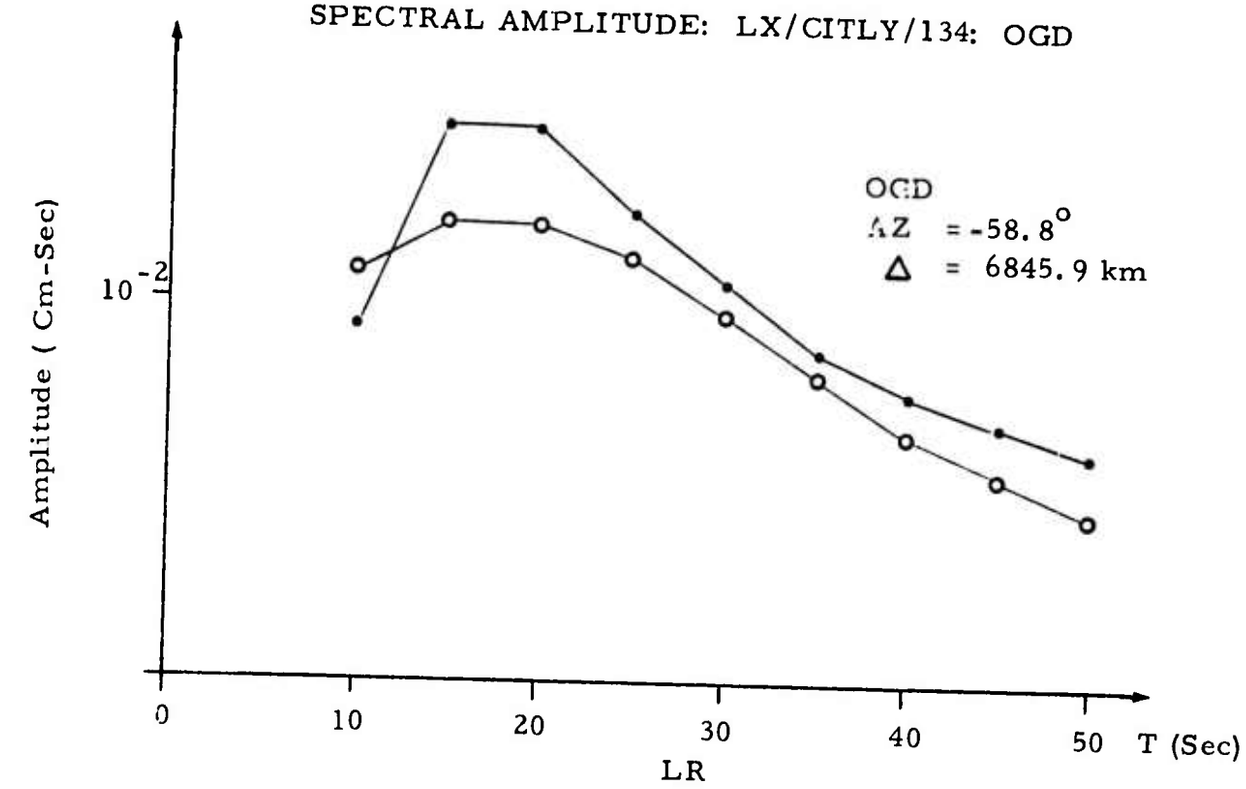

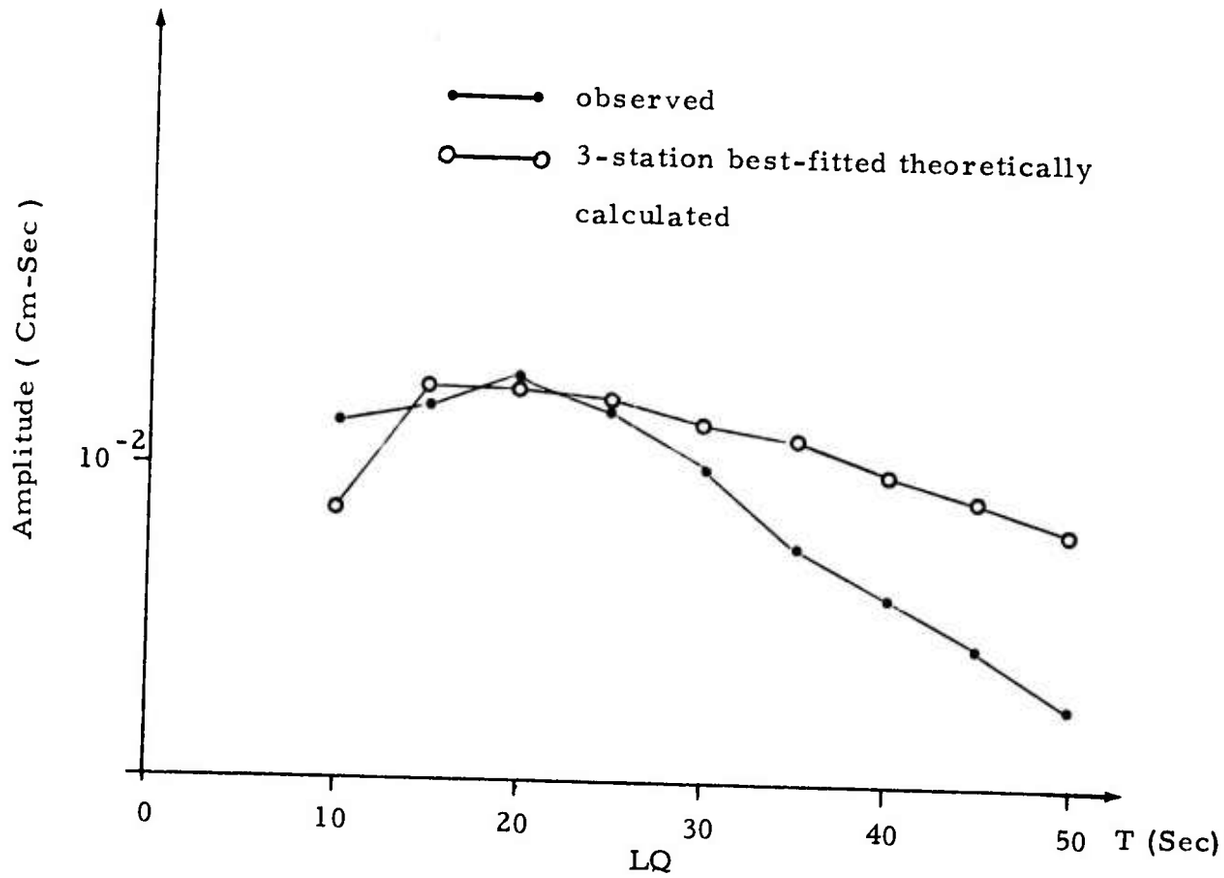

FIGURE V-5c

SPECTRAL AMPLITUDE: LX/CITLY/134: TLO

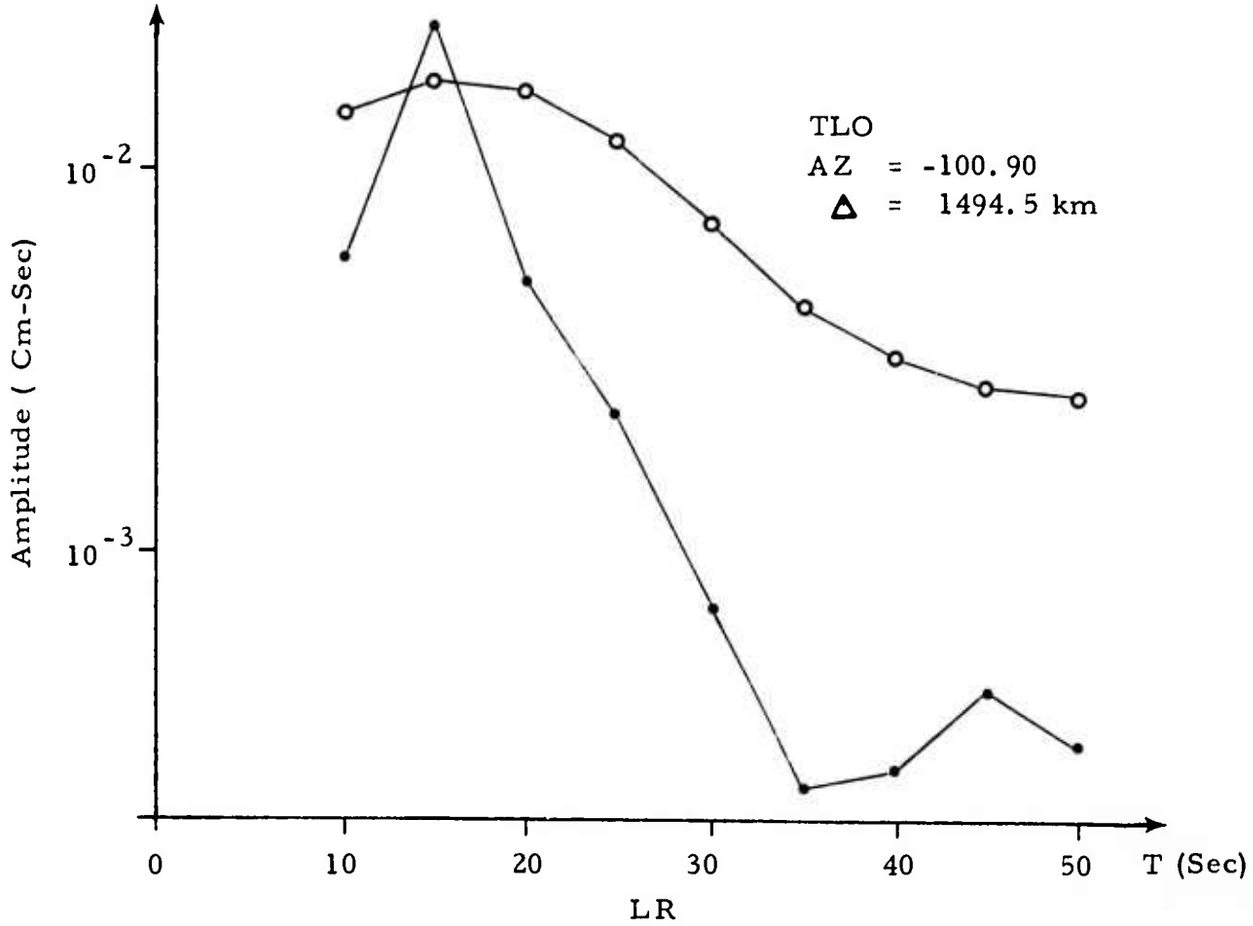

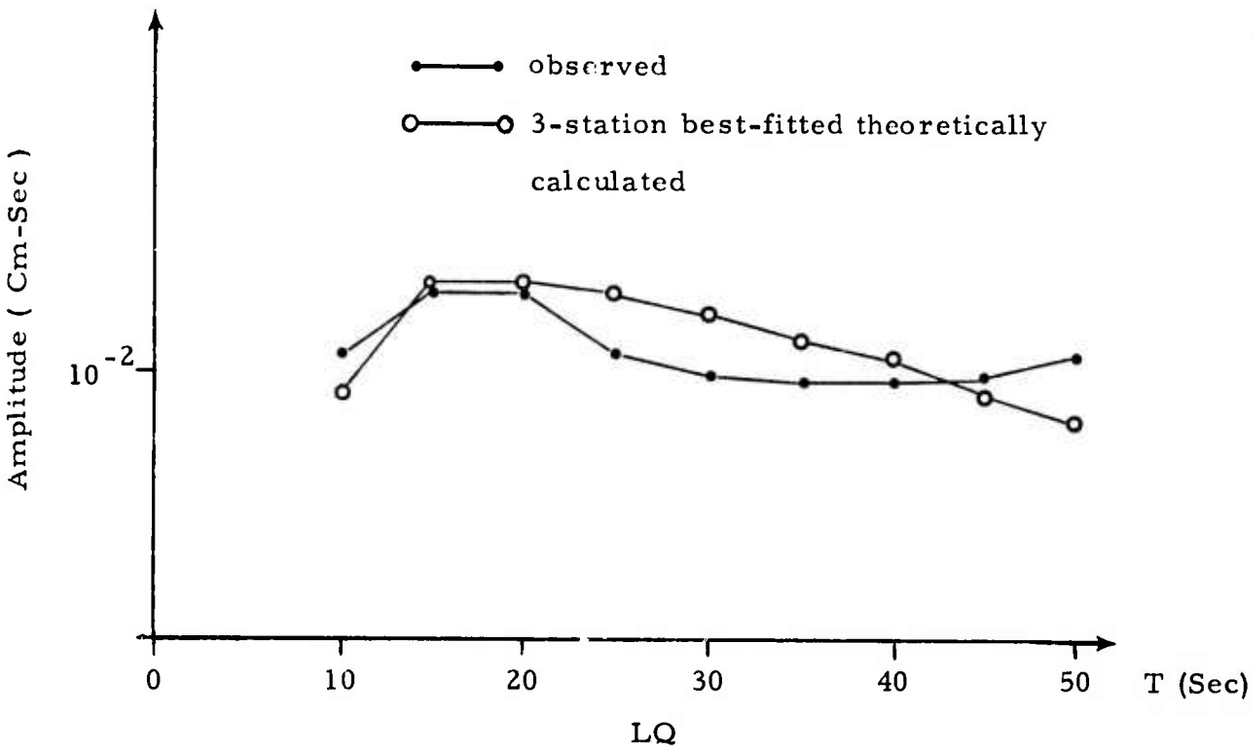

and Figures V-6 show the same for CITLY/143. For both events, we see that the spectral match at TLO breaks down completely at longer periods. Evidently, our effective Q is not modeling the actual attenuation. Future studies will be directed at obtaining an accurate estimate.

Finally, two other cases of interest were analyzed, and the results are summarized below:

- Using Event CITLY/134 as a reference, CITLY/143 was analyzed using spectral ratios. The depth estimate was 22 km, with the possible range 22 to 26 km containing 80 per cent of the models.

- Both events were analyzed individually using only two stations, KON and OGD. The depth estimate for both events was 24 km, but the other parameters varied a great deal from the three station fit, with the seismic moments for both events about a third larger.

FIGURE V-6a

SPECTRAL AMPLITUDE: LX/CITLY/143: KON

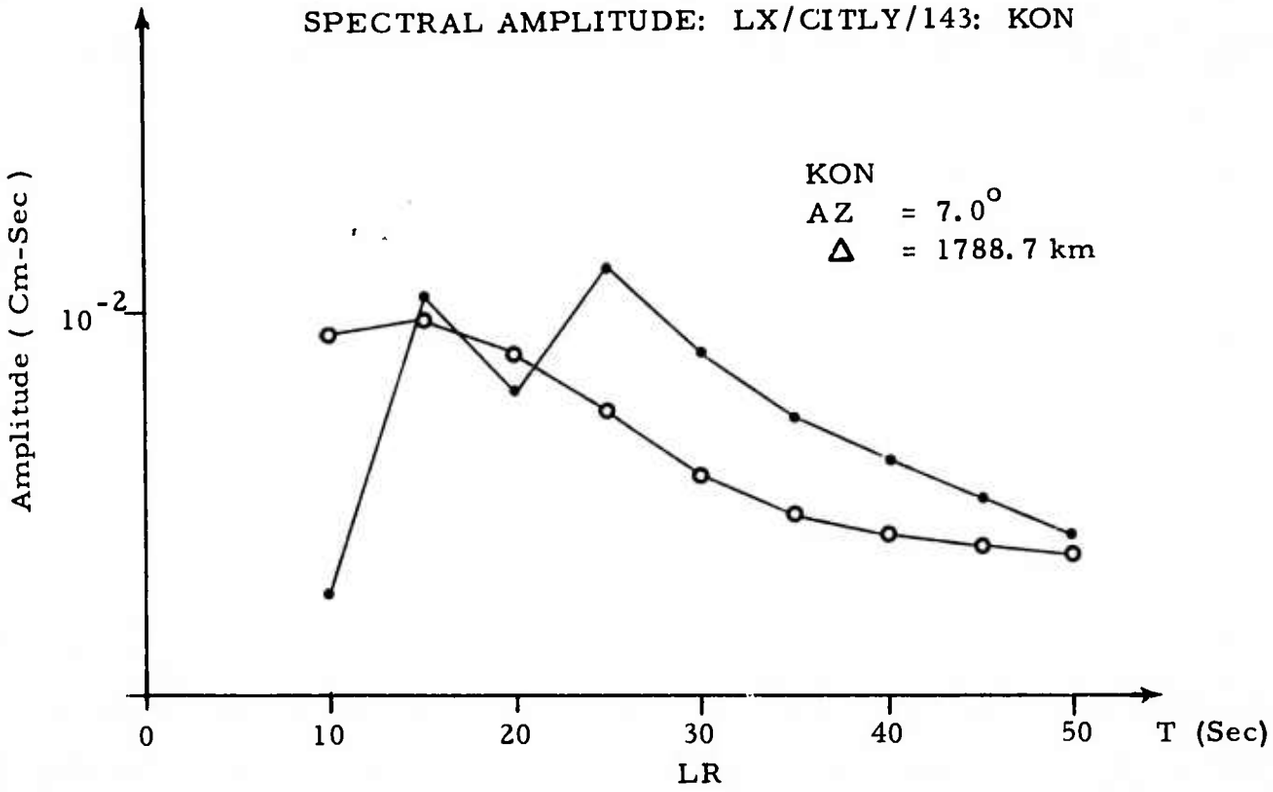

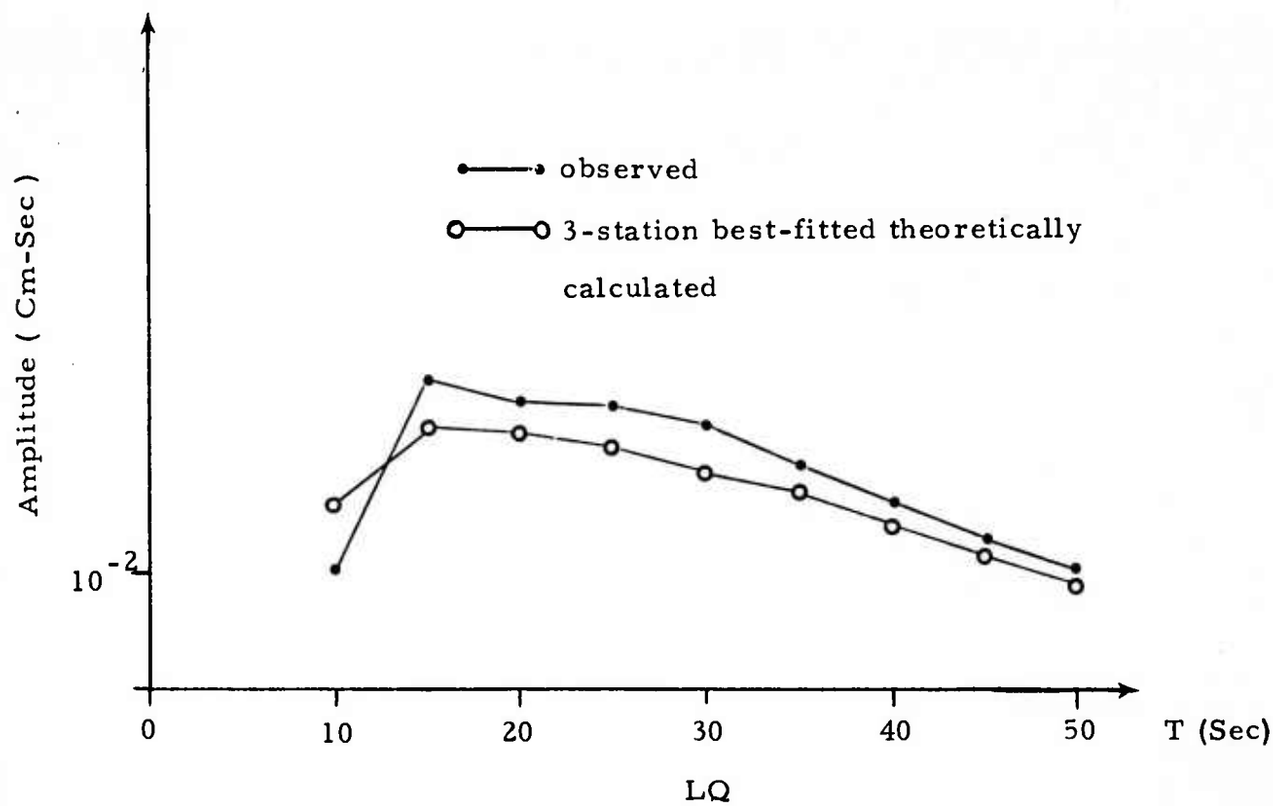

FIGURE V-6b

SPECTRAL AMPLITUDE: LX/CITLY/143: OGD

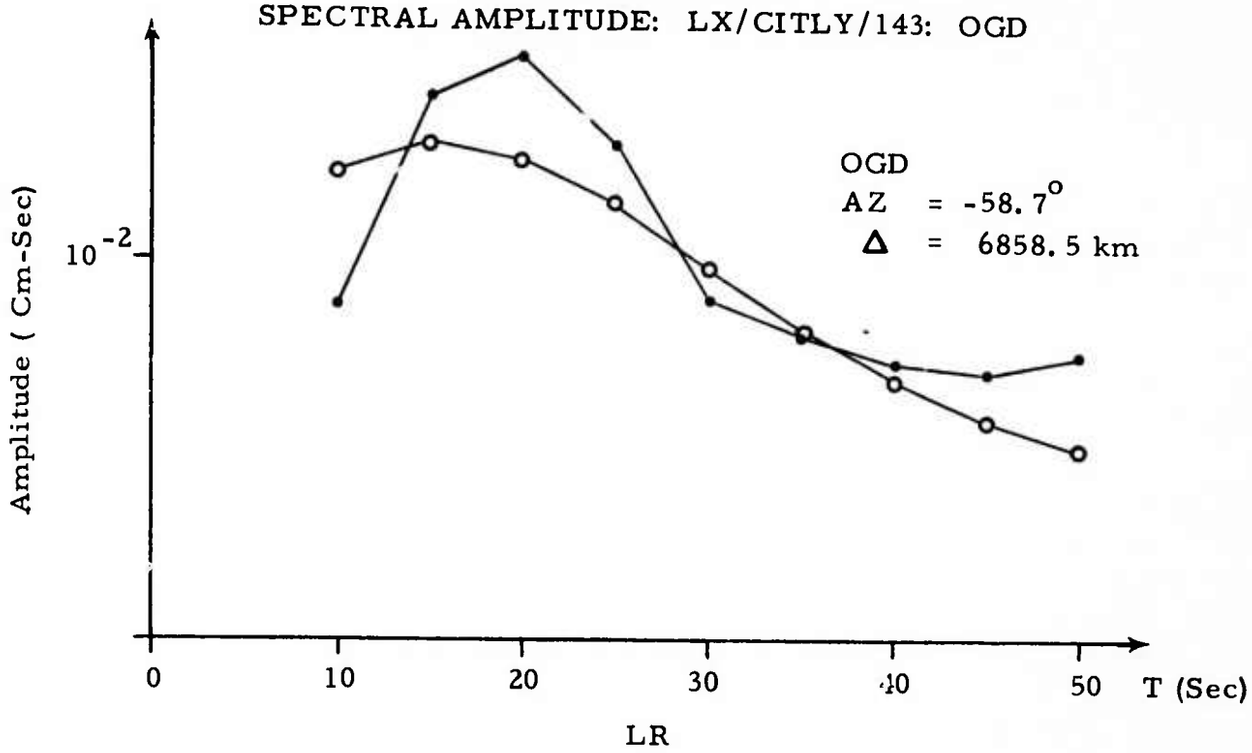

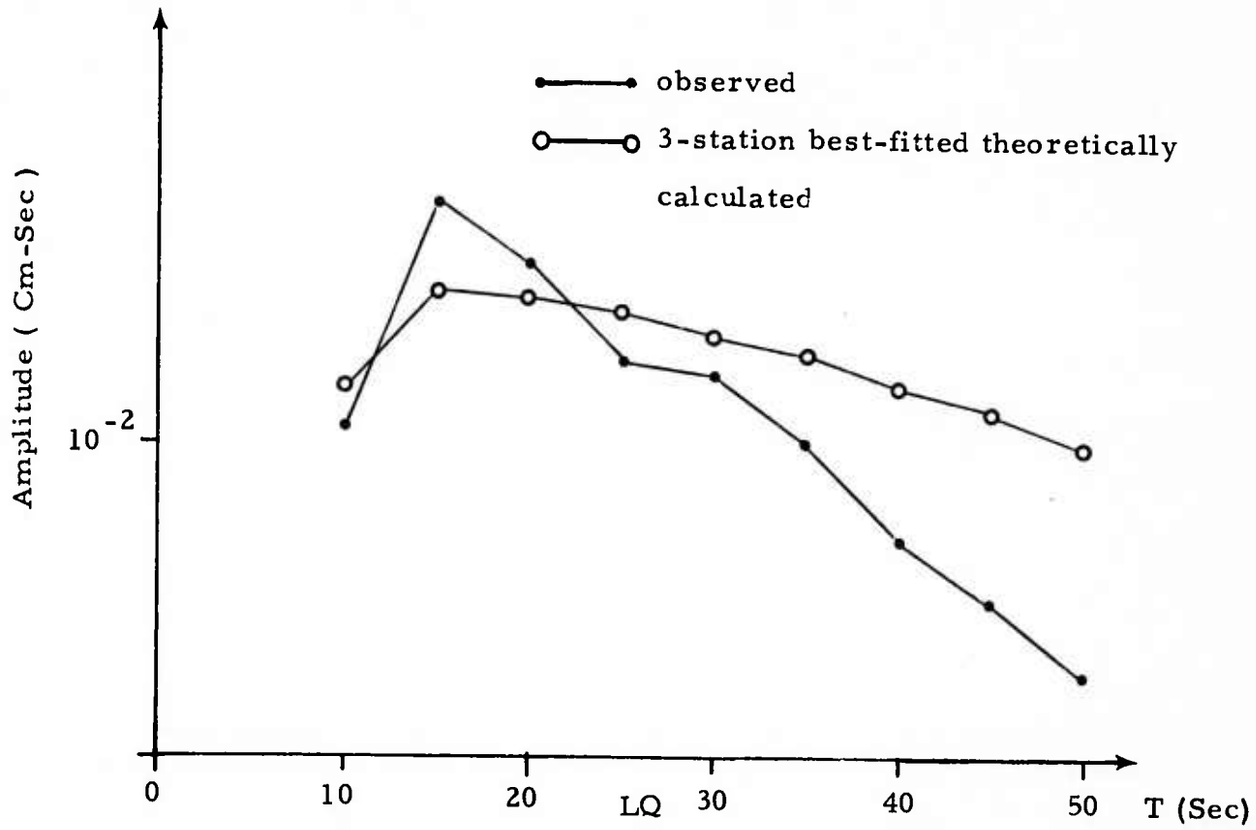

FIGURE V-6c

SPECTRAL AMPLITUDE: LX/CITLY/143: TLO

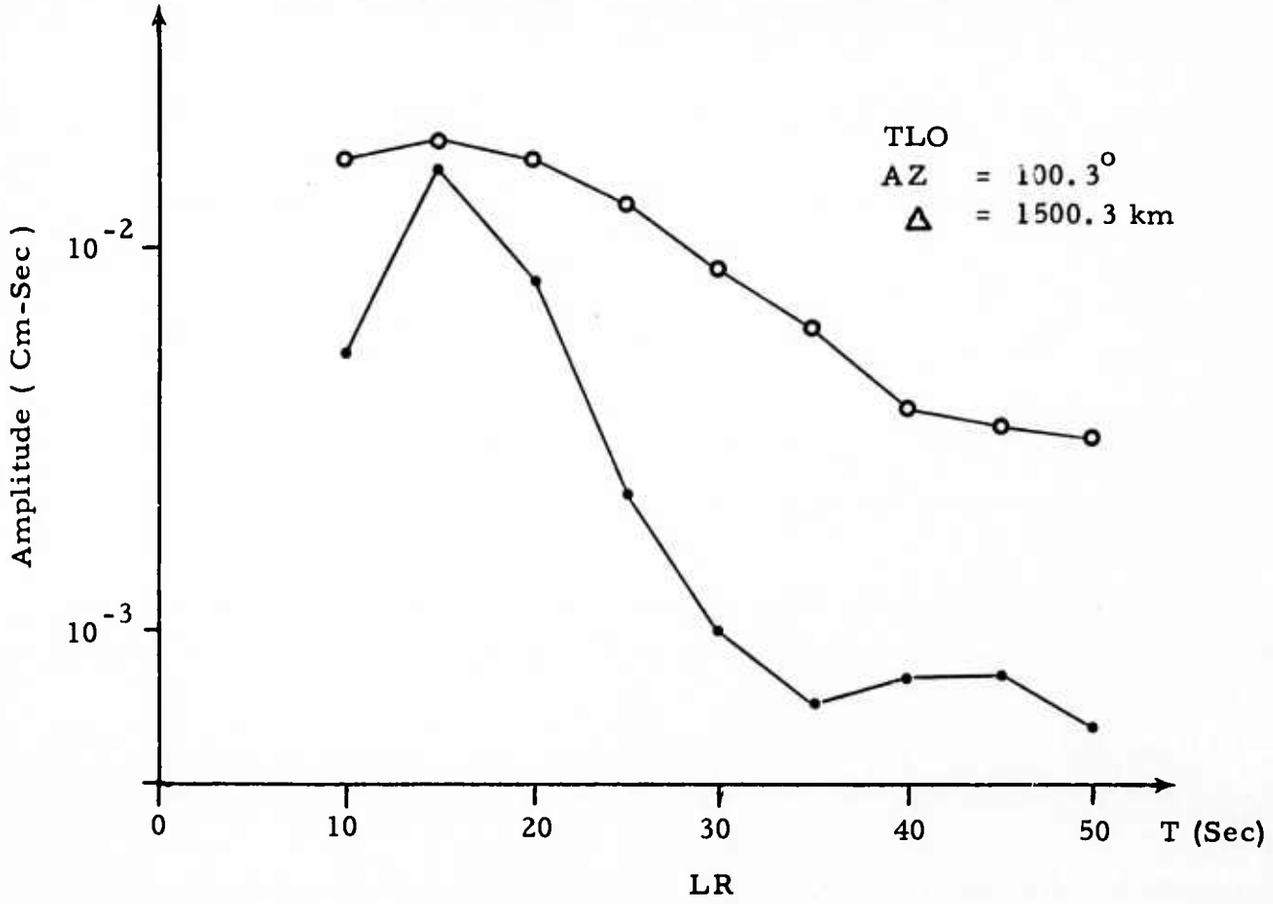

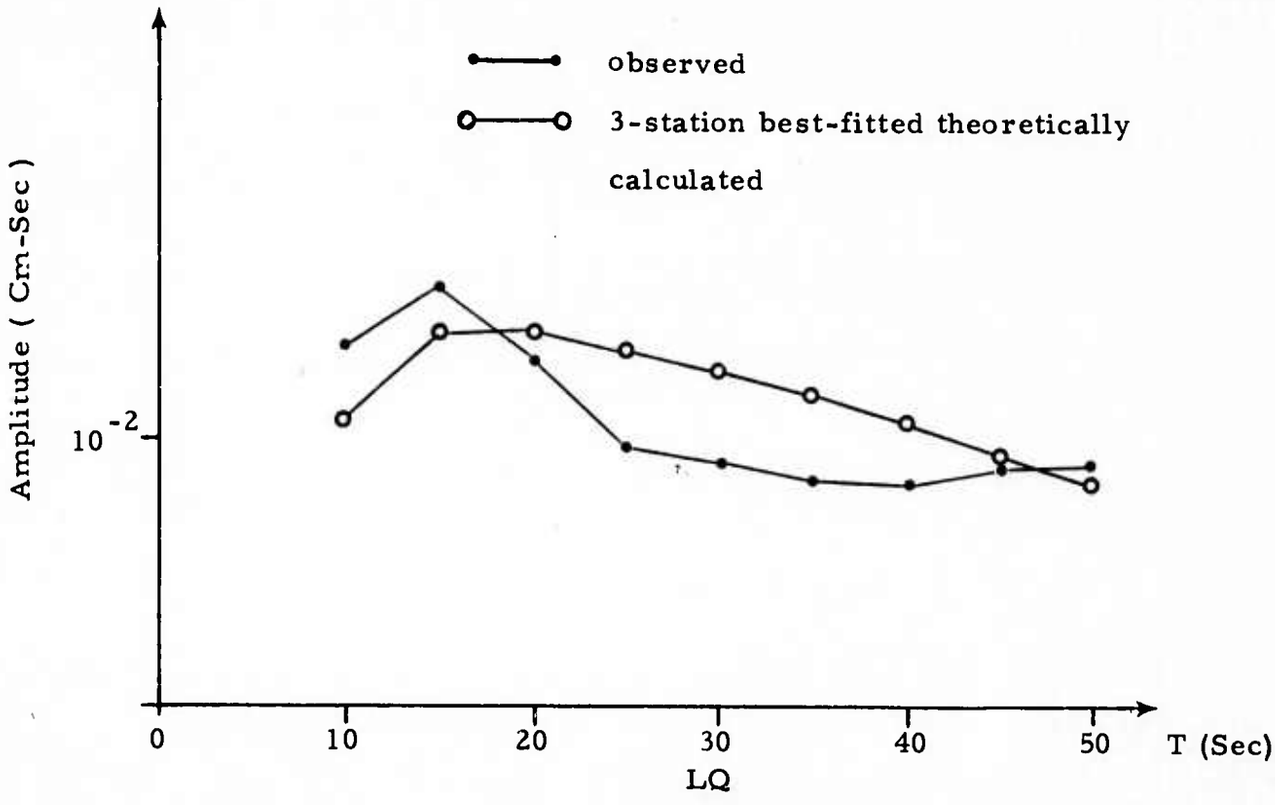

SECTION VI

EARTHQUAKES IN SINKIANG

Having analyzed events with varying degrees of control on the source parameters, we will now analyze six earthquakes in Sinkiang, China, for which we have no reliable independent estimates of the source parameters. These events have been chosen from about thirty events which originated in that region during 1972, the sole criteria being that they were observed at two or more VLPE stations. The locations of these events are displayed in Figure VI-1, with their locations, date and origin time, and body wave magnitude given in Table VI-1. Information concerning the observation stations is given in Table VI-2 for each event.

This section is divided into three parts. In the first we will discuss attenuation and multipathing corrections. The second part contains solutions and residual distributions for each event, and the third part presents solutions obtained through spectral ratios.

A. PATH CORRECTIONS

Narrow band filter analysis, as discussed in Appendix B, was applied to every Rayleigh and Love wave record. Examples of the narrow band output are given in Appendix H, with the associated group velocity curves. Observed Rayleigh wave amplitude spectra was available for all eight sampled periods (T = 15 to 50 seconds, ΔT = 5 sec) of the six events at most of the observation stations; while for the Love waves, the observed amplitude spectra was incomplete at most stations. Except for event LX/KIRSI/059, the spectral amplitudes are relatively small. For station CHG, though, the spectral amplitudes are unreasonably small, indicating unusual attenuation. (The source-station path of Sinkiang to CHG is shown

CENTRAL ASIA - SOUTH SINKIANG

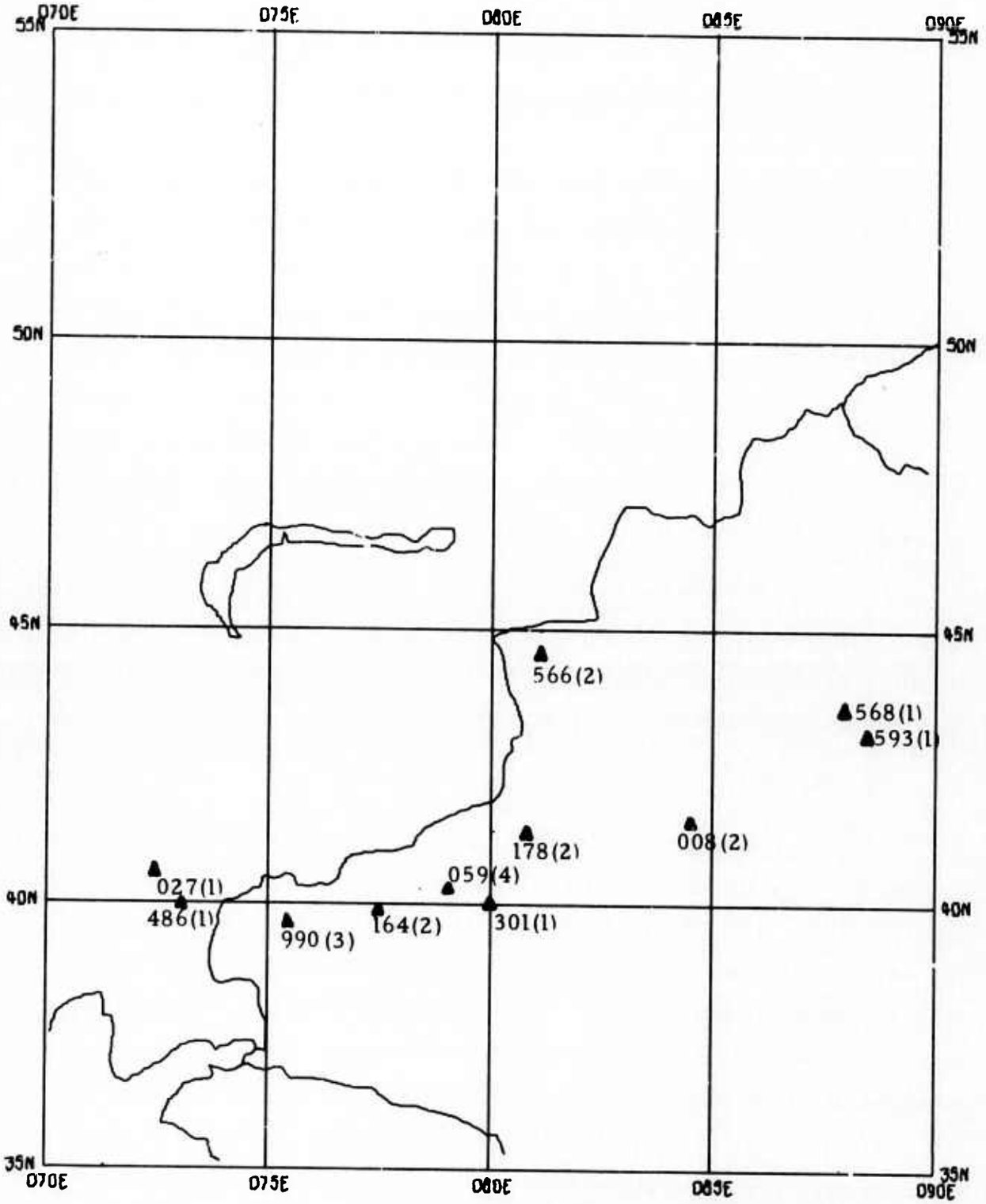

FIGURE VI-1

LOCATION OF SINKIANG EVENTS, WITH THE NUMBER OF STATIONS RECORDING EACH EVENT IN PARENTHESIS

TABLE VI-1

SINKIANG EARTHQUAKES

Event I. D.	Location		Date and Time	M_b
	Latitude	Longitude		
LX/KIRSI/059	40.3N	79.0E	01/15/72 20.21.50	5.4
LX/SSINK/990	39.4N	75.3E	12/03/72 08.54.47	5.0
LX/NSINK/008	41.8N	84.5E	01/02/72 10.27.35	5.2
LX/SINKI/178	41.7N	80.7E	02/16/72 23.19.20	4.8
LX/NSINK/566	44.6N	81.1E	07/05/72 01.09.53	4.6
LX/SINKI/164	39.9N	77.4E	02/11/72 05.55.46	4.9

TABLE VI-2

OBSERVATION STATIONS FOR SINKIANG EARTHQUAKES

Event I. D.	Site I. D.	Azimuth To Source (+ for N-E)	Δ In Degree	Δ In km
LX/KIRSI/059				
	2 CHG	135.4	27.5	3056.3
	3 FBK	19.5	68.7	7648.4
	4 TLO	-60.6	61.0	6790.0
	7 OGD	-19.7	95.3	10604.7
LX/SSINK/990				
	2 CHG	128.2	29.0	3226.0
	6 KON	-40.7	45.0	5004.0
	9 ALQ	1.5	105.9	11775.9
LX/NSINK/008				
	2 CHG	147.3	26.1	2896.9
	4 TLO	-58.8	63.8	7105.3
LX/SINKI/178				
	3 FBK	20.3	67.0	7453.5
	6 KON	-41.7	45.9	5113.6
LX/NSINK/566				
	4 TLO	-61.7	60.3	6711.0
	8 KIP	53.2	94.9	10563.4
LX/SINKI/164				
	3 FBK	18.9	69.5	7735.1
	6 KON	-40.9	45.6	5079.8

in Figure VI-2, as well as paths for all the VLPE stations.) This high attenuation also shows up in the amplitude spectra for explosions in Eastern Kazakh. Listed in Table VI-3 are event information for two of these.

The explosions were used in an attempt to obtain an effective Q for the Sinkiang - CHG travel path from Tryggvason's method (Appendix A). His method assumes that equal energy is transmitted in all directions from the source, which is ideally suited for explosion data. In Figure VI-3 are shown energy attenuation coefficients k_e for the two explosions determined by Tryggvason's method. The results are hard to interpret, mainly because his method needs good azimuthal coverage and purely continental paths. We tried to adjust the amplitudes of EKAZH/013 using Von Seggern's (1971) amplitude equalization technique for estimating differences between continental and oceanic paths, and then apply Tryggvason's technique. Again, the results are difficult to interpret for the reasons given above. We finally decided to implement a two-station correction (Appendix A) between CHG and ALQ using Tryggvason's energy attenuation coefficient. Although CHG and ALQ are not on the same great circle path through the source area, we are using explosion data, and the ALQ travel path is mostly continental (as shown consistently by group velocity curves from the Sinkiang region). The results of this technique are shown in Figure VI-4. The energy attenuation coefficient for CHG is quite high, indicating high absorption over the frequencies of interest.

B. AMPLITUDE SPECTRAL FITTING FOR INDIVIDUAL EVENTS

As with the Italian data, the quality is highly variable, and we only applied the modified Tsai's method, with the accuracy furnished by the residual distributions thought to be sufficient. The optimal solutions of source parameters for these six earthquakes are listed in Table VI-4, and the probable ranges with percentage confidences of the source parameters are listed in Table VI-5. The distributions of minimum residuals of each

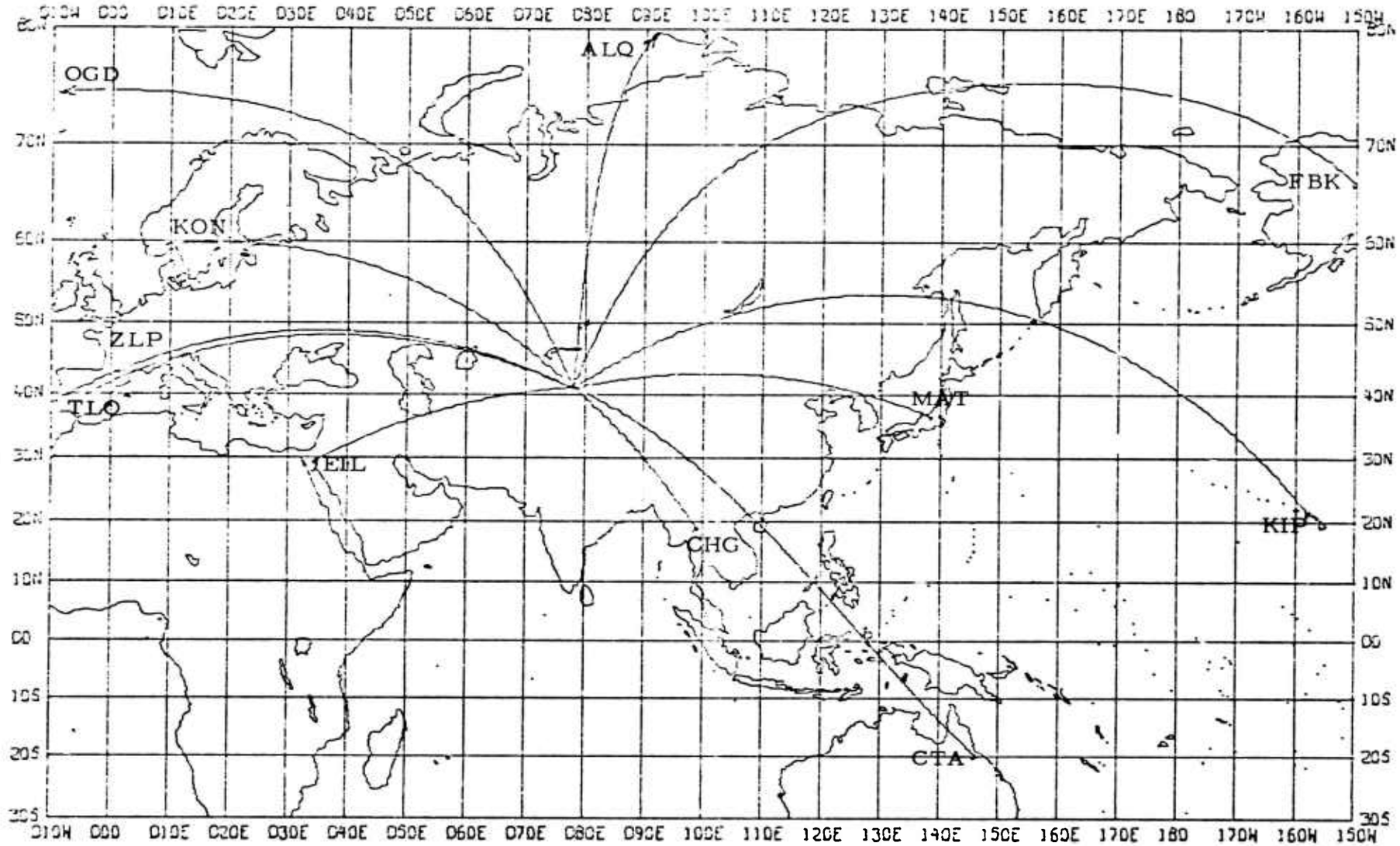

FIGURE VI-2

SOURCE-STATION PATHS FOR THE VLPE STATIONS FROM SINKIANG EVENTS

TABLE VI-3

TWO EXPLOSIONS FROM EASTERN KAZAKH

LX/EKAZH/013: Location: 49.8 N Lat., 78.1 E Long.
Magnitude: m_b = 5.7
Date: 12/10/72
Origin Time: 04:26:58

Recording Station	Location		Azimuth From Source	Δ (km)
	Lat.	Long.		
CHG	18.8 N	99.0 E	144.0°	3911.2
KIP	21.4 N	158.0 W	50.6°	10385.8
ALQ	34.9 N	106.5 W	3.8°	10611.3
ZLP	16.5 S	68.1 W	-51.1°	15233.3

LX/EKAZH/876: Location: 49.9 N Lat., 78.8 E Long.
Magnitude: m_b = 6.2
Date: 11/2/72
Origin Time: 01:26:58

Recording Station	Location		Azimuth From Source	Δ (km)
	Lat.	Long.		
KON	59.7 N	9.6 E	-48.4	4364.0
KIP	21.4 N	158.0 W	51.2	10339.7
ALQ	34.9 N	106.5 W	4.4	10596.7

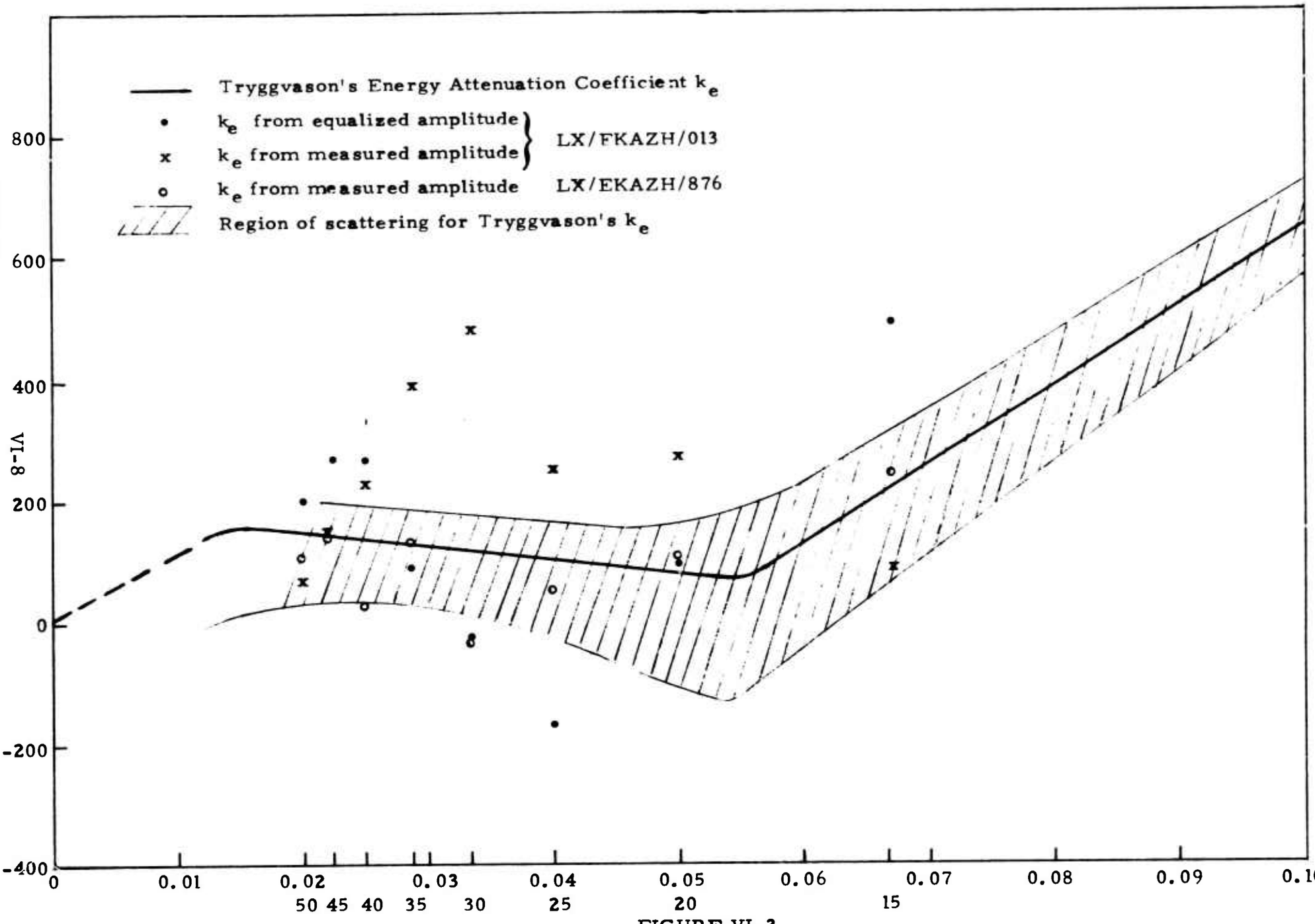

FIGURE VI-3

DETERMINATION OF ENERGY ATTENUATION COEFFICIENTS FROM TWO EXPLOSIONS IN EASTERN KAZAKH

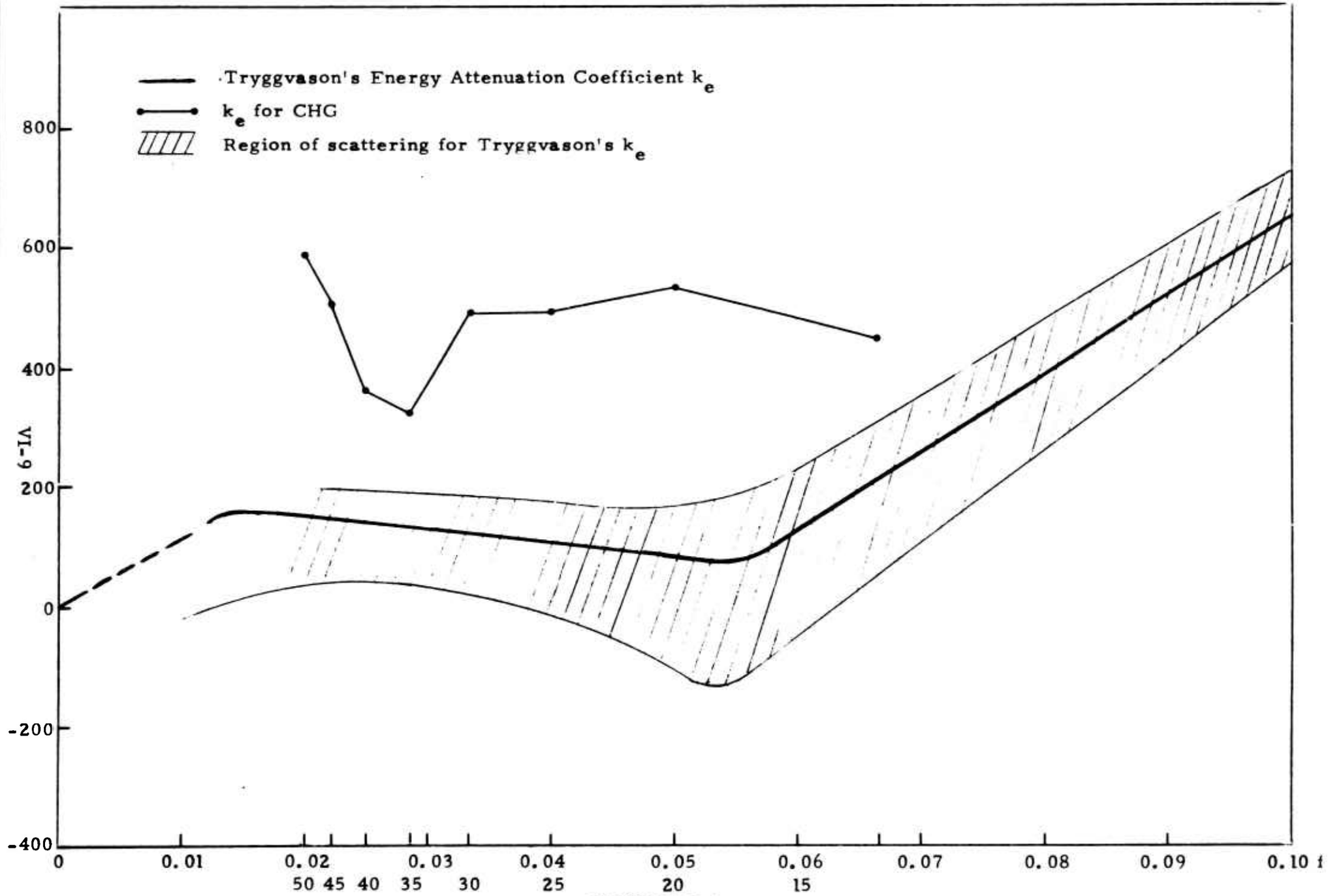

FIGURE VI-4
ENERGY ATTENUATION COEFFICIENT k_e FOR CHG

TABLE VI-4

ESTIMATIONS OF SOURCE PARAMETERS
OBTAINED BY AMPLITUDE SPECTRAL FITTING
BASED ON MINIMUM-RESIDUAL CRITERION

Event I. D.	Optimal Solution				
	Depth h km	Dip Angle δ Degree	Slip Angle λ Degree	Strike $N\phi^{o}E$	Moment 10^{25} dyne-cm
LX/KIRSI/059	42.5	40.0	0.0	170.0	0.768E-01
LX/SSINK/990	47.5	50.0	-60.0	120.0	0.103E-02
LX/NSINK/008	4.0	30.0	30.0	165.0	0.669E-03
LX/SINKI/178	10.0	40.0	60.0	150.0	0.452E-03
LX/NSINK/566	14.0	60.0	30.0	20.0	0.338E-03
LX/SINKI/164	6.0	40.0	30.0	150.0	0.512E-03

TABLE VI-5

ESTIMATIONS OF SOURCE PARAMETERS
OBTAINED BY AMPLITUDE SPECTRAL FITTING
BASED ON DISTRIBUTION OF MINIMUM RESIDUAL CRITERION

Event I. D.	Source Parameters							
	Depth h km		Dip Angle δ^{o}		Slip Angle λ^{o}		Strike Nϕ^{o}E	
	Probable Range[1]	% Confidence	Probable Range[2]	% Confidence	Probable Range[3]	% Confidence	Probable Range[4]	% Confidence
LX/KIRSI/059	40-52.5	83	30-40 70-90	46 37	-60 0-60	25 55	75-100 160-180	37 25
LX/SSINK/990	42.5-55	78	40-60	90	30, 60	71	115-125 155-180	23 41
LX/NSINK/008	4-8	85	30 60-80	30 55	90 -60, 30	42 48	-	-
LX/SINKI/178	6-12	80	30-60	80	30, 60	83	100-135 150-170	48 20
LX/NSINK/566	8-18	75	60-80	75	30	78	15-35 105-125	49 41
LX/SINKI/164	2-8	89	30-40 70-80	54 25	30, 60	75	150-165	39

1. $\Delta h = 2$ km, $0<h<20$ km, $\Delta h = 2.5$ km, $h>20$ km
2. $\Delta\delta = 10^{o}$
3. $\Delta\lambda = 30^{o}$
4. $\Delta\phi = 5^{o}$

parameter of each event is shown in Figures VI-5 to VI-10 with their spectral fits.

Referring to Table VI-4, these six events may be divided into two groups according to their focal depth: (1) LX/KIRSI/059 and LX/SSINK/990 have the deeper focal depth at about 45 km; (2) the other four have shallow focal depths around 5 to 15 km. From the dip angle estimation, these six earthquakes have fault planes dipping from 30° to 60°. The strikes of all but one event, LX/NSINK/566, are oriented approximately N 150° E. The magnitudes of the seismic moments estimated for these events agree with their m_b values from the PDE list in the sense that the larger the m_b values are, the larger the seismic moments will be for the same focal depth.

In general, the percentage confidence of the focal depth estimation is about 80% for about 6 km uncertainty in the shallow focal depths and about 10 km uncertainty in the deeper focal depths. The resolution of the rest of the source parameters is mixed, with the strike distributions generally poor. This might be due to the insufficient azimuthal coverage and incomplete Love wave spectra.

Visually judging the spectral fits, those for the four shallow earthquakes are reasonably good at both stations, while those for the two deeper events are mixed and, in general, are just fair.

C. AMPLITUDE SPECTRAL FITTING USING SPECTRAL RATIOS

Among the six Sinkiang earthquakes, there are two pairs of events which have common observation stations. Referring to Table VI-2, they are: (1) LX/KIRSI/059 and LX/NSINK/008; (2) LX/SINKI/178 and LX/SINKI/164. Common observation stations for the first pair are CHG and TLO; and those for the second pair are FBK and KON. Both pairs of events occur within 5°.

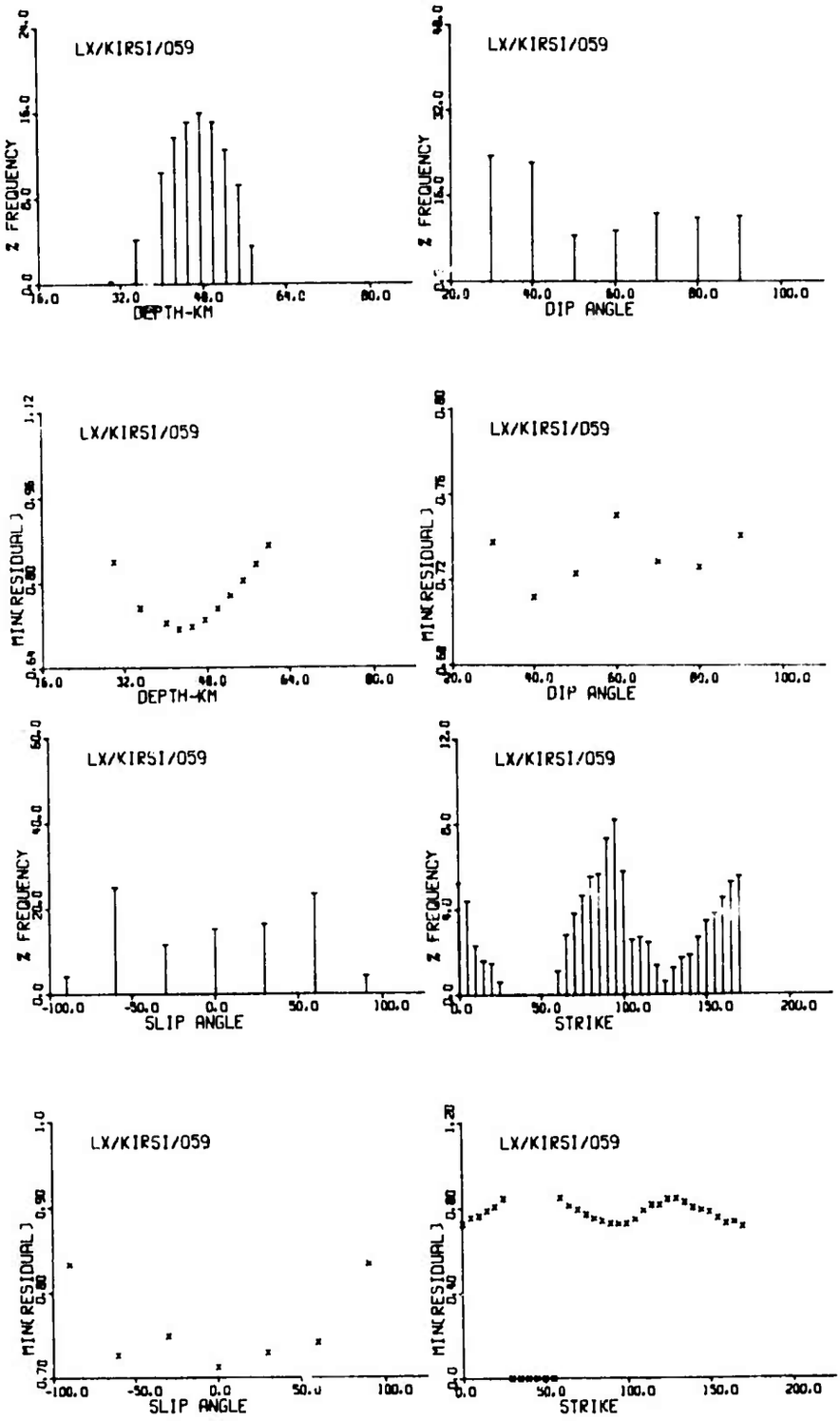

FIGURE VI-5a

RESIDUAL DISTRIBUTIONS FOR LX/KIRSI/059

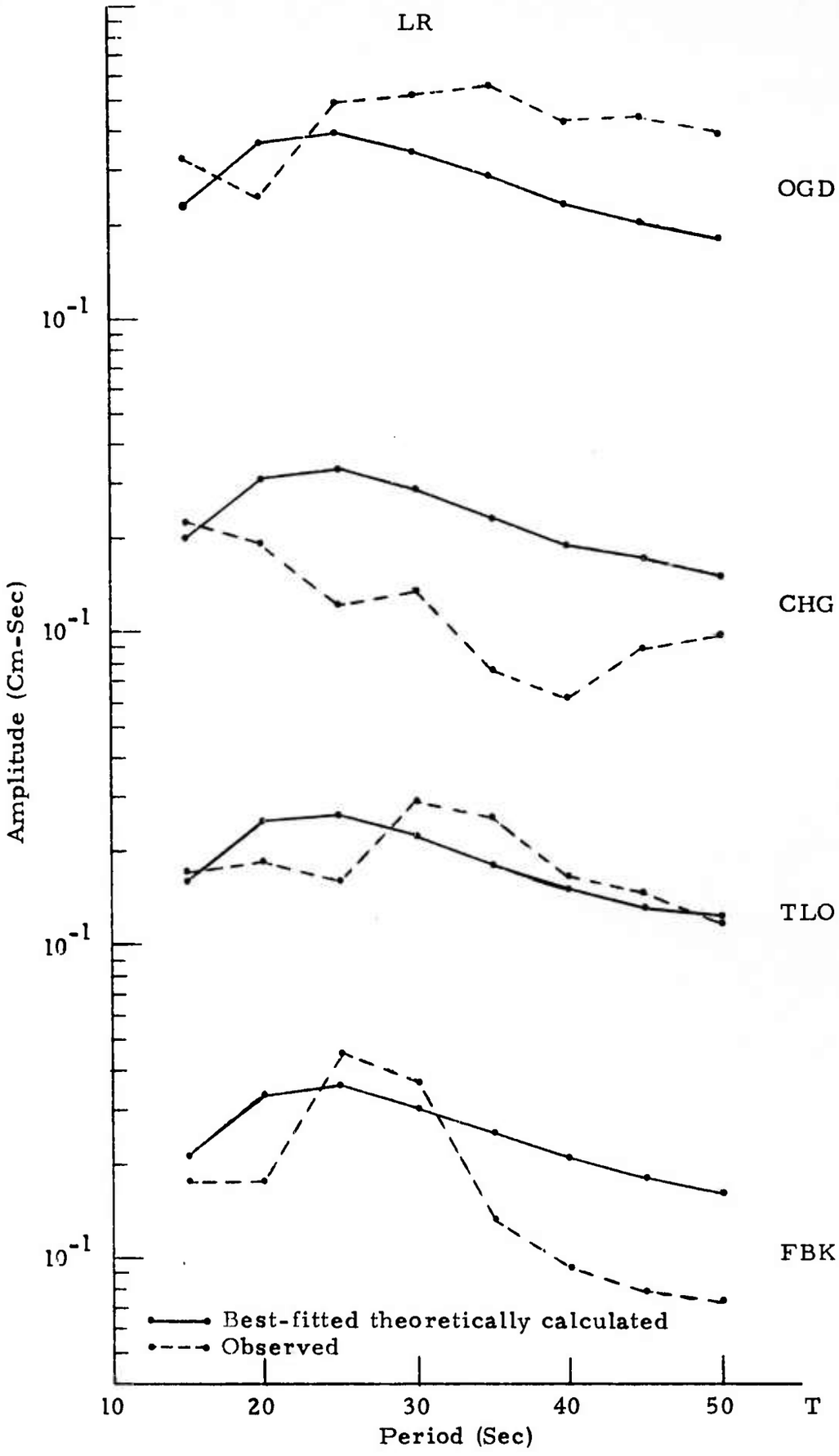

FIGURE VI-5b

RAYLEIGH WAVE SPECTRAL FITS FOR LX/KIRSI/059

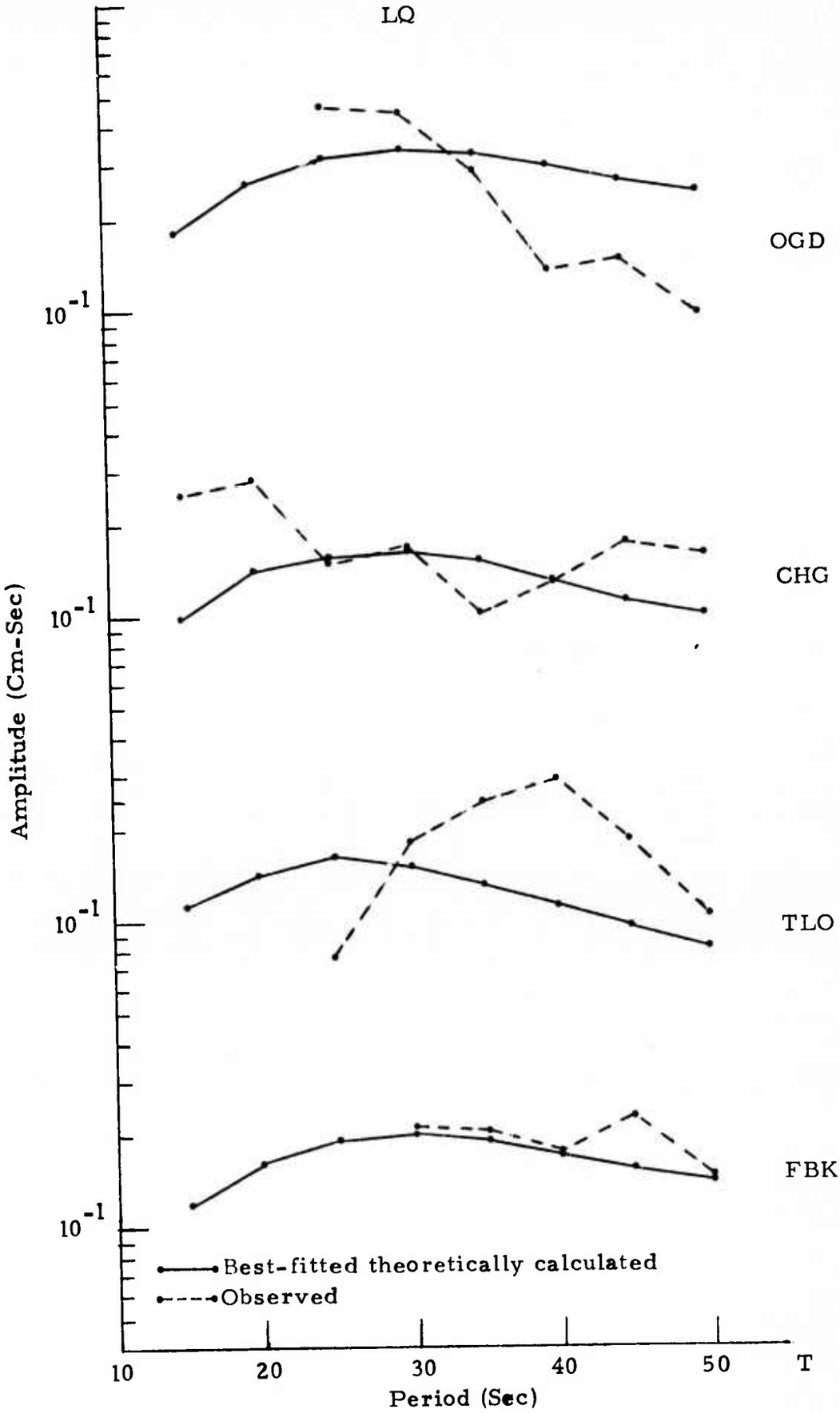

FIGURE VI-5c
LOVE WAVE SPECTRAL FITS FOR LX/KIRSI/059

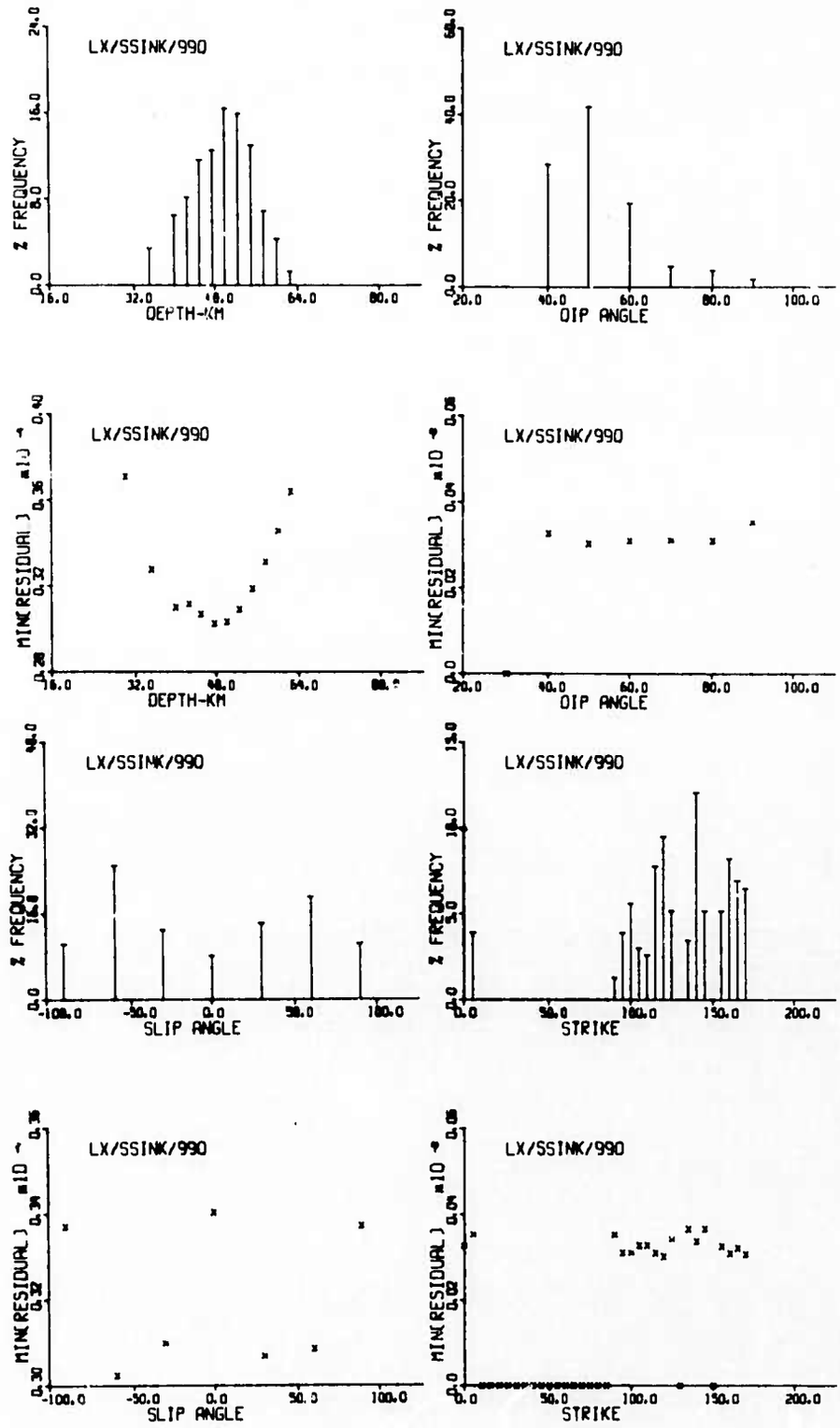

FIGURE VI-6a

RESIDUAL DISTRIBUTIONS FOR LX/SSINK/990

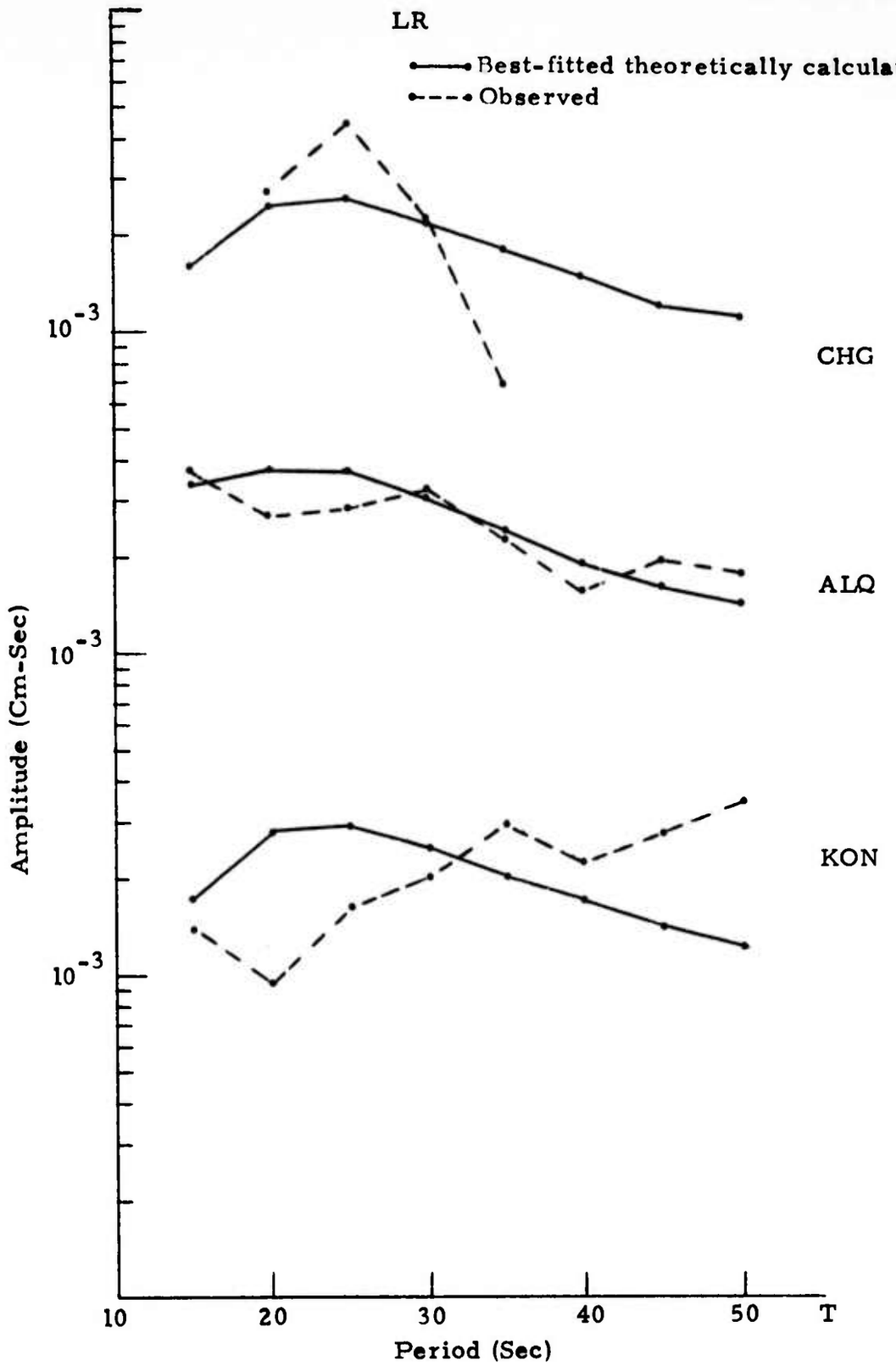

FIGURE VI-6b
RAYLEIGH WAVE SPECTRAL FITS FOR LX/SSINK/990

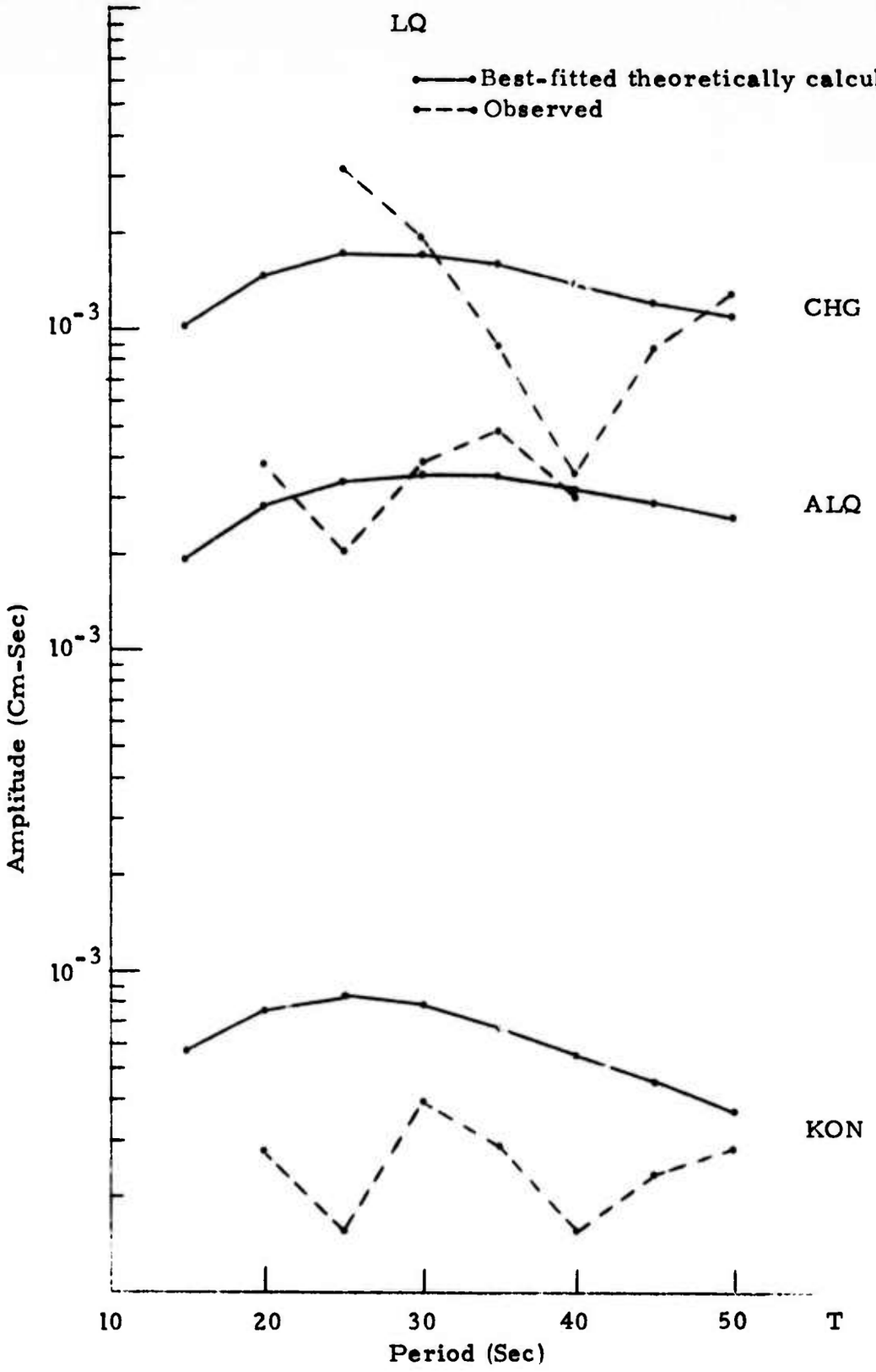

FIGURE VI-6c

LOVE WAVE SPECTRAL FITS FOR LX/SSINK/990

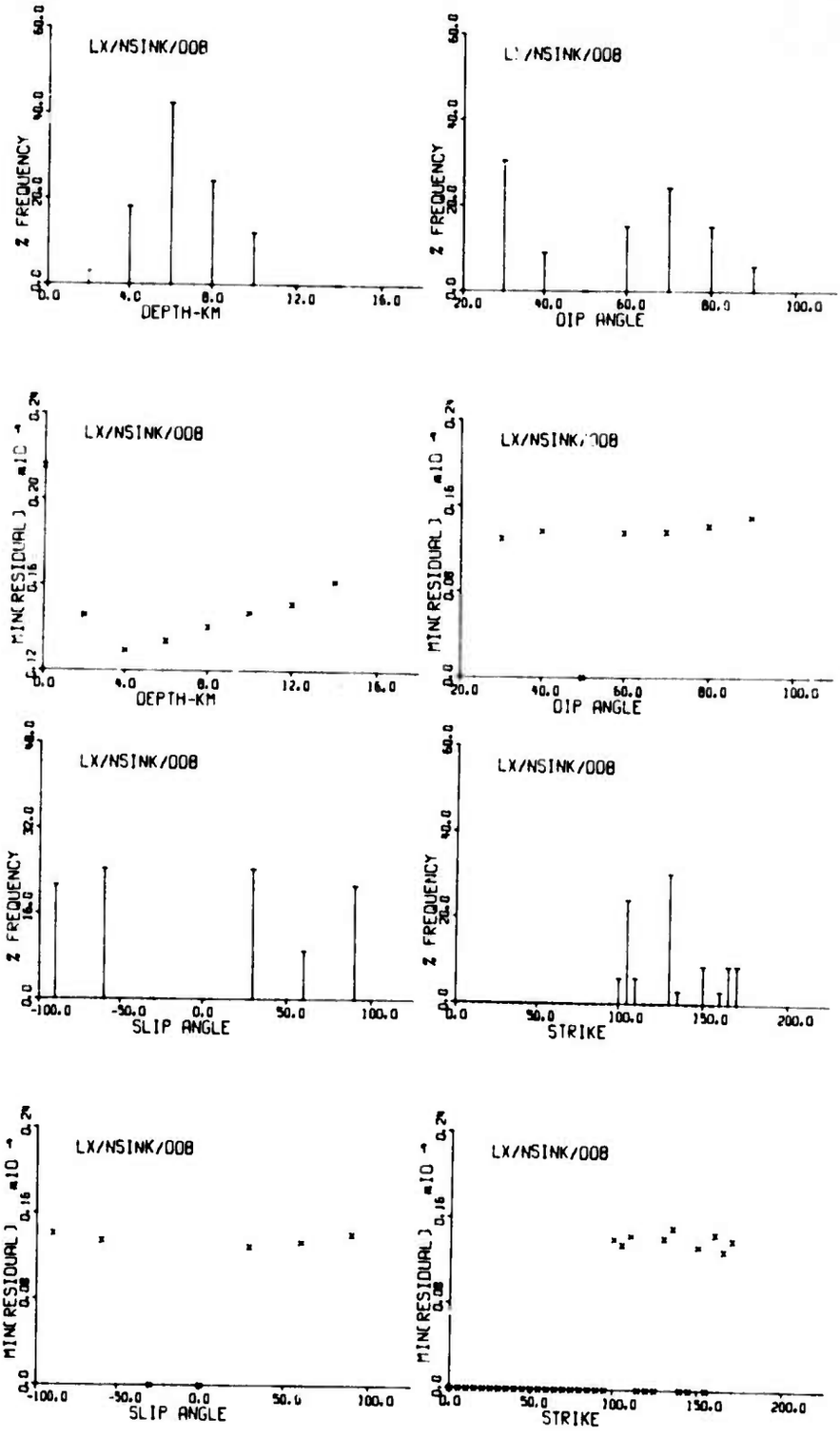

FIGURE VI-7a

RESIDUAL DISTRIBUTIONS FOR LX/NSINK/008

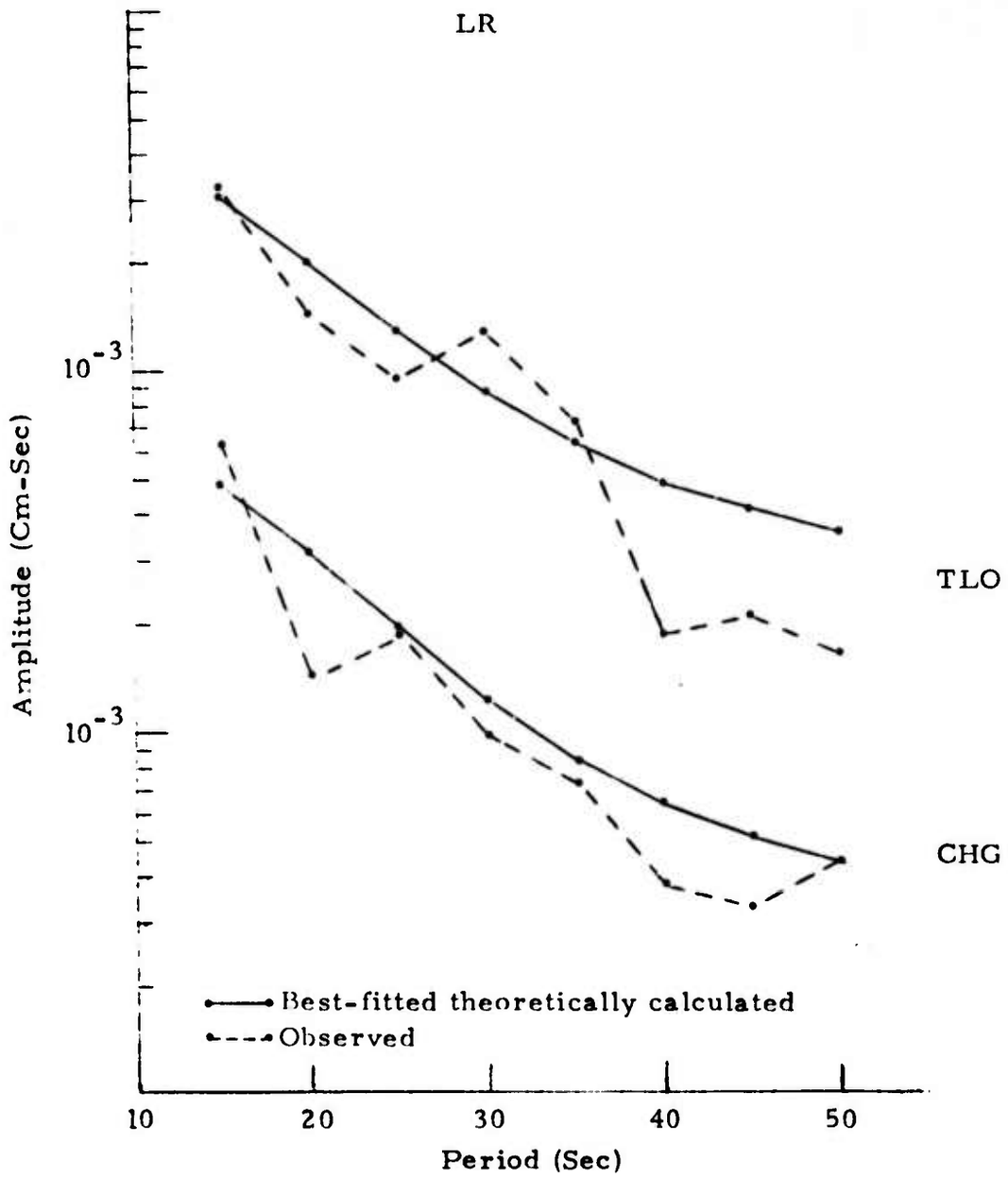

FIGURE VI-7b

RAYLEIGH WAVE SPECTRAL FITS FOR LX/NSINK/008

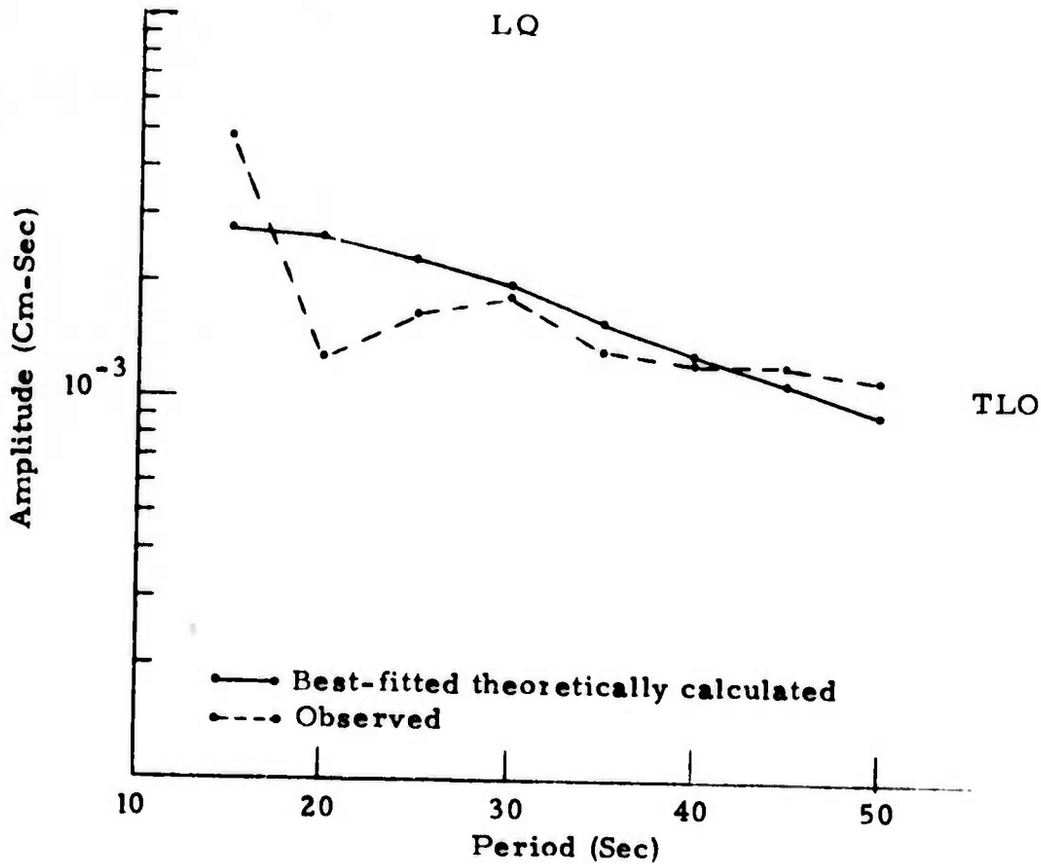

FIGURE VI-7c

LOVE WAVE SPECTRAL FITS FOR LX/NSINK/008

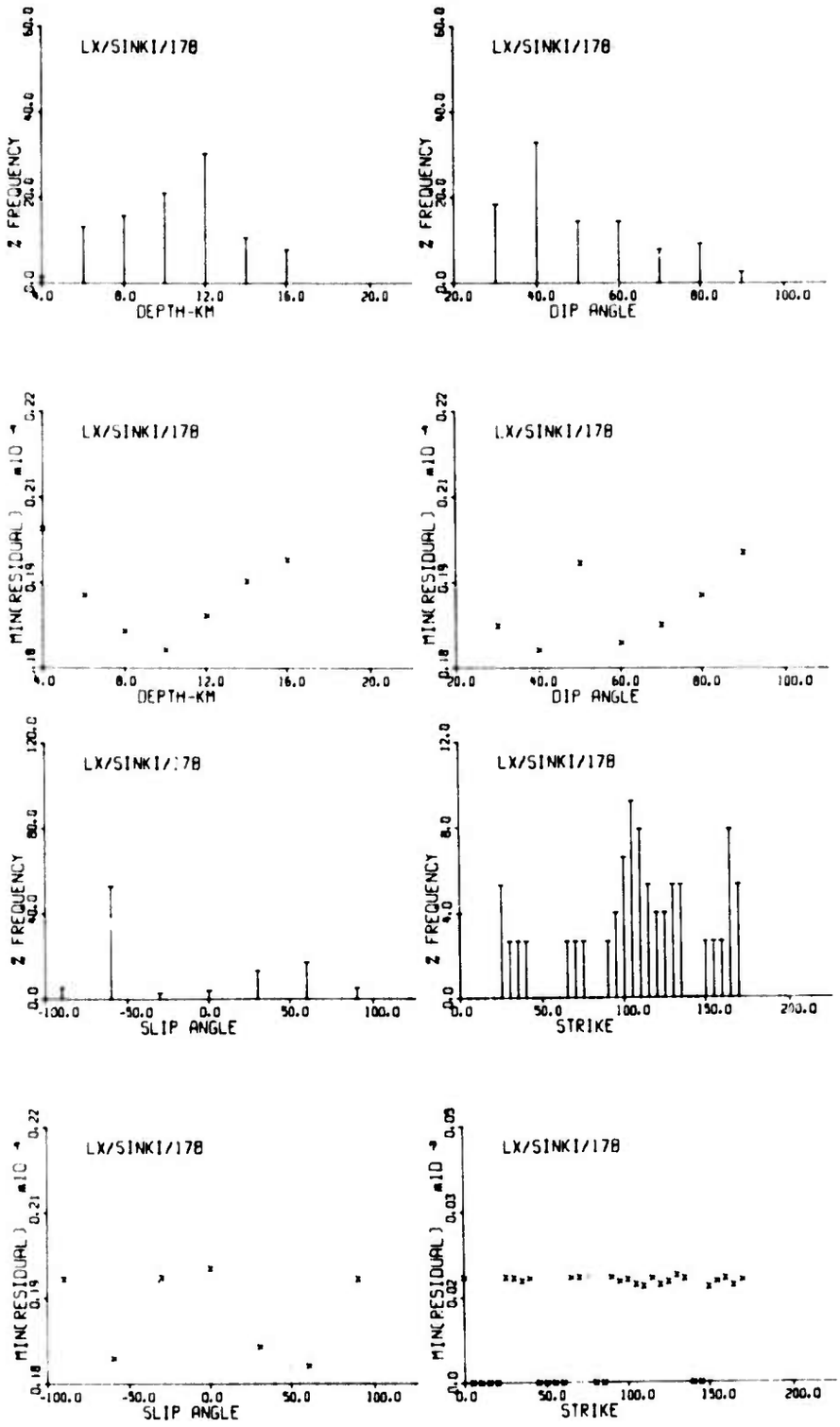

FIGURE VI-8a

RESIDUAL DISTRIBUTIONS FOR LX/SINKI/178

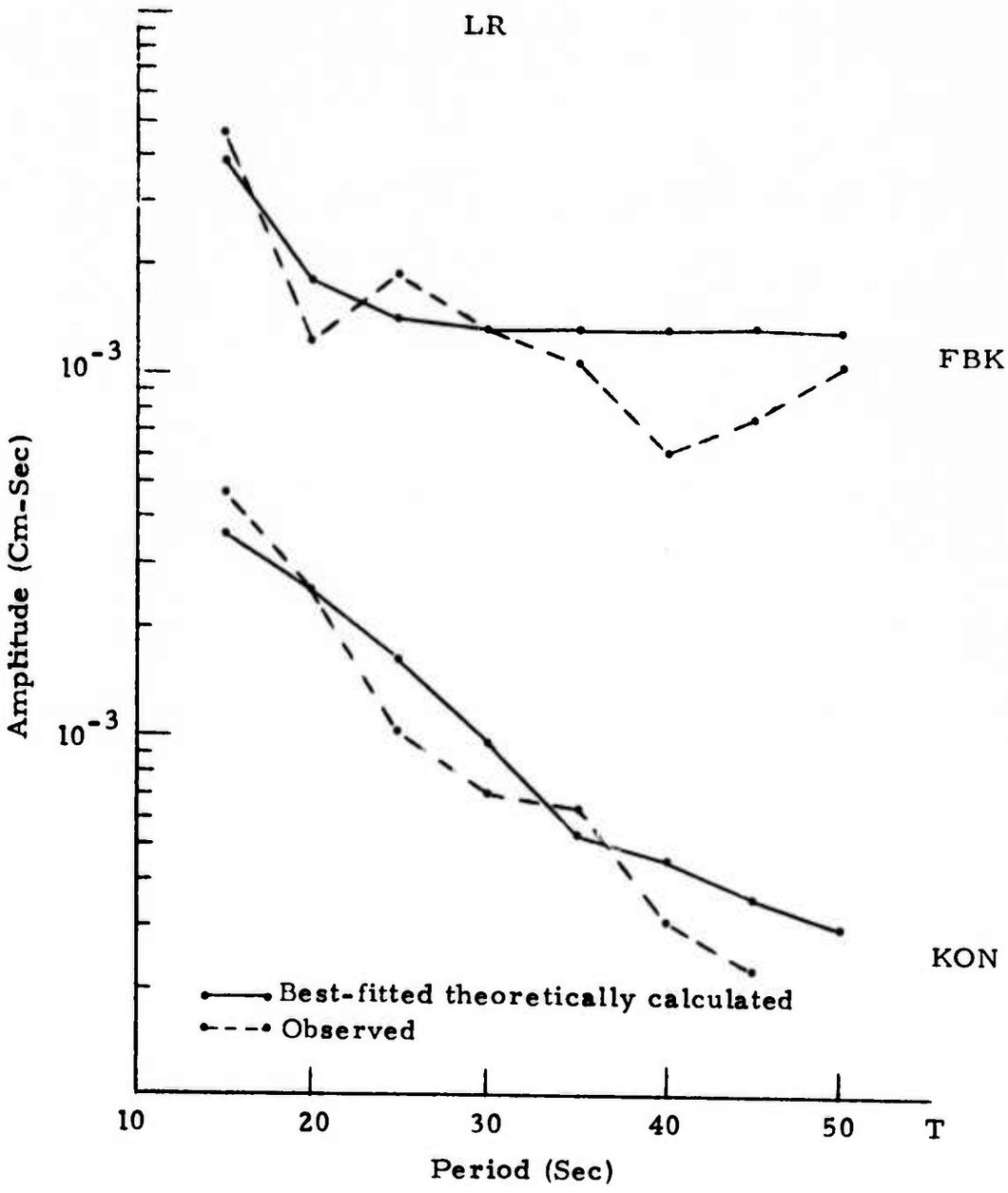

FIGURE VI-8b

RAYLEIGH WAVE SPECTRAL FITS FOR LX/SINKI/178

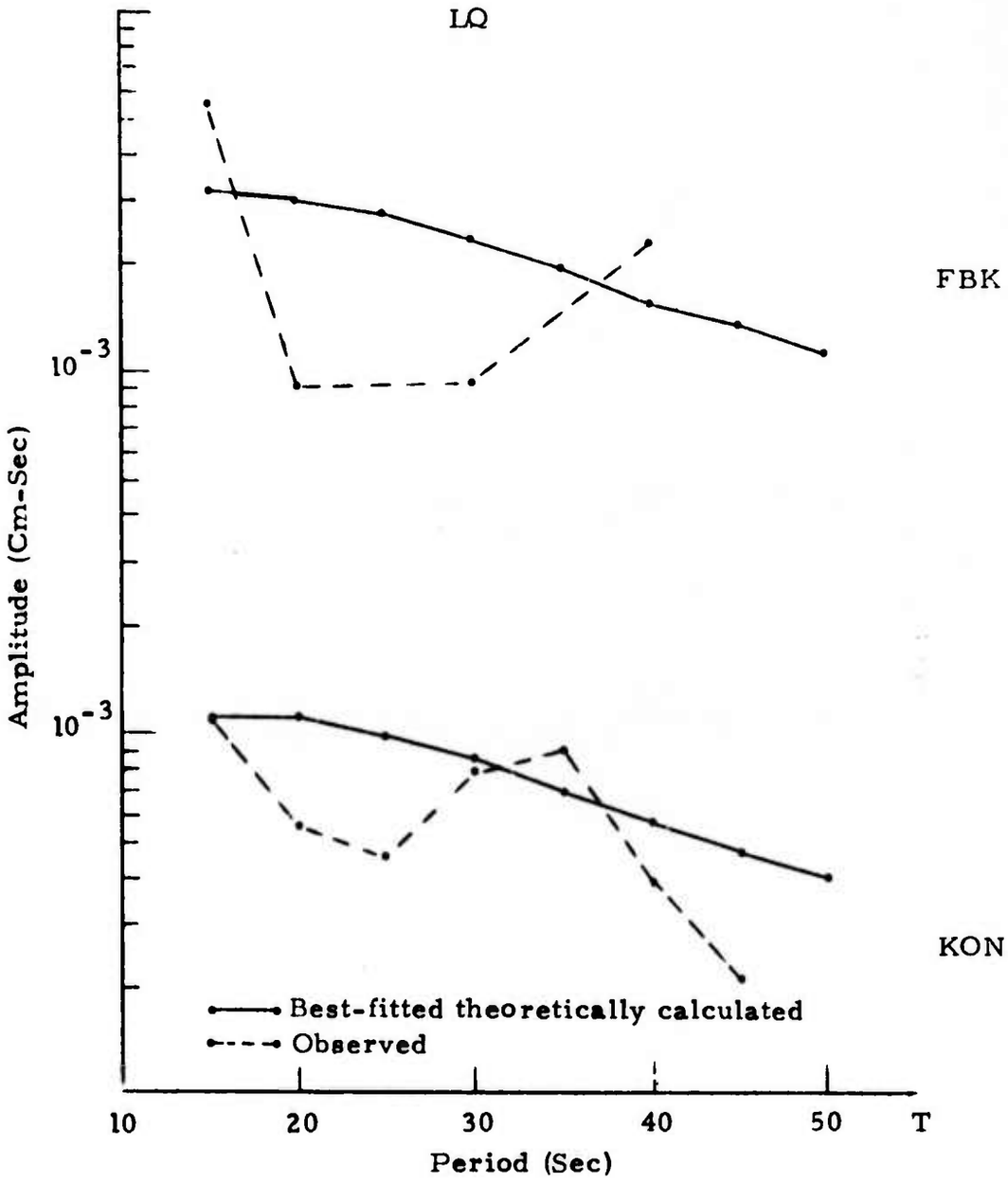

FIGURE VI-8c

LOVE WAVE SPECTRAL FITS FOR LX/SINKI/178

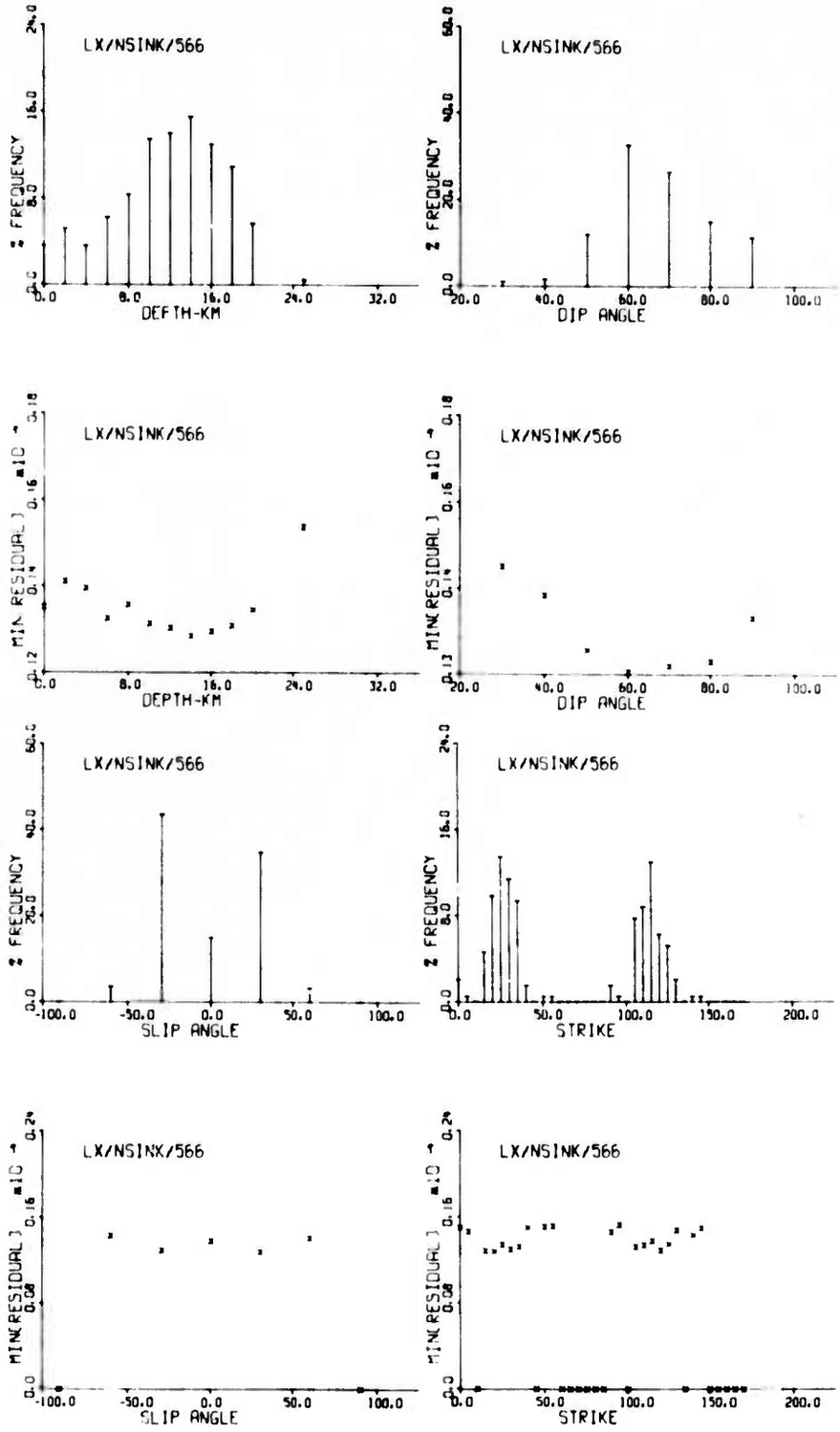

FIGURE VI-9a

RESIDUAL DISTRIBUTIONS FOR LX/NSINK/566

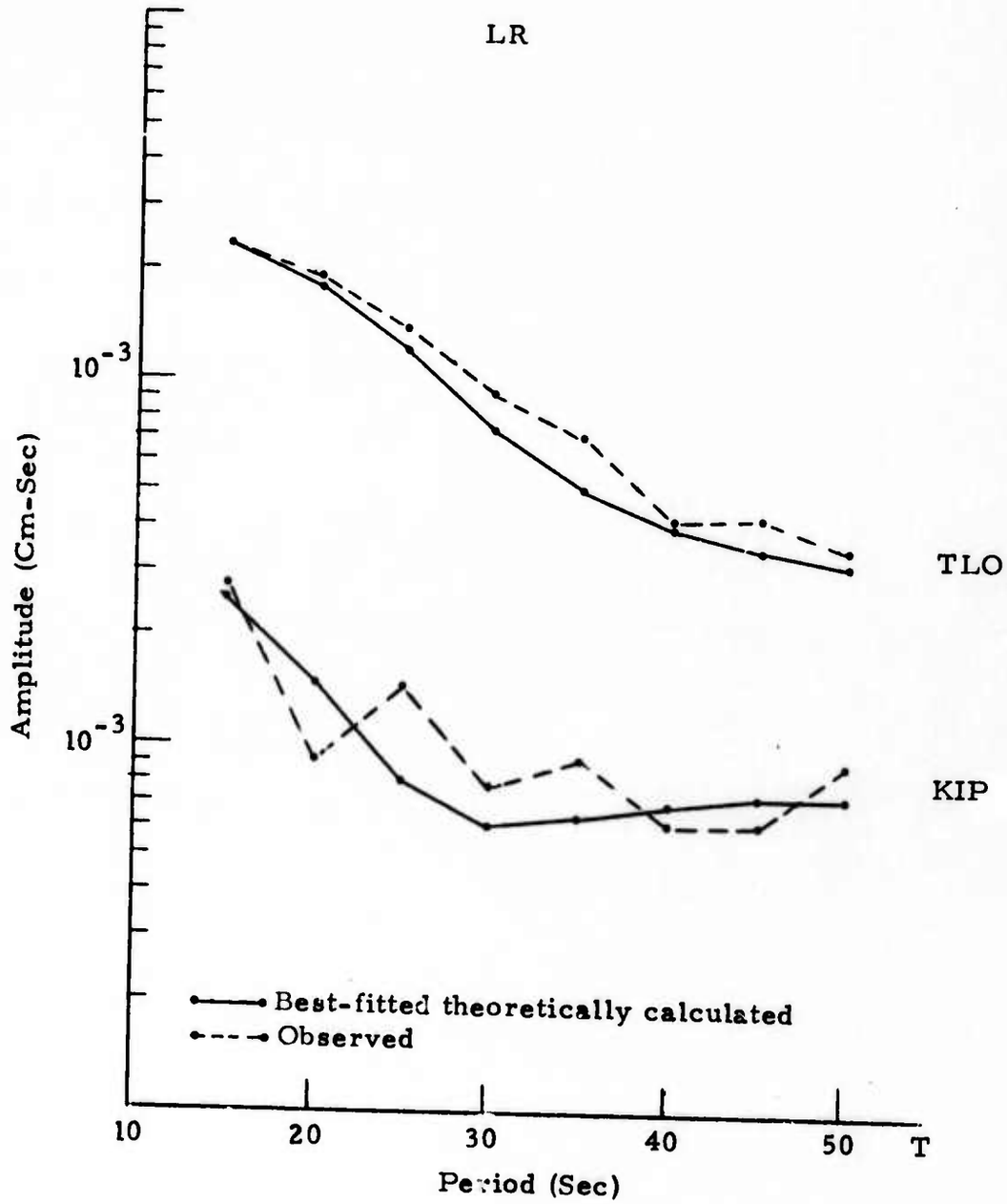

FIGURE VI-9b

RAYLEIGH WAVE SPECTRAL FITS FOR LX/NSINK/566

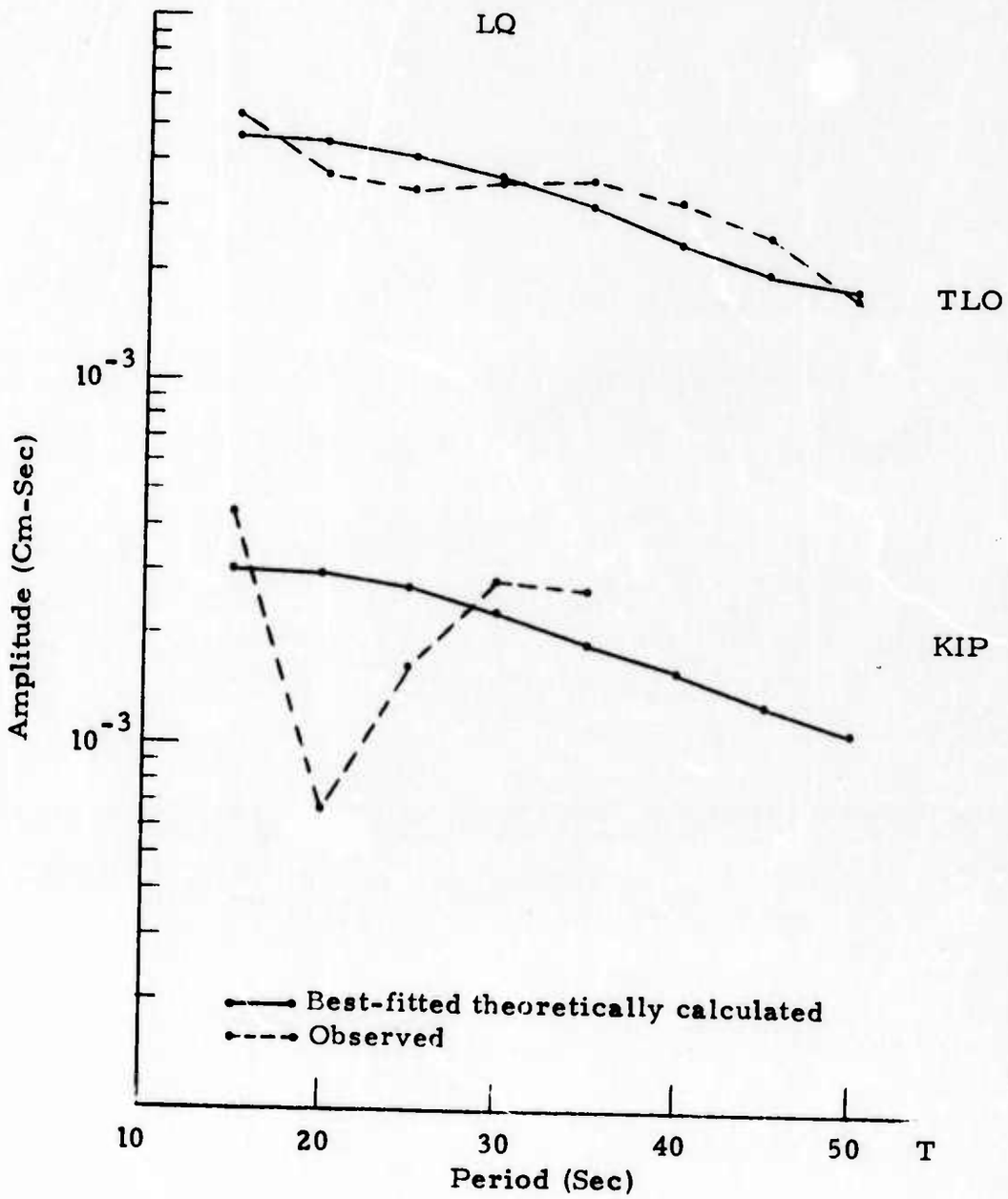

FIGURE VI-9c

LOVE WAVE SPECTRAL FITS FOR LX/NSINK/566

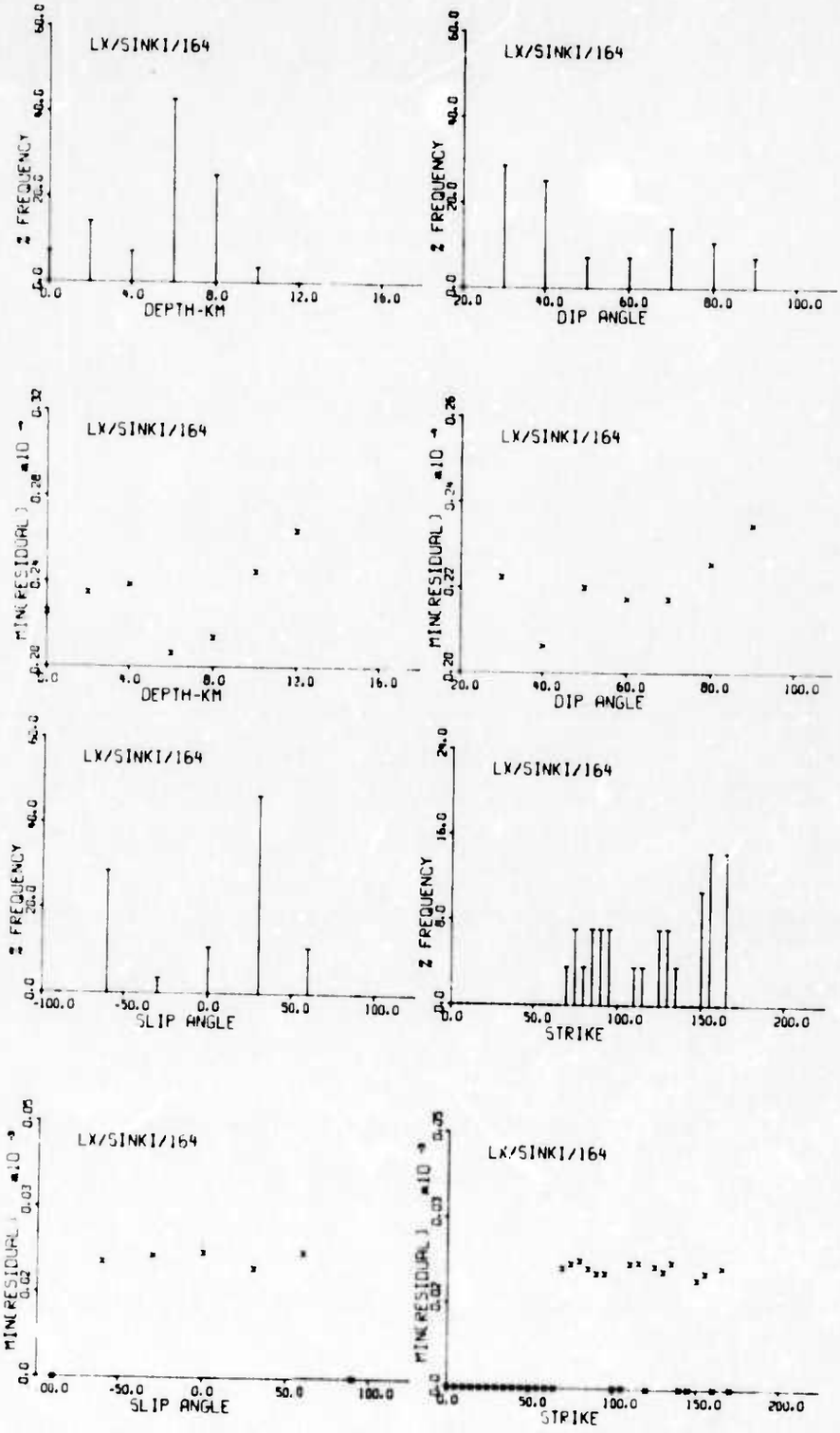

FIGURE VI-10a

RESIDUAL DISTRIBUTIONS FOR LX/SINKI/164

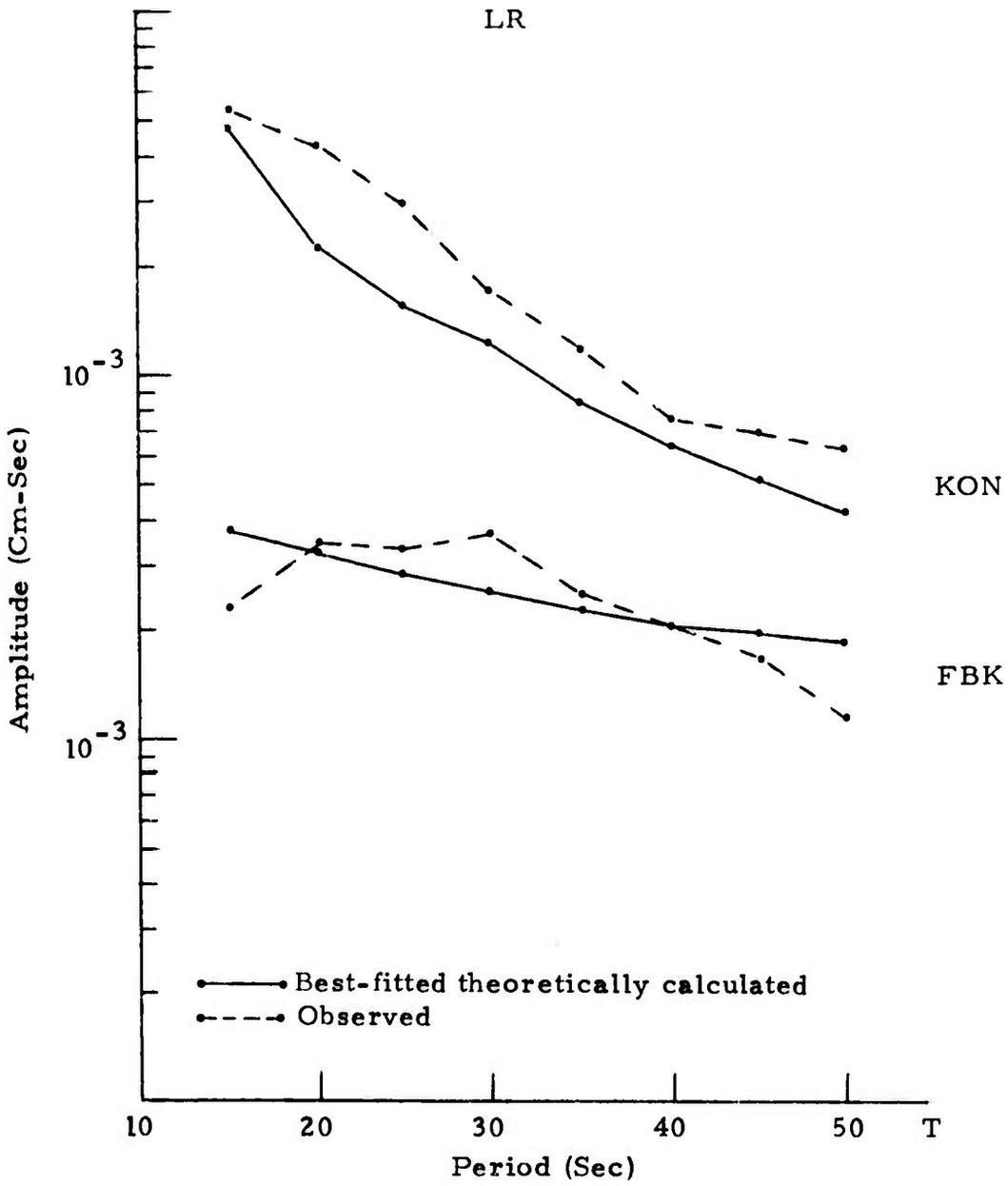

FIGURE VI-10b

RAYLEIGH WAVE SPECTRAL FITS FOR LX/SINKI/164

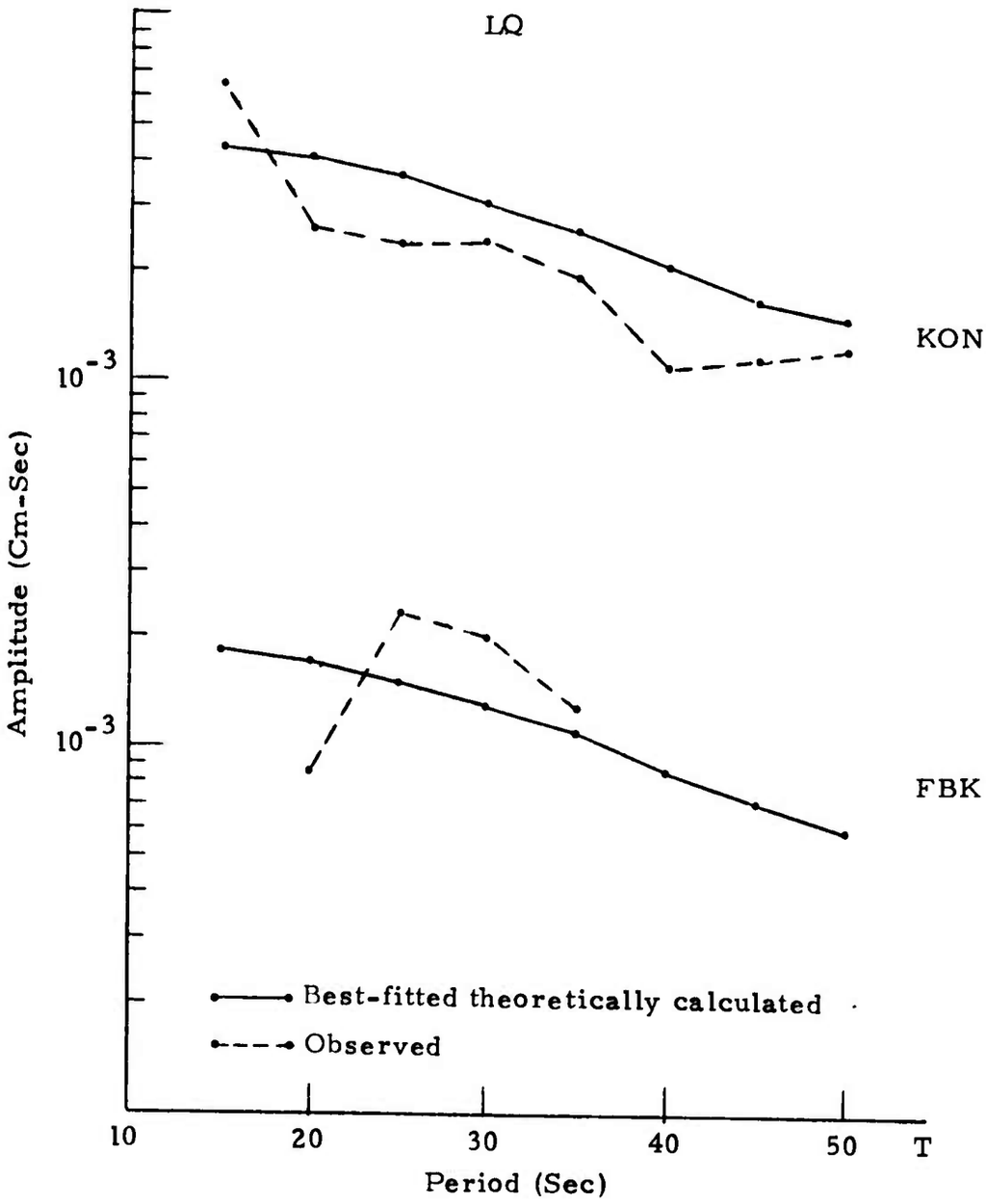

FIGURE VI-10c

LOVE WAVE SPECTRAL FITS FOR LX/SINKI/164

The estimations of source parameters for events LX/NSINK/008, LX/SINKI/178, and LX/SINKI/164 using ratio-of-events fitting with minimum residual and distribution-of-minimum-residual criteria are given in Tables VI-6, VI-7, and VI-8 respectively. The residual distributions are also displayed in Figures VI-11, VI-12, and VI-13. From these results, we can reach the following conclusions:

- For event LX/NSINK/008, the optimal solution of source parameters obtained from the ratio-of-events fitting is somewhat different from that obtained with the individual spectral fit, except for the focal depth estimation. This discrepancy may be due to two reasons: (1) the locations of the two events are not close enough, or (2) the original parameter estimation of LX/KIRSI/059, the reference event, may be not good enough.

- For events LX/SINKI/178 and LX/SINKI/164, the source parameter estimations from spectral ratios are quite comparable with those from amplitude spectral fitting. This seems to firm the good spectral fits obtained for the shallow events.

TABLE VI-6

LX/NSINK/008
ESTIMATIONS OF SOURCE PARAMETERS
OBTAINED BY RATIO-OF-EVENTS FITTING

REFERENCE EVENT: LX/KIRSI/059

SOLUTIONS FOR EVENT: LX/NSINK/008

A. Solution by Minimun-Residual Criterion

Event I. D.	Optimal Solution				
	Depth h km	Dip Angle δ Degree	Slip Angle λ Degree	Strike $N\phi^{o}E$	Moment 10^{25} dyne-cm
LX/NSINK/008	8.0	90.0	$\pm$90.0	130	0.126E-02

B. Solution by Distribution-of-Minimum-Residual Criterion

Event I. D.	LX/NSINK/008	
Source Parameter	Probable Range	% Confidence
h	6-10	86
δ	70-90	83
λ	$\pm$90	74
ϕ	125-130	47

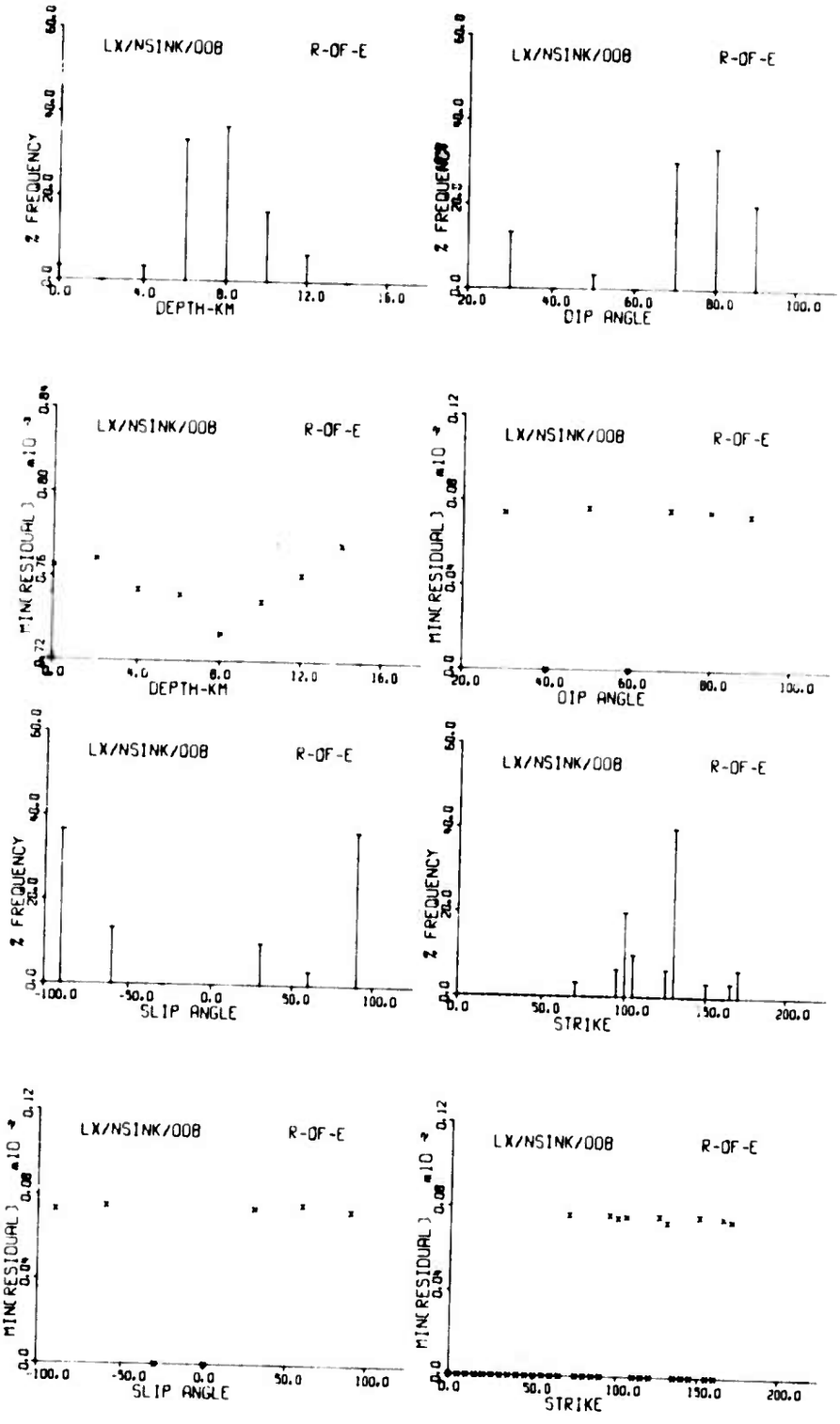

FIGURE VI-11

RESIDUAL DISTRIBUTIONS FOR LX/NSINK/008
DETERMINED BY RATIO OF EVENTS

TABLE VI-7

LX/SINKI/178

ESTIMATIONS OF SOURCE PARAMETERS
OBTAINED BY RATIO-OF-EVENTS FITTING

REFERENCE EVENT: LX/SINKI/164

SOLUTIONS FOR EVENT: LX/SINKI/178

A. Solution by Minimun-Residual Criterion

Event I. D.	Optimal Solution				
	Depth h km	Dip Angle δ Degree	Slip Angle λ Degree	Strike Nϕ^{o}E	Moment 10^{25} dyne-cm
LX/SINKI/178	12.0	30, 60	$\pm$90.0	125.0	0.377E-03

B. Solution by Distribution-of-Minimum-Residual Criterion

Event I. D.	LX/SINKI/178	
Source Parameter	Probable Range	% Confidence
h	10-14	85
δ	30, 60-70	93
λ	$\pm$90	96
ϕ	120-125	89

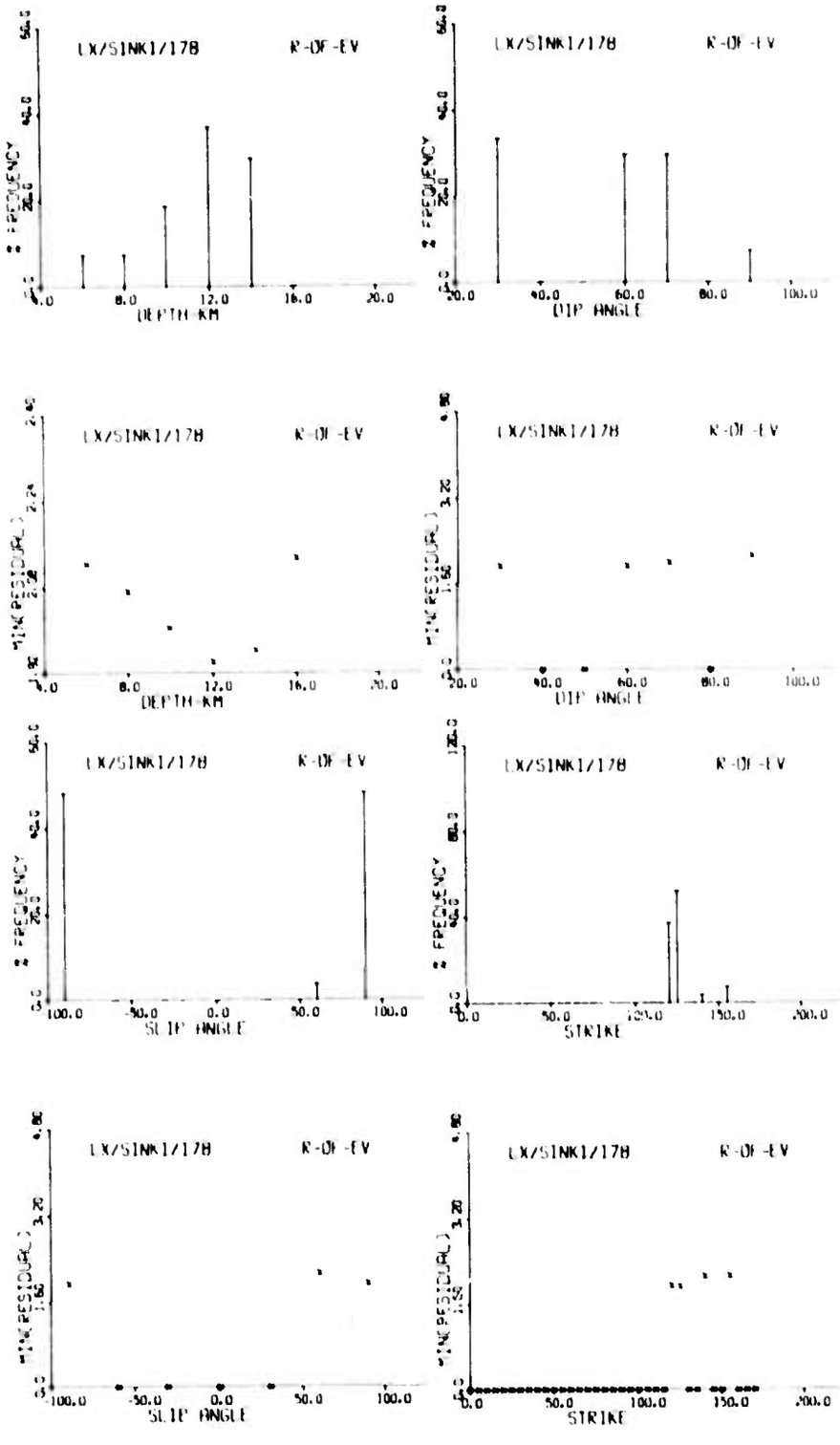

FIGURE VI-12

RESIDUAL DISTRIBUTIONS FOR LX/SINKI/178
DETERMINED BY RATIO OF EVENTS

TABLE VI-8

LX/SINKI/164

ESTIMATIONS OF SOURCE PARAMETERS
OBTAINED BY RATIO-OF-EVENTS FITTING

REFERENCE EVENT: LX/SINKI/178

SOLUTIONS FOR EVENT: LX/SINKI/164

A. Solution by Minimun-Residual Criterion

Event I. D.	Optimal Solution				
	Depth h km	Dip Angle δ Degree	Slip Angle λ Degree	Strike Nϕ^{o}E	Moment 10^{25} dyne-cm
LX/SINKI/164	6.0	60.0	30.0	160.0	0.667E-03

B. Solution by Distribution-of-Minimum-Residual Criterion

Event I. D.	LX/SINKI/164	
Source Parameter	Probable Range	% Confidence
h	4-8	78
δ	50-80	83
λ	$\pm$30	70
ϕ	155-160	57

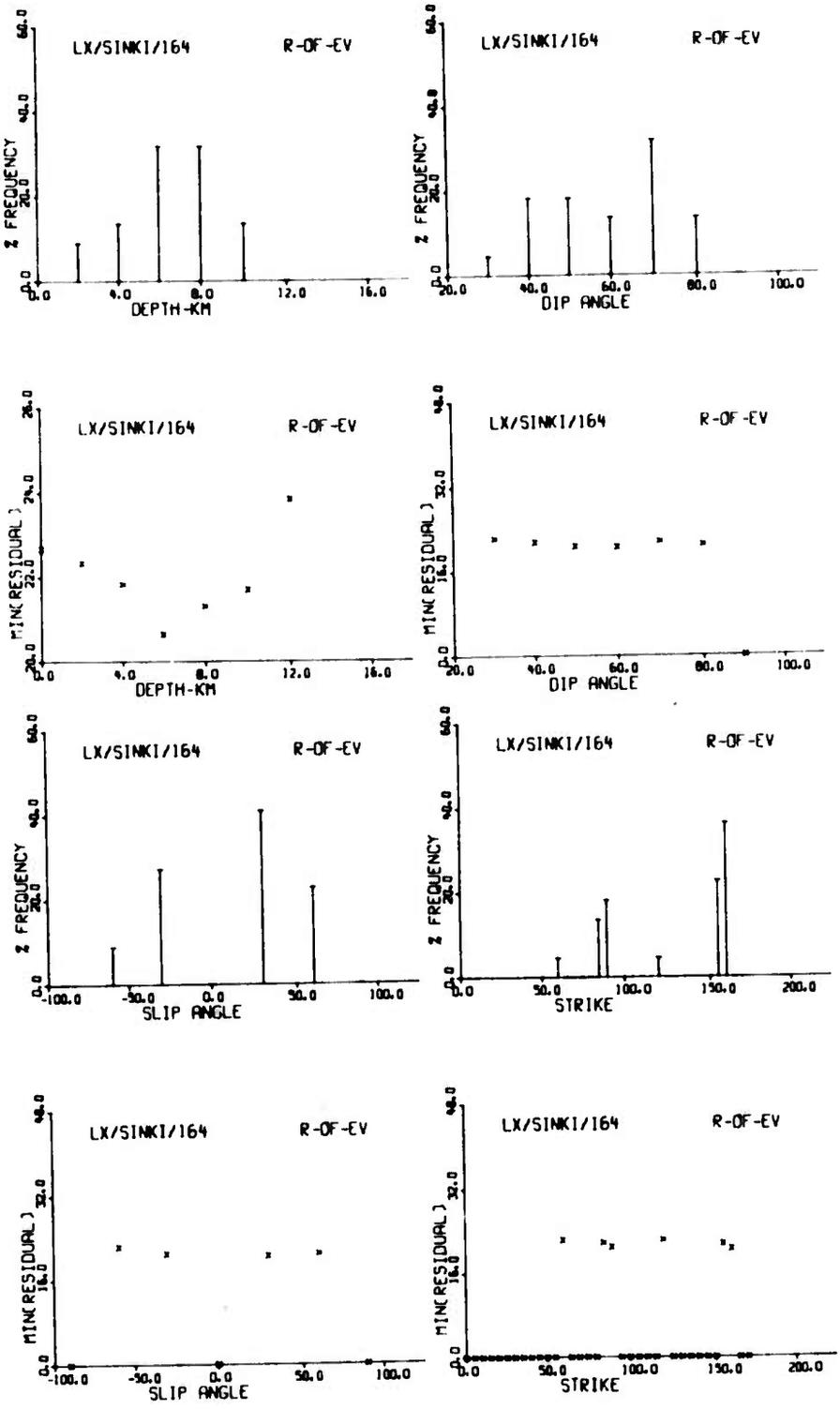

FIGURE VI-13

RESIDUAL DISTRIBUTIONS FOR LX/SINKI/164
DETERMINED BY RATIO OF EVENTS

SECTION VII
CONCLUSIONS AND DISCUSSIONS

The following remarks summarize the results in the preceeding sections concerning source parameter estimates obtained from surface wave data using spectral fitting procedures, both exhaustive and iterative:

- In an effort to examine the uniqueness of our parameter estimates under the minimum residual criteria, initial studies yielded the following results: (1) spectral shape is most sensitive to variations in depth; (2) No readily observable general spectral property characterizes a source parameter's value. Holes in the Rayleigh wave spectrum exist only for almost vertical strike slip faults; (3) A double couple source applied to theoretical Rayleigh wave data yields a non-shallow depth estimate, but from the distribution of possible strike angles, radiation pattern shape, and spectral shape, we see that this solution is an exception. Future studies will examine the source description and layered half space physical properties to see what parameter affects spectral shape the most.

- Analysis of the high quality Rayleigh wave data from the Southeastern Missouri Earthquake of October 21, 1965, yielded good parameter corroboration (4 km depth vs. < 6 km body wave estimate) and excellent spectral fits. Although other parameter estimates varied, the depth estimate did not change for two stations in successive quadrants. Parameter estimates were obtained using four different layered earth models, and

yielded the puzzling result of very little effect on the depth estimate (Δh = 2 km), although the other parameters, including seismic moment, varied a great deal. Future studies will examine this problem in detail.

- The analysis of two, low magnitude ($m_b \doteq 4.1$) Italian events yielded good corroboration with body wave data. These results were obtained using three VLPE stations. Each surface wave record was analyzed for multipathing using narrow band filters, and very little of it was found. This method has proved to be successful, and the results are easy to interpret. These events were also analyzed using spectral ratios. This method assumes that master events, with accurate source parameter estimates, have been obtained for the region of interest. Therefore, by taking spectral ratios, travel path effects have been eliminated. Comparison of this technique with the individual fits were favorable. One problem, though, arose in the spectral fit at TLO. An attenuation study of this travel path will be undertaken.

- Six events from Sinkiang, recorded at VLPE stations during 1972, were analyzed. Because of the mixed quality of the data, the minimum residual distribution statistics were particularly helpful in analyzing the optimal solution. Severe multipathing rendered some Love wave data useless. The effective Q corrections are thought to be inadequate, especially for the CHG travel path. The source parameter analysis yielded mixed results, with the four shallow events thought to have the better solutions. Greater azimuthal coverage should reduce much of the uncertainty. Future studies will include the analysis of seismic regions within Eurasia using VLPE data.

SECTION VIII
REFERENCES

Alexander, S. S., 1963, Surface Wave Propagation in the Western United States, Ph. D. Thesis, Calif. Inst. of Tech., Pasadena, California.

Archambeau, C. B., 1964, Elastodynamic Source Theory, Ph. D. Thesis, Calif. Inst. of Tech., Pasadena, California.

Archambeau, C. B., J. C. Bradfor, P. W. Broome, W. C. Dean, E. A. Flinn and R. L. Sax, 1965, Data Processing Techniques for the Detection and interpretation of Teleseismic Signals, Proc. IEEE, 53, 1860-1884.

Ben-Menaham, A. and D. G. Harkrider, 1964, Radiation Patterns of Seismic Surface Waves from Buried Dipolar Point Sources in A Flat Stratified Earth, J. Geophys. Res., 69, 2605-2620.

Closs, H., 1969, Explosion Seismic Studies in Western Europe, The Earth's Crust and Upper Mantle, Geophys. Mon. 13, 178-188.

Draper, N. R. and H. Smith, 1968, Applied Regression Analysis, Wiley Pub.

Evernden, J. F., 1953, Direction of Approach of Rayleigh Waves and Related Problems (I), Bull. Seismol. Soc. Amer., 27, 393.

Glover, P. and S. S. Alexander, 1969, Lateral Variations in Crustal Structure Beneath the Montana LASA, J. Geophys. Res., 74, 505.

Harkrider, D. G., 1964, Surface Waves in Multilayered Elastic Media: I. Rayleigh and Love Waves from Buried Sources in A Multilayered Elastic Half-Space, Bull. Seismol. Soc. Amer., 54, 627-679.

Lambert, D. G., E. A. Flinn and C. B. Archambeau, 1972; A Comparative Study of the Elastic Wave Radiation from Earthquakes and Underground Explosions, Geophys. J. R. Astr. Soc., 29, 403, 432.

Linville, A. F., 1971, Rayleigh-Wave Multipath Analysis Using A Complex Cepstrum Technique: Special Report No. 2, Texas Instruments, Incorporated, Dallas, Texas.

McEvilly, T. V., 1963, Central U. S. Crust-Upper Mantle Structure from Love and Rayleigh Wave Phase Velocity Inversion, Bull. Seismol. Soc. Amer., 54. 1997-2015.

McKenzie, D., 1972, Active Tectonics of the Mediterranean Region, Geophys. J. R. Astr. Soc., 30, 109-186.

Mitchell, B. J., 1973; Radiation and Attenuation of Rayleigh Waves from the Southeastern Missouri Earthquake of October 21, 1965, J. Geophys. Res., 78, 886-899.

Newton, C. A., 1973, An Investigation of Rayleigh Wave Ellipticity with Applications to Earth Structure, Ph. D. Thesis, Pa. State Uni.

Saito, M., 1967, Excitation of Free Oscillations and Surface Waves by A Point Source in A Vertically Heterogeneous Earth, J. Geophys. Res., 72, 3689-3699.

Tryggvason, E., 1965, Dissipation of Rayliegh Wave Energy, J. Geophys. Res., 70, 1449-1455.

Tsai, Y. B. and K. AKi, 1970a, Source Mechanism of the Truckee, California Earthquake of September 12, 1966, Bull. Seismol. Soc. Amer., 60, 1199-1208.

Tsai, Y. B. and K. AKi, 1970b, Precise Focal Depth Determination from Amplitude Spectra of Surface Waves, J. Geophys. Res., 75, 5729-5743.

Tsai, Y. B., 1972a, Utility of Tsai's Method for Seismic Discrimination: Semiannual Technical Report No. 1, Texas Instruments, Incorporated, Dallas, Texas.

Tsai, Y. B. and W. W. Shen, 1972, Utility of Tsai's Method for Seismic Discrimination: Final Technical Report, Texas Instruments, Incorporated, Dallas, Texas.

Turnbull, L. S., 1972, Surface Wave Radiation from A Buried Volume Relaxation Source in A Multilayered Half-Space, 53rd Annual Meeting, American Geophys. Union.

Turnbull, L. S. and S. S. Alexander, 1973, Determination of Source Parameters for Several Mid-Atlantic Ridge Events Using Surface Wave Radiation Patterns, Seismol. Soc. Amer. Meeting.

Von Seggern, D. H., 1971, Effects of Propagation Paths on Surface-Wave Magnitude Estimates, SDL Rept. No. 279, Teledyne Geotech.

Weidner, D. J., 1972, Rayleigh Waves from Mid-Ocean Ridge Earthquakes: Source and Path Effects, Ph. D. Thesis, MIT, Cambridge, Mass.

APPENDIX A

TWO METHODS FOR DETERMINING AN EFFECTIVE Q

All methods for correcting for effective attenuation involves a correction for geometrical spreading, which can be written:

$$A_{cr_o} = A_{op} \left(\frac{R_e \sin \Delta_p}{r_o} \right) \qquad \text{(A-1)}$$

where: A_{cr_o} - Amplitude corrected to field point r_o
A_{op} - Observed amplitude at field point p
Δ_p - Distance between source and field point p
R_e - Radius of Earth

The geometrical spreading correction is included in the equations of both of the following corrections.

TRYGGVASON'S APPROACH

The basic assumption in Tryggvason's (1965) approach is that equal energy is transmitted in all directions from the source. Therefore, this method is particularly useful when applied to explosion data. It is also assumed that wave energy is not transferred from one frequency band to another. In other words, spectral modulations resulting from multipathing have been eliminated. The total energy in a narrow frequency band at distance D from the source is:

$$E_o = E_o e^{-Dk} = C_1 A^2 \sin \Delta \qquad \text{(A-2)}$$

where: E_o - total energy of the frequency band at the source

k - coefficient of energy dissipation

A - Fourier amplitude

Δ - epicentral distance in radians

C_1, C_2 - constants for each frequency

Taking natural logarithms of equation (A-2)

$$\ln E_o - Dk = \ln C_1 + 2\ln A + \ln \sin\Delta \qquad \text{(A-3)}$$

Letting $E_o = C_1 A_o^2$ and $C_2 = 2\ln A_o$, then

$$2\ln A + \ln \sin\Delta = C_2 - Dk \qquad \text{(A-4)}$$

A least squares fit of the points obtained at several azimuths and distances will yield an average k (attenuation coefficient) for the region.

TWO-STATION METHOD

By simply equalizing the amplitude between two stations (Tsai and Aki, 1970a) we obtain

$$Q(f) = \frac{\pi f (r_2 - r_1)}{U(f)} \Big/ \ln \frac{A_1(f)}{A_2(f)} \sqrt{\frac{\sin\Delta_1}{\sin\Delta_2}} \qquad \text{(A-5)}$$

where: $U(f)$ - group velocity

$A_1(f)$ - spectral amplitude at station 1

$A_2(f)$ - spectral amplitude at station 2

r_1, r_2 - epicentral distances in km

Δ_1, Δ_2 - epicentral distances in radians

This method demands high quality spectra. It is also highly desirable to have several stations along the great circle path to eliminate minor spectral perturbations.

APPENDIX B

DETERMINATION OF FUNDAMENTAL MODE AMPLITUDE SPECTRA AND GROUP VELOCITIES BY NARROW BAND FILTERING

It has been shown by Evernden (1953) that the propagation paths for surface waves are greatly altered by lateral velocity changes along the path and depend on frequency. Further evidence of such effects was given by Alexander (1963), Glover and Alexander (1969), and Newton (1973). The result of this phenomenon, known as multipathing, should be analyzed as a function of frequency. The effect of multipathing is usually an introduction of anomalies (short period peaks) into the power spectrum of the signal. Because the determination of source parameters from far-field radiation patterns involves studying fundamental mode amplitude spectra, a method for de-multipathing a spectrum is required.

One method which has proved to be successful in de-multipathing is the application of a series of narrow band filters [Alexander (1963), Archambeau et al (1965), Newton (1973)]. Given a signal's time series f(t) and power spectrum $F(\omega)$, one chooses a frequency to be examined ω_o. A narrow band,

$$B = \left[\omega_o - \frac{\Delta\omega}{2}, \ \omega_o + \frac{\Delta\omega}{2}\right]$$

defines a unit rectangular function by

$$H(\omega) = 1 \text{ if } \omega \in B \ [\text{then } \hat{F}(\omega) = F(\omega)\, H(\omega)]$$

$$= 0 \text{ otherwise.}$$

If $\Delta\omega$ is sufficiently small, the inverse Fourier transform of $\hat{F}(\omega)$ will be a well behaved oscillating function, $\hat{f}(t)$, which attains one or more distinct local maxima

$$\hat{f}_1 = \hat{f}(t_1) \geq \hat{f}_2 = \hat{f}(t_2) \geq \hat{f}_3 = \hat{f}(t_3) \geq \ldots$$

The times $[t_i]_{i=1}^{N}$ indicate the relative arrival time of wave groups represented by the superposition of frequencies in the band B. When multipathing occurs, N>1 for some periods(s), $T_o = \frac{2\pi}{\omega_o}$.

Now suppose one chooses as the frequencies to be examined

$$\omega_{o,K} = T_{o,K}^{-1} \cdot 2\pi = (10+5K)^{-1} \cdot 2\pi \qquad K = 1, 2, \ldots 10$$

(or periods (T) 10 to 60 seconds), and we want the wave packet functions $\hat{f}_{i,K}$ to exhibit M cycles. From Fourier transform theory,

$$\Delta t \Delta\omega \doteq 4\pi^2 \longrightarrow \Delta\omega \doteq \frac{4\pi^2}{\Delta t}$$

and

$$M = \frac{\omega_{o,K}}{2\pi} \Delta t = \frac{\Delta t}{T_{o,K}} \longrightarrow \Delta t = T_{o,K} M$$

Therefore

$$\Delta\omega_K \doteq 4\pi^2 / T_{o,K} M \qquad K = 1, 2, \ldots 10$$

Using this technique, we obtain the relative arrival times $[t_i]_{L=1}^{N_K}$, and using

the station to source distance (Δ), the origin time of the event (t_o), the trace start time, t_s, we obtain group velocities

$$\left[U_{i,K} = \frac{\Delta}{t_s - t_o + t_{i,K}}\right]_{i=1}^{N(K)}, \qquad K=1, 2, \ldots 10$$

Comparing these group velocity points to average group velocity curves enables one to choose a "best" $U_{i,K}$ and corresponding $\hat{f}_{i,K}$ for each frequency (K).

APPENDIX C

A DISLOCATION EARTHQUAKE SOURCE-TIME FUNCTION

If we designate the source-time function of the theoretical earthquake dislocation as D(t), then the time function of the theoretical force system (single, couple, douple couple, etc. forces) which causes that dislocation should be proportional to the second derivative of D(t); therefore

$$F(t) \alpha \frac{d^2 D(t)}{dt^2} \tag{C-1}$$

Thus, if a unit-step function (which is the limiting form of a ramp function) is chosen for the theoretical dislocation, i.e.

$$\begin{aligned} D(t) = C_1 U(t) &= \lim_{\tau \to 0} C_1 \left(1 - e^{-t/\tau}\right) \qquad t \geq 0 \\ &= 0 \qquad\qquad\qquad\qquad\quad t < 0 \end{aligned} \tag{C-2}$$

where: C_1 and τ are constants

$$\begin{aligned} U(t) &= 1 \qquad t \geq 0 \\ &= 0 \qquad t < 0 \end{aligned}$$

then the time function of the force system will be a doublet function according to (C-1). Therefore,

$$F(t) \alpha \frac{d^2 U(t)}{dt^2}$$

$$\alpha \frac{d\delta(t)}{dt} = \delta\rho(t) \tag{C-3}$$

where: $\delta(t)$ is a Dirac delta function

$\delta_\rho(t)$ is a doublet function

Now, let the spectral amplitudes of the surface waves due to the douple couple force of 1 dyne-cm seismic moment with temporal variation of a Dirac delta function as given by Saito (1967) or Harkrider (1964) be $A_\delta^{DC}(\omega)$. Then the spectral amplitude of the surface waves due to double couple forces with general temporal variation as $L_\ell(t)$ will be

$$A_{M_\ell}^{DC}(\omega) = M_\ell \, L_\ell(\omega) A_\delta^{DC}(\omega) \qquad \text{(C-4)}$$

$$\text{where } L_\ell(\omega) = \left| \int_{-\infty}^{\infty} L_\ell^o(t) e^{-i\omega t} \, dt \right|$$

$$\text{with } L_\ell(t) = M_\ell \, L_\ell^o(t)$$

For douple couple forces varying with time as a doublet function as given in (C-3), corresponding to a unit-step function of the dislocation, then according to (C-4), we have

$$A_{M_\ell}^{DC}(\omega) = (M_\ell \, \omega) \, A_\delta^{DC}(\omega) \qquad \text{(C-5)}$$

since $L_\ell(t) = M_\ell \, \delta_\rho(t)$, then $L_\ell(\omega) = \omega$.

APPENDIX D
REPRESENTATIVE EARTH STRUCTURES

In order to determine the effect of earth structure on the source parameters obtained from either an exhaustive or non-linear regression approach, a series of representative structures must be analyzed. Because we are mainly concerned with events originating in Eurasia, four continental structures have been chosen.

A Gutenburg-Bullen standard earth model is shown in Figure D-1, with its normal high velocity crust. A thicker, higher velocity crust on top of this standard model is shown in Figure D-2. This model is a good approximation for the Tibetian Plateau. Figure D-3 shows a model for the Central United States (McEvilly, 1963) which differs from the standard model by higher crustal density and shear wave velocity (V_s). Finally, a very low velocity crust reflecting sedimentary layers is given by the Hamilton-Healy Earth Model in Figure D-4.

Rayleigh and Love group velocity curves are shown in Figures D-5 and D-6, respectively. We see that while the Central U.S. and Gutenburg-Bullen structures yield almost identical curves, the Hamilton-Healy yields lower velocities at shorter periods while the Tibetian Plateau yields lower velocities at longer periods.

FIGURE D-1
GUTENBERG - BULLEN EARTH MODEL

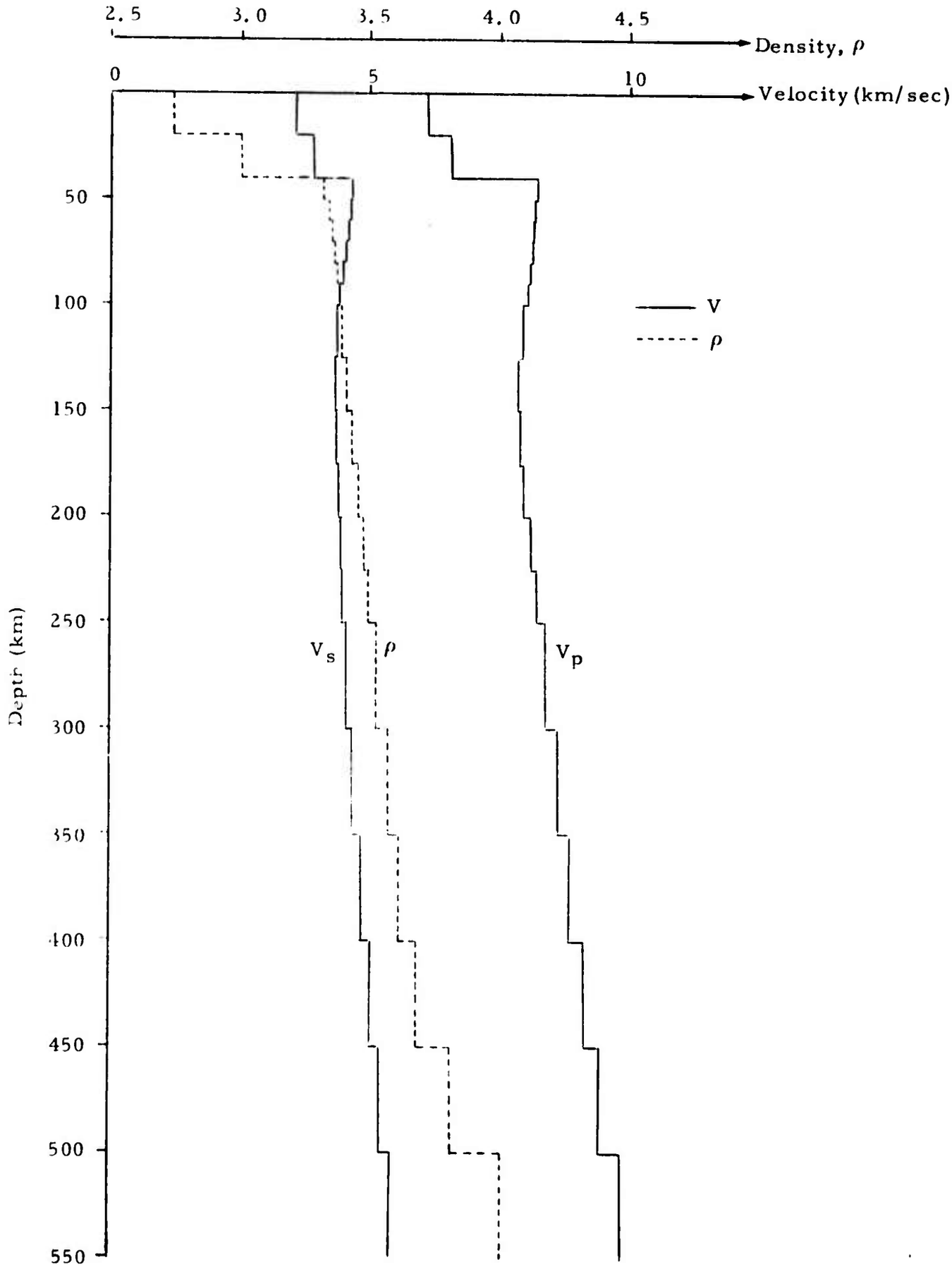

FIGURE D-2

A 56-Km CRUSTAL MODEL FOR TIBET PLATEAU

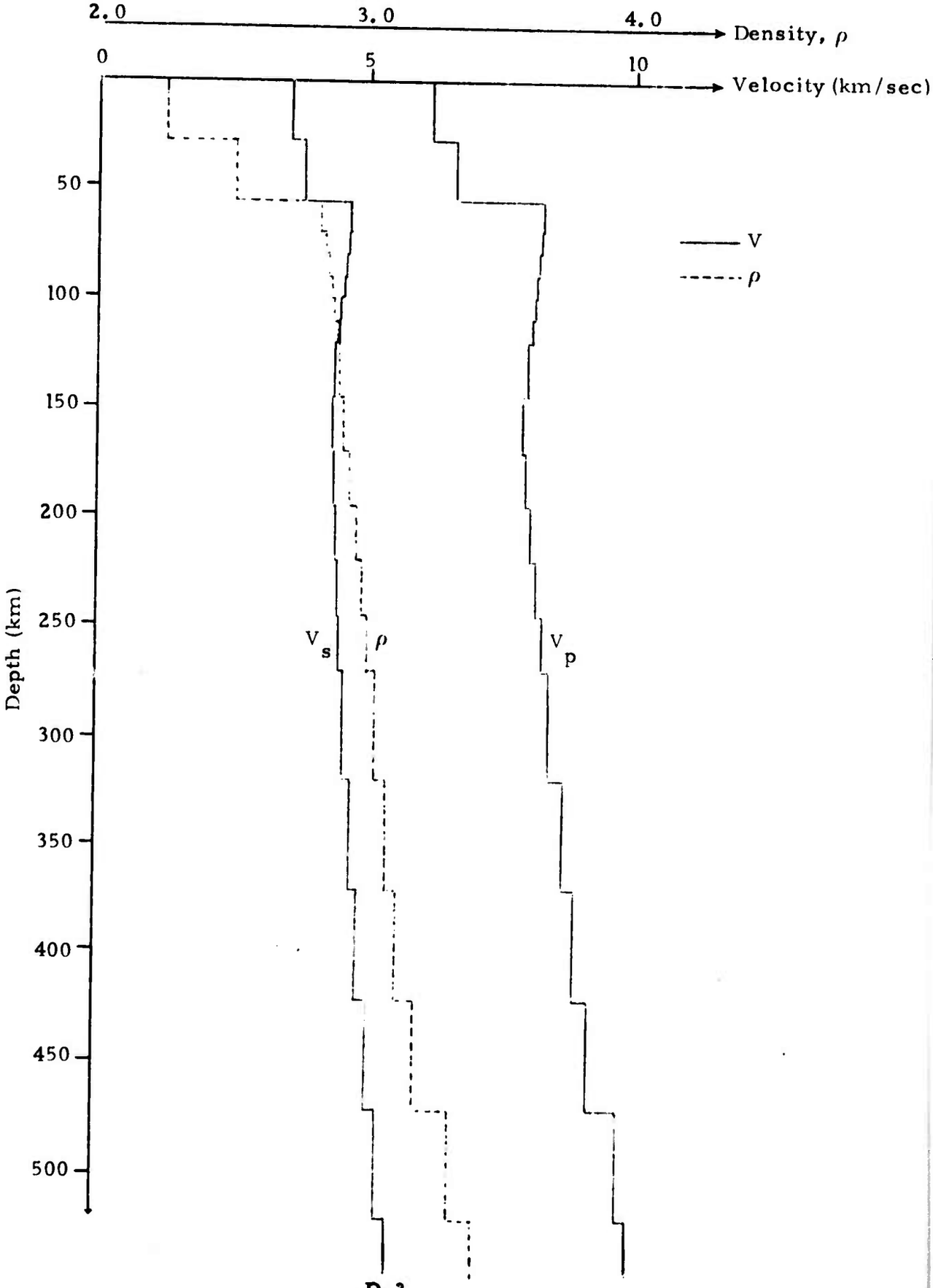

FIGURE D-3

CENTRAL U.S. EARTH MODEL

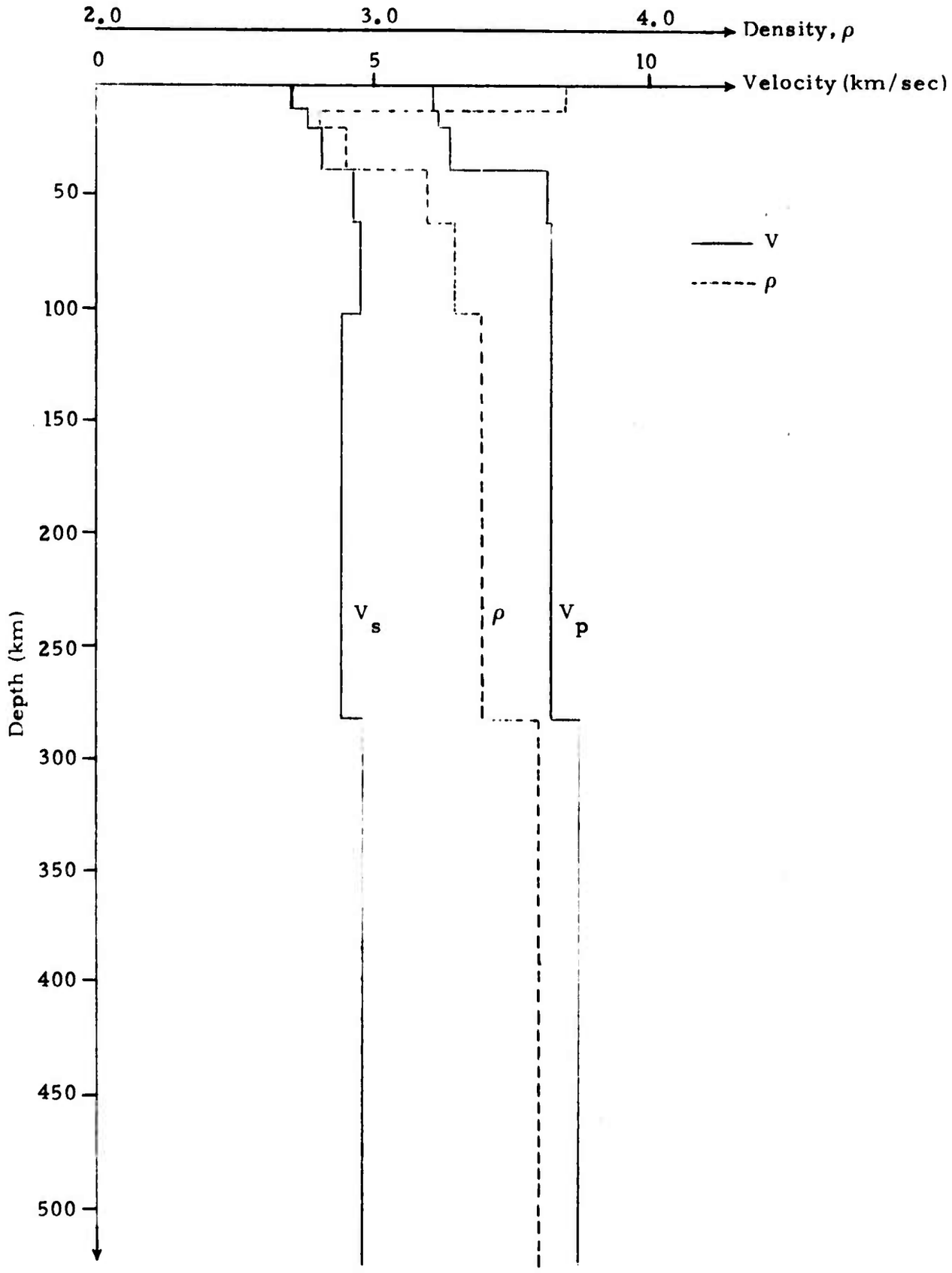

FIGURE D-4
HAMILTON - HEALY EARTH MODEL

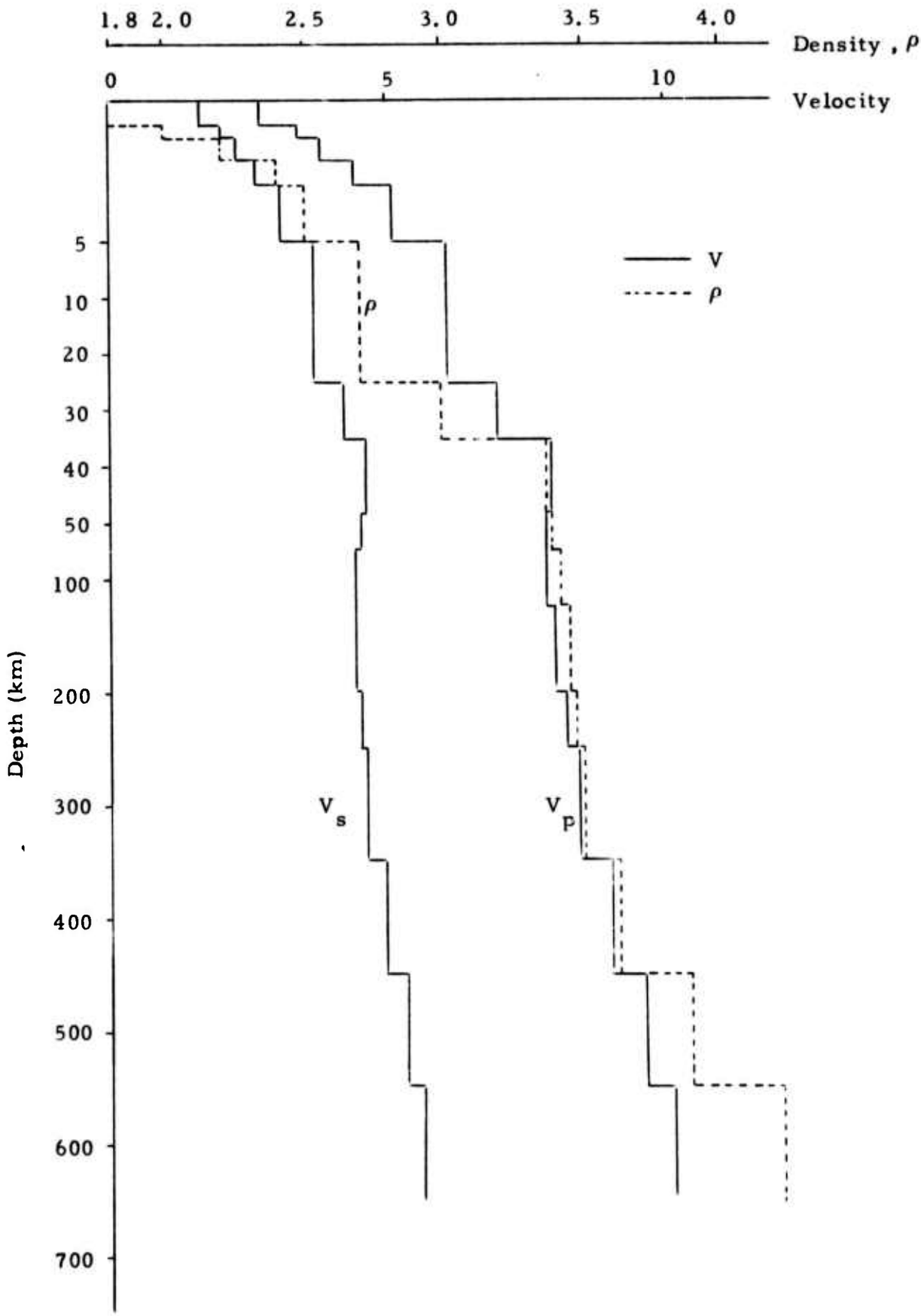

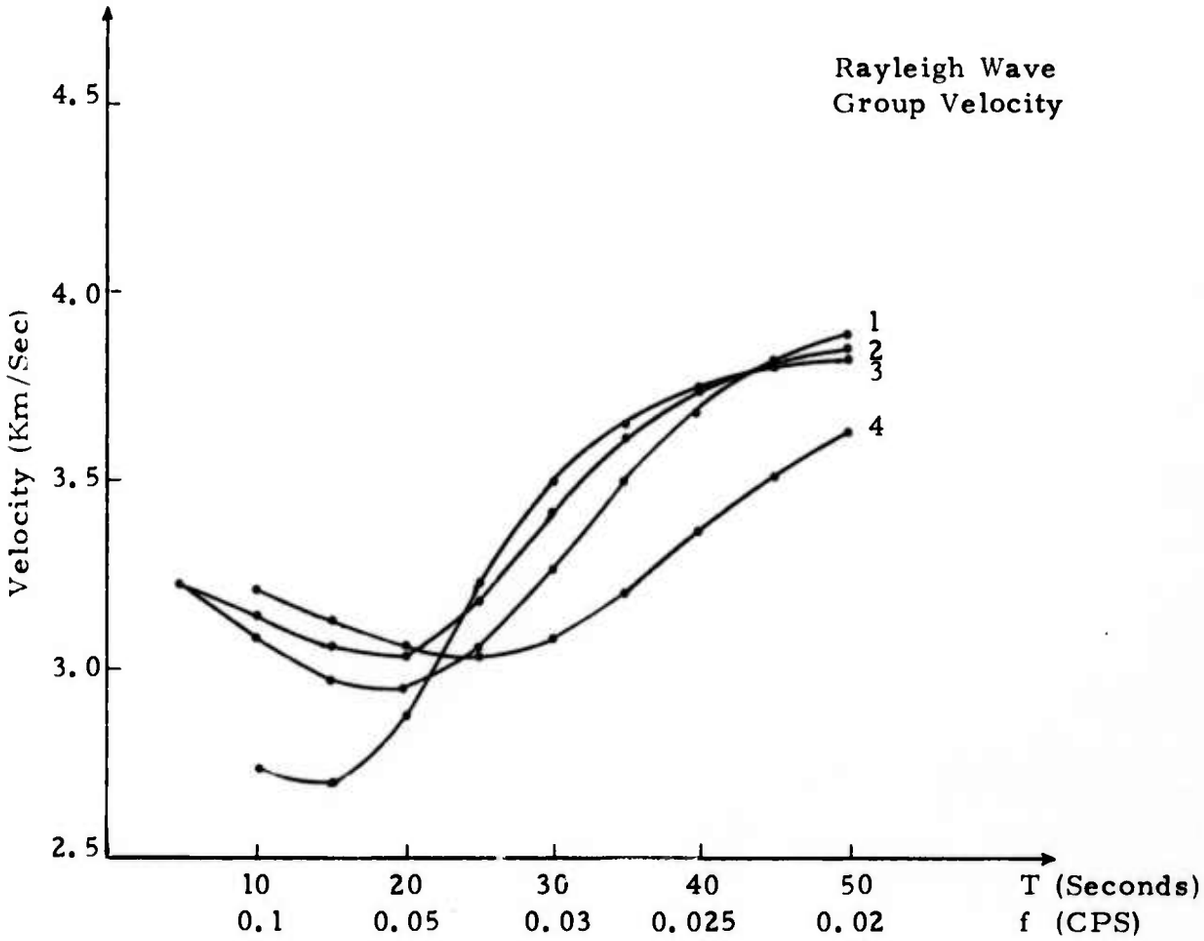

1. Central U. S. Earth Model
2. Gutenberg-Bullen Earth Model
3. Hamilton-Healy Earth Model
4. A 56-Km Crustal for Tibet Plateau

FIGURE D-5

THEORETICAL RAYLEIGH WAVE GROUP VELOCITY CURVES FOR VARIOUS EARTH STRUCTURES

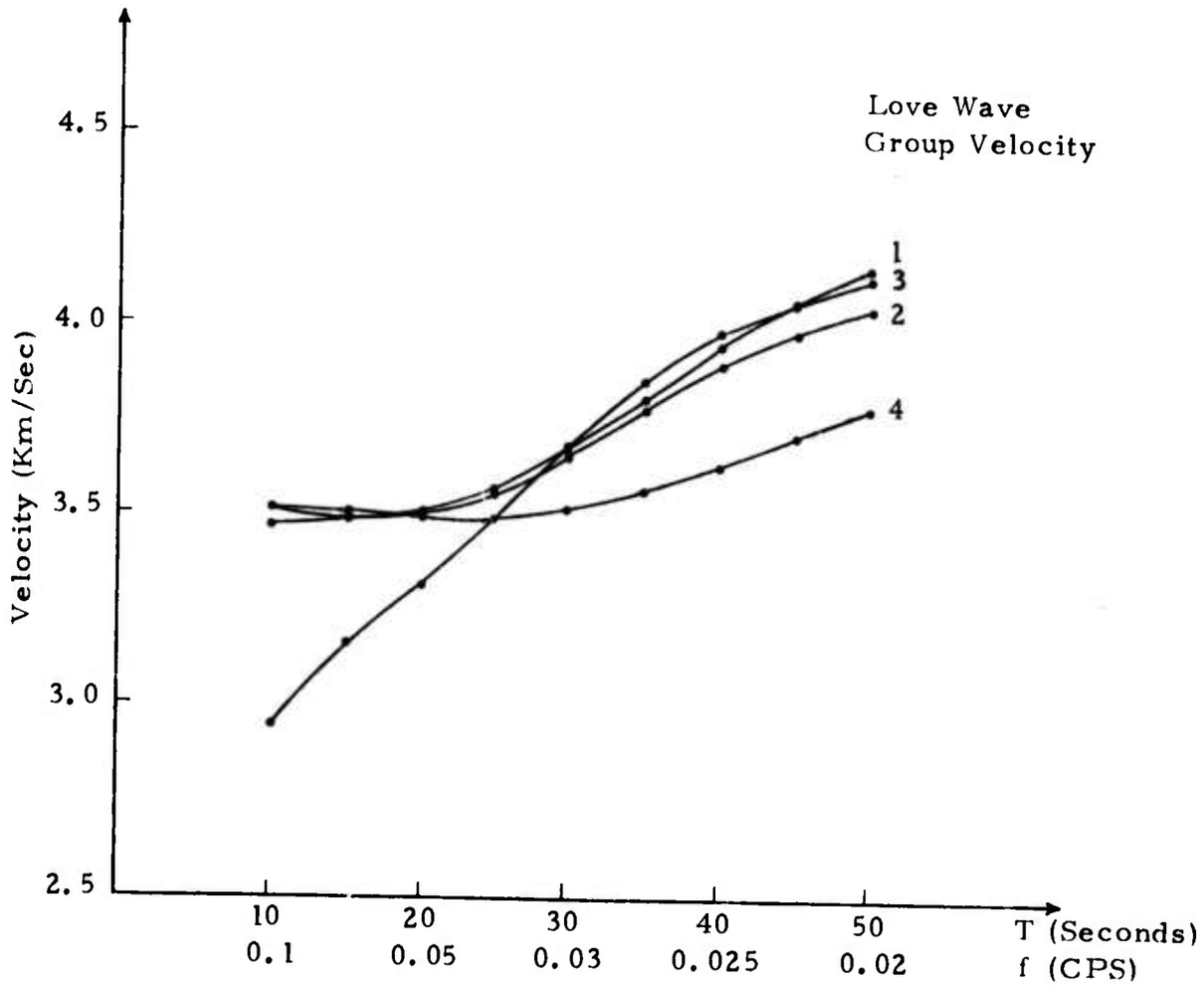

1. Central U. S. Earth Model
2. Gutenberg-Bullen Earth Model
3. Hamilton-Healy Earth Model
4. A 56-Km Crustal for Tibet Plateau

FIGURE D-6

THEORETICAL LOVE WAVE GROUP VELOCITY CURVES
FOR VARIOUS EARTH STRUCTURES

APPENDIX E
REVIEW OF TSAI'S METHOD

Tsai's method for the estimation of seismic source parameters, namely focal depth (h), dip angle (δ), slip angle (λ), strike (ϕ), and seismic moment (M), is the exhausted searching scheme in finding the best fit between the observed and the theoretically calculated surface wave amplitude spectra for one or more observation sites. The exhausted search is in the sense that every combination of δ, λ, ϕ, and h in a predefined set of these parameters has been tested, and the best fit is defined by the minimum of the least squares error among all members in that predefined set. In Tsai's method, the set of δ, λ, ϕ, and h is usually defined by:

$\delta_k = 60^\circ - 90^\circ$	$\Delta\delta_k = 10^\circ$	$k = 4$
$\lambda_\ell = -90^\circ - 90^\circ$	$\Delta\lambda_\ell = 30^\circ$	$\ell = 7$
$\phi_n = 0 - 180^\circ$	$\Delta\phi_n = 10^\circ$	$n = 19$
$h_m = 0 - 125$ km	$\Delta h_m = 5$ km	$m = 26$

Thus, there are 13832 members in the set. A detailed description of Tsai's method is given by Tsai and Shen (1972 b).

By Tsai's method, the optimal estimation of seismic source parameters will be obtained by examining 28 $\epsilon_{k\ell}$ which have been obtained through the least-squares fitting process, picking up the Min$[\epsilon_{k\ell}]$ and assigning δ_k, λ_ℓ, ϕ_n, h_m and M the values which correspond to that Min$[\epsilon_{k\ell}]$. Thus, it is strictly a minimum ϵ criterion. The distribution and magnitude of these 28 $\epsilon_{k\ell}$ have not been taken into consideration, because the distribution is incomplete and the magnitudes of the 28 $\epsilon_{k\ell}$ are widely scattered with little trend to follow.

In order to attain a greater degree of confidence in using the minimum residual Min$[\epsilon_{k\ell}]$ solution, a detailed knowledge of the residual distribution would be helpful in determining the distribution about the absolute minimum and guard against a possible spurious minimum generated by poor quality data. Examining only those 28 $\epsilon_{k\ell}$ which correspond to the pre-determined 28 combinations of dip and slip angles somehow implies before-hand knowledge obtained from a body-wave fault plane solution. It will not affect the optimal source parameter estimation based on the Min($\epsilon_{k\ell}$) criterion, but it will definitely make differences in the distribution and magnitude of $\epsilon_{k\ell}$. For events originating in Eurasia, body-wave data with good azimuthal coverage are usually not immediately available. Therefore, if we are depending only on surface wave data, residual distribution information is important. The following changes were instituted in Tsai's method to obtain optimal source parameter estimation:

- In the fitting process, the focal depth will be varied last, because the depth (h) will effect the shape of the theoretical surface wave amplitude spectra the most, especially for Rayleigh Waves (see Section III). There will be one ϵ^h_{min} for each group at one focal depth (there will be 26 groups with 532 members in each group for the set of δ, λ, ϕ, and h described earlier).

- The variation of ϵ^h_{min} with respect to focal depth will be obtained and a standard value of ϵ, $[\epsilon^h_{min}]_{STANDARD}$, will be determined from those ϵ^h_{min} for the purpose of picking appropriate members in the set of δ, λ, ϕ, and h to form a sample group.

- Members in the set of δ, λ, ϕ, and h whose ϵ is less than $[\epsilon^h_{min}]_{STANDARD}$ will be taken into consideration in forming the distribution of ϵ with respect to focal depth.

Examples of these distributions for each source parameter are given in Sections IV, V, and VI.

APPENDIX F

NON-LINEAR REGRESSION OF SEISMIC SOURCE PARAMETERS FROM SURFACE WAVE DATA

We will assume that the seismic source as observed in the far-field can be represented by a simple double couple in the form developed by Harkrider (1964). This representation may not be the most accurate, but for this discussion we will assume that higher order components are not needed (Turnbull, 1972). The general form for the far-field Rayleigh and Love wave radiation from a double couple source may be written as:

$$U = Sk_n e^{-i\frac{3\pi}{4}} N(h)\, X(\theta, h) \frac{e^{-ik_n r}}{r^{\frac{1}{2}}} \qquad (F\text{-}1)$$

where

U : spectral horizontal Rayleigh or Love wave displacement

S : spectral source function (For step function = M/ω)

k_n: ω/c Rayleigh or Love wave angular wave number

N(h) : either $N_\theta(h)$ or $N_{rz}(h)$ - response functions from the layered half space for Love and Rayleigh waves respectively

$X(\theta, h)$: the complex radiation pattern function which can be written as:

$$X(\theta, h) = d_o + i(d_1 \sin\theta + d_2 \cos\theta) + d_3 \sin 2\theta + d_4 \cos 2\theta \qquad (F\text{-}2)$$

The coefficients d_i are given below for a double couple:

	LOVE	RAYLEIGH
d_o	0	$\frac{1}{2}\sin\lambda\sin 2\delta B(h)$
d_1	$\cos\lambda\cos\delta G(h)$	$-\sin\lambda\cos 2\delta C(h)$
d_2	$-\sin\lambda\cos 2\delta G(h)$	$-\cos\lambda\cos\delta C(h)$
d_3	$\frac{1}{2}\sin\lambda\sin 2\delta V(h)$	$\cos\lambda\sin\delta A(h)$
d_4	$\cos\lambda\sin\delta V(h)$	$-\frac{1}{2}\sin\lambda\sin 2\delta A(h)$

where θ is the azimuth angle, δ the dip angle, λ the slip angle, and

$$A(h) = -\left[\dot{u}_s^*(h)/\dot{w}_o\right]$$

$$B(h) = -\left[\left(3-4\frac{\beta_s^2}{\alpha_s^2}\right)\left[\dot{u}_s^*(h)/\dot{w}_o\right] + \frac{2}{\rho_s\alpha_s^2}\left[\sigma^*_{r_s}(h)/(\dot{w}_o/C_r)\right]\right]$$

$$C(h) = -\frac{1}{\mu_s}\left[\tau_{r_s}(h)/(\dot{w}_o/C_r)\right]$$

$$V(h) = \left[\dot{v}_s(h)/\dot{v}_o\right]$$

$$G(h) = \frac{1}{\mu_s}\left[\tau_{l_s}^*(h)/\left(\dot{v}_o/C_l\right)\right]$$

where:

$\frac{\dot{u}_s(h)}{\dot{w}_o}, \frac{\dot{w}_s(h)}{\dot{w}_o}, \frac{\dot{v}_s(h)}{\dot{v}_o}$ - Haskell's plane wave particle velocity (or displacement) ratios

$\sigma_{r_s}(h)$ - Depth-dependent factor of normal stress associated with the Rayleigh waves

$\tau_{r_s}(h)$, $\tau_{l_s}(h)$ - Depth-dependent factors of tangential stresses associated with the Rayleigh and Love waves.

The fault plane geometry is shown below.

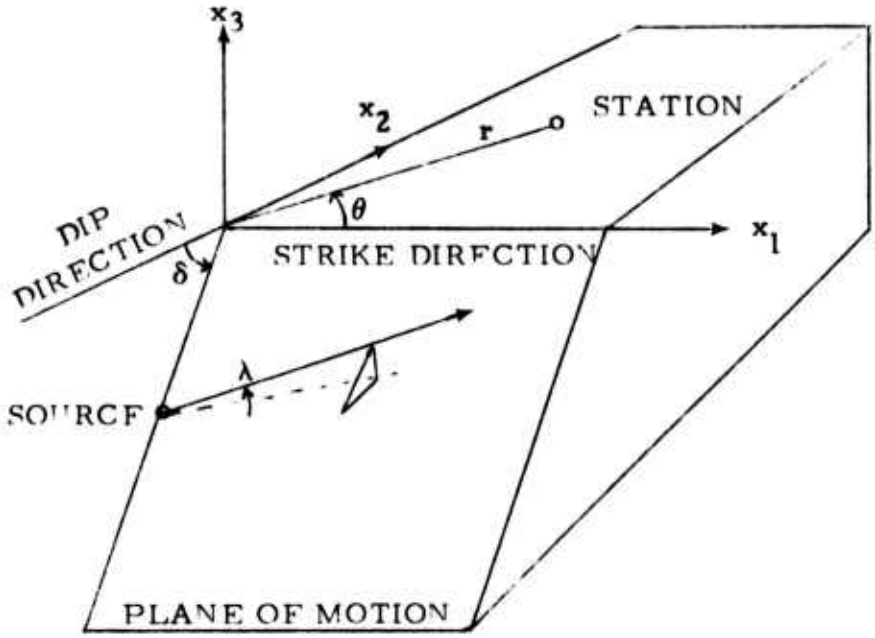

FIGURE F-1

FAULT PLANE GEOMETRY
After Harkrider (1964)

If we are to fit the radiation patterns described by the displacement function U, we must determine which parameters would be feasible to use in a regression analysis. We first realize that a fit must be made for each frequency (or wave number), because radiation patterns vary with frequency for an earthquake. [This is due to the effect of rupture velocity (Archambeau, 1964)]. Also, the variation of depth in the regression procedure requires a significant effort, because a different placement of the source in the layered half space would involve a complicated variation of the response functions N(h), A(h), B(h), C(h), G(h), and V(h). As a first attempt, the depth is estimated using an exhaustive technique such as Tsai's method. Regression is then performed at each of several reasonably spaced depths bracketing this estimated depth, the final depth being that which produces the minimum residual.

The parameters which easily lend themselves to this type of regression analysis are λ(slip angle), δ(dip angle), θ(strike angle), and M(seismic moment). Upon examination of expression (F-2), we see that a linear regression approach would involve significant errors because the angles are arguments of trigonometric functions.

There are several approaches available for non-linear regression, but possibly the most direct and easily understood involves making a Taylor Series approximation (Draper and Smith, 1968). The objective of this procedure is to obtain the expressions involving strike, dip, slip, and seismic moment using the first terms in Taylor Series expansion, and obtain values for the regression parameters with an iterative technique.

By assuming the theoretical description of the source, we have the set of theoretical equations

$$Y = f(x_i, \beta_j) \tag{F-3}$$

where:

$x_i = x_1, x_2, \ldots x_n$ independent variables (in our case, we have depth and azimuth).

$\beta_j = \beta_1, \beta_2, \ldots \beta_p$ regression parameters (in our case, strike, dip, and slip).

The objective is to find the estimates of β_j which minimize the

$$\text{"error of squares"} = S(\beta_j) = \sum_{u=1}^{n} E_u^2 = \sum_{u=1}^{n} (Y_u - f_u(x_i, \beta_j))^2 \tag{F-4}$$

where:

Y_u = observed dependent variables (u = 1, 2, . . ., n) (in our case, the amplitude variation with azimuth for a particular period)

E_u = observed deviation about predicted equation

$$Y_u = f_u(x_i, \beta_j) + E_u \text{ for each } u\ (u = 1, 2, \ldots, n) \qquad (F\text{-}5)$$

Regression satisfying condition (F-4) may be achieved using the 'linearization' or 'Taylor Series' method.

Carrying out a Taylor Series expansion of $f(x_i, \beta_j)$ about the point β_j^0 and curtailing expansion at the first derivative yields

$$f_u(x_i, \beta_j) \doteq f_u(x_i, \beta_j^0) + \sum_{j=1}^{P} \left| \frac{\partial f_u(x_i, \beta_j)}{\partial \beta_j} \right|_{\beta_j = \beta_j^0} \cdot (\beta_j - \beta_j^0) \qquad (F\text{-}6)$$

where β_j and β_j^0 are separated by the small increment Δ.

Now setting

$$f_u^0 = f_u(x_i, \beta_j^0) \qquad (F\text{-}7)$$

$$\Delta_j = \beta_j - \beta_j^0 \qquad (F\text{-}8)$$

$$Z_{j,u}^0 = \left| \frac{\partial f_u(x_i, \beta_j)}{\partial \beta_j} \right|_{\beta_j = \beta_j^0} \qquad (F\text{-}9)$$

yields

$$Y_u - f_u^0 = \sum_{j=1}^{P} \Delta_j \cdot Z_{j,u}^0 + E_u \qquad (F\text{-}10)$$

which is a linearized form of expression (F-5).

Applying the least-squares condition (F-4) to (F-10) gives as the "sum of squares"

$$SS(\beta_j) = \sum_{u=1}^{n} \left[Y_u - f_u^0 - \sum_{j=1}^{P} \Delta_j \cdot Z_{j,u}^0 \right]^2 = E_u^2 \qquad \text{(F-11)}$$

Minimizing F_u^2 with respect to Δ gives

$$\frac{\partial F_u^2}{\partial \Delta_j} = 2 \sum_{u=1}^{n} \left[Y_u - f_u^0 - \sum_{j=1}^{P} \Delta_j \cdot Z_{j,u}^0 \right] \left[\sum_{u=1}^{n} Z_{j,u}^0 \right] = 0 \qquad \text{(F-12)}$$

or

$$\sum_{u=1}^{n} \left[Y_u - f_u^0 \right] = \sum_{u=1}^{n} \sum_{j=1}^{P} \Delta_j \cdot Z_{j,u}^0 \qquad \text{(F-13)}$$

as a non-trivial solution of (F-12). These expressions (F-13) are sometimes called the normal equations.

For purposes of clarity and computation, we can write equation (F-13) in matrix notation. Therefore, we have

$$\Delta = \begin{bmatrix} \beta_1 - \beta_1^0 \\ \beta_2 - \beta_2^0 \\ \beta_p - \beta_p^0 \end{bmatrix} \quad \text{(pxl)} \qquad \text{(F-14)}$$

$\downarrow$ p (regression parameters)

In our case, p = 4 for ϕ, λ, δ, M

$$\Delta = \begin{bmatrix} \beta_\phi - \beta_\phi^o \\ \beta_\lambda - \beta_\lambda^o \\ \beta_\delta - \beta_\delta^o \\ \beta_M - \beta_M^o \end{bmatrix}$$

$$Z^0 - \underset{\substack{\text{(nxp) or (nx4)} \\ \text{(p} \longrightarrow \text{regression parameters)}}}{\begin{bmatrix} Z^0_{11} & Z^0_{21} & \cdots & Z^0_{p1} \\ Z^0_{12} & \cdots & \cdots & Z^0_{p2} \\ Z^0_{in} & \cdots & \cdots & Z^0_{pn} \end{bmatrix}} \quad \text{n (number of observations)} \qquad \text{(F-15)}$$

In our case,

$$Z^0_{1n} - \left|\frac{\partial fn}{\partial \beta_\phi}\right| \beta_j = \lambda, \delta, M \qquad Z^0_{3n} = \left|\frac{\partial fn}{\partial \beta_\delta}\right| \beta_j = \phi, \lambda, M$$

$$Z^0_{2n} - \left|\frac{\partial fn}{\partial \beta_\lambda}\right| \beta_j = \phi, \delta, M \qquad Z^0_{4n} = \left|\frac{\partial fn}{\partial \beta_M}\right| \beta_j = \lambda, \delta, \phi$$

$$Y^0 = \underset{\text{(nxl)}}{\begin{bmatrix} Y_1 - f^0_1 \\ Y_2 - f^0_2 \\ Y_n - f^0_n \end{bmatrix}} \quad \text{n (number of observations)} \qquad \text{(F-16)}$$

Then expression [F-13] is given by

$$\left[\beta_j - \beta_j^0\right] = \vec{\Delta} = (\underset{pxn}{\vec{Z}^{0T}} \underset{nxp}{Z^0})^{-1} \cdot \underset{pxn}{\vec{Z}^{0T}} \cdot \underset{nxl}{\vec{Y}^0} \qquad \text{(F-17)}$$

$$\underset{pxp}{\qquad\qquad} \qquad \underset{pxl}{\qquad}$$

$$\underset{pxl}{\qquad\qquad\qquad}$$

The above equation may be solved iteratively for estimates β_j^0 of the true regression parameters β_j by making a first guess at β_j^0 and using (F-17) to give β_j. This is used as a new estimator β_j^0 which is used to calculate β_j and so on until the iteration converges.

Before we proceed further with this discussion, a note must be made on applying this technique to our source description. We see from equation (F-2) that the radiation pattern is given by a complex expression. This form does not lend itself to a regression analysis. Instead, we can work with the modulus squared. Therefore, we are working with a quantity directly proportional to the energy in the seismic wave rather than the amplitude. We can therefore write

$$X(\theta)X^*(\theta) = d_0^2 + d_3^2 \sin^2 2\theta + d_4^2 \cos^2 2\theta + 2d_3d_0 \sin 2\theta + 2d_4d_0 \cos 2\theta$$
$$+ 2d_3d_4 \sin 2\theta \cos 2\theta + d_1 \sin 2\theta + d_2 \cos 2\theta + 2d_1d_2 \sin\theta\cos\theta \qquad \text{(F-18)}$$

with the d_l defined as before. Then $X(\theta)X^*(\theta)$ will be the function $f_u(x_i, \beta_j)$.

APPENDIX G

REPRESENTATIVE SPECTRA AND RADIATION PATTERNS

The following spectra and radiation patterns were generated using a theoretical double couple point source placed in a Guttenburg layered half space:

Figures G-1a, b, c to G-4a,b,c - Rayleigh, Love, and Love/Rayleigh amplitude spectra for a vertical strike-slip fault at 30^{o} azimuth showing variation of depth, dip, slip, and strike respectively.

Figures G-5a, b, c - Rayleigh, Love, and Love/Rayleigh amplitude spectra for an approximately vertical strike-slip fault at 30^{o} azimuth showing variation of depth.

Figures G-6a, b, c to G-9a, b, c - Rayleigh, Love, and Love/Rayleigh amplitude spectra for a dip-slip type fault at 30^{o} azimuth showing variation of depth, dip, slip, and strike respectively.

Figures G-10a, b to G-14a, b - Rayleigh and Love wave radiation patterns for h = 15 km, $\delta = 60^{o}$, $\lambda = -30^{o}$, and $\phi = 20^{o}$ for periods 50, 40, 30, 20, and 10 seconds respectively.

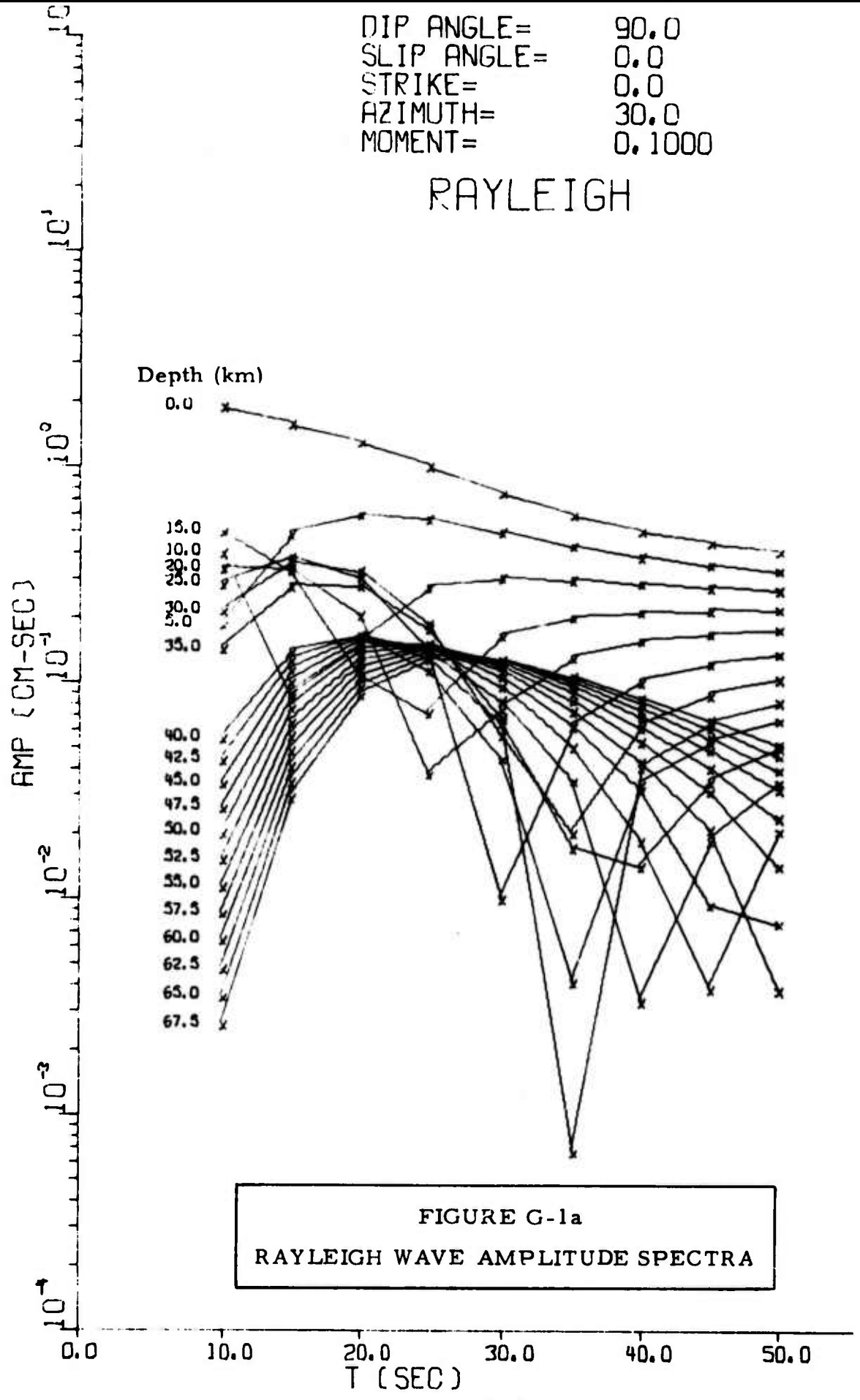

FIGURE G-1a

RAYLEIGH WAVE AMPLITUDE SPECTRA

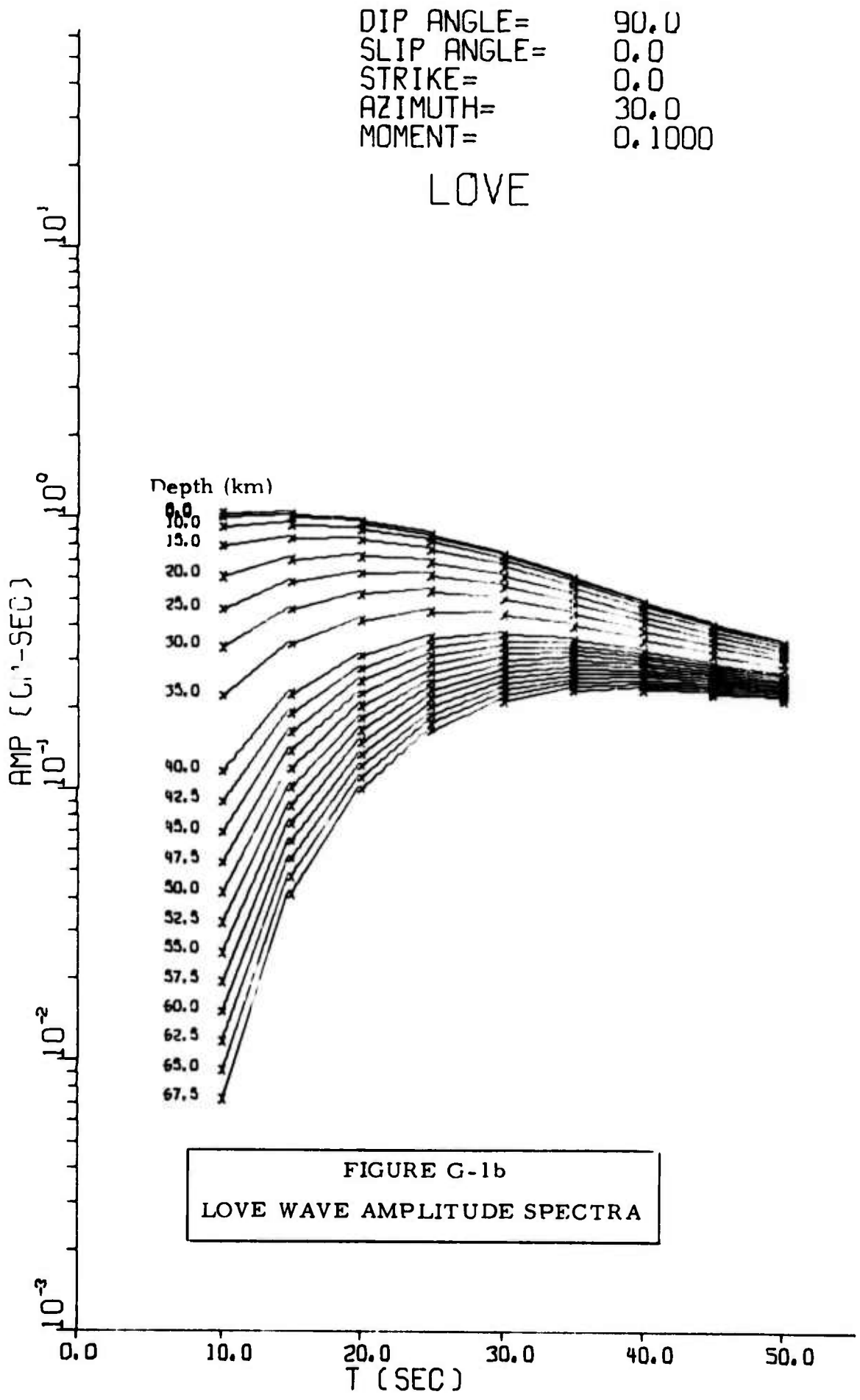

FIGURE G-1b

LOVE WAVE AMPLITUDE SPECTRA

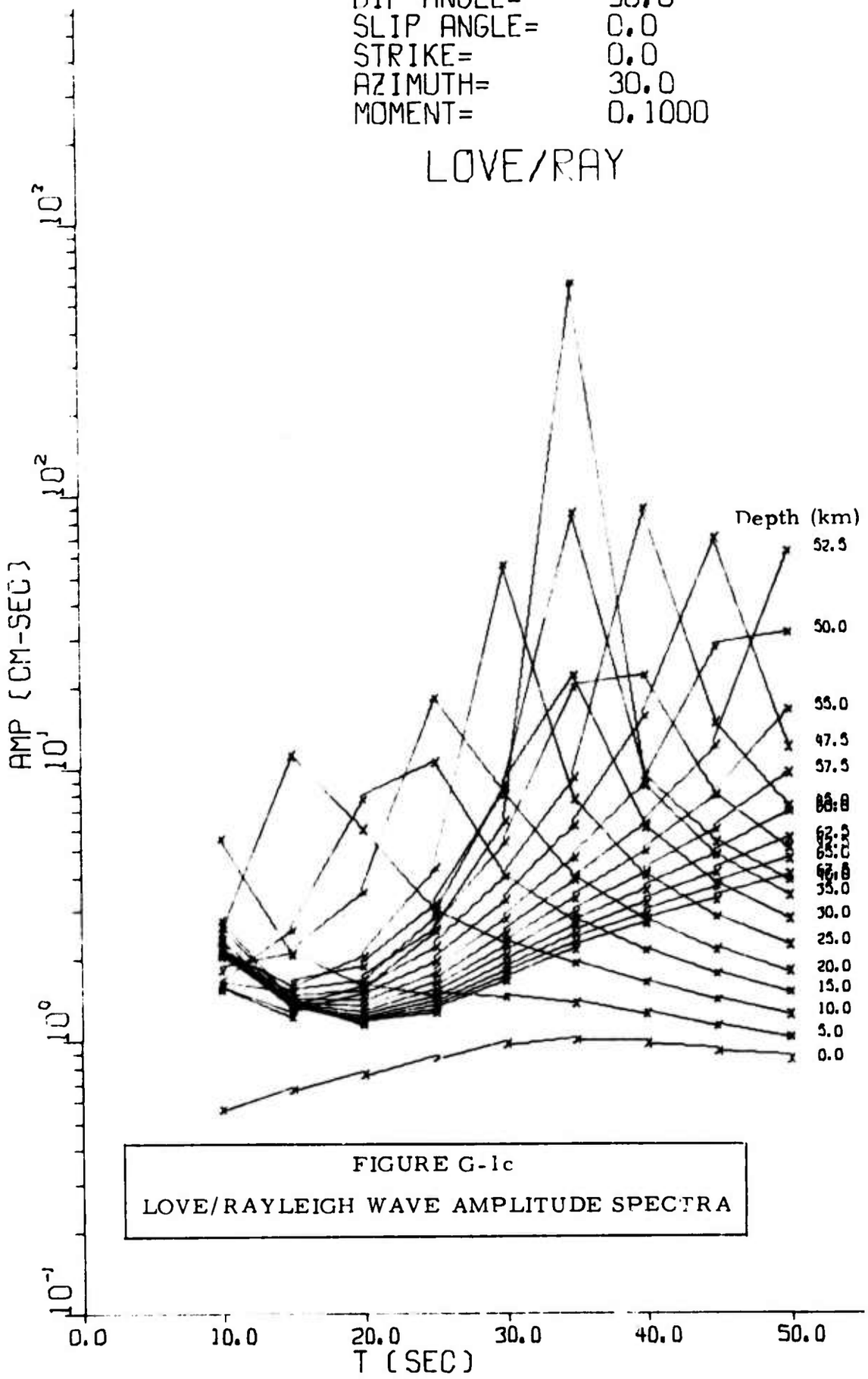

FIGURE G-1c

LOVE/RAYLEIGH WAVE AMPLITUDE SPECTRA

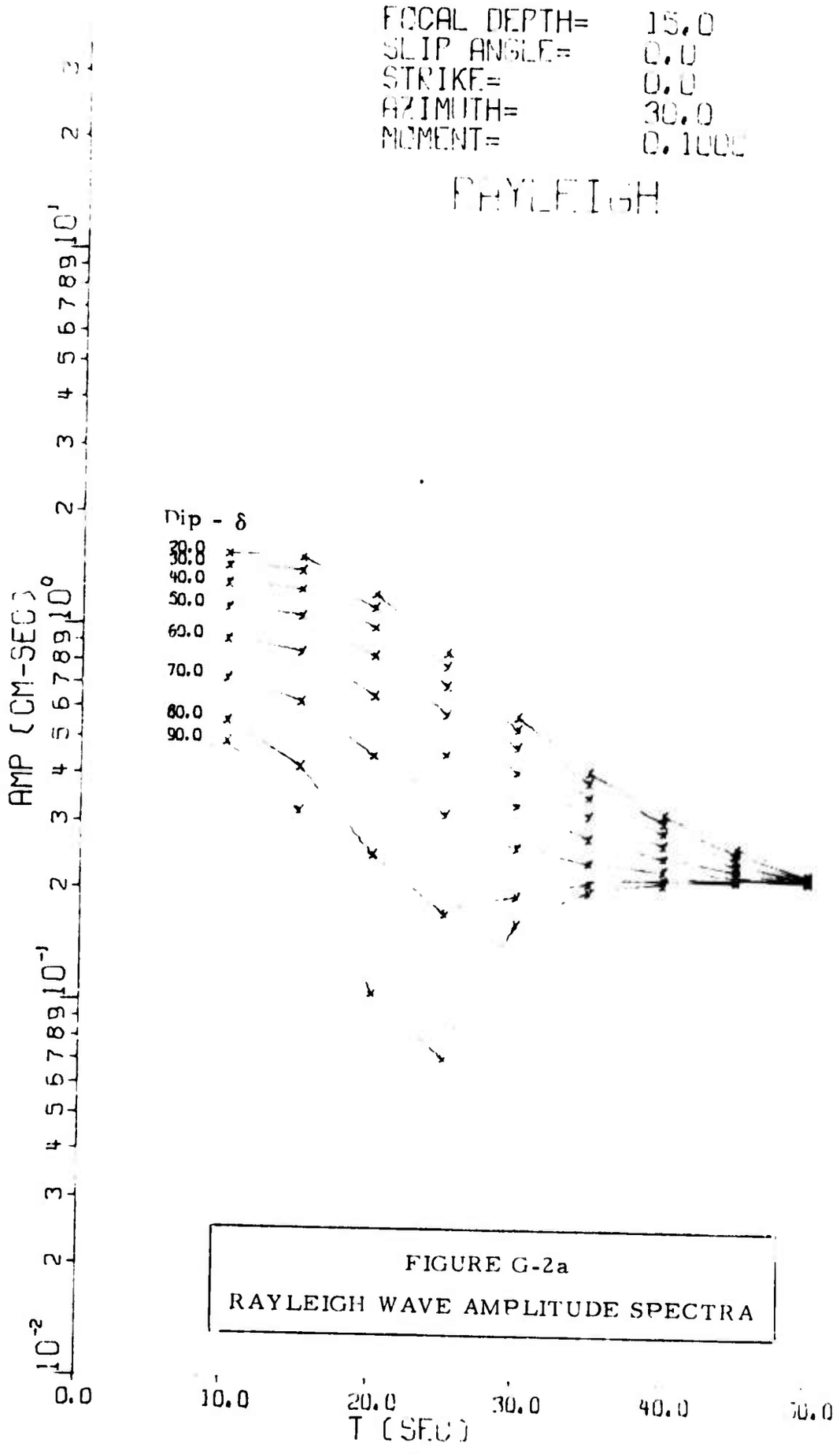

FIGURE G-2a

RAYLEIGH WAVE AMPLITUDE SPECTRA

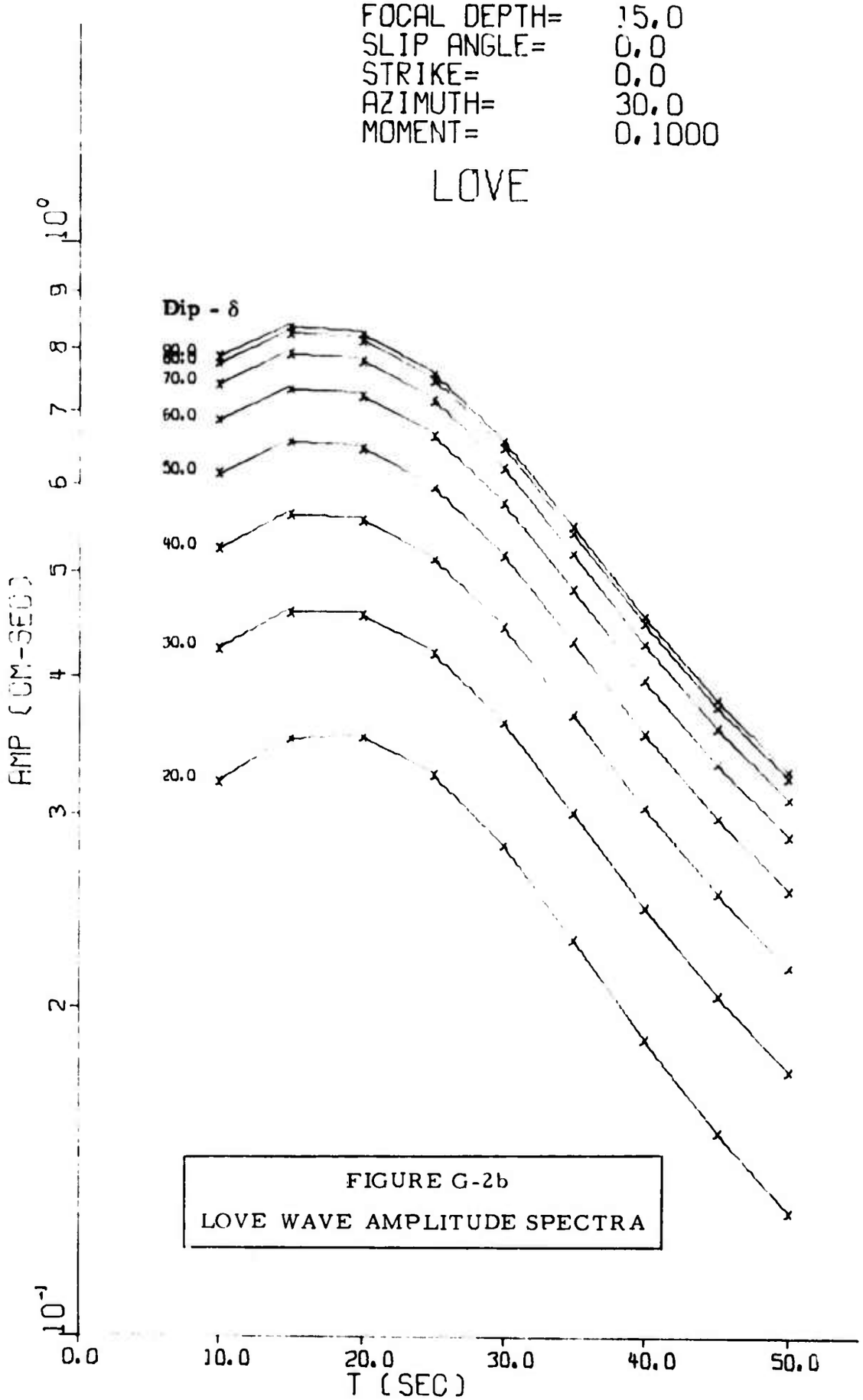

FIGURE G-2b

LOVE WAVE AMPLITUDE SPECTRA

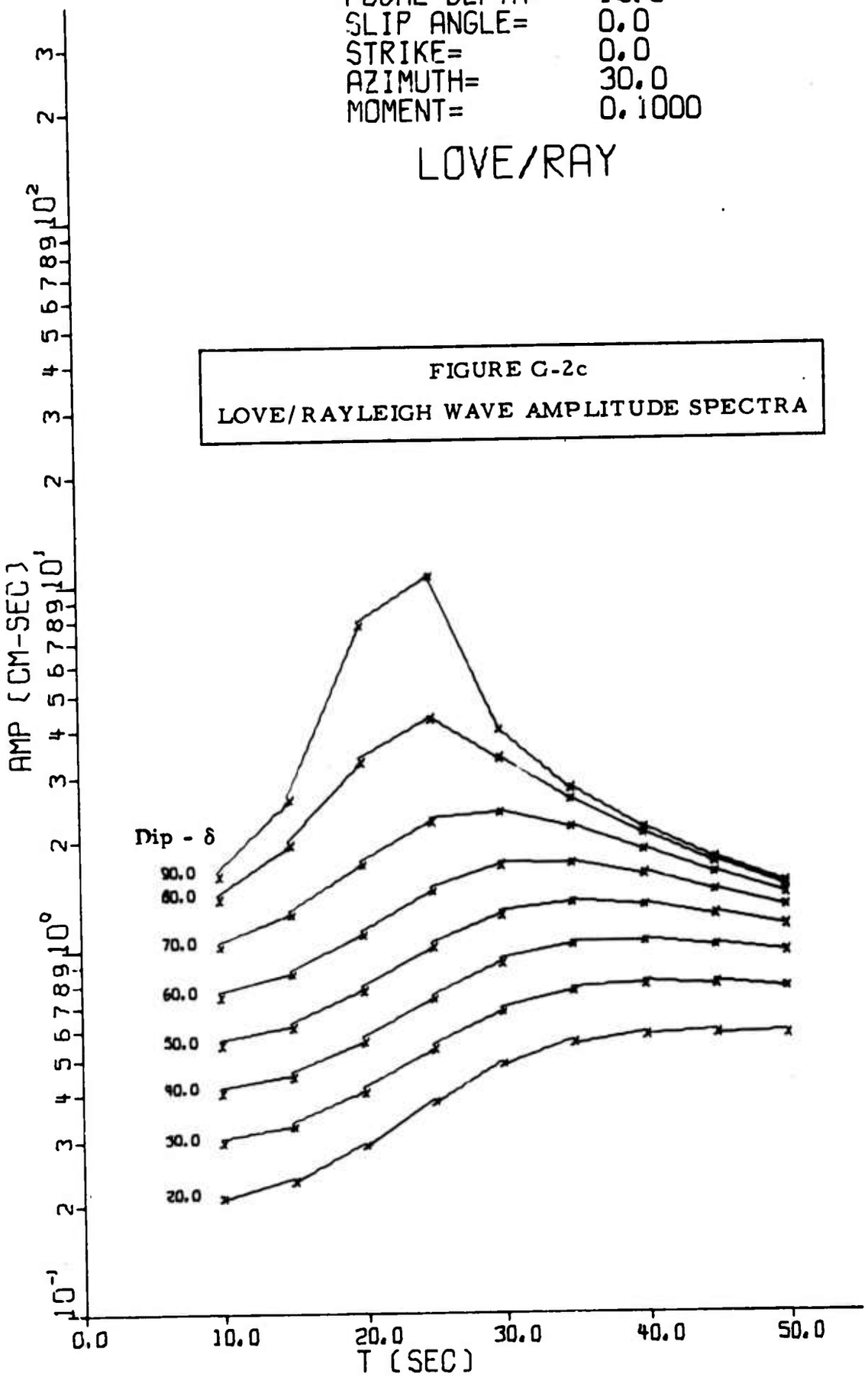

FIGURE G-2c

LOVE/RAYLEIGH WAVE AMPLITUDE SPECTRA

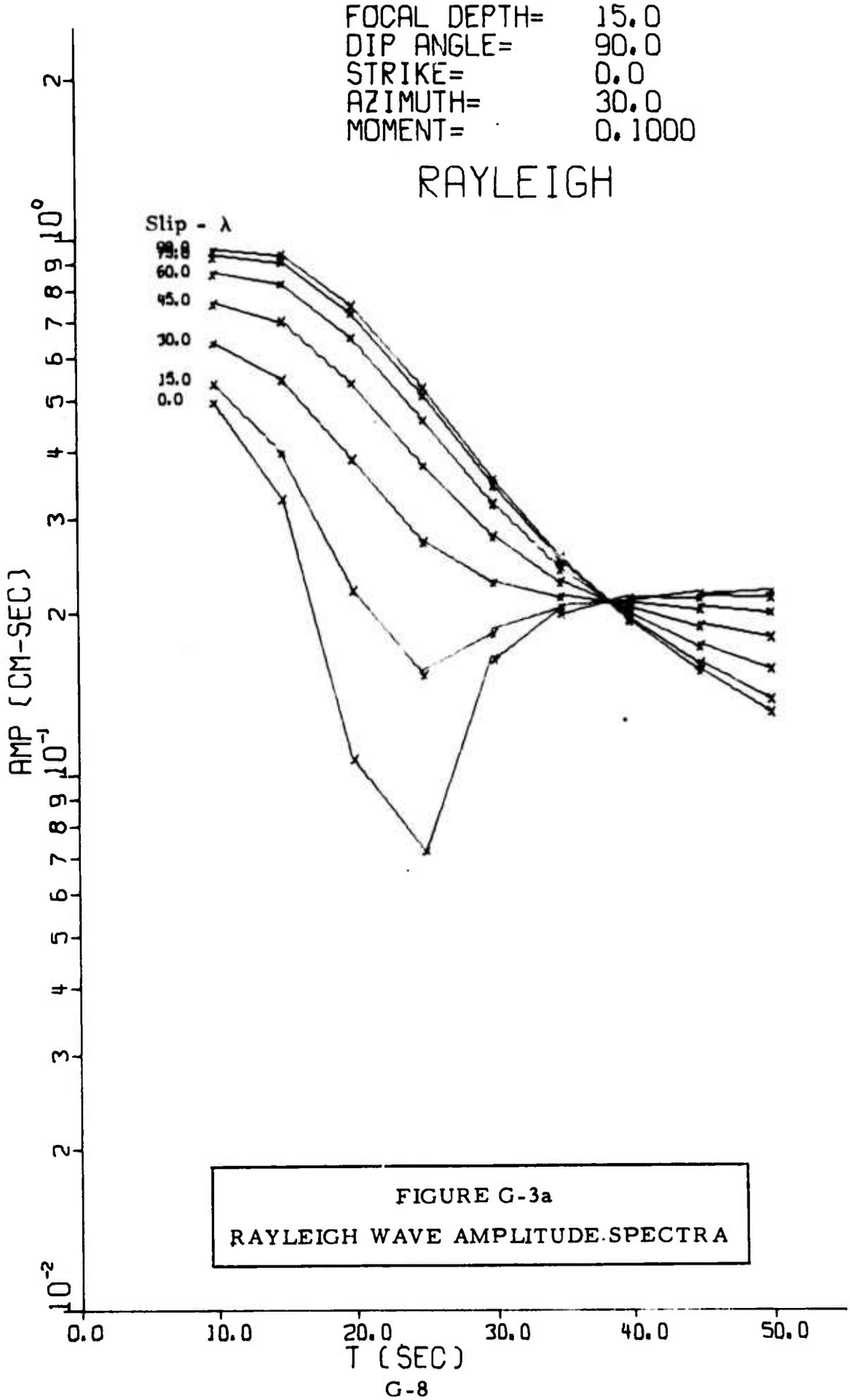

FIGURE G-3a

RAYLEIGH WAVE AMPLITUDE SPECTRA

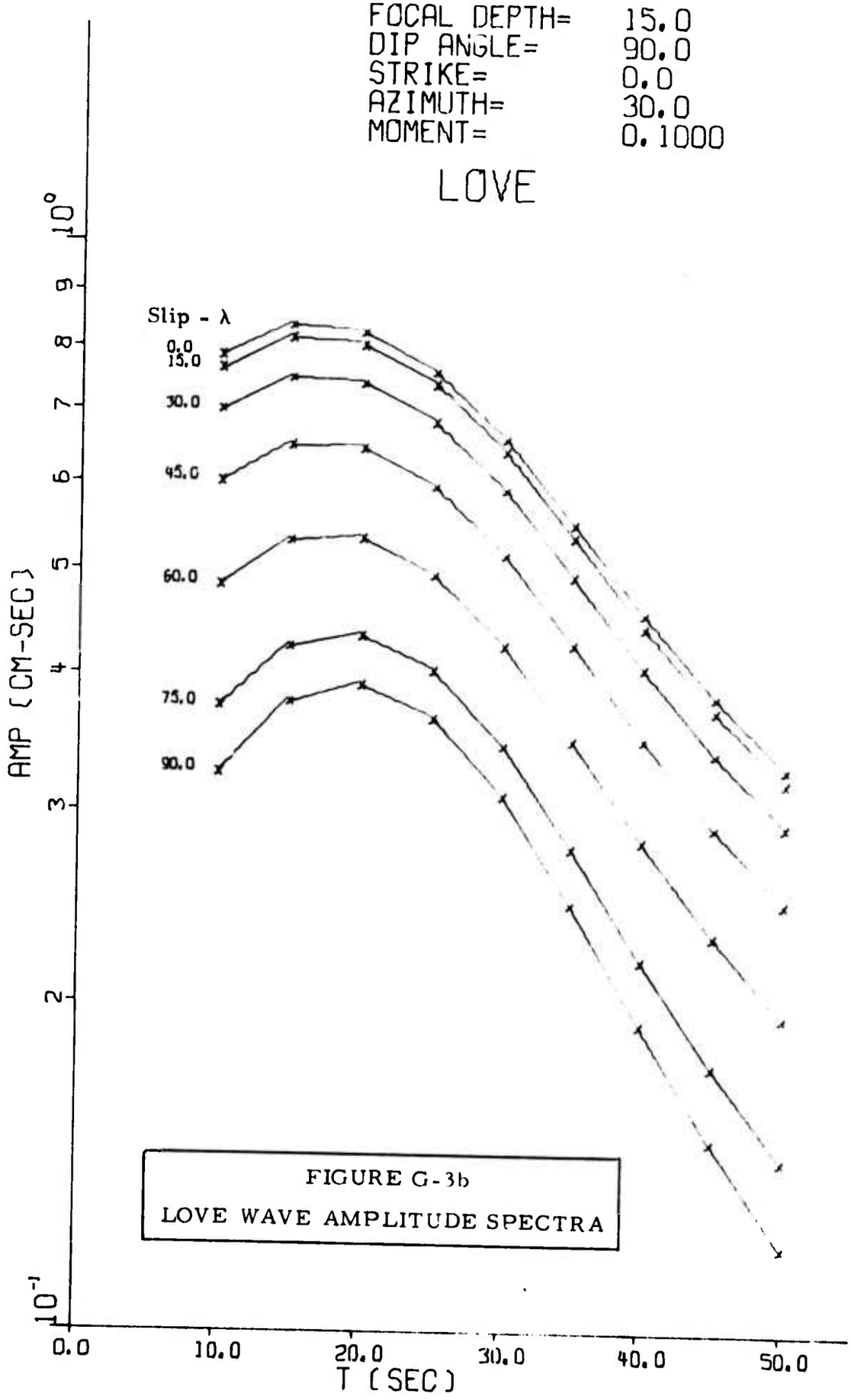

FIGURE G-3b

LOVE WAVE AMPLITUDE SPECTRA

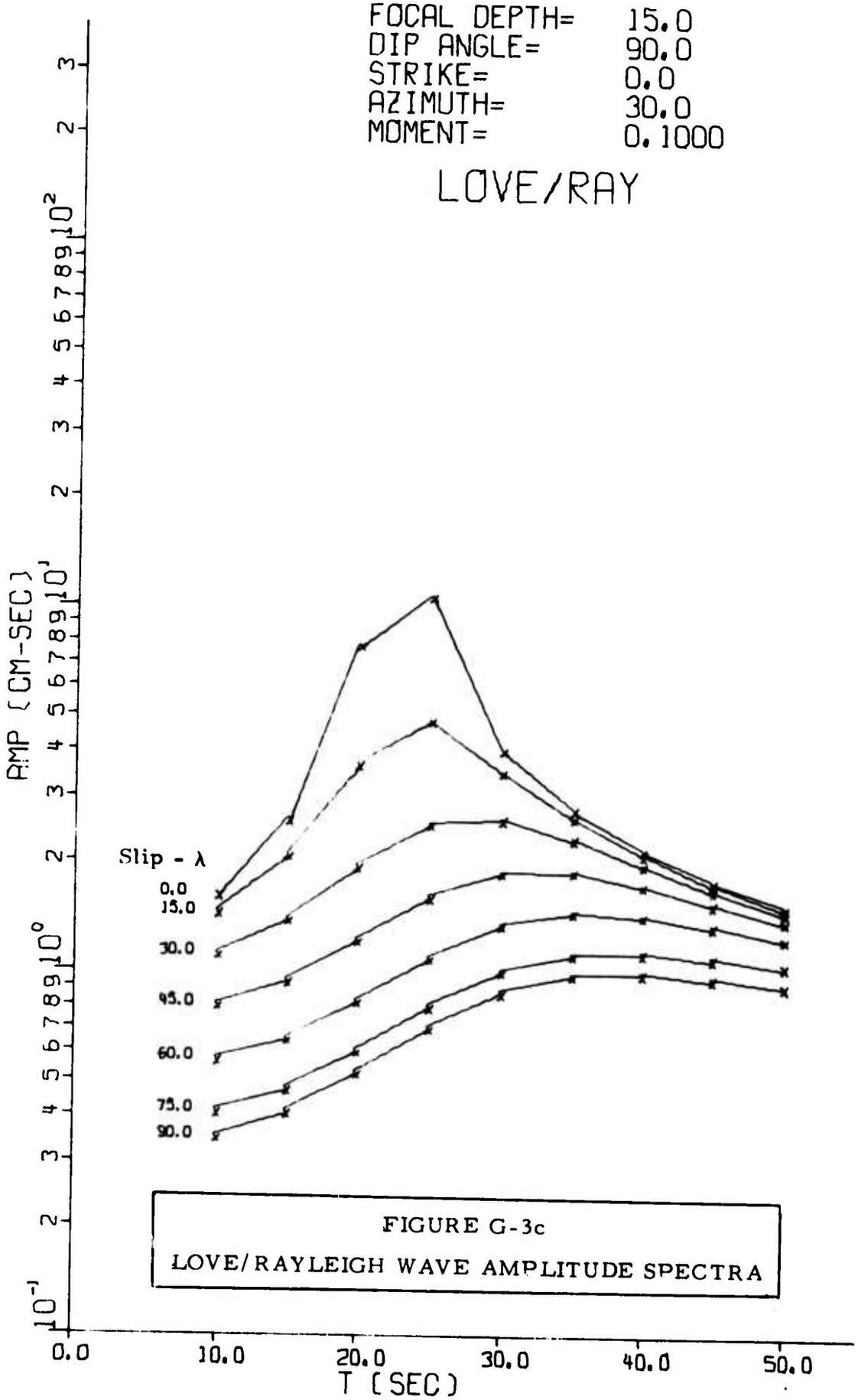

FIGURE G-3c

LOVE/RAYLEIGH WAVE AMPLITUDE SPECTRA

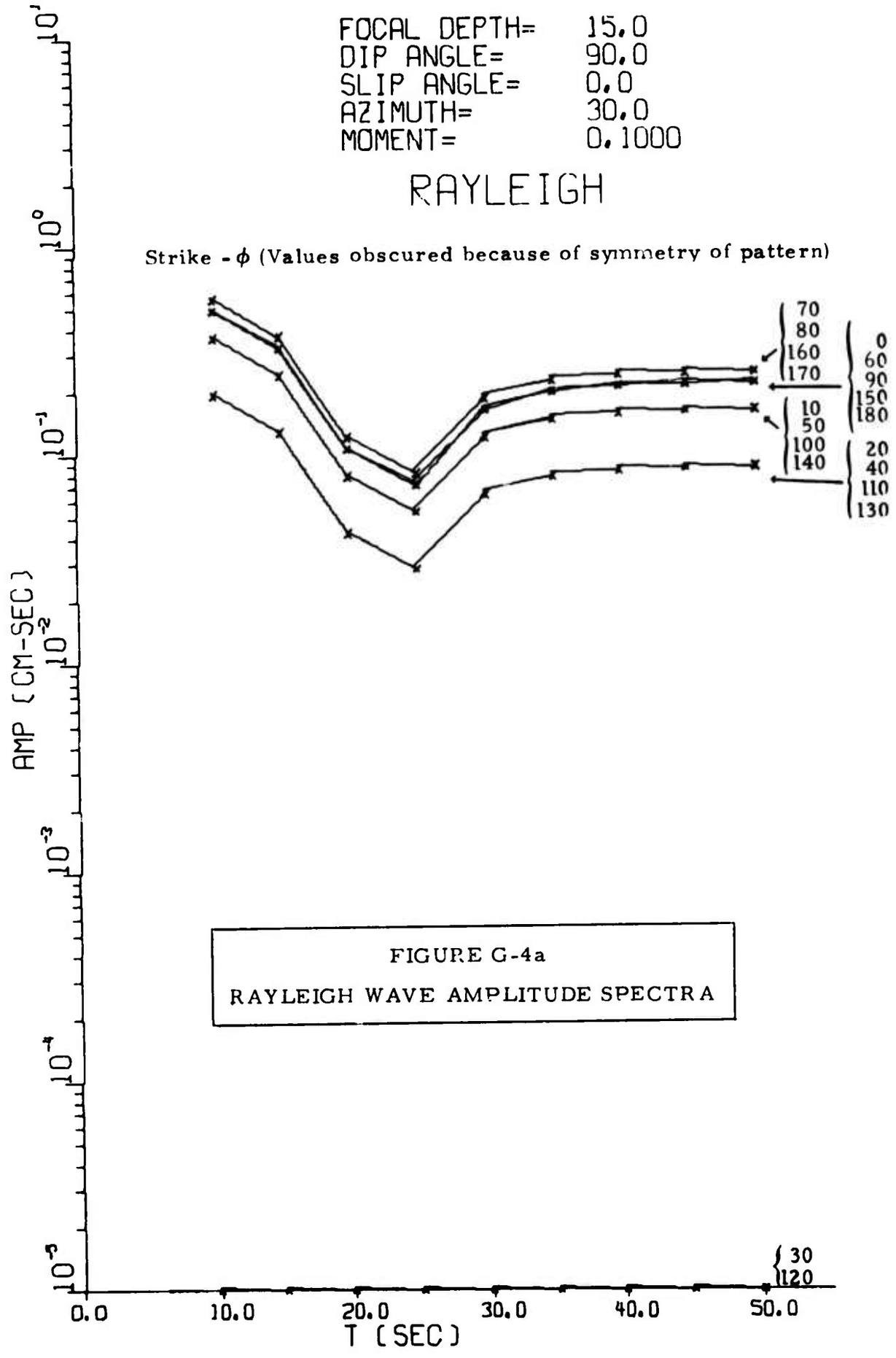

FIGURE G-4a

RAYLEIGH WAVE AMPLITUDE SPECTRA

FOCAL DEPTH= 15.0
DIP ANGLE= 90.0
SLIP ANGLE= 0.0
AZIMUTH= 30.0
MOMENT= 0.1000

LOVE

FIGURE G-4b

LOVE WAVE AMPLITUDE SPECTRA

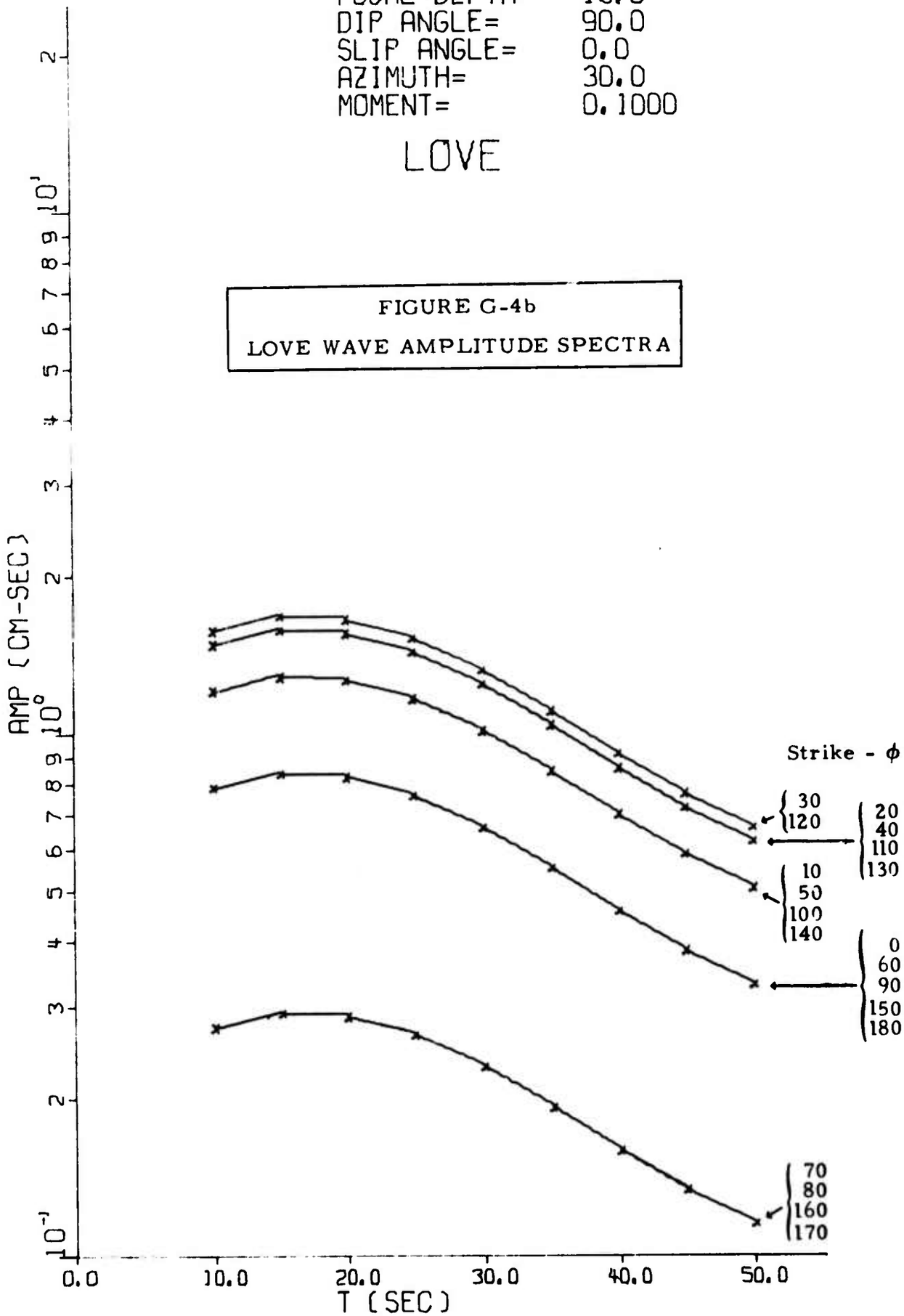

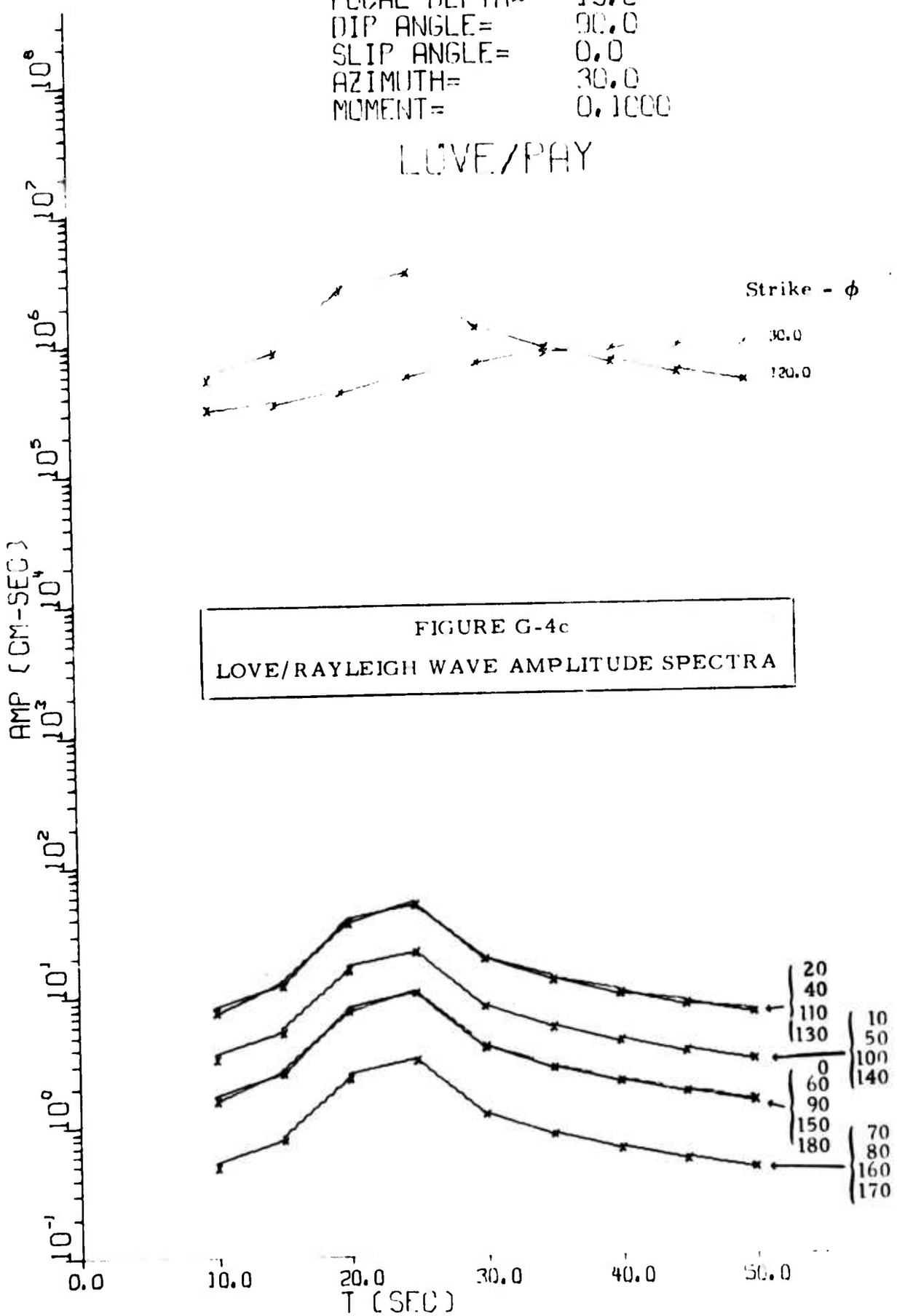

FIGURE G-4c

LOVE/RAYLEIGH WAVE AMPLITUDE SPECTRA

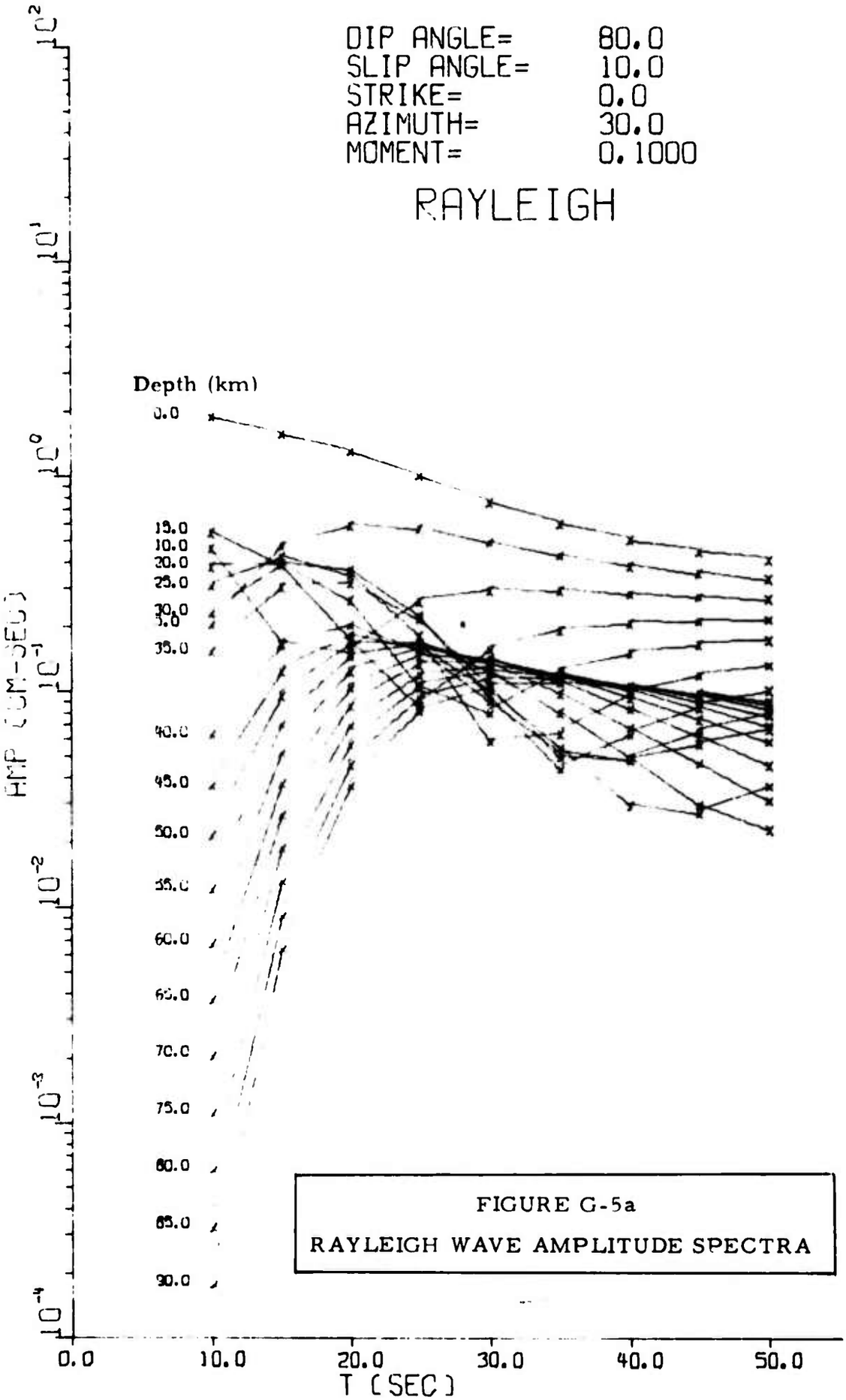

FIGURE G-5a

RAYLEIGH WAVE AMPLITUDE SPECTRA

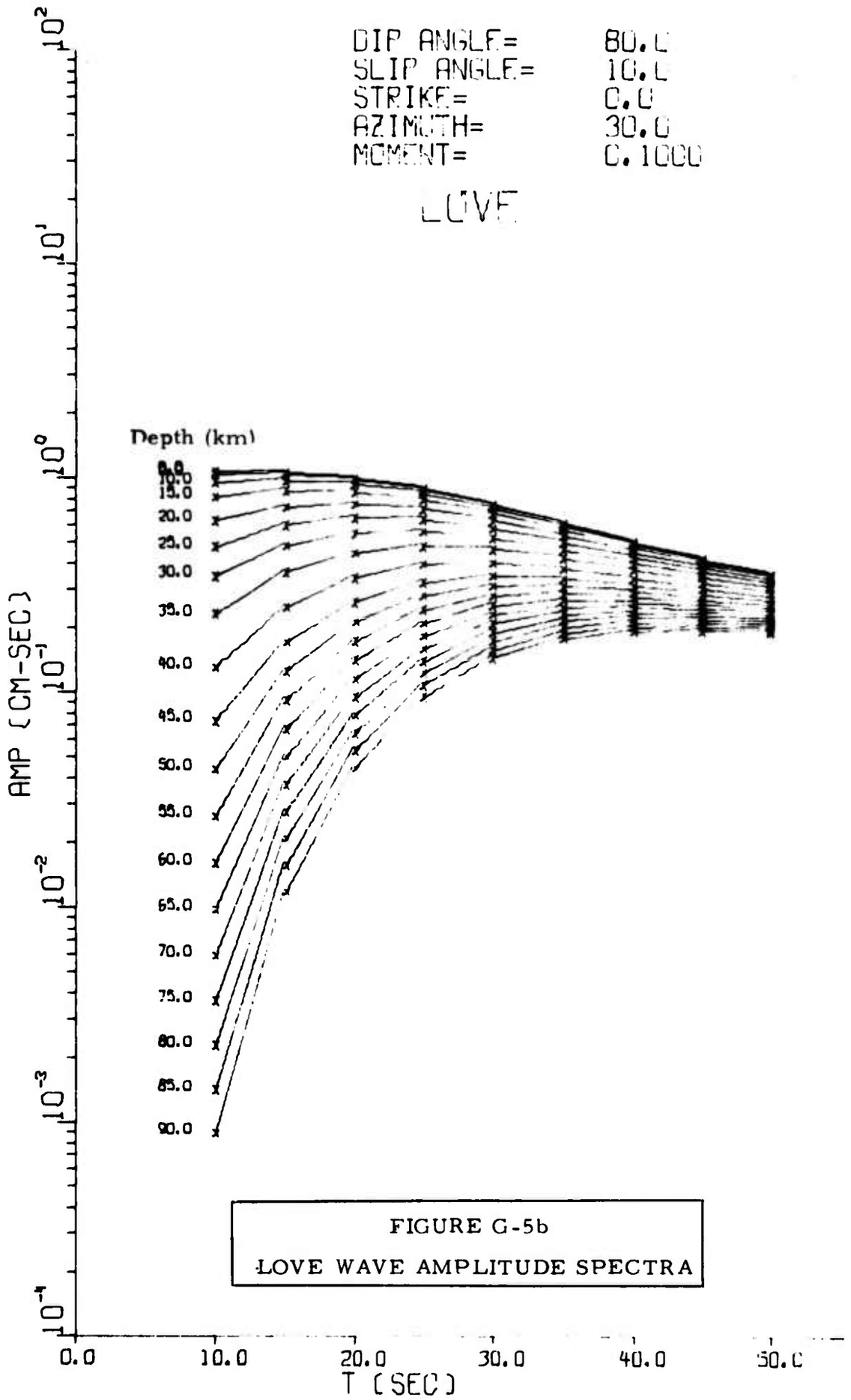

FIGURE G-5b

LOVE WAVE AMPLITUDE SPECTRA

DIP ANGLE= 80.0
SLIP ANGLE= 10.0
STRIKE= 0.0
AZIMUTH= 30.0
MOMENT= 0.1000

LOVE/RAY

FIGURE G-5c

LOVE/RAYLEIGH WAVE AMPLITUDE SPECTRA

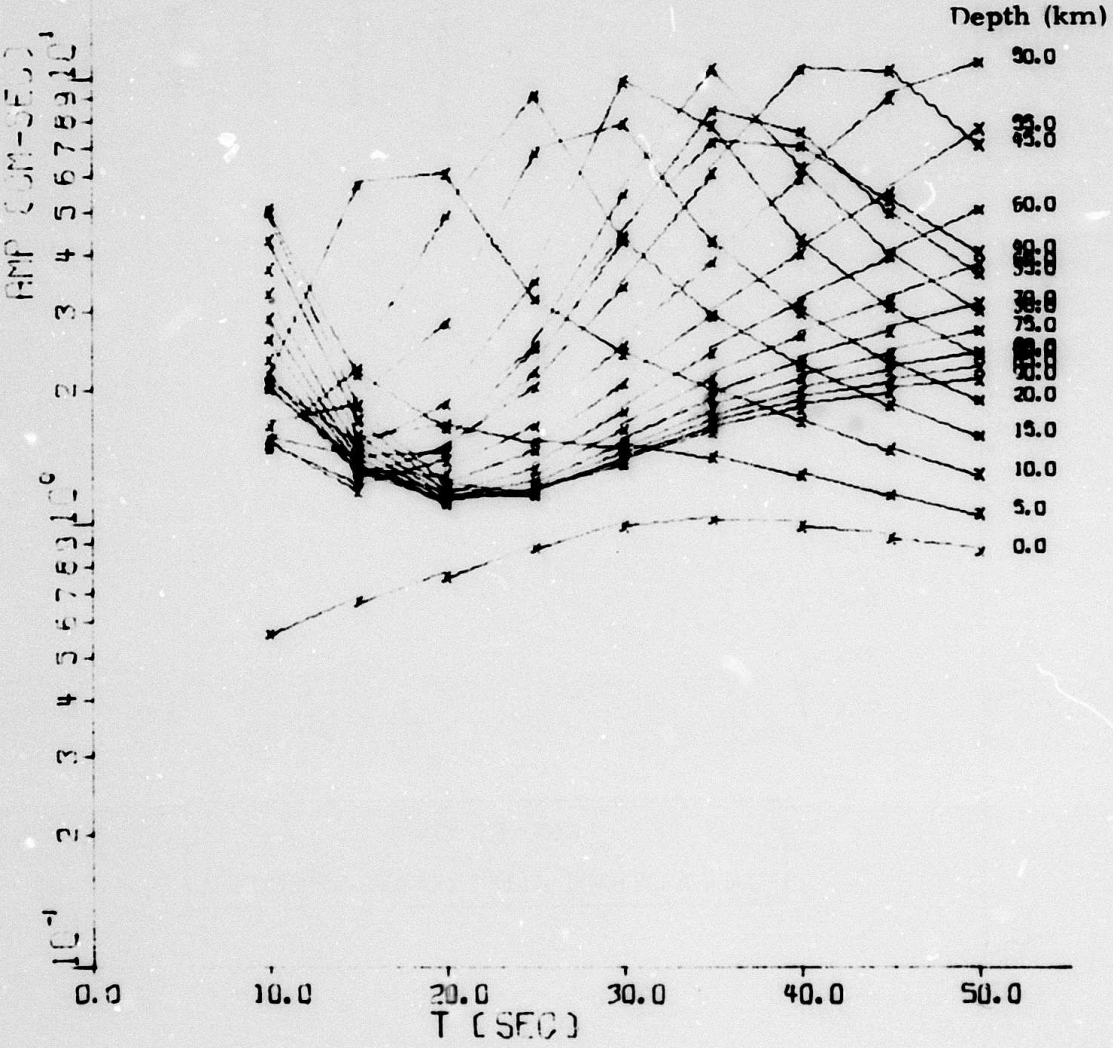

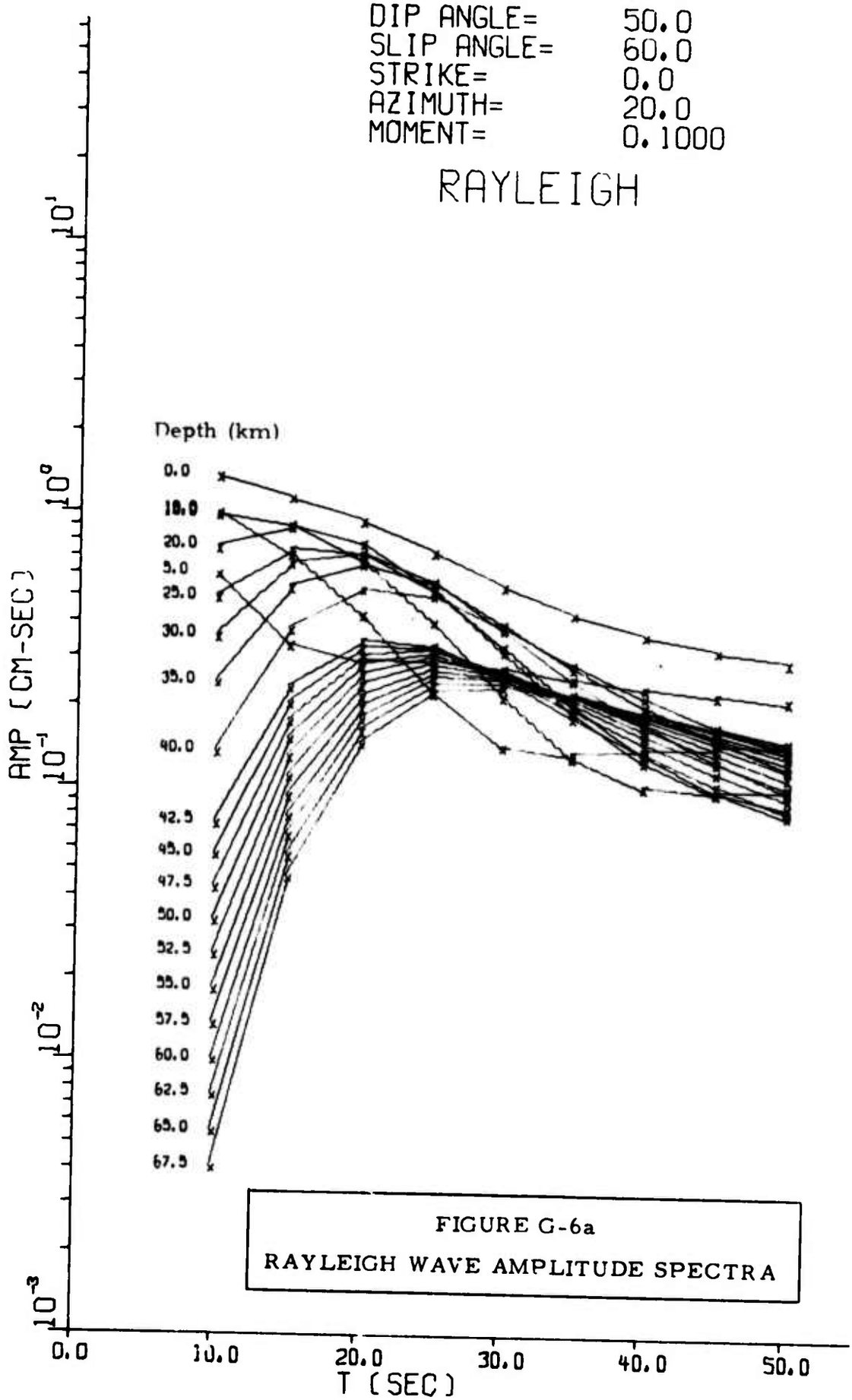

FIGURE G-6a

RAYLEIGH WAVE AMPLITUDE SPECTRA

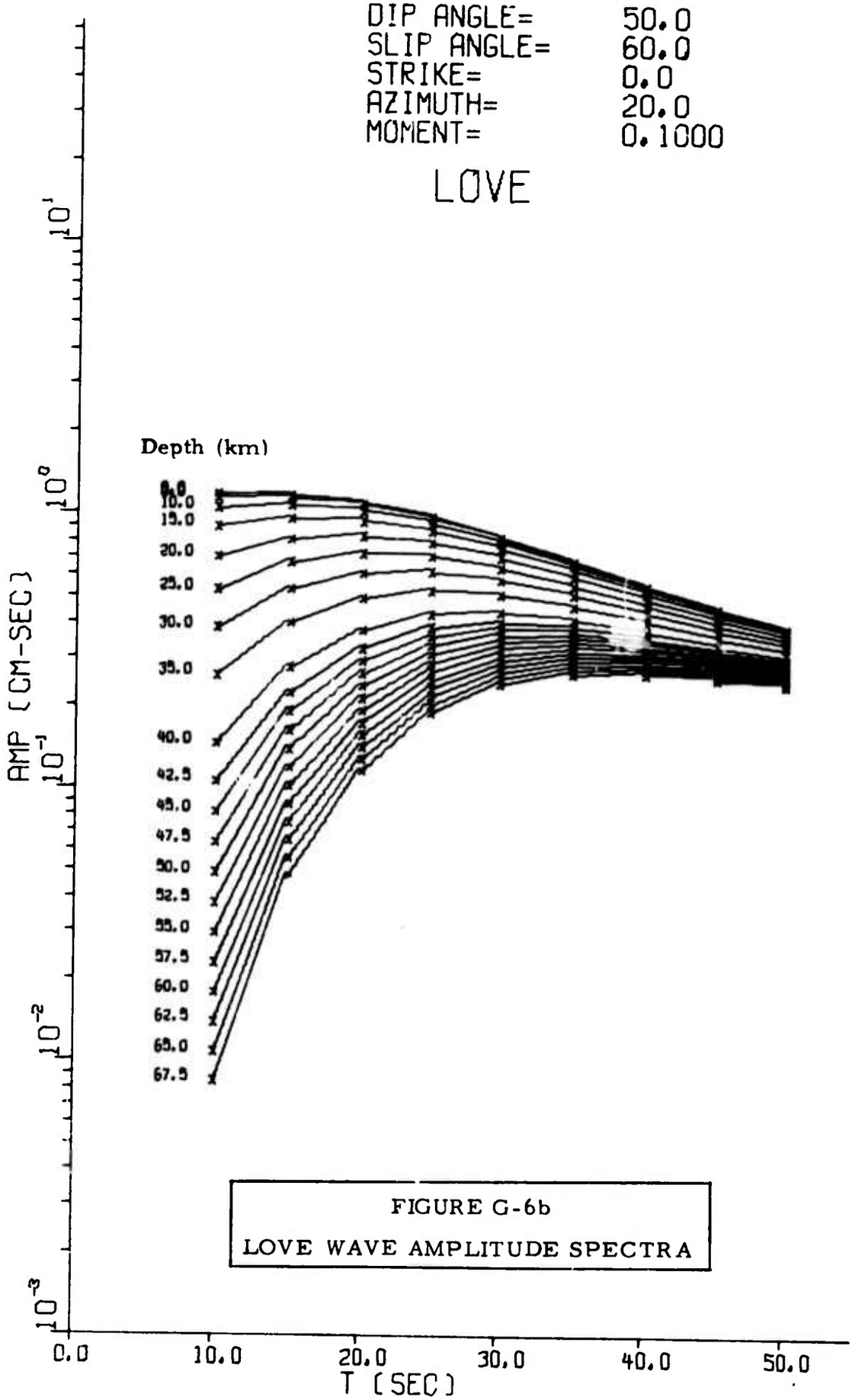

FIGURE G-6b

LOVE WAVE AMPLITUDE SPECTRA

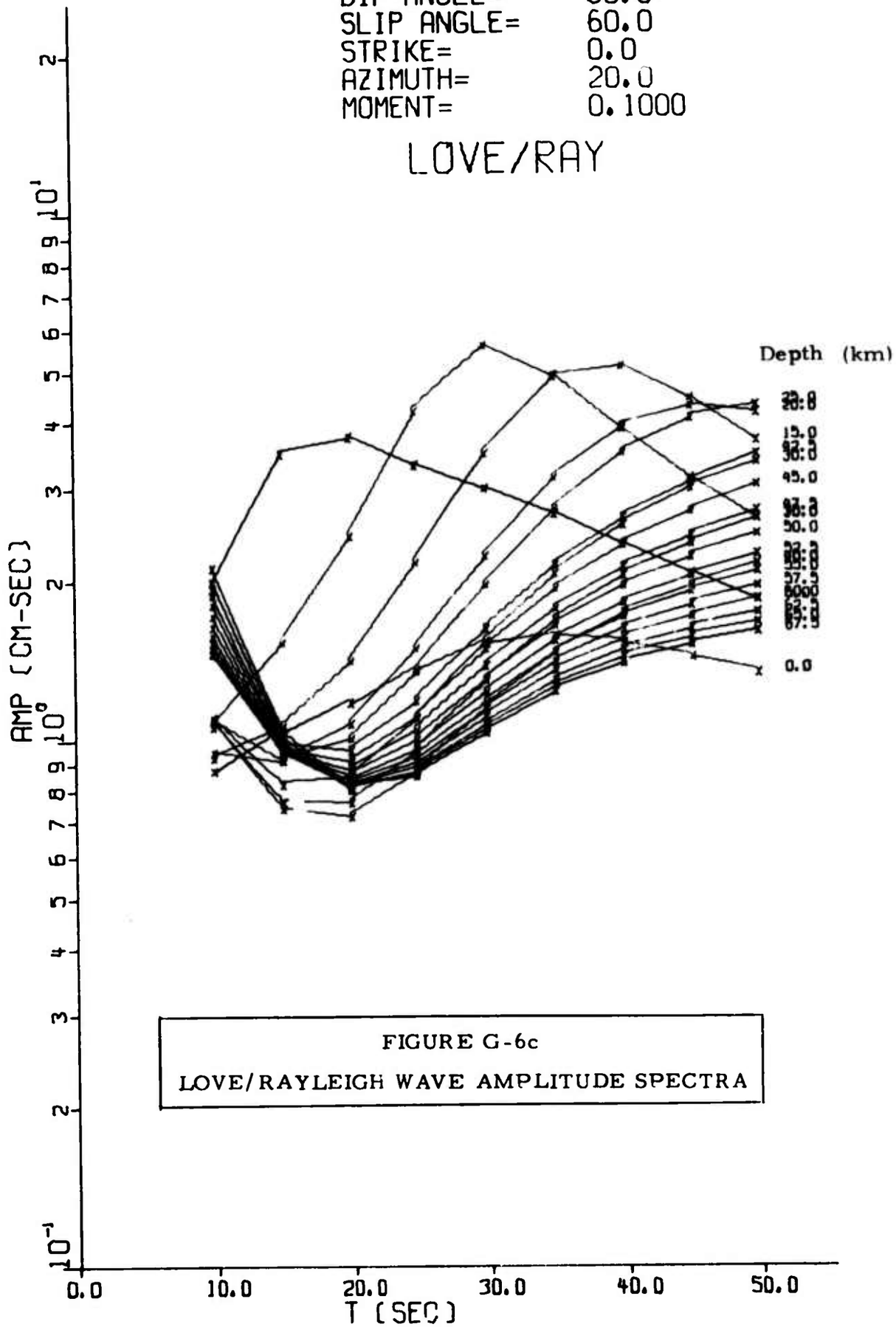

FIGURE G-6c

LOVE/RAYLEIGH WAVE AMPLITUDE SPECTRA

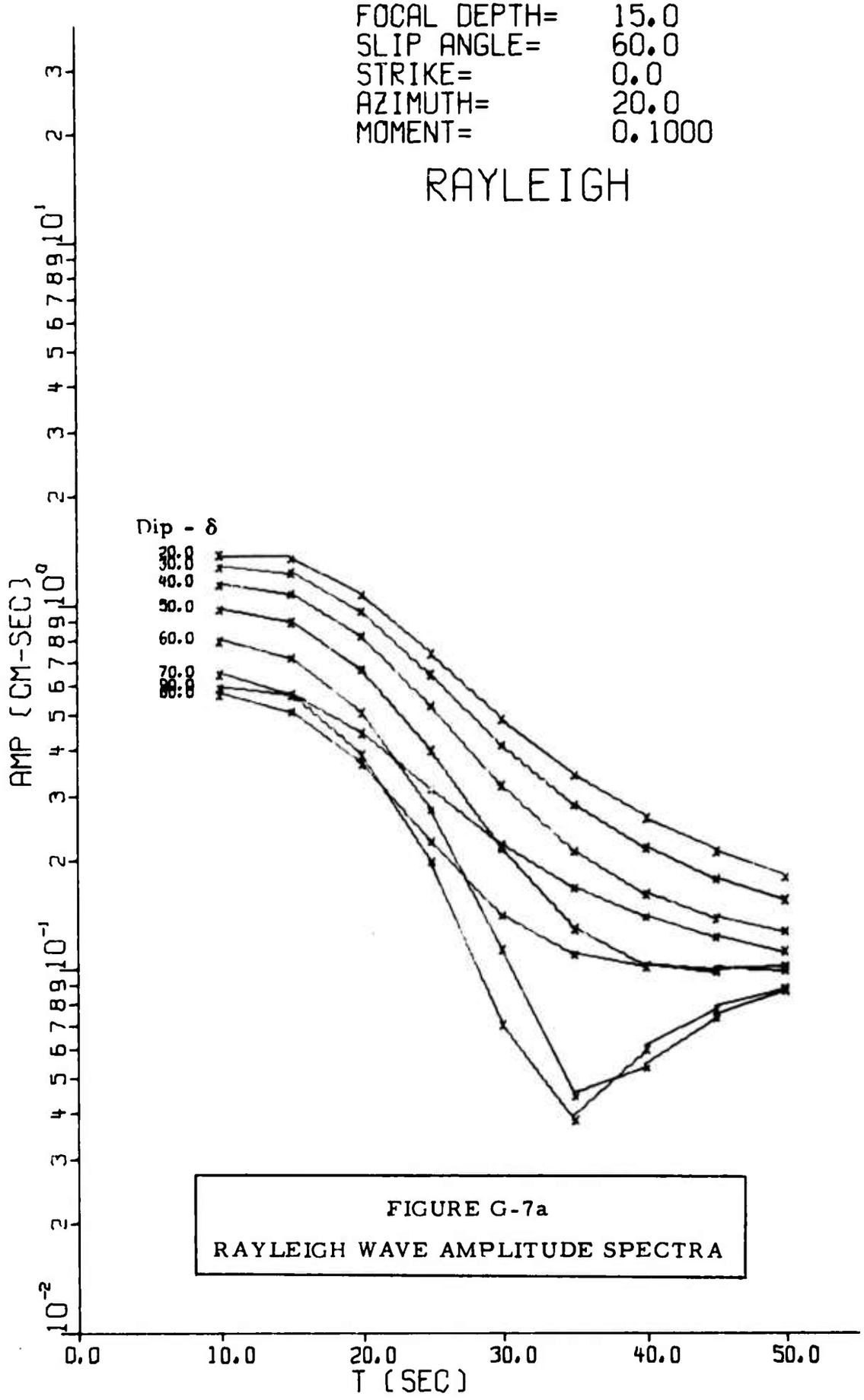

FIGURE G-7a

RAYLEIGH WAVE AMPLITUDE SPECTRA

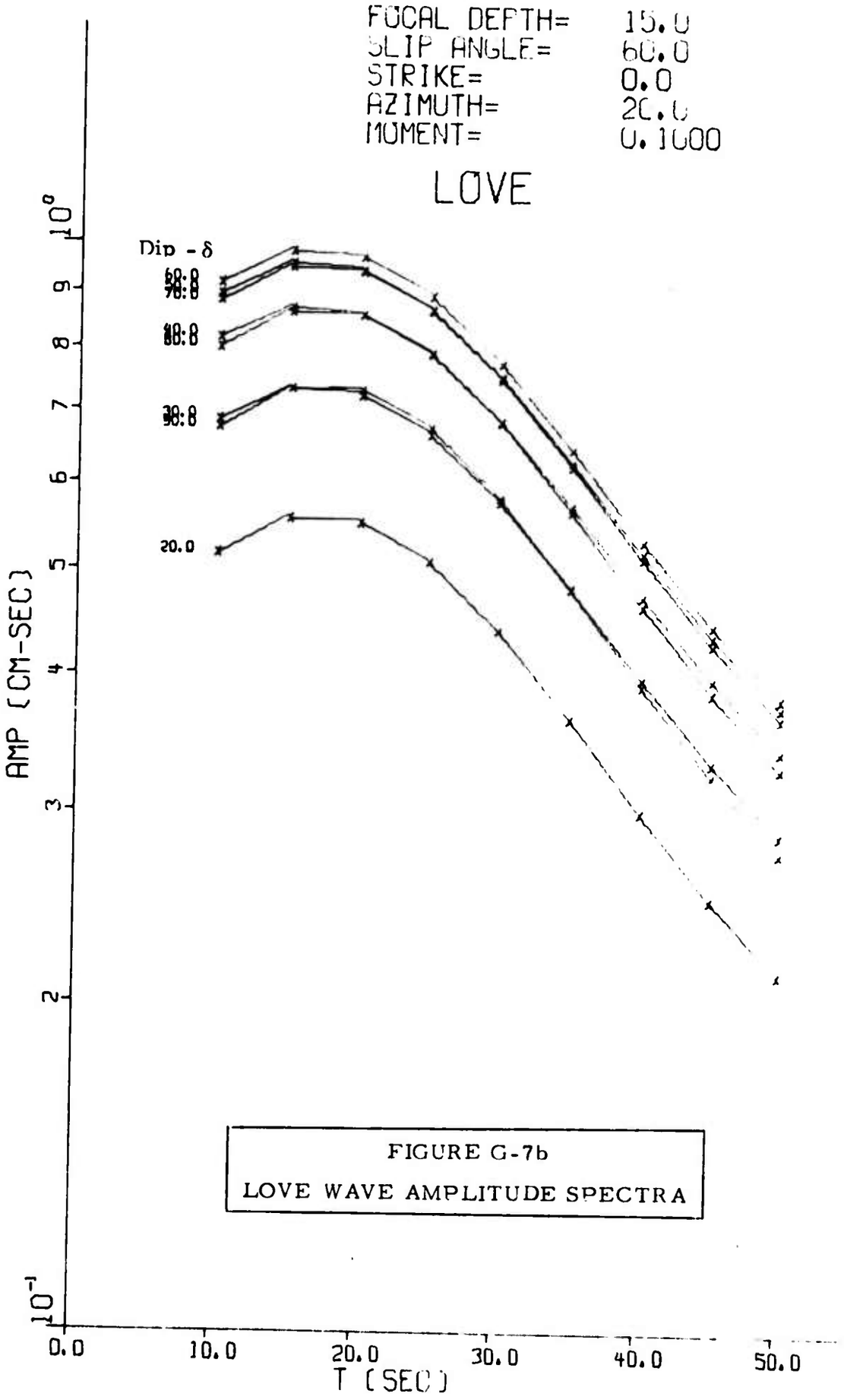

FIGURE G-7b

LOVE WAVE AMPLITUDE SPECTRA

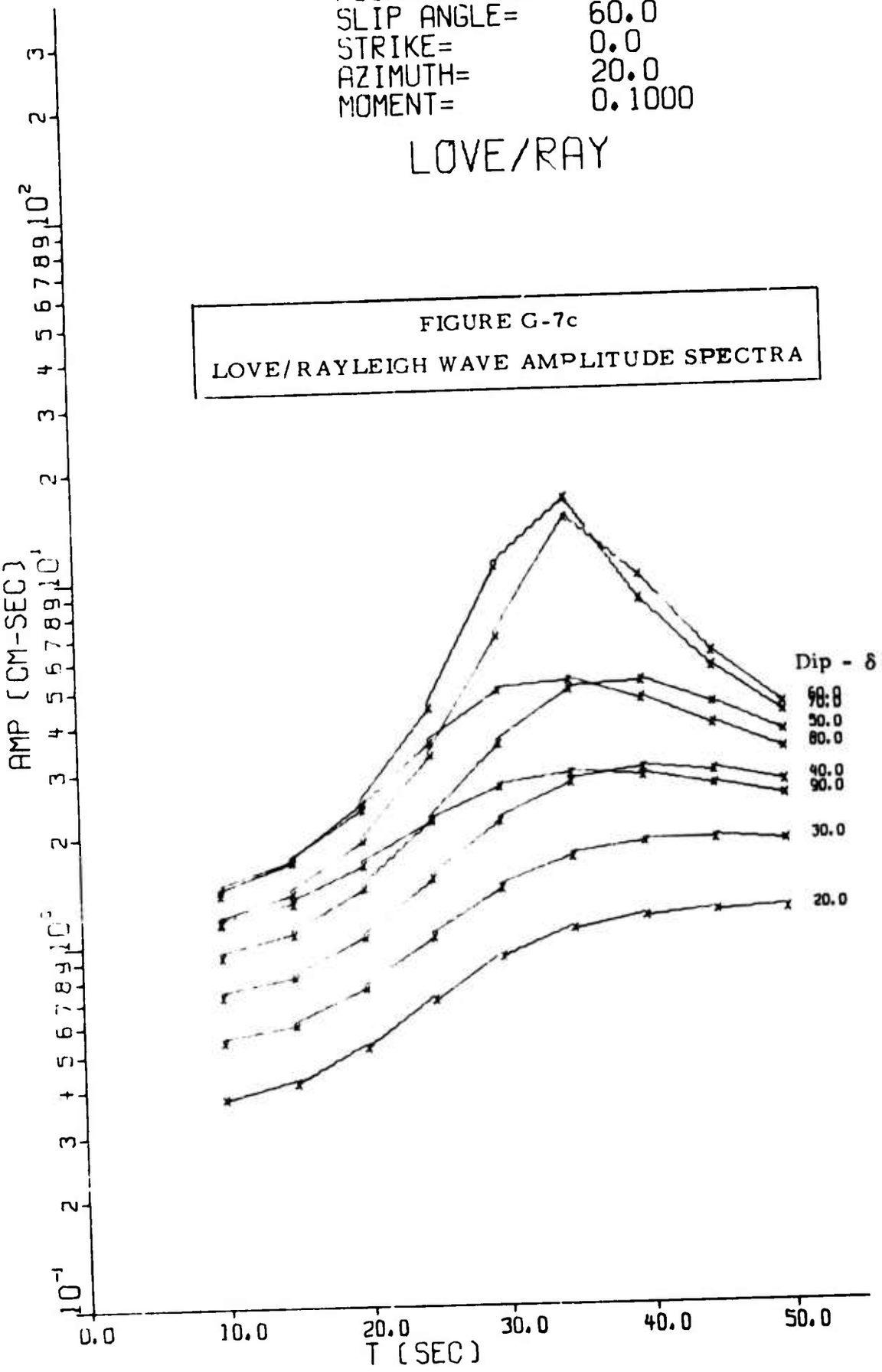

FIGURE G-7c

LOVE/RAYLEIGH WAVE AMPLITUDE SPECTRA

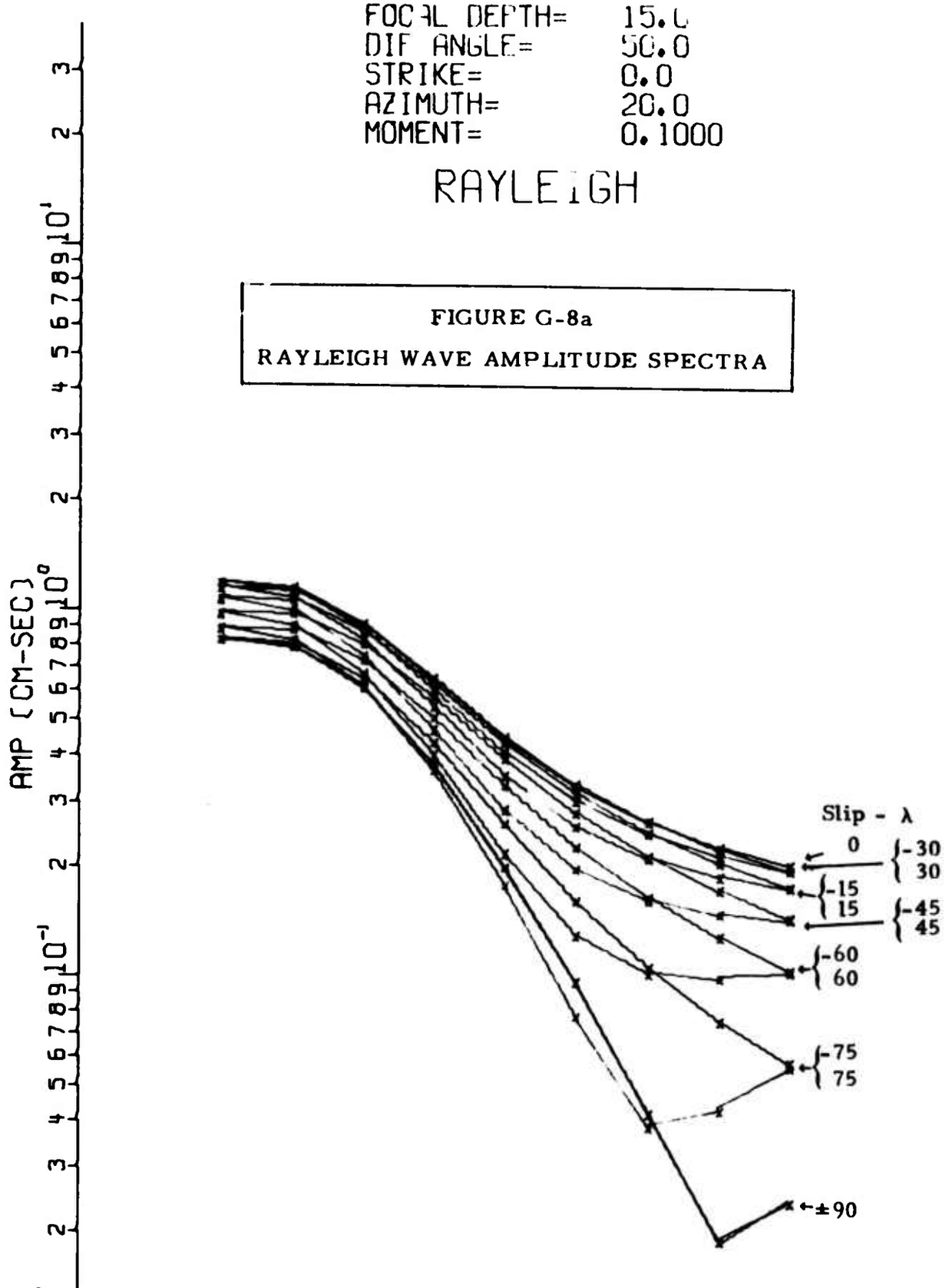

FIGURE G-8a

RAYLEIGH WAVE AMPLITUDE SPECTRA

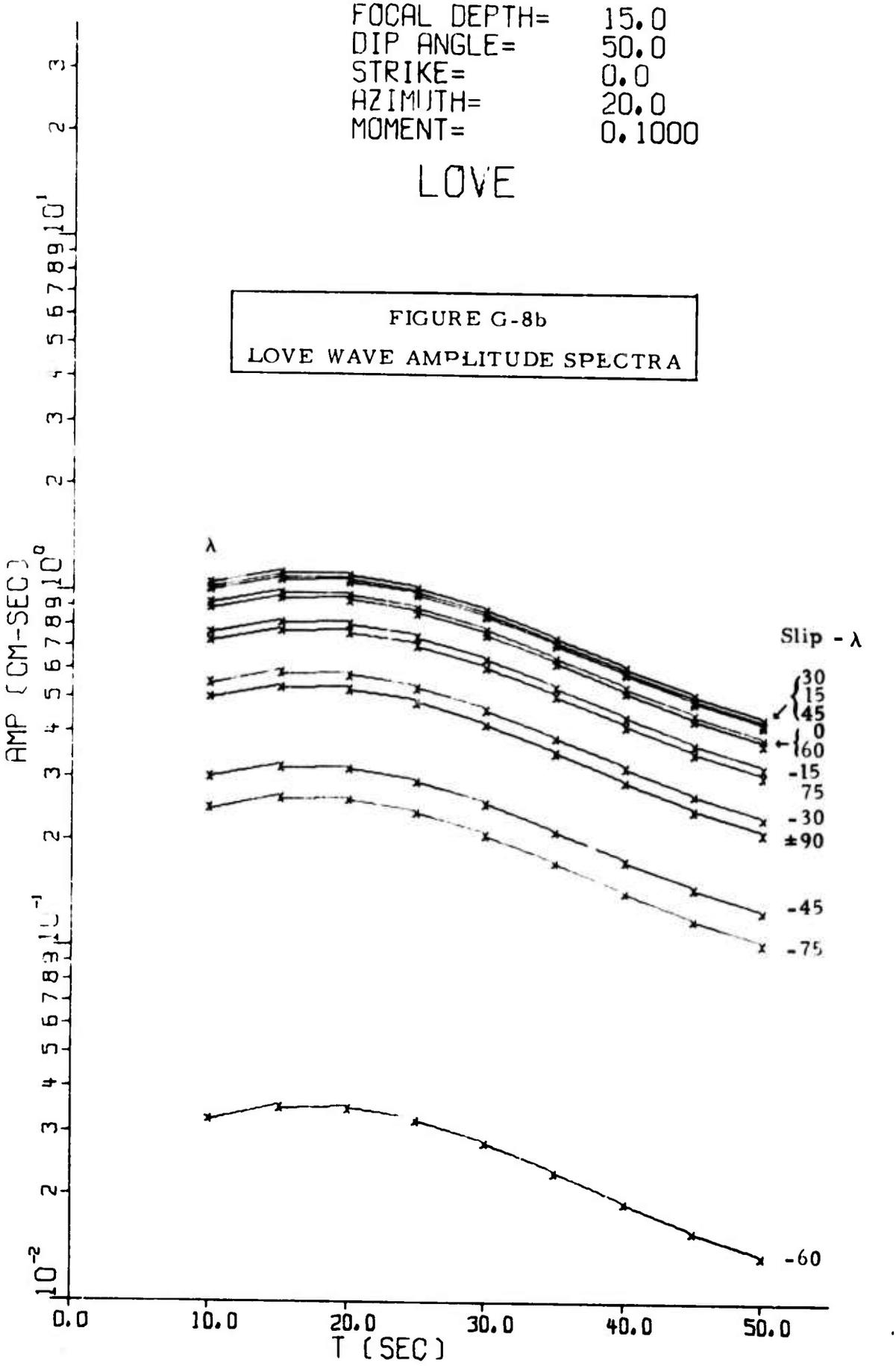

FIGURE G-8b

LOVE WAVE AMPLITUDE SPECTRA

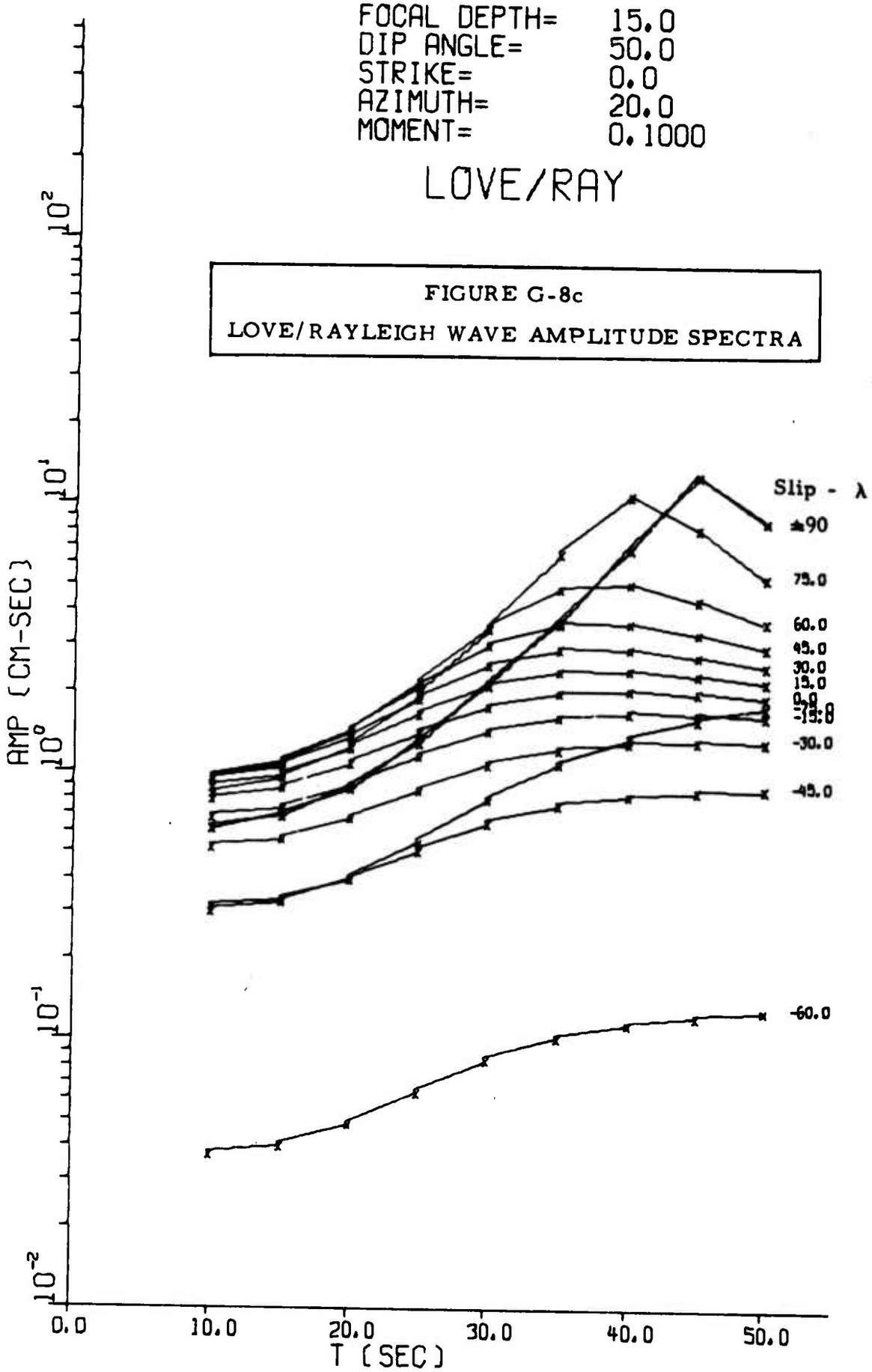

FIGURE G-8c

LOVE/RAYLEIGH WAVE AMPLITUDE SPECTRA

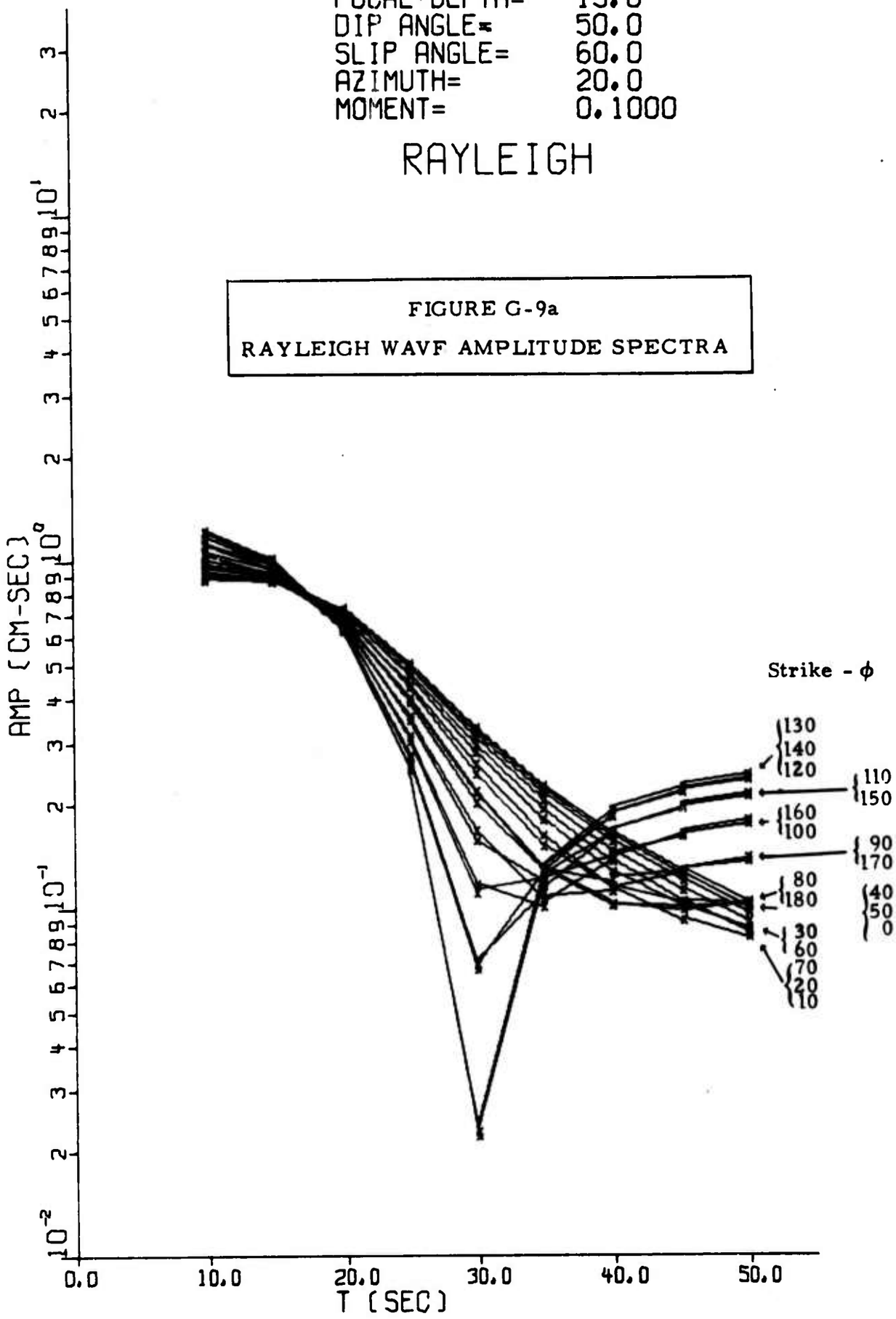

FIGURE G-9a

RAYLEIGH WAVF AMPLITUDE SPECTRA

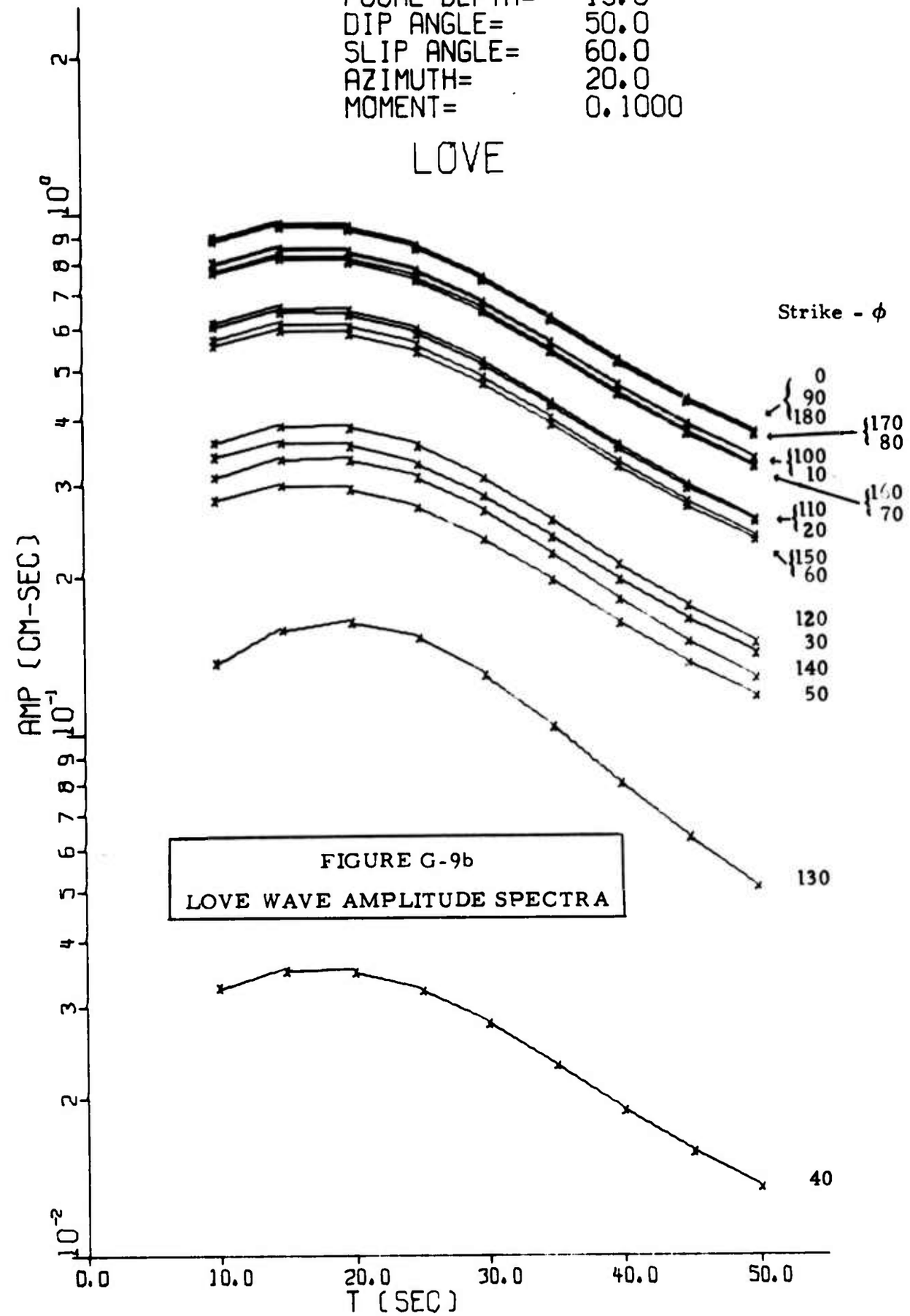

FIGURE G-9b

LOVE WAVE AMPLITUDE SPECTRA

FOCAL DEPTH= 15.0
DIP ANGLE= 50.0
SLIP ANGLE= 60.0
AZIMUTH= 20.0
MOMENT= 0.1000

LOVE/RAY

FIGURE G-9c

LOVE/RAYLEIGH WAVE AMPLITUDE SPECTRA

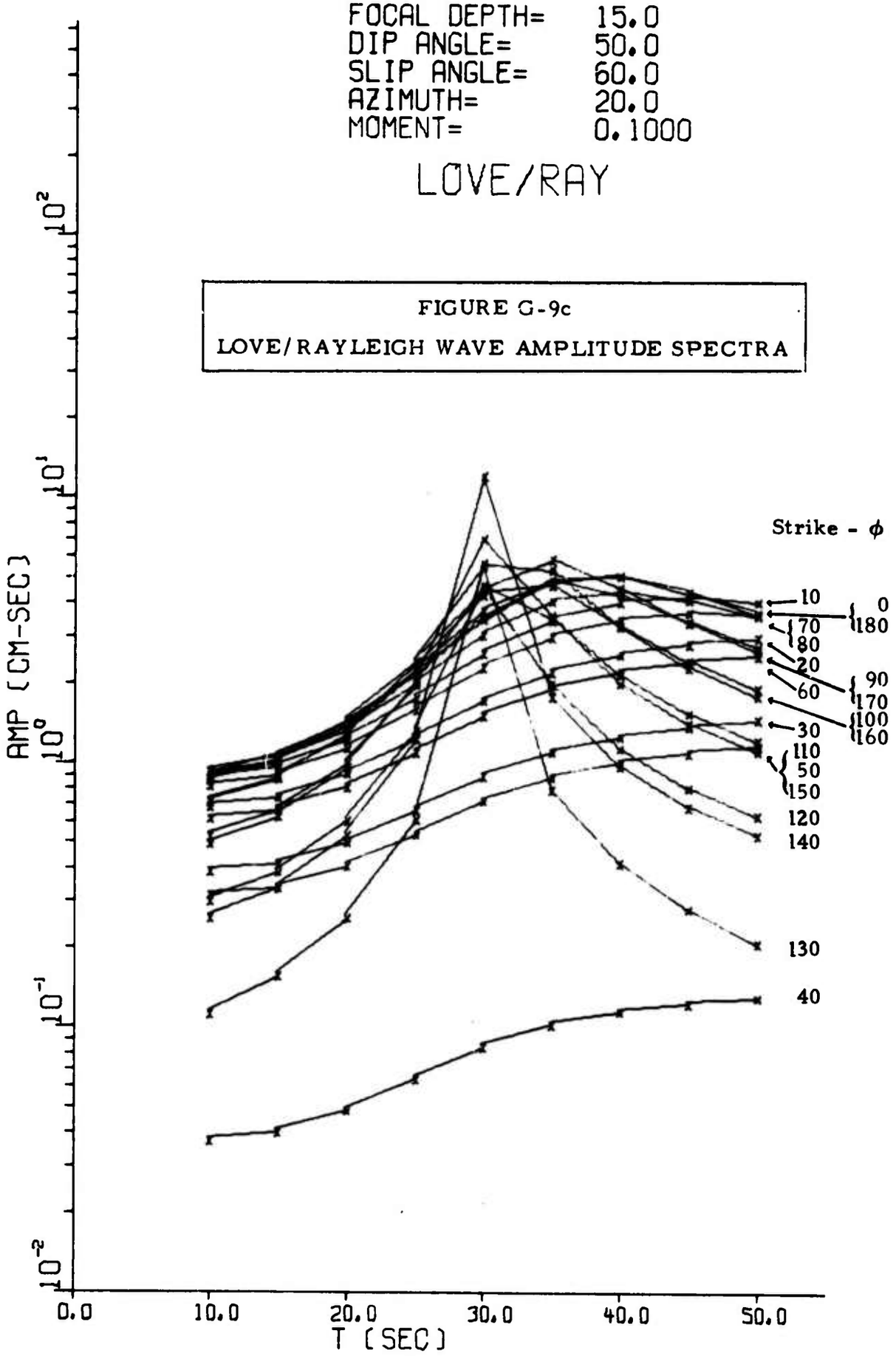

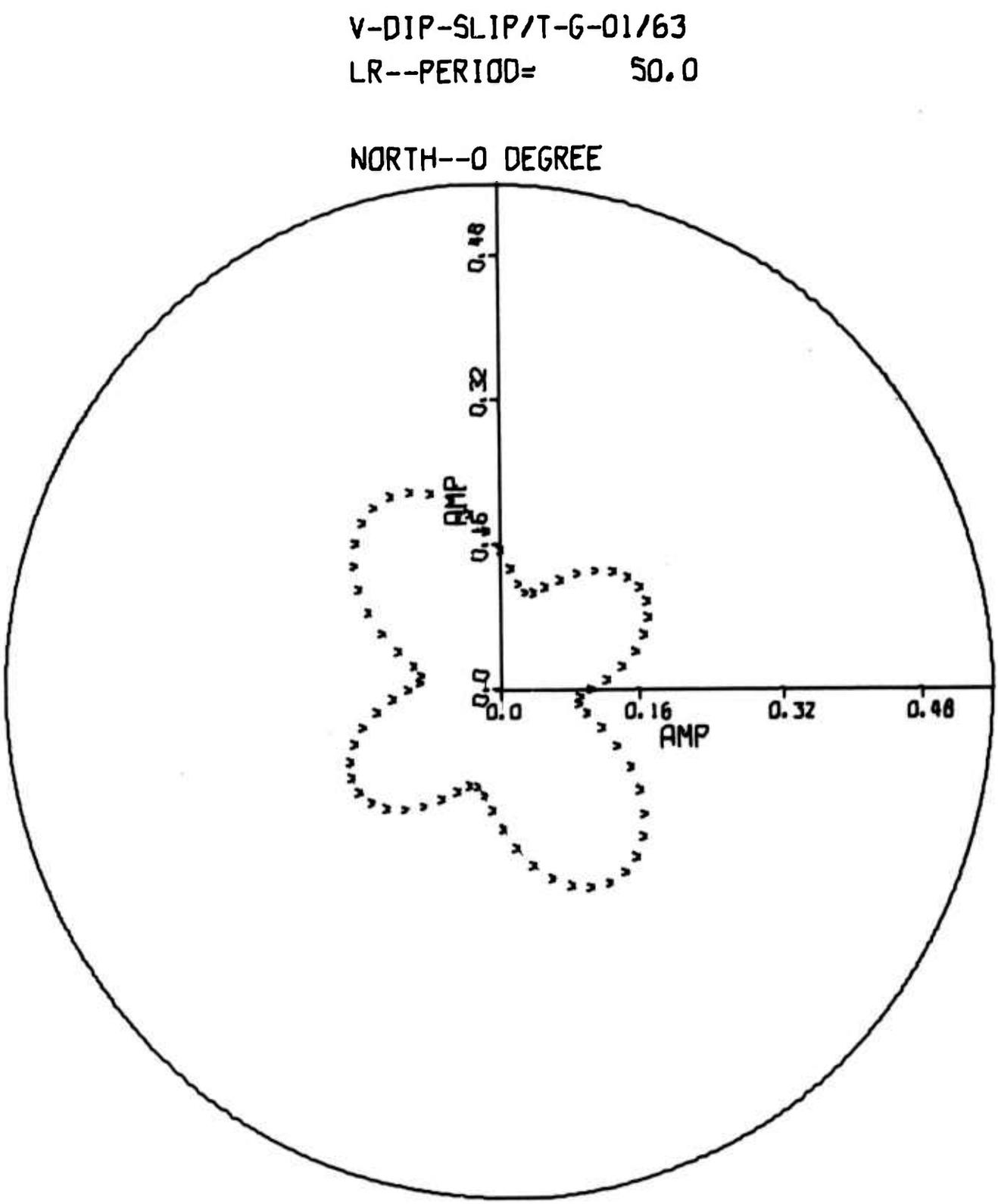

FIGURE G-10a

RAYLEIGH WAVE RADIATION PATTERNS

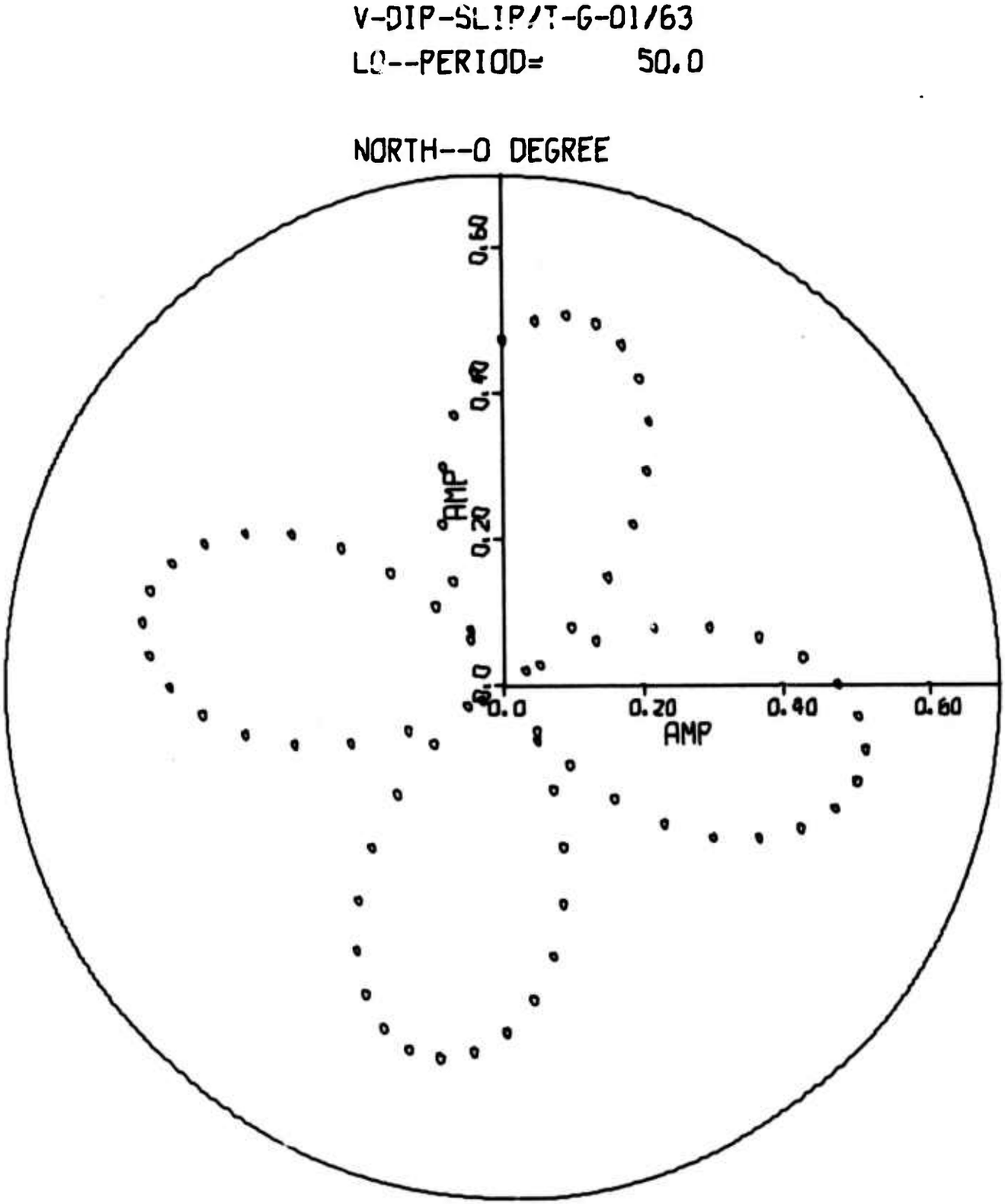

FIGURE G-10b

LOVE WAVE RADIATION PATTERNS

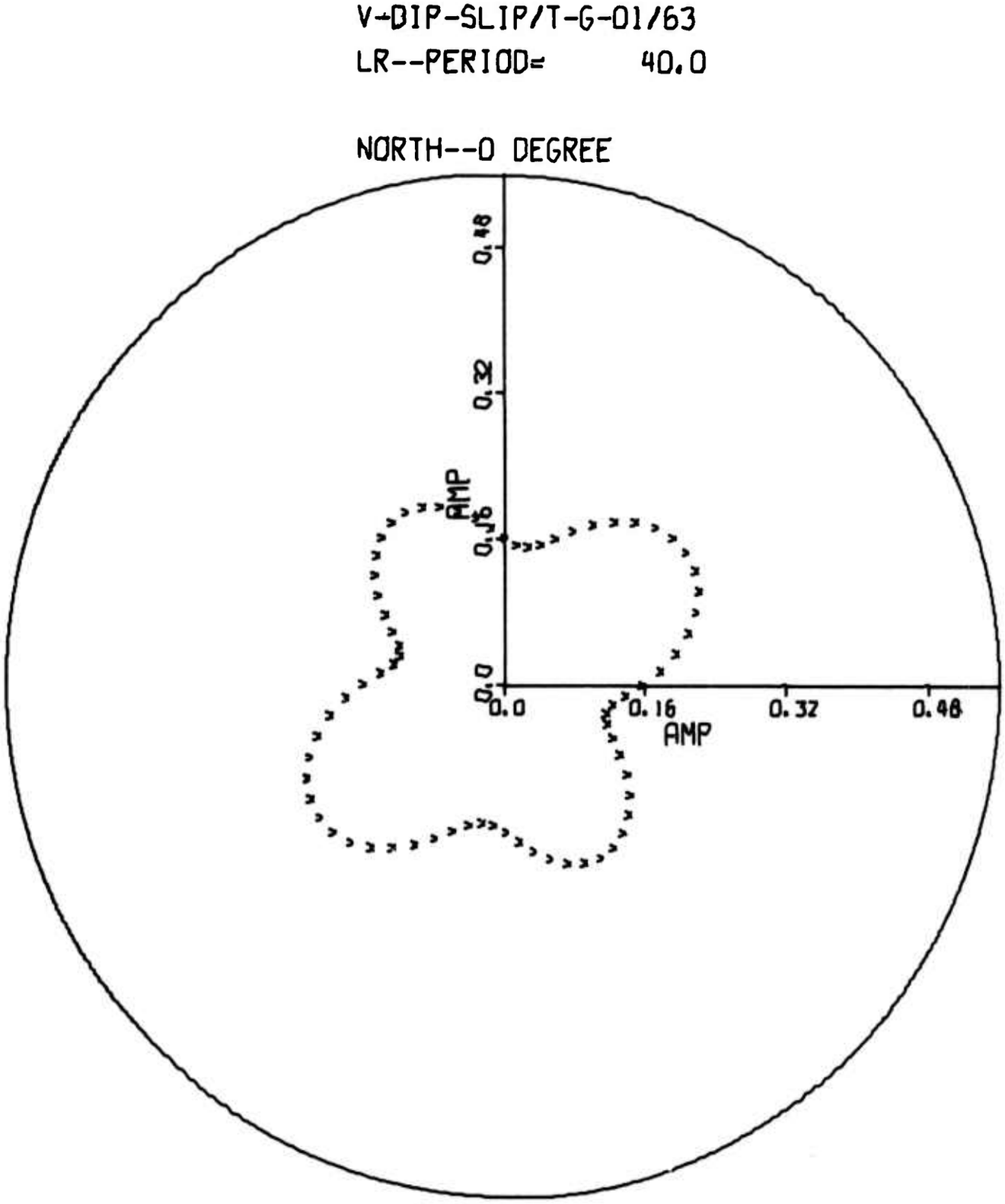

FIGURE G-11a

RAYLEIGH WAVE RADIATION PATTERNS

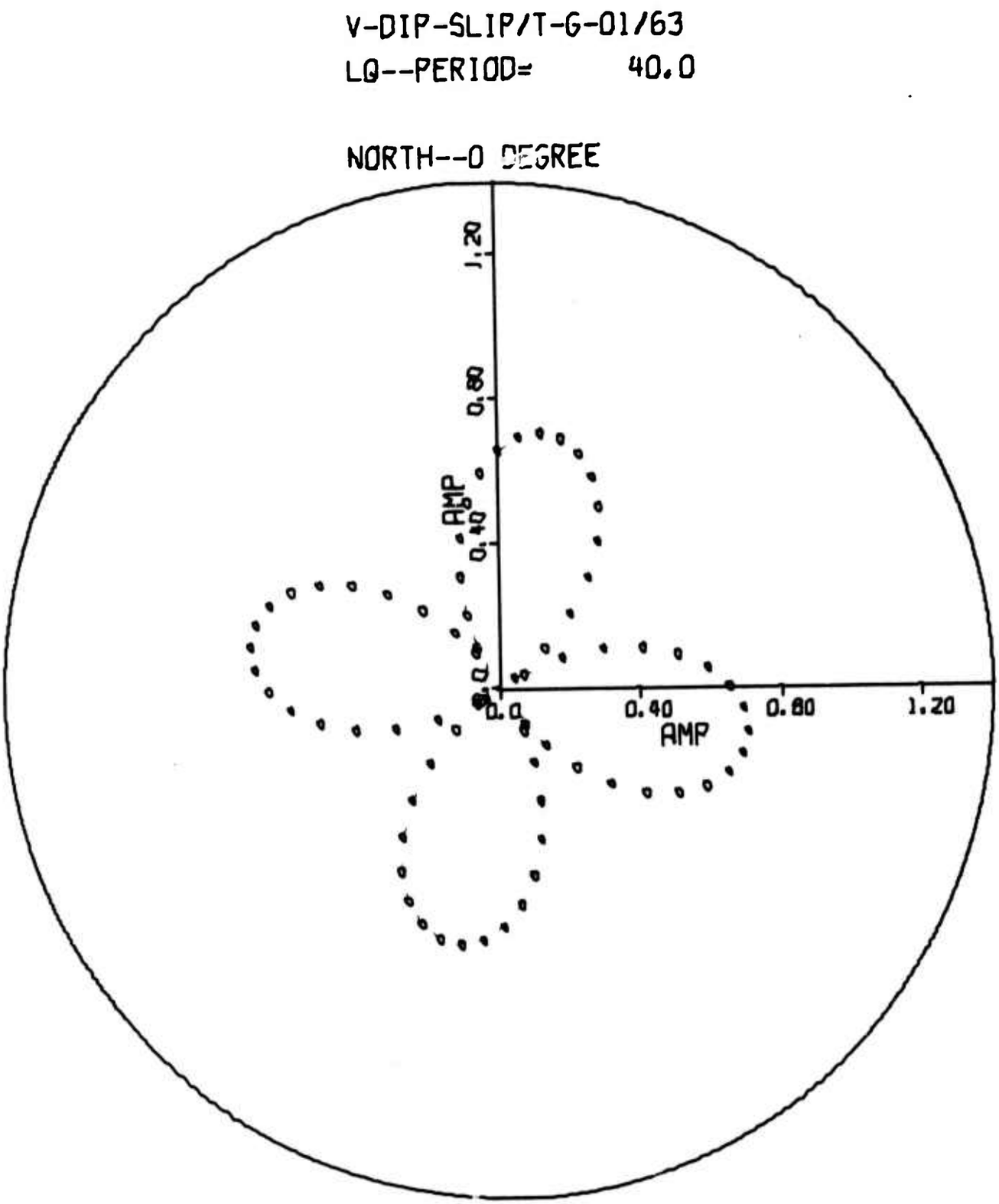

FIGURE G-11b

LOVE WAVE RADIATION PATTERNS

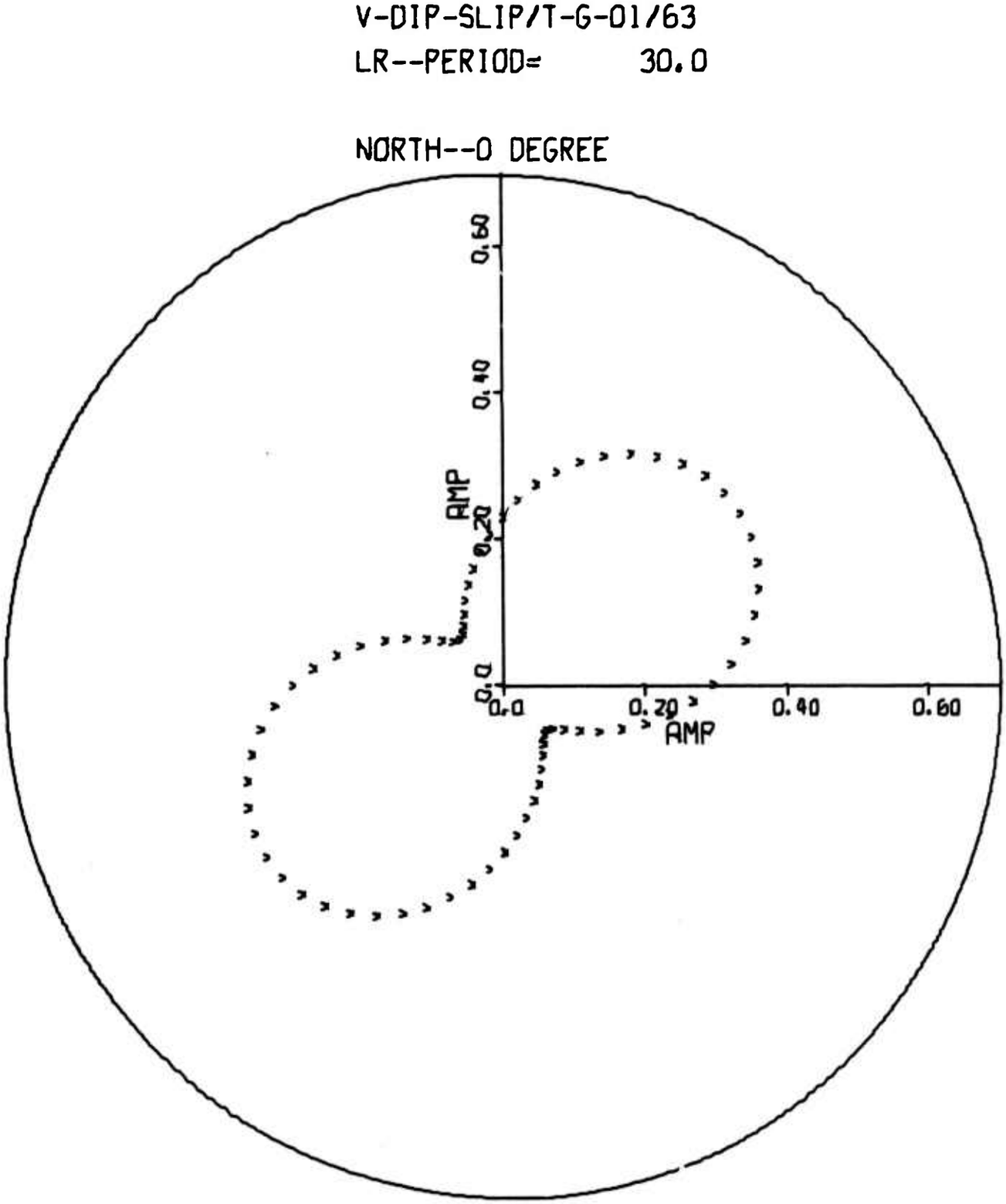

FIGURE G-12a

RAYLEIGH WAVE RADIATION PATTERNS

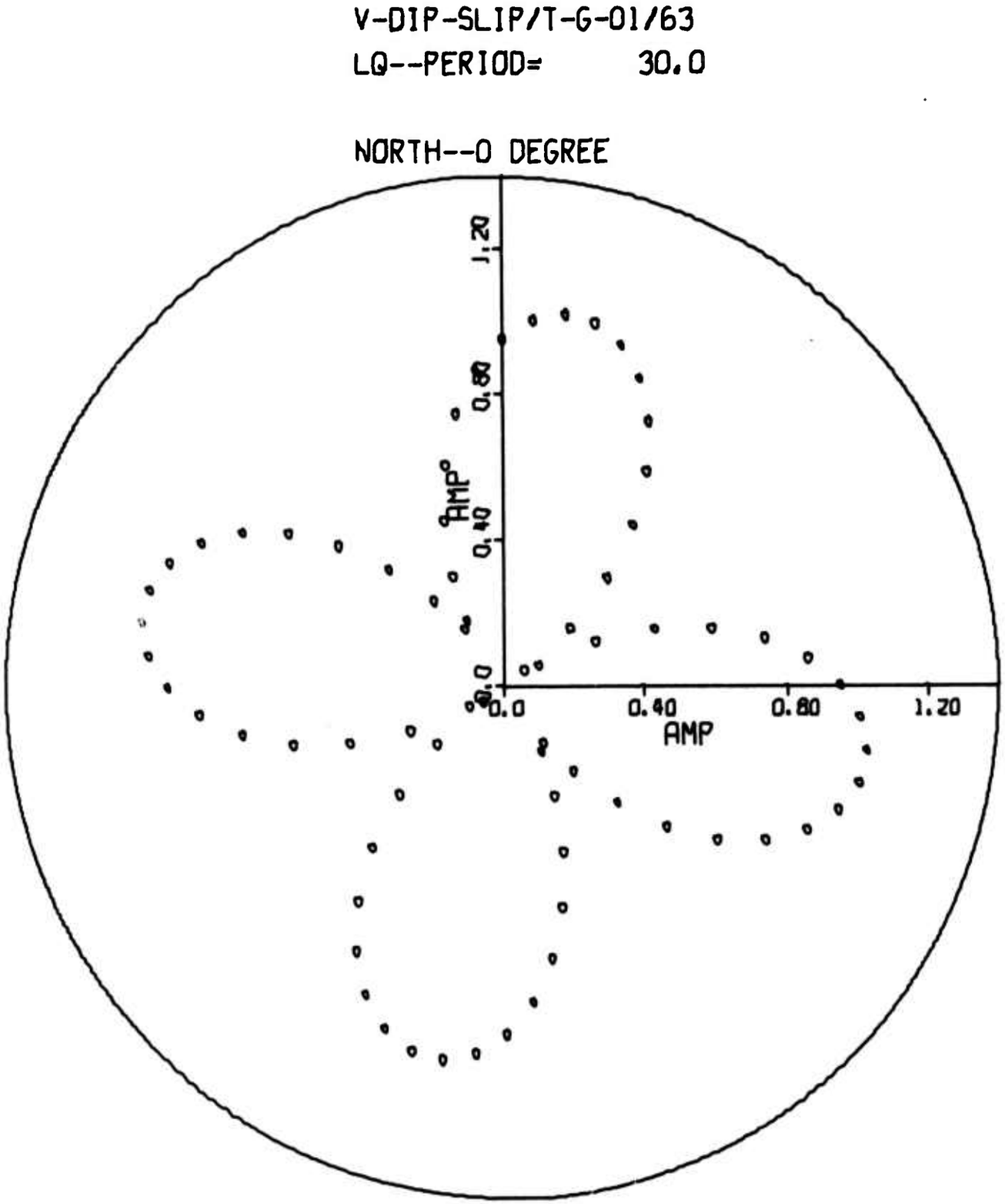

FIGURE G-12b

LOVE WAVE RADIATION PATTERNS

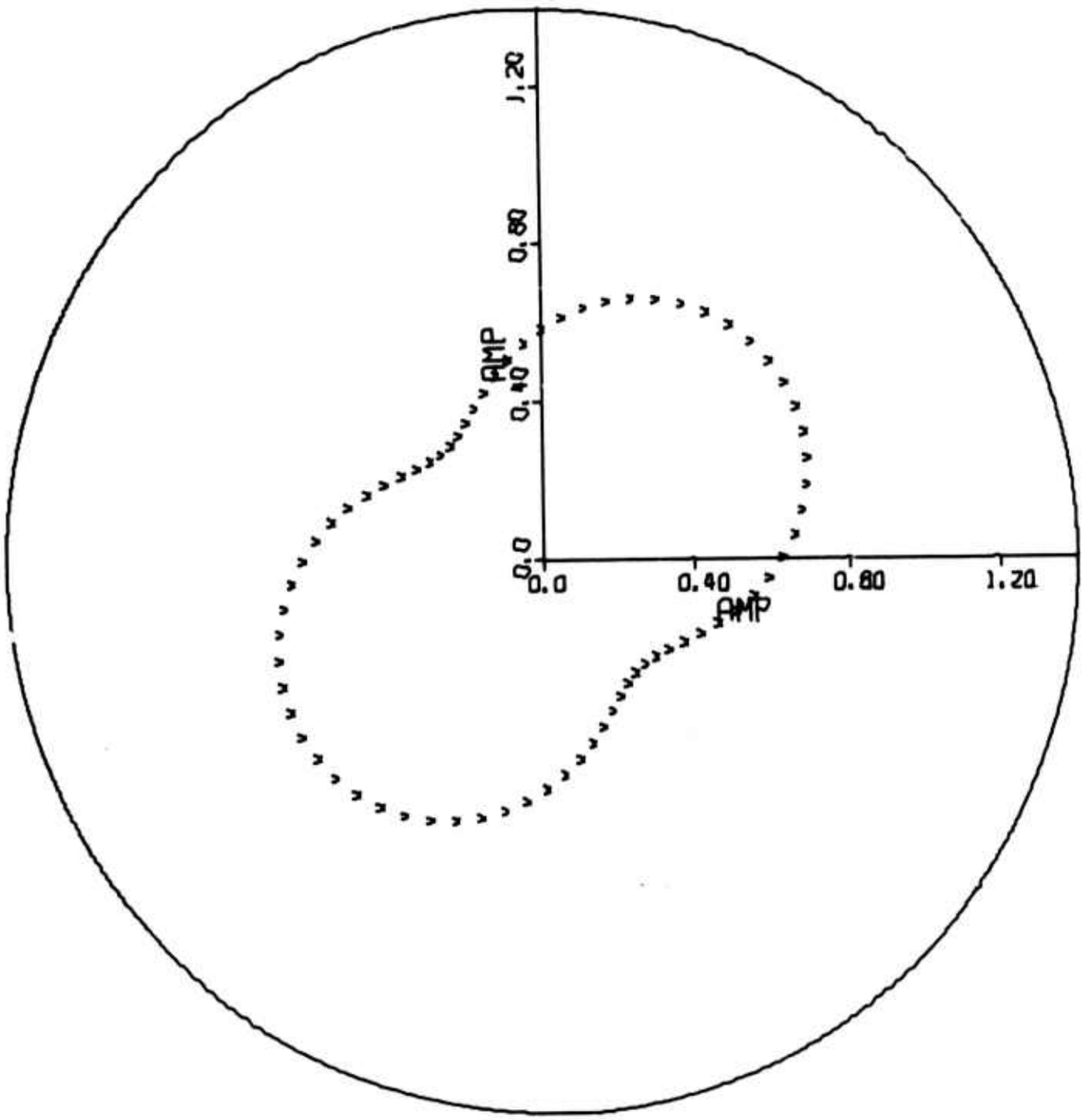

FIGURE G-13a

RAYLEIGH WAVE RADIATION PATTERNS

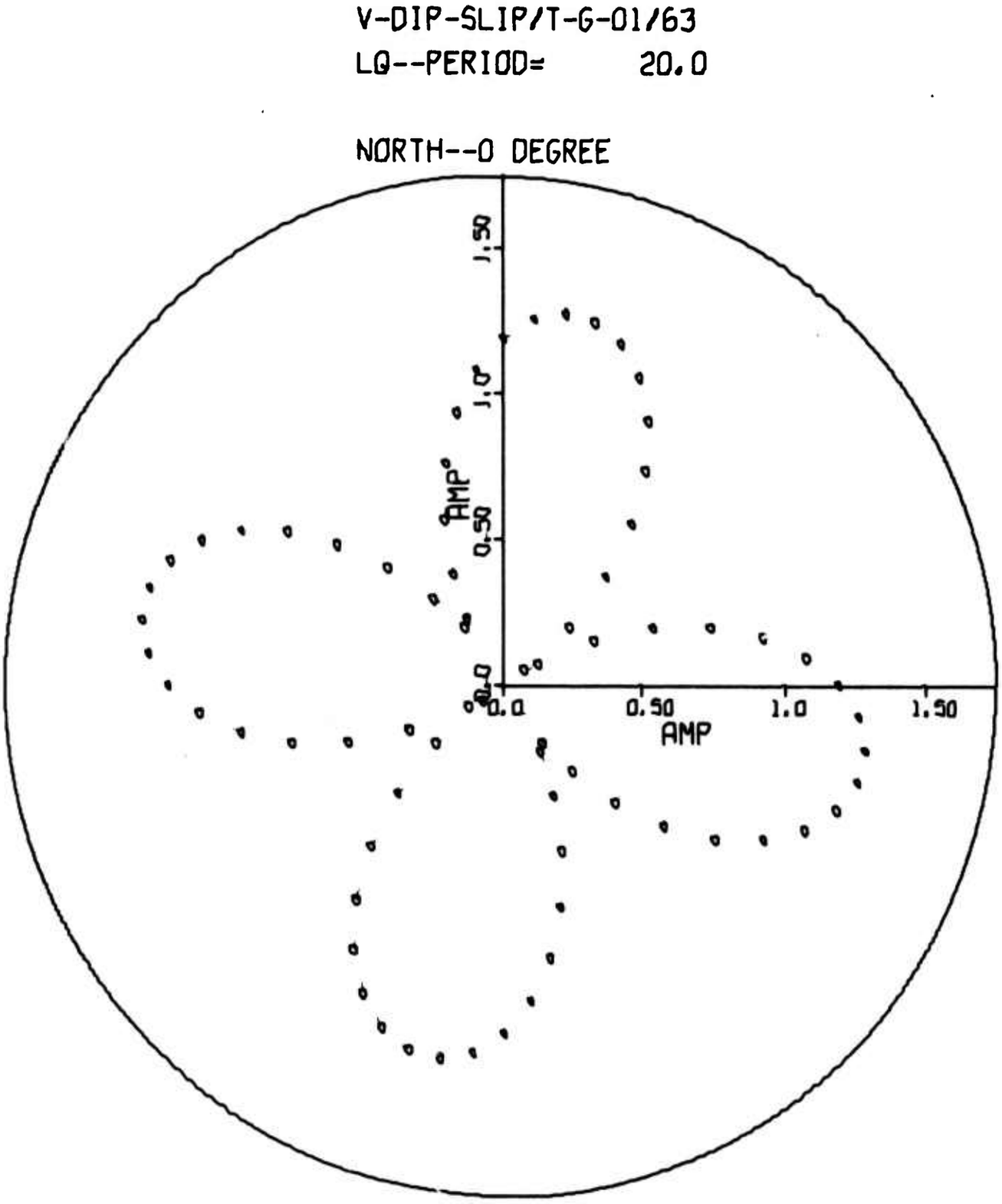

FIGURE G-13b

LOVE WAVE RADIATION PATTERNS

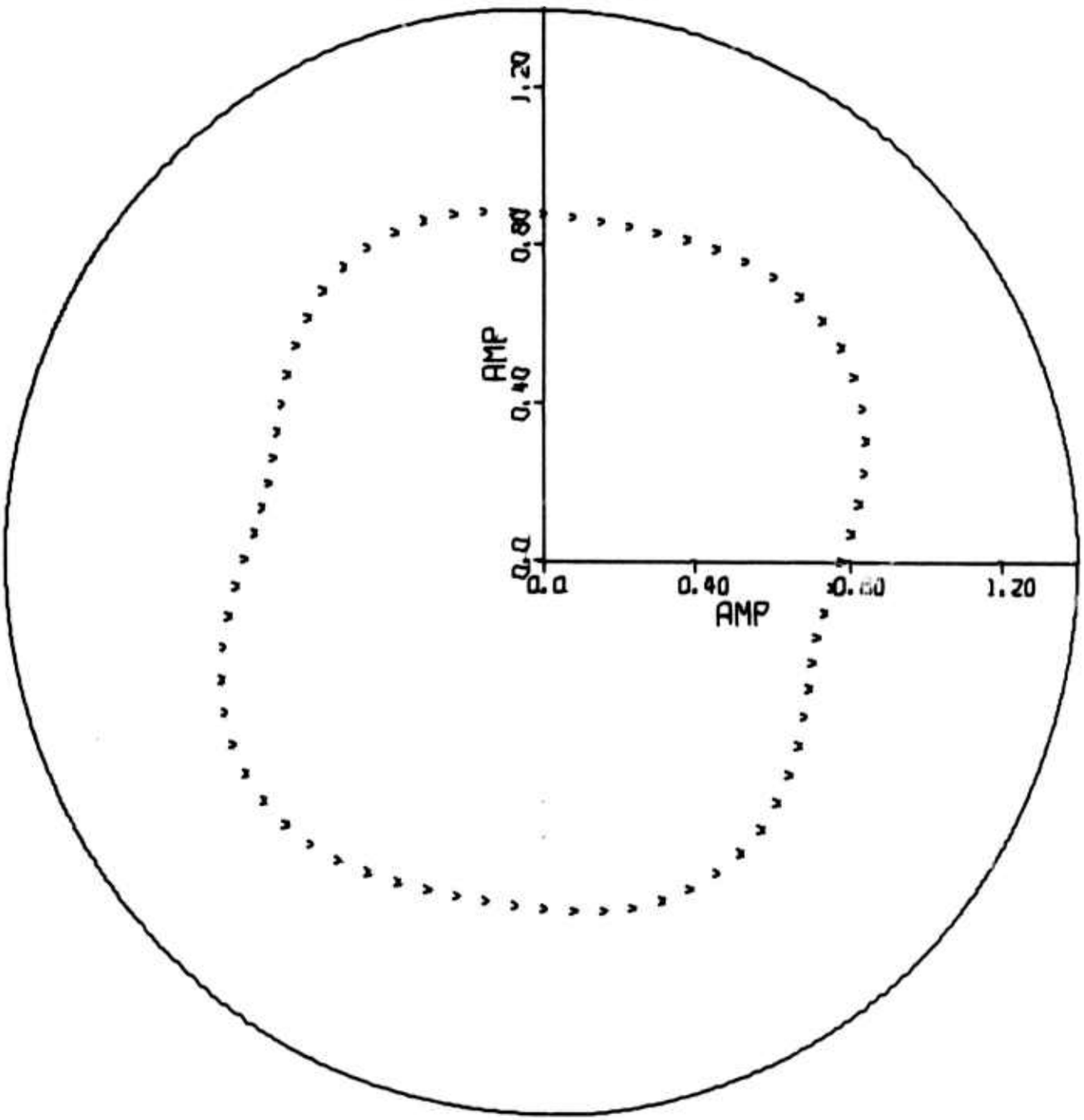

FIGURE G-14a

RAYLEIGH WAVE RADIATION PATTERNS

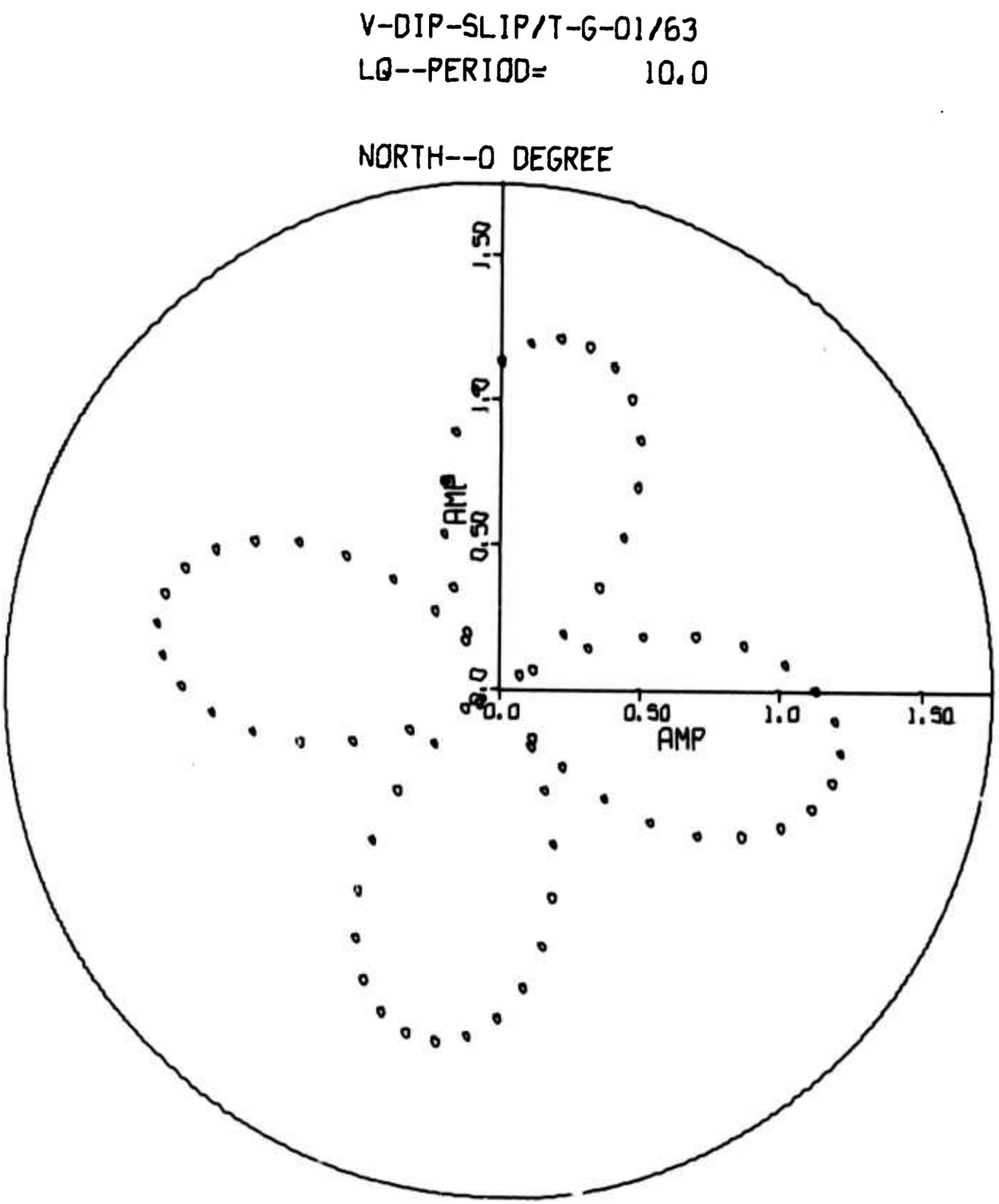

FIGURE G-14b

LOVE WAVE RADIATION PATTERNS

APPENDIX H

EXAMPLES OF MULTIPATHING FROM SINKIANG TO SELECTED VLPE STATIONS

For practically all VLPE records of Sinkiang events, severe multipathing occurred. Figures H-1 show the results of narrow band filters applied to the record at CHG from event KIRSI/059, with Figure H-2 showing the group velocities of the wave packet peaks at each period plotted with standard group velocity curves. The wave packet peaks are numbered in order of descending amplitude. We see that by matching a general trend of the curves with the plotted points, direct path amplitudes are obtained. For both the Rayleigh and Love waves (Figures H-3: narrowband filters, and Figure H-4: Love wave group velocities) recorded at CHG, we see very low group velocities (although some of this could be due to group delay of the instrument). Two other sets of Rayleigh and Love wave group velocity curves are shown in Figures H-5 to H-8, demonstrating 'typ paths encountered. Figures H-5 and H-6 for event KIRSI/059 recorded at FBK, show fairly close adherence to the Rayleigh wave group velocity curve, while severe multipathing occurs for the Love waves below 30 seconds period. Figures H-7 and H-8 for the same event recorded at KIP show the effects that a part continental-part oceanic path have on the group velocity curve.

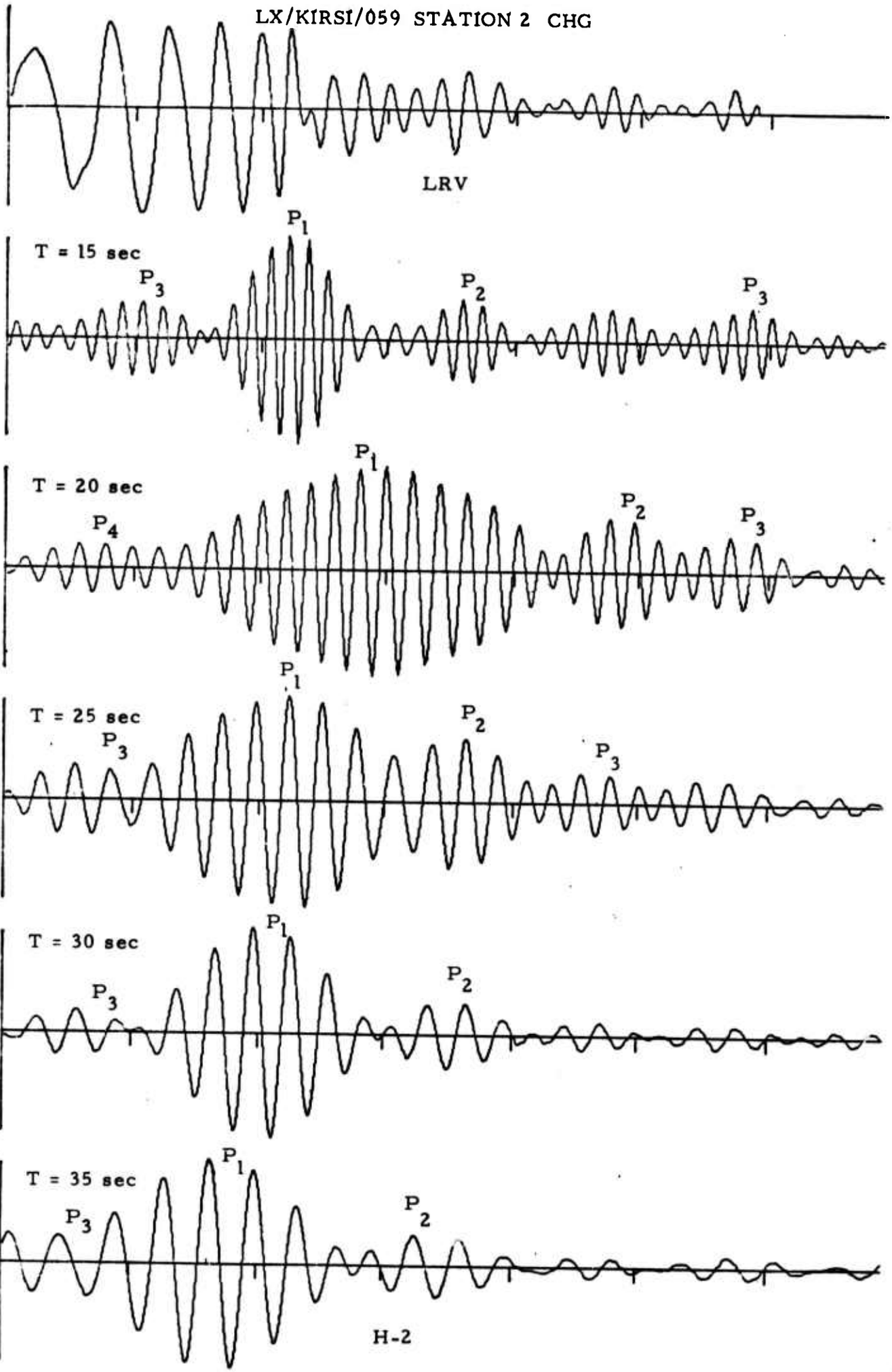

FIGURE H-1a
NARROWBAND FILTER ANALYSIS OF THE VERTICAL RAYLEIGH WAVE
OF EVENT LX/KIRSI/059 RECORDED AT CHG

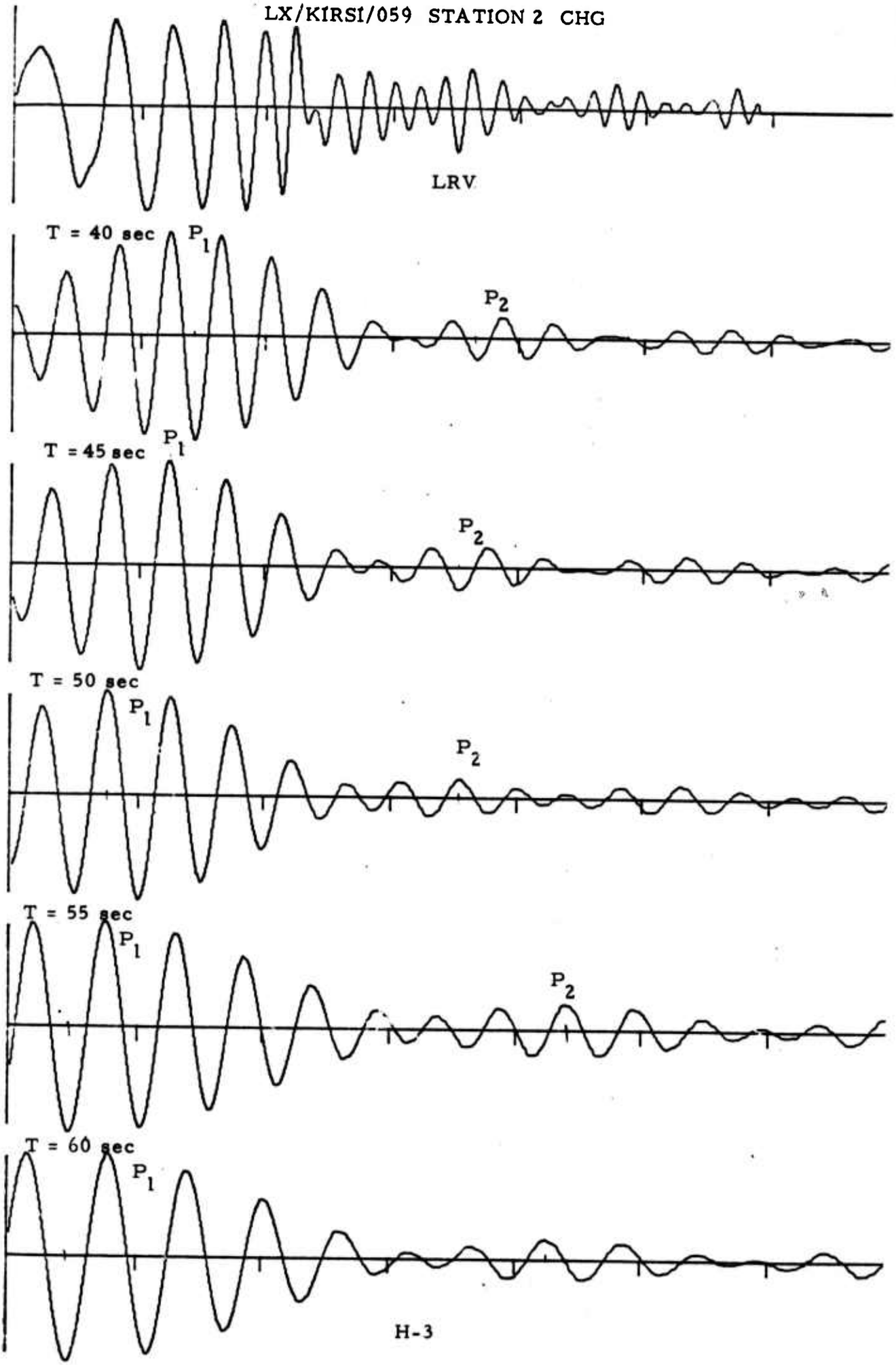

FIGURE H-1b
NARROWBAND FILTER ANALYSIS OF THE VERTICAL RAYLEIGH WAVE
OF EVENT LX/KIRSI/059 RECORDED AT CHG

FIGURE H-2

GROUP VELOCITY DETERMINATION FROM NARROWBAND OUTPUT
OF RAYLEIGH WAVES FOR EVENT LX/KIRSI/059
RECORDED AT CHG

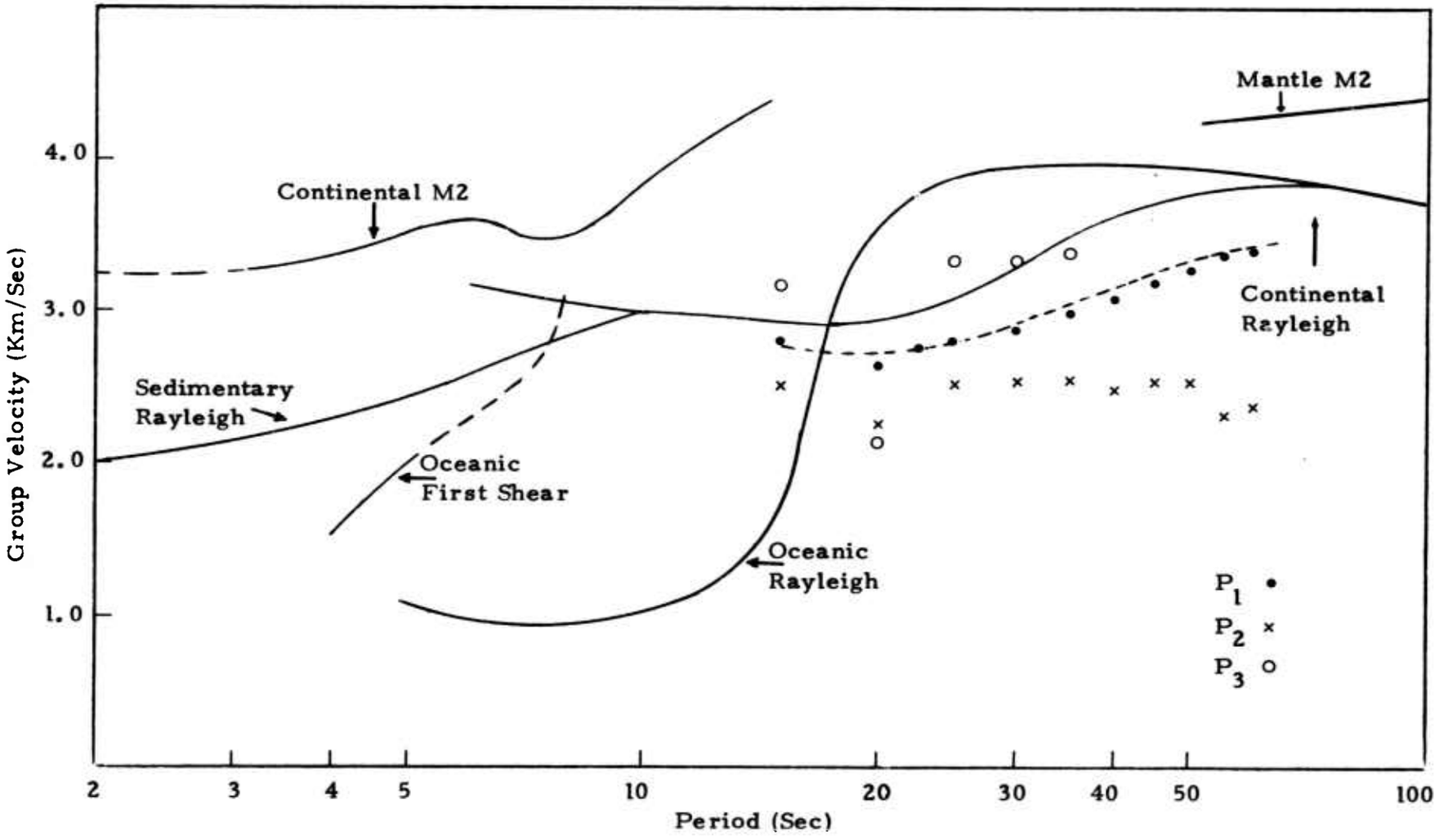

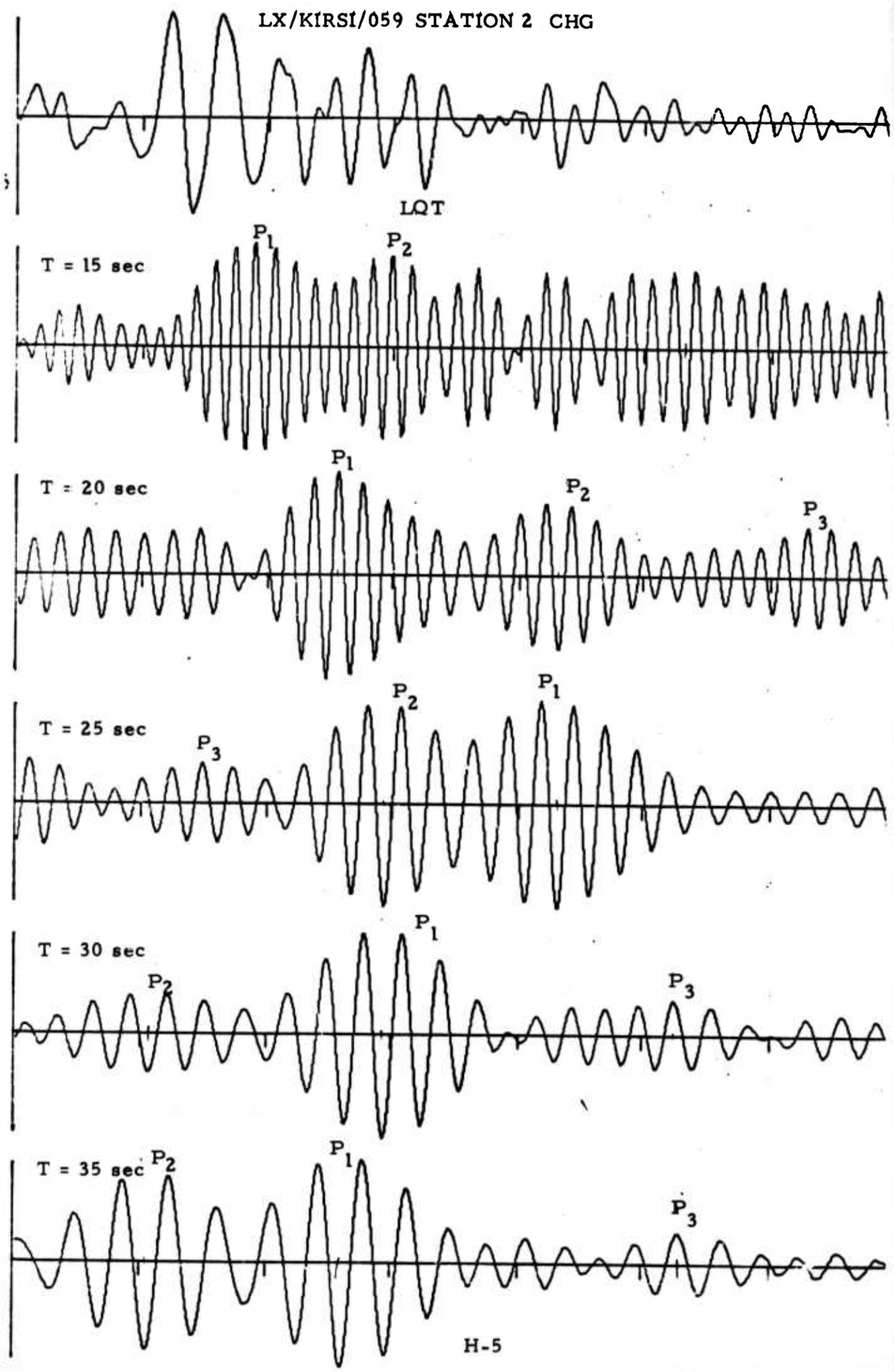

FIGURE H-3a

NARROWBAND FILTER ANALYSIS OF THE LOVE WAVES OF EVENT LX/KIRSI/059 RECORDED AT CHG

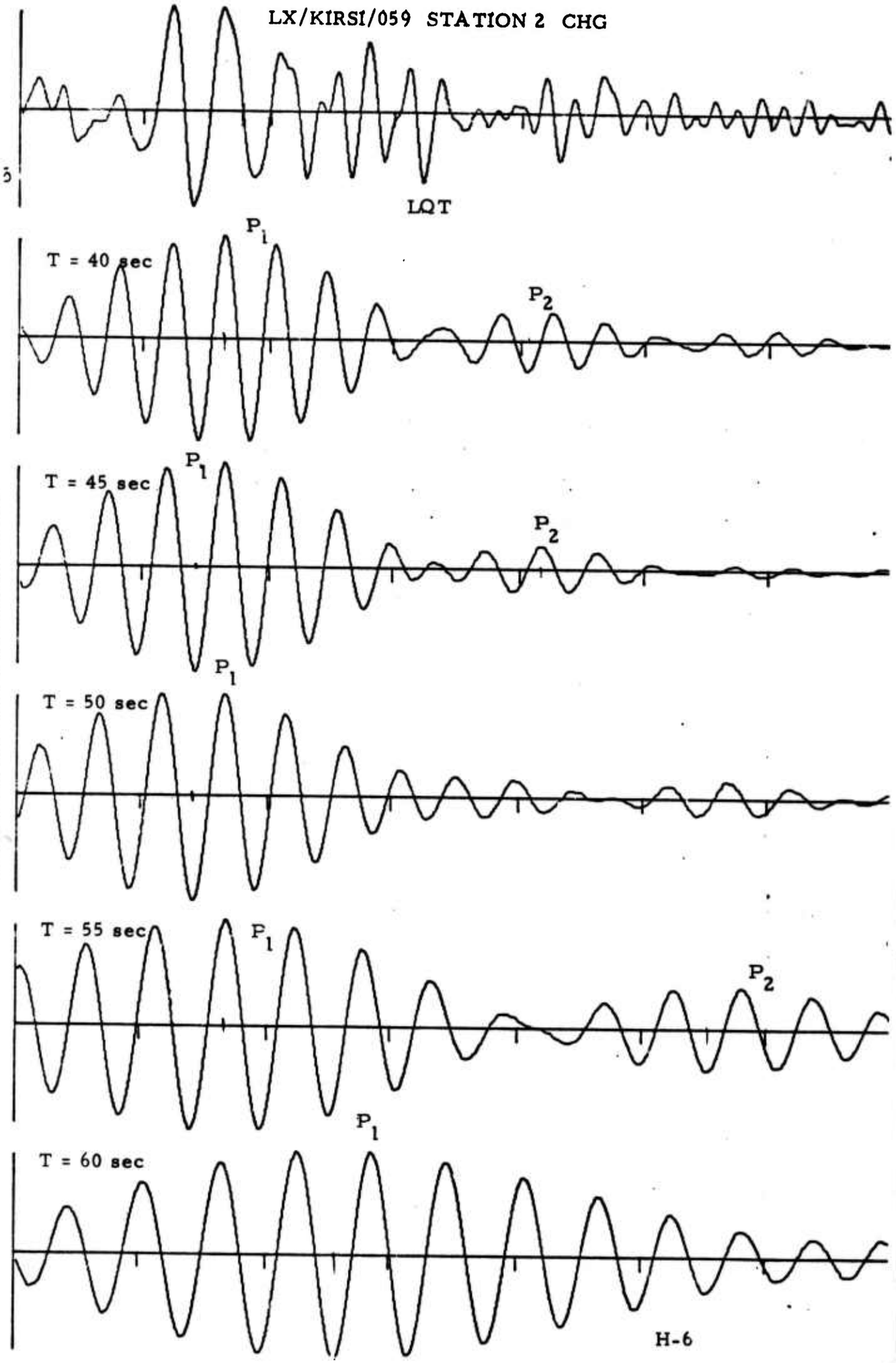

FIGURE H-3b
NARROWBAND FILTER ANALYSIS OF THE LOVE WAVES OF EVENT LX/KIRSI/059 RECORDED AT CHG

FIGURE H-4

GROUP VELOCITY DETERMINATION FROM NARROWBAND OUTPUT
OF LOVE WAVES FOR EVENT LX/KIRSI/059
RECORDED AT CHG

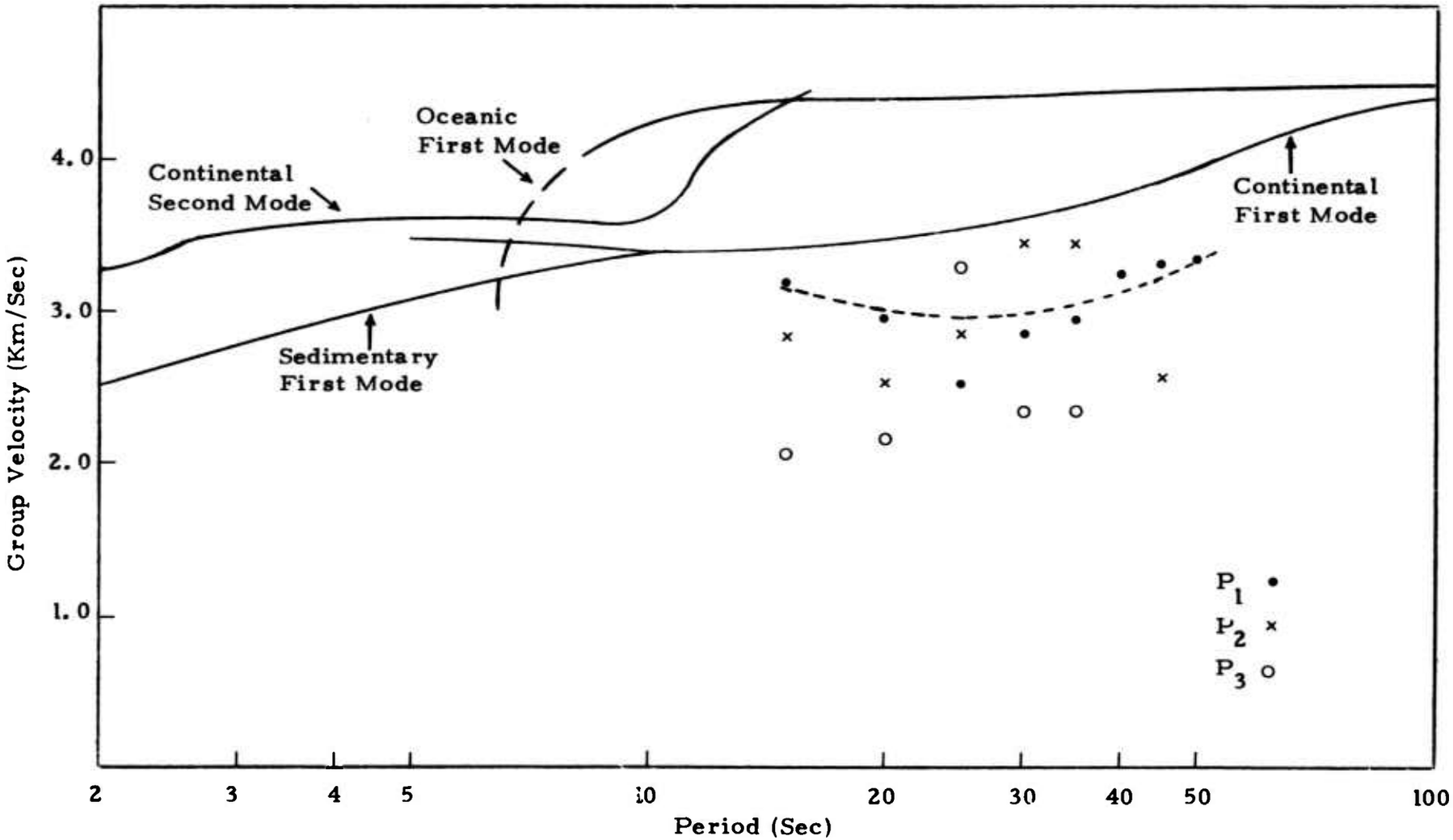

FIGURE H-5

GROUP VELOCITY DETERMINATION FROM NARROWBAND OUTPUT OF RAYLEIGH WAVES FOR EVENT LX/KIRSI/059 RECORDED AT FBK

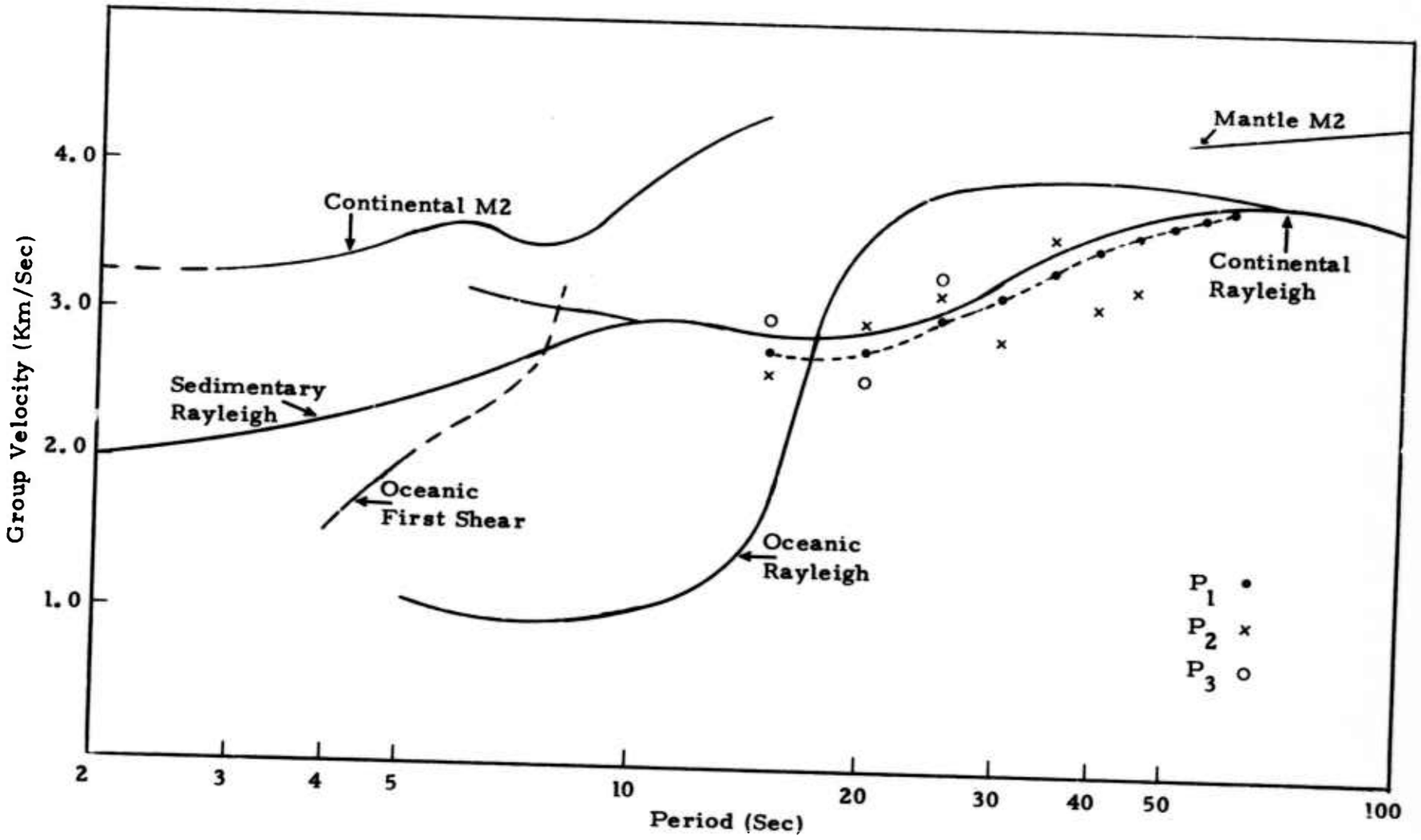

FIGURE H-5

GROUP VELOCITY DETERMINATION FROM NARROWBAND OUTPUT
OF RAYLEIGH WAVES FOR EVENT LX/KIRSI/059
RECORDED AT FBK

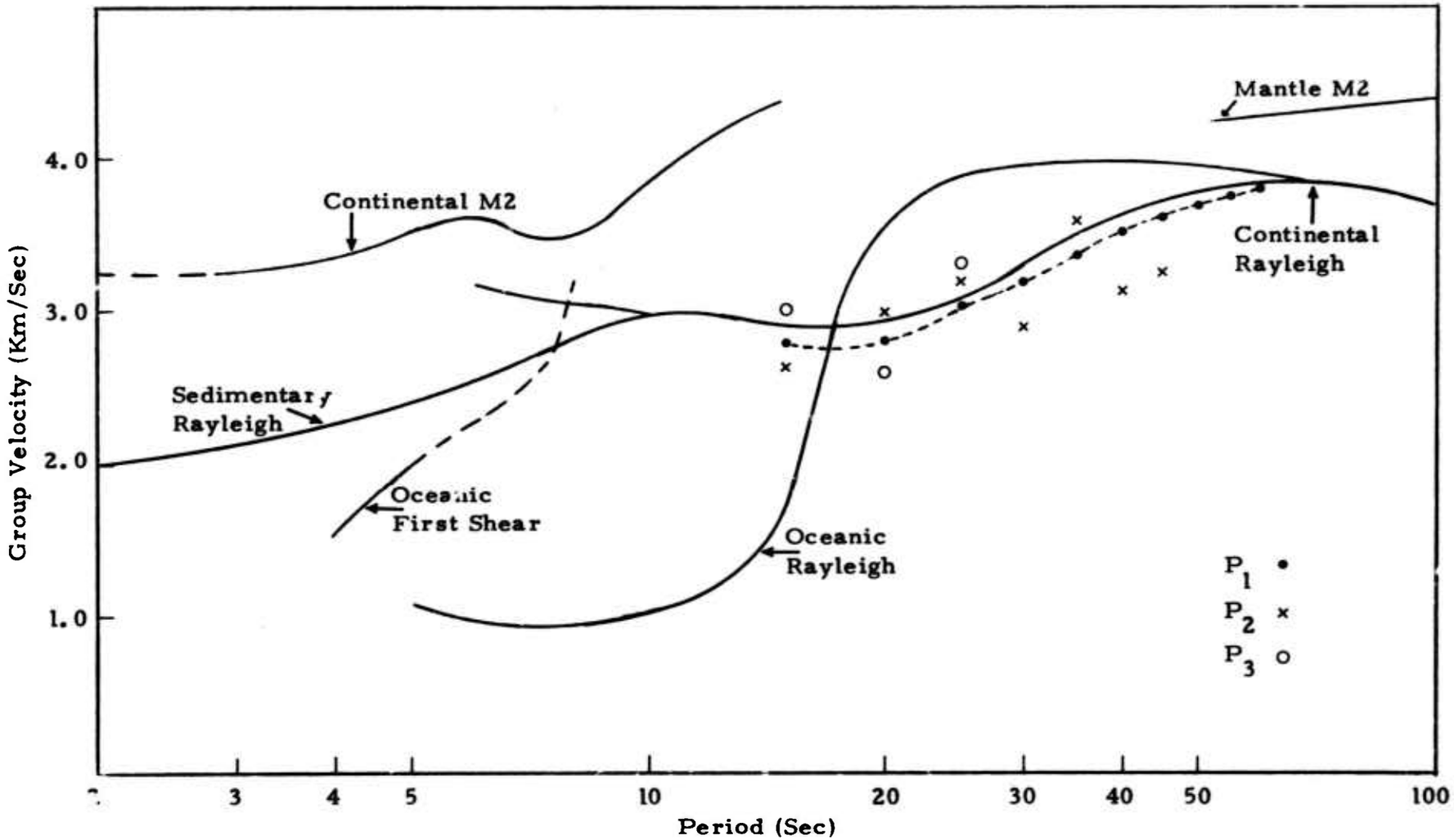

FIGURE H-6

GROUP VELOCITY DETERMINATION FROM NARROWBAND OUTPUT
OF LOVE WAVES FOR EVENT LX/KIRSI/059
RECORDED AT FBK

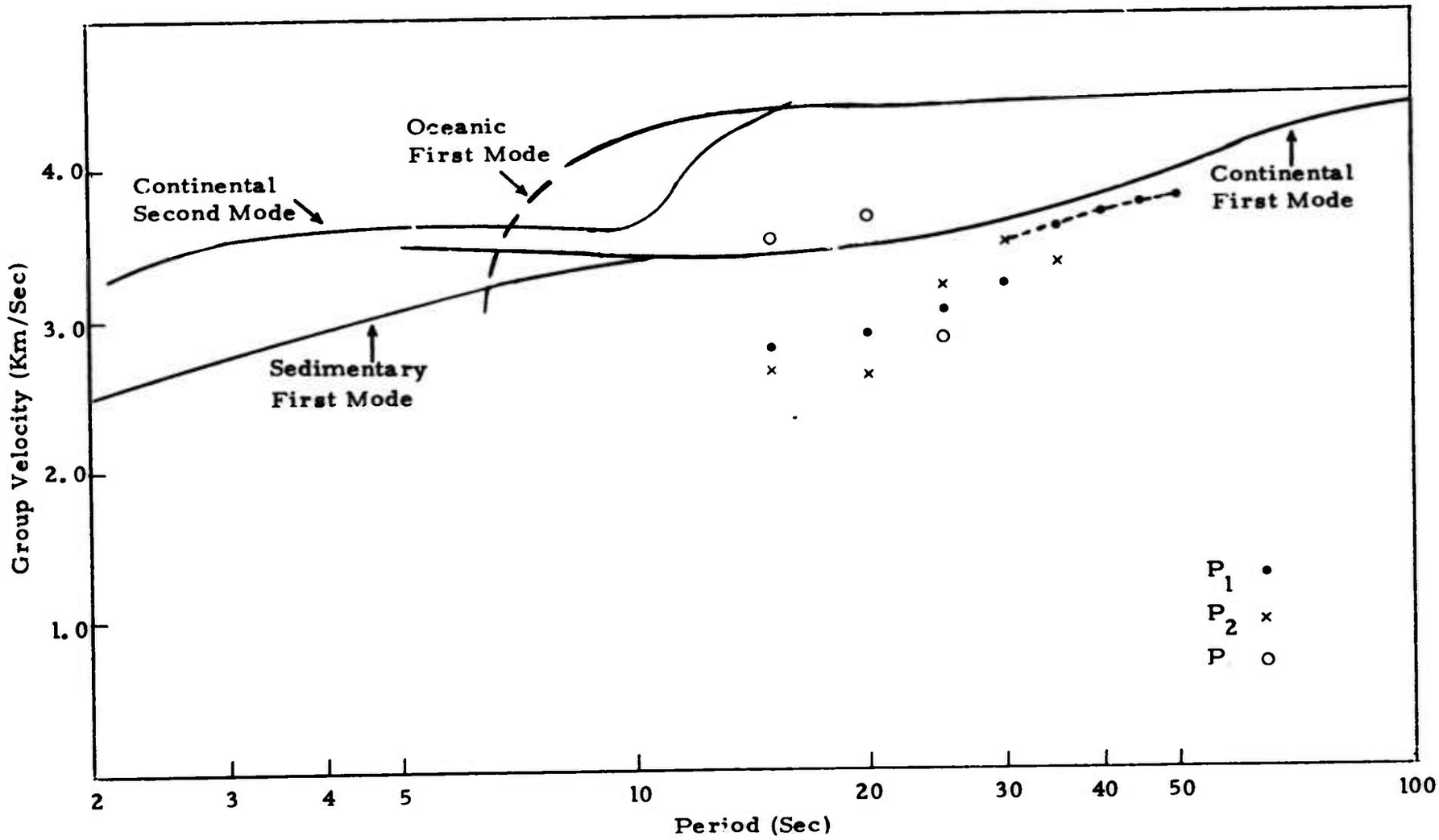

FIGURE H-7

GROUP VELOCITY DETERMINATION FROM NARROWBAND OUTPUT
OF RAYLEIGH WAVES FOR EVENT LX/KIRSI/059
RECORDED AT KIP

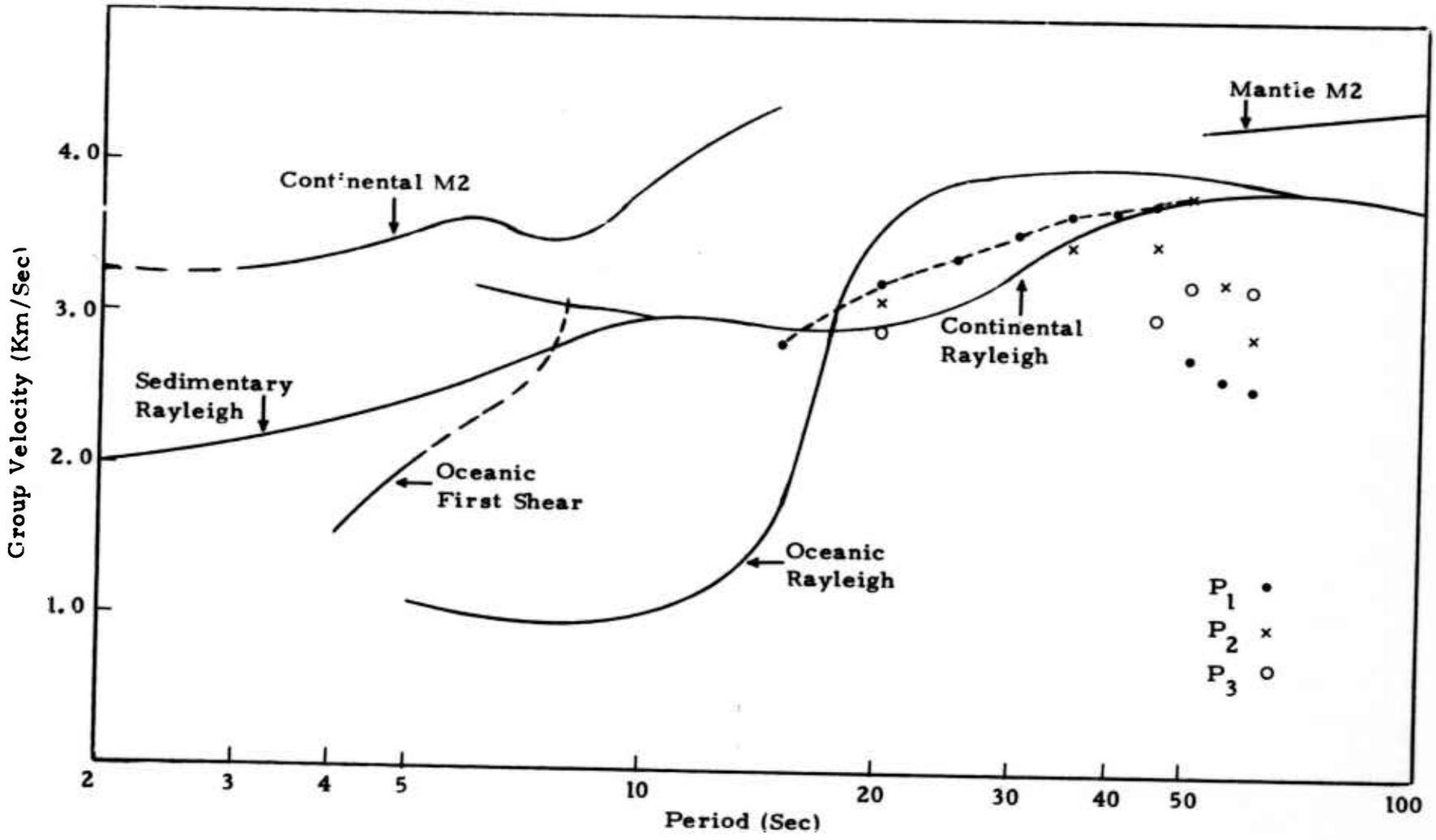

FIGURE H-8

GROUP VELOCITY DETERMINATION FROM NARROWBAND OUTPUT
OF LOVE WAVES FOR EVENT LX/KIRSI/059
RECORDED AT KIP